University of Sheffield

Reversible Acrylic Adhesives based on Covalent Adaptable Networks

Xander Praet

A thesis submitted in partial fulfilment of the requirements for the degree of Doctor of Philosophy

The University of Sheffield

Faculty of Science

Department of Chemistry

March 2023

Declaration

I, Xander Praet, confirm that the Thesis is my own work. I am aware of the University's Guidance on the Use of Unfair Means (*www.sheffield.ac.uk/ssid/unfair-means*). This work has not been previously been presented for an award at this, or any other, university. All the work is the original work of the author, except where acknowledged.

Signature: .....

March 2023

- DMTA data in Chapters 2-5 was obtained by Nicholas Hawkins (University of Oxford)
- Tensile testing data of ageing and recycling experiments in Chapters 2-5 was obtained by Jennifer Hughes (Natural Materials Lab, University of Sheffield)
- Rheology data in Chapter 4 was obtained by Bernhard De Meyer (University of Ghent)
- Creep data in Chapters 5 was obtained by Neil Lunt (University of Sheffield)

My PhD journey in 10 film quotes

And I have to get my monthly report in by tomorrow.

-Tony Wendice, Dial M for Murder (1954)

60% of the time, it works every time.

-Brian Fantana, Anchorman: The Legend of Ron Burgundy (2004)

Yeah, it's really cold in here too.

-Jason Bourne, The Bourne Identity (2002)

It's far too hot in here and you're fully dressed.

-Villefort, The Count of Monte Cristo (2002)

I'm sorry, Herr Direktor, but you're running very late.

-Itzhak Stern, Schindler's List (1993)

Are all the machines out of order today?

-Ben, Dark Floors (2008)

I think I left something in the oven.

-Chicha, The Emperor's New Groove (2000)

I'm gonna need a cup of coffee.

-Jim Gordon, The Dark Knight (2008)

I just want to sleep.

-Indy, Indiana Jones and the Raiders of the Lost Ark (1981)

Just when I thought I was out, they pull me back in.

-Michael Corleone, The Godfather: Part III (1990)

Acknowledgements

Here we are, after 1604 days at the University of Sheffield, after 1 successful Brexit (or so I've been told), 1 devastating global pandemic and 4 not so equally incumbent prime ministers, at the top of the proverbial mountain, which often felt steeper than Conduit Road.

First and foremost, I'd like to thank my supervisor Professor Andrew Slark for his guidance through this eventful PhD project. His trust in me to help build, shape and be part of the brand-new Slark research group really humbles me. It's easy to *sgorio cais* with him as the *mewnwr.* He genuinely is the *Seren y Gêm.*

Thanks to the UKRI for funding my project and all the people I've met from the CDT. All our workshops (and free lunches) definitely made me a better researcher. Next, I'd like to thank a few members of the Slark group because all that I have achieved was only possible by collaborating with these brilliant people. Thanks to Neil Lunt for all his help with the creep experiments, Jenny Hughes for helping me with the tensile testing and thanks to Tom Jackson for the help with the thermal analysis. Also, a huge thanks goes out to our Postdocs James and Devanshi for their immense support of our young research group. Finally, I like to thank my oldest colleague, part-time mountaineer and full-time friend Simon Fawcett, who joined me on this adventure from the absolute beginning and was always the canniest of us all.

Further, I want to thank Chris Holland for sharing his tensile testing equipment and Nick Hawkins at Oxford University for helping with DMTA. I also want to thank a few members of the Du Prez group at the University of Ghent. Many thanks to Tim Maiheu, Bernhard De Meyer and Filip Van Lysebetten for the help with the stress-relaxation experiments and the fruitful discussions. Also, many thanks to Stefan Lawrenson at Scott Bader for his feedback while I was writing up.

A group of people that were of paramount importance for making it through these past years were my friends to whom I owe a massive thank you for always including me in their colourful lives. I simply could not have done this without all of you.

Finally, I'd like to thank my family for their tremendous support, even though it was mostly given remotely. All that I am is because of my amazing parents and my inspiring sister Nore. They truly enable me to accomplish astonishing feats and keep reminding me of one of our favourite motivational mottos "*Weir doen voesj".*

This PhD thesis is brought to you by the following sponsors: Falafel King Friday, coffee, scores written by Hans Zimmer, persistent grit, breadsticks and houmous, power naps and Wednesday footy organised by Neil and Jonny (a.k.a. the cofounder of the Slark group film jamborees, I know, where does that man find the time?).

Abstract

Covalent Adaptable Networks (CANs) are a new paradigm in polymer science and consist of dynamic cross-links. A range of chemical routes has been reported, which tend to proceed *via* a dissociative or associative mechanism. However, the understanding of the physical and mechanical properties of CANs is limited.

In this work, three different types of dynamic exchange reactions are comprehensively compared – Diels-Alder cycloaddition, transamination of vinylogous urethanes and phthalate monoester transesterification. Functional comonomers furfuryl methacrylate (FMA), acetoacetoxyethyl methacrylate (AEMA), 2-hydroxylethyl methacrylate (HEMA) are copolymerised with 2-ethylhexyl methacrylate (EHMA) using standard free-radical polymerisation techniques (FRP) with *n*-dodecyl mercaptan (DDM) as a chain transfer agent (CTA). The three types of dynamic networks are formed by further reacting with different bifunctional aliphatic cross-linkers. The incorporation of the functional comonomers is varied systematically from 5 to 20 mol.% to critically examine material properties in the same acrylic network. Furthermore, two molecular weights were investigated, namely 10 and 40 $kg.mol^{-1}$. Our aim is to understand the influence of specific network chemistry, prepolymer molecular weight and cross-link density on the rheological, thermal and mechanical properties. Therefore, all prepared networks are fully characterised using thermogravimetric analysis (TGA), differential scanning calorimetry, solubility tests, stress-relaxation experiments, dynamic mechanical thermal analysis (DMTA), tensile testing, ageing and recyclability experiments. First, the properties were compared with the literature within each dynamic chemistry. Then, a comparison was conducted between all three reversible chemistries.

The knowledge will be used to help design new acrylic polymer networks, which perform in use as adhesives but can be triggered to provide reversibility and enable re-use of materials.

Table of Contents

List of Abbreviations

AEMA	Acetoacetoxyethyl methacrylate
AIBN	Azobisisobutyronitrile
atm	Standard atmosphere (1.01325 bar)
ATRP	Atom transfer radical polymerisation
BA	N-butyl acrylate
BMA	N-butyl methacrylate
BPO	Benzoyl peroxide
CANs	Covalent adaptable networks
CDM-AA	Cyclohexane dimethanol bisacetoacetate
$CHCl_3$	Chloroform
CPD	Cyclopentadiene
CRP	Controlled radical polymerisation
CTA	Chain transfer agent
$Đ$	Dispersity
DA	Diels-Alder
DA_{INV}	Inverse electron demand Diels-Alder reaction
DA_{NED}	Normal electron demand Diels-Alder reaction
DDM	N-dodecyl mercaptan
DEPD	Diethyl-1,5-pentanediol
DGEBA	Diglycidyl ether of bisphenol A
DMTA	Dynamic mechanical thermal analysis

DP	Degree of polymerisation
DSC	Differential scanning calorimetry
e	Euler's number
E	Young's modulus
E_a	Activation energy
EHMA	2-ethylhexyl methacrylate
EtOAc	Ethyl acetate
FMA	Furfuryl methacrylate
FTIR	Fourier-transform infrared spectroscopy
G	Relaxation modulus
G'	Storage modulus
G''	Loss modulus
GAC	General acid catalysis
GBC	General base catalysis
H_2SO_4	Sulfuric acid
HEMA	2-hydroxethyl methacrylate
HMA	Hexyl methacrylate
HOMO	Highest occupied molecular orbital
I	Initiator
IUPAC	International Union of Pure and Applied Chemistry
LMA	Lauryl methacrylate
LUMO	Lowest unoccupied molecular orbital
LVR	Linear viscoelastic region
m.p.	Melting point

M_c	Critical molecular weight
MCR	Mid-chain radical
M_e	Entanglement molecular weight
META	4-methacryloxyethyl trimellitic anhydride
MMA	Methyl methacrylate
M_n	Number-average molecular weight
NGP	Neighbouring group participation
NMP	Nitroxide Mediated Polymerisation
NMP	N-methyl-2-pyrrolidone
NMR	Nuclear Magnetic Resonance
p	Fractional monomer conversion
PBD	Poly(butadiene)
PBT	Poly(butylene terephtalate)
PCL	Poly(ε-caprolactone)
PEG	Poly(ethylene glycol)
PEHMA	Poly(2-ethylhexyl methacrylate)
PET	Poly(ethylene terephthalate)
PFMA	Poly(furfuryl methacrylate)
PILs	Polymerised ionic liquids
PLMA	Poly(lauryl methacrylate)
PME	Phthalate monoesters
PMMA	Poly(methyl methacrylate)
PTHF	Poly(tetrahydrofuran)
p-TsOH	p-Toluene sulfonic acid

RAFT	Reversible addition/fragmentation chain transfer
rDA	Retro-Diels-Alder
RDRP	Reversible-deactivation radical polymerisation
RDS	Rate determining step
SEC	Size exclusion chromatography
SPR	Secondary propagating radical
T^{-1}	Inverse temperature
TBD	Triazabicyclodecene
$T_{deg5\%}$	5% mass degradation temperature
T_g	Glass-transition temperature
TGA	Thermogravimetric analysis
THF	Tetrahydrofuran
TMAC	Trimellitic anhydride chloride
TMP	Trimethylolpropane
TREN	Tris(2-aminoethyl)amine
TS	Transition state
T_v	Topology freezing temperature
VCM	Vacuum compression moulding
vs.	*Versus*
WLF	Williams-Landel-Ferry
WRAP	Waste & Resources Action Programme
X_n	Number-average degree of polymerisation
$Zn(ac)_2$	Zinc acetate
$Zn(acac)_2$	Zinc acetyl acetonate

Zn-PAM	Poly(acrylonitrile-co-zinc methacrylate)
ε_b	Elongation at break
η	Intrinsic viscosity
σ_b	Stress at break
τ	Relaxation time

Chapter 1 Introduction

1.1 Adhesives

1.1.1 Introduction

The process of bonding is the joining of two substrates using an adhesive to resist separation. Adhesives are often defined as a non-metal that acts as a binder based on cohesion and adhesion. Both cohesion and adhesion depend on intermolecular forces, which can be weak (*e.g.* van der Waals interactions) or strong (*e.g.* covalent bond) chemical bonds depending on the adhesive/substrate system. An adhesive bond can be divided into different zones, namely a cohesion zone in the centre and an adhesion zone at the interface with the substrate (*Figure 1*). Additionally, there is a transition zone present in between both zones.

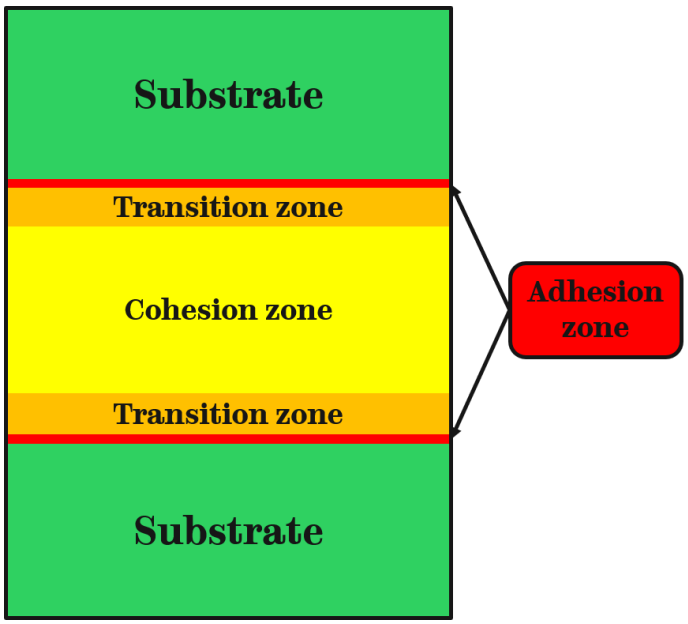

Figure 1: A cross-section of an adhesive binder, highlighting the adhesion, transition and cohesion zones between substrates.

The macroscopic properties of the adhesive are different in the cohesion zone when compared to the adhesion zone. This is a result of the difference in state of the material. In the cohesion zone, the adhesive behaves as a uniform homogeneous bulk material. Conversely, the microstructure and composition of the adhesion zone is altered due to the interfacial interaction with the substrate surface. There is also a transition zone present between the two that has gradually changing macroscopic properties. Further, the properties of these zones will define the performance of the adhesive.

A first important prerequisite for bonding is good wetting of the substrate surface. Wetting is the ability of the adhesive to spread and cover the substrate surface evenly.[1] This wetting depends on the properties of the substrate surface, which describes a preference towards some adhesives based on the balance of surface and interfacial forces. Hence, good wetting can significantly improve the quality of the adhesive bond by increasing the contact area. Further, this increased contact area can be attained by increasing the surface roughness, which in turn improves the mechanical interlocking of the adhesive/substrate system.[2] In examples where there is an incompatibility between surfaces, a promotor (*e.g.* a primer) can be used to improve adhesion. Furthermore, cleaning of the surface or using pre-treatment methods can significantly increase the wetting of the surface. This can be rationalised by the removal of weak boundary layers (*e.g.* grease, inorganic contaminants, rust). Moreover, the wetting performance of an adhesive is predominantly determined by its rheological properties. The most important rheological property is the viscosity, which determines how well the adhesive can flow and make intimate surface contact. The viscosity of the material depends on

the molecular structure of the adhesive polymer (*e.g.* the average chain length, presence of side chains). In the field of pressure-sensitive adhesives, the molecular structure plays an important role in determining how tacky or "sticky" the material is. Increasing the tack will consequently increase the resistance to peel, which can be defined as the force required to remove the adhesive from the substrate. Thus, the performance depends on the molecular structure of the adhesive polymer.

A second prerequisite is a hardening step to ensure that the cohesive strength is adequate for the application. This hardening will also significantly improve the resistance to shear, which is the property related to the lateral creep of the material.

1.1.2 Classification

Adhesives can be classified based on their chemical basis or the bonding mechanism. Furthermore, within these subclasses, a further distinction can be made based on the number of components in the formulation systems. The two main bonding mechanisms include physical hardening and chemical curing.

An example of the first mechanism are the so-called hot melt adhesives. Here, the adhesive is heated to a viscous liquid and coated onto a substrate surface before it cools back down to a solid. These hot melt adhesives can also be reactive, which leads to additional chemical bonds after cooling down (*e.g.* hydrogen bonding). These additional bonds improve the adhesion and resistance to heat and moisture. In industry, they are valued for their shelf life, safety and convenience.

The second bonding mechanism usually involves a two-part system, namely the resin and the hardener. These are mixed to achieve the desired setting time, which is the shortest time required by the adhesive to develop strength for the handling.

The one-part formulation has to be stored at low temperatures to avoid premature curing reactions. Hence, the shelf life will significantly decrease at higher temperatures.

Different chemistries and monomers can be used for the latter. Urethane-based adhesives have the largest market share, followed by epoxy- and acrylic-based systems (*Figure 2*). The urethane chemistry is based on the reaction of isocyanates and polyols and extensively used as an adhesive in footwear, flexible packaging, transportation, furniture and construction.[3] Epoxy chemistry is one of the oldest adhesive chemistries and it is based on the reaction of epoxides and polyols or polyamines. Due to its low shrinkage, good wettability, high corrosion resistance and good mechanical strength, it is widely used in the electronics, sports, construction, automotive, aerospace and aeronautics industry.[4-7]

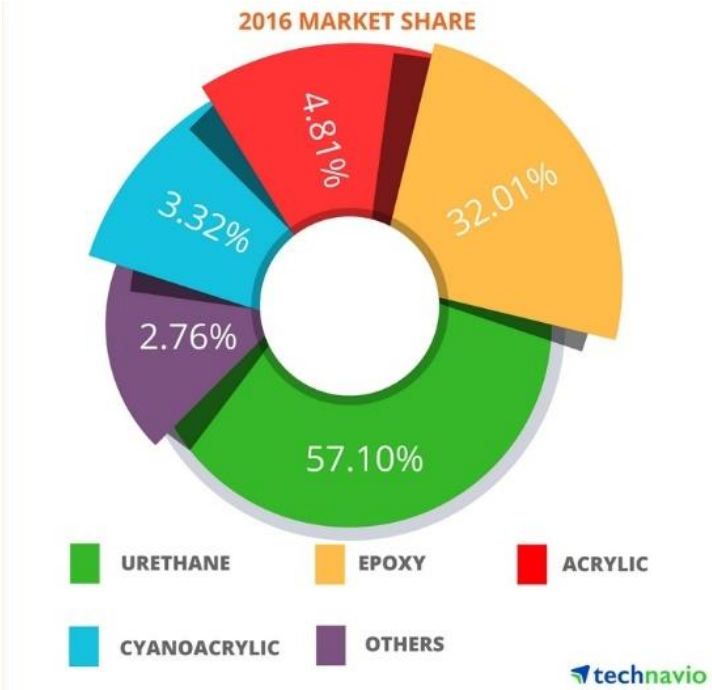

Figure 2: Global structural adhesives market by product type. Copyright of Infiniti Research Ltd.[8]

Acrylic adhesives are based on the chain-growth polymerisation reaction of (meth)acrylic monomers and will be further discussed in the next section. The urethane- and epoxy-based adhesives are beyond the scope of this work. Furthermore, there are diverse adhesive types including one-component or two-component formulations, liquids, pastes, pellets and films. Some key manufacturers and suppliers in this field are 3M, Arkema, Ashland, Henkel and Sika.

1.1.3 Acrylic adhesives

Acrylic adhesives based on acrylate and methacrylate monomers have been used on a commercial scale for decades.[9] Generally, these consist of two components that are usually mixed directly before applying to the substrates. Acrylates are often less frequently employed due to their pungent odour when compared to methacrylates.[9]

Polymer systems based on methyl methacrylate (MMA) are one of the most widely used adhesives on the market.[9] Initially, they were used as bonding agents for poly(methyl methacrylate) (PMMA) in the 1950s. For example, one of the components can contain an oxidising agent (*e.g.* peroxide species) while the reducing agent (*e.g.* metal salt) is added to the other component. In order to improve toughness and increase the compatibility with a wider variety of substrates, manufacturers started to introduce elastomers to supplement or substitute the former PMMA additive in the 1960s. Other well-known acrylic polymer systems are often based on butyl acrylate. These systems are generally lightly cross-linked and employed as pressure-sensitive adhesives (*e.g.* sticky notes, gaffer tape) and can even be biobased.[10]

Furthermore, to meet new performance requirements of specific applications, new functional monomers were introduced in the formulations. The ability to tailor the adhesive formulation to distinct and demanding niche applications drove the extensive development of these commercial polymer systems to the high performing standard they are today. Hence, their applications range from medical, dental[11, 12] to composites and construction.[13, 14] At the end-of-life phase of an assembled product, adhesives can also play an important role in the recycling (*e.g.* debonding on demand) and reducing the overall carbon footprint.[15]

1.1.4 Recycling

For a long time, it was virtually impossible to recycle assemblies containing chemically cured adhesive bonds since there was a lack of reversibility in these bonds. Initially, systems were introduced based on additives that could act as a susceptor (*e.g.* carbon nanotubes, ferromagnetic materials).[16, 17] These susceptors enabled heat generation upon the application of an external electromagnetic field. Consequently, this heat facilitated the disruption of the joint. Alternatively, microspheres filled with a liquid hydrocarbon were added. Upon heating, these spheres undergo a significant volume expansion, which ultimately leads to rupture of the joint.[18, 19] Onusseit *et al.* researched the influence of adhesives on recycling and stated: “In order to simplify recycling for the future, adhesives with “switches enclosed” are being developed which will allow us to disbond system components into separate parts after use for reuse or material recycling.”[20]

Recent developments on the introduction of recyclability in cured systems will be discussed in the next chapters. This recyclability is important since the waste

production in the UK has become a large issue with most of the materials used in manufacturing products ending up as waste. In 2011, the Waste & Resources Action Programme (WRAP) found that the construction industry was responsible for 120 million tonnes of waste, which was estimated as being a third of all UK waste.[21] Landfill is approaching capacity in most places and an increase in consumer waste is projected (*Figure 3*).[21-23] In recent years, a trend is emerging in the chemical industry to strive for a so-called circular economy.[24]

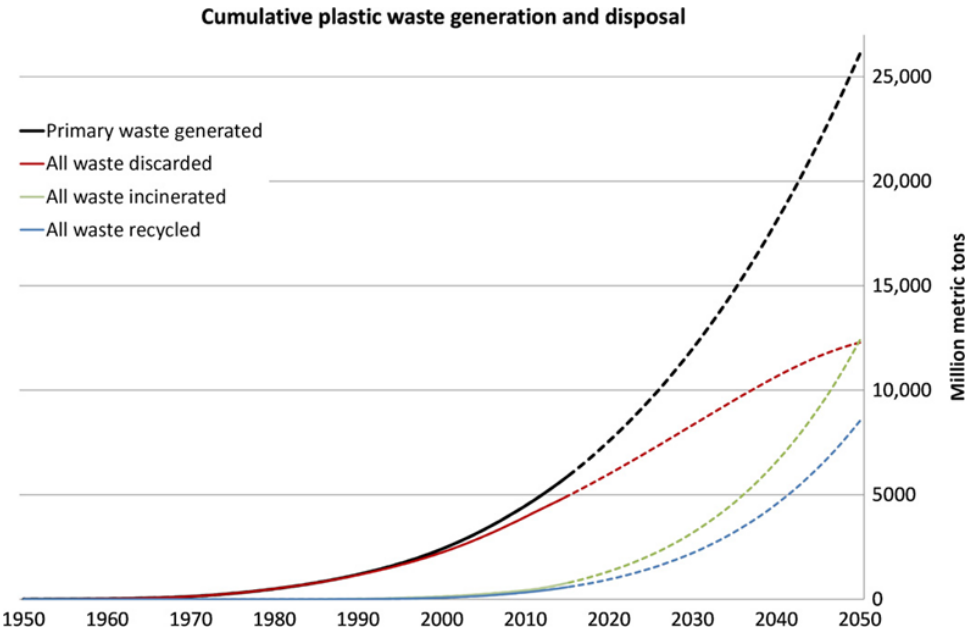

Figure 3: Cumulative plastic waste generation and disposal (in million metric tons). Solid lines show historical data from 1950 to 2015; dashed lines show projections of historical trends to 2050. Figure reproduced with permission from Science Advances.[23]

Nowadays, end-of-life requirements (recycling, re-use and remanufacturing) need to be considered in the fabrication of new products (*Figure 4*). Generally, custom engineering and new technologies allow the manufacturer to increase the recyclability of the products and minimise the waste stream going to landfill. It is currently impossible to fully separate components which are bonded using conventional, irreversible adhesives. New smart polymers are required, which can

be easily applied as adhesives, provide high performance during its life cycle but which can be triggered to enable separation of substrates and consequently their reuse.

Figure 4: Different stages of the life cycle of a product. Copyright of Carbon Footprint Ltd.

1.2 Thermoplastics *vs.* Thermosets

Polymers can be subdivided classically into two major classes, namely thermoplastics and thermosets. The former class can be seen as a collection of long chains, which can entangle (*Figure 5*). An important property of thermoplastics is that upon sufficient heating these long chains flow to a certain degree. This flow enables easy (re)processing. Despite the possibility to flow, the viscosity is a few orders of magnitude larger than the viscosity of common fluids such as water or even honey. Thermoplastics are extensively used in the food packaging industry due to their low cost and excellent processability.[25] Another advantage is their light weight causing a high strength-to-weight ratio. The main drawbacks of this class are their sensitivity towards solvents and their low mechanical strength.[26] In contrast, a thermoset is a type of polymer that has molecular bridges, so-called cross-links,

between individual polymer chains resulting in a three-dimensional covalently bonded network (*Figure 5*).

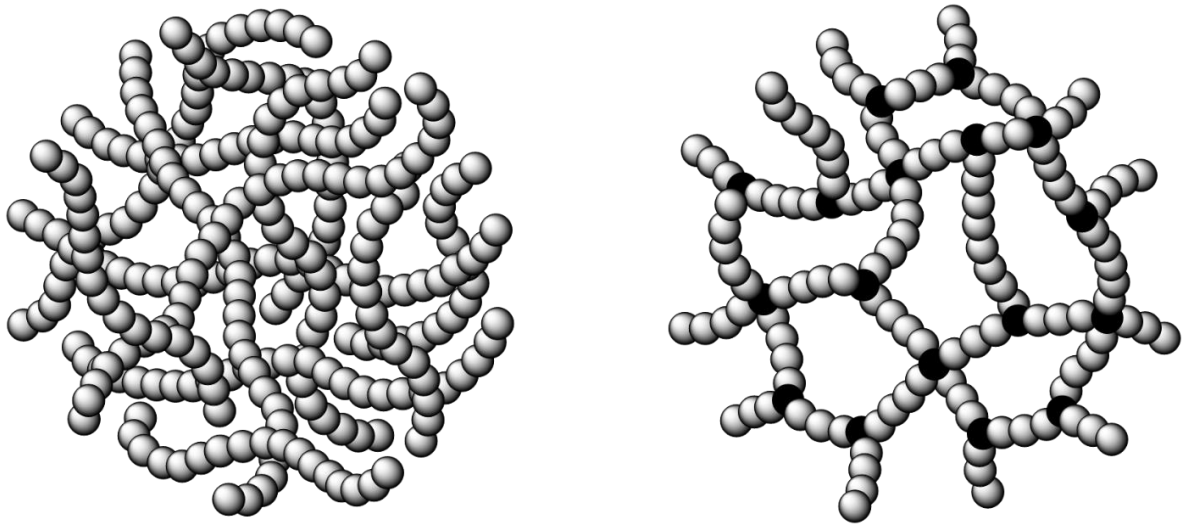

Figure 5: Graphical representation of a thermoplastic (left) consisting of individual linear polymer chains and a cross-linked thermoset polymer (right).

This network has specific attributes such as high mechanical strength, thermal stability and solvent resistance. The cross-linking process or curing usually happens in a mould. This three-dimensional cast is responsible for the shape given to the desired product. Once cured, reshaping or reprocessing has traditionally proved impossible. This means that recycling by repetitive reheating followed by a processing step such as extrusion, injection moulding or cast moulding is not possible for thermoset materials in contrast with thermoplastics.

A lot of applications require polymers with high mechanical strength and thermosets are the most suited material for such uses. In 2015, the world production of thermosets amounted to 79 million metric tons.[27] That was approximately a quarter of the total world production of plastics. Unlike the circular economy that is theoretically possible for thermoplastics, thermosets lack reprocessability.[28] This

necessitates the design of more reprocessable materials with the properties of thermosets.

Since then thermosets proved themselves to be exceptionally useful for a whole range of applications such as electrical insulators,[29] coatings,[30] sealants,[31] biocompatible implants,[32] flooring and fibre-reinforced composites in the automotive and aircraft industry.[33] Hence, they are strong and reliable materials for more demanding tasks that thermoplastics are unable to fulfil.

Despite these properties, conventional thermosets, consisting of irreversible cross-links, still have the major disadvantage of lacking reprocessability. Recent efforts have therefore attempted to design materials that introduce reversibility into the network in order to facilitate the reprocessing.[34] This can be achieved by using labile bonds or linkages to obtain degradable thermosets. Further, dynamic, instead of irreversible, chemistries can be introduced in either the cross-links or the polymer backbone resulting in covalent adaptable networks (*vide infra*).

1.2.1 Polymer networks

Polymer networks can be made *via* two methods. A first one includes the step-growth reaction between at least a bifunctional and trifunctional monomer, which is often referred to as a polyaddition reaction. The second method involves a chain-growth polymerisation that incorporates monomers with a functional handle that can react with a cross-linker molecule in a subsequent curing step (*Scheme 1*). The main structural difference between these two types of networks is the number of cross-links per unit of volume (cross-link density). This plays an important role in the

gelation process and exchange reactions, when reversible cross-linking chemistries are incorporated (*vide infra*).

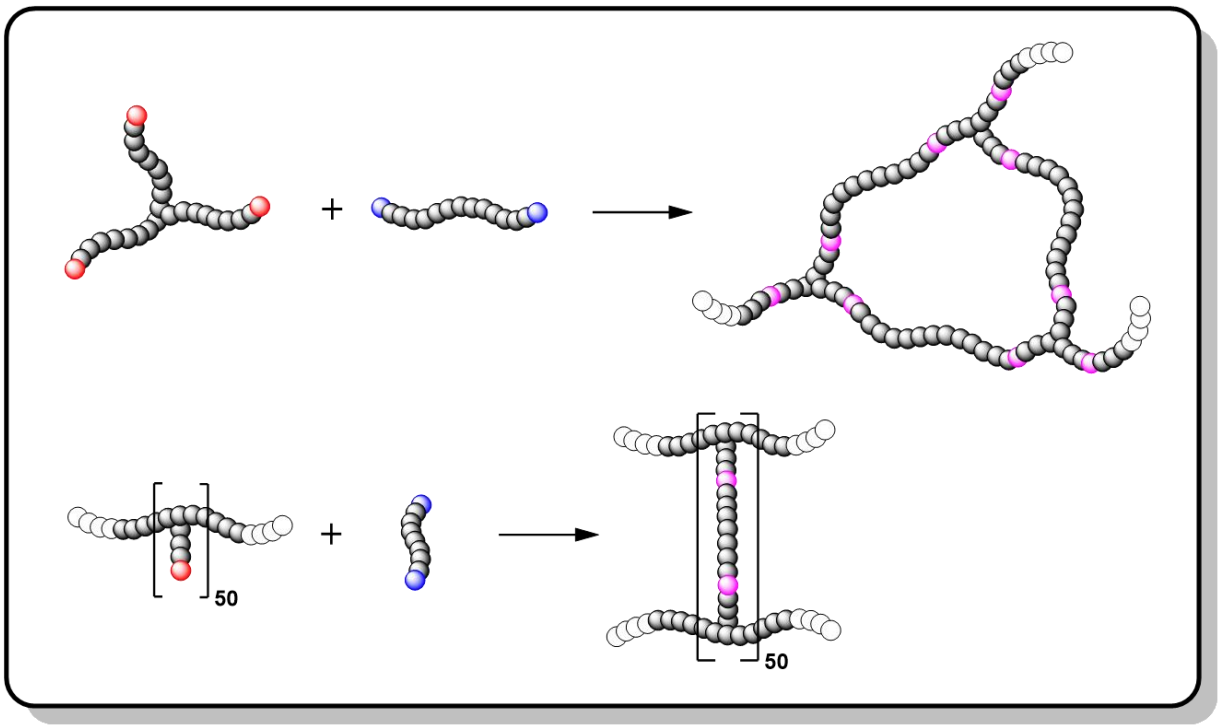

Scheme 1: General cross-linking types with the polyaddition approach (top) and the pendant group approach (bottom).

The Carothers theory describes the influence of fractional monomer conversion (p) on the number-average degree of polymerisation (X_n) in step-growth polymerisations (*Equation 1*).[35] From this equation, we can deduce that high monomer conversions are needed to achieve high degrees of polymerisation. For example, p of 0.99 is required for X = 100.

$$\bar{X}_n = \frac{1}{1-p} \qquad (1)$$

The Flory-Stockmayer theory is an extension of the Carothers theory and describes the relation between functionality of the monomers, conversion and gelation point

(*Equation 2 - 3*).[36-39] The conversion of bifunctional groups B at the gelation point (p_{Bg}) can be calculated *via*:

$$p_{Bg} = \frac{1}{\sqrt{r(f_A-1)(f_B-1)}} \quad (2)$$

$$r = \frac{N_B}{N_A} \quad (3)$$

where r is the ratio of the number of A and B groups present initially, f_A and f_B are the number of reactive functional A and B groups, respectively.

Considering the example from *Scheme 1 (top)* between a trifunctional A monomer (f_A = 3) and bifunctional B monomer (f_B = 2), assuming the number of reactive functional groups A and B are the same (r = 1), the conversion of B groups at the gelation point is p_{Bg} = 0.71.

For the pendant group approach, high molecular weights are already achieved during the chain-growth copolymerisation when incorporating the functional comonomers. Hence, gelation will occur at significantly lower conversions compared to the polyaddition approach. For example, considering the reaction from *Scheme 1 (bottom)* between polymer chains with 50 pendant A groups (f_A = 50) and bifunctional cross-linking B groups (f_B = 2), assuming the number of reactive functional groups A and B are the same (r = 1), the conversion of B groups at the gelation point is p_{Bg} = 0.14.

The main conclusion is that significantly higher conversions are needed to reach gelation in step-growth networks than chain-growth networks, as the degree of

polymerisation is mainly achieved during the copolymerisation. This work will focus exclusively on the use of the latter approach.

1.2.2 Free radical polymerisation

Methacrylate monomers are commonly polymerised *via* chain-growth polymerisation techniques in industry.[40, 41] Chain-growth polymerisation consists of the sequential addition of monomer building blocks onto the polymer chain. This reaction can occur *via* two mechanisms, namely an ionic or a radical mediated pathway.[42] Industrially, free radical polymerisation has been used for a long time to produce commodity thermoplastics.[43] The major advantage is the robustness and scalability of the technique, which enables large batch reactions.[44] Monomers are combined with an initiator in a reaction vessel in solvent or in bulk. Various monomers are compatible with this method such as styrene, acrylates, methacrylates, vinyl chloride, ethene and propene[45]. The mechanism consists of three main steps; namely initiation, propagation and termination (*Scheme 2*).[46]

An additional side reaction, the transfer reaction, can also occur depending on the application, this side reaction can either be detrimental or beneficial. It is considered detrimental when these transfer reactions cause a broad dispersity when narrow dispersities are required. However, transfer reactions to a chain transfer agent can be beneficially used to control the molecular weight.[46]

Initiation occurs when an initiator molecule is exposed to a suitable stimulus, such as heat, light or a redox initiator, upon which a labile bond within the initiator undergoes homolytic decomposition to generate the desired radicals (*Scheme 2*). Commonly used thermal initiators include benzoyl peroxide (BPO) and azobisisobutyronitrile (AIBN).

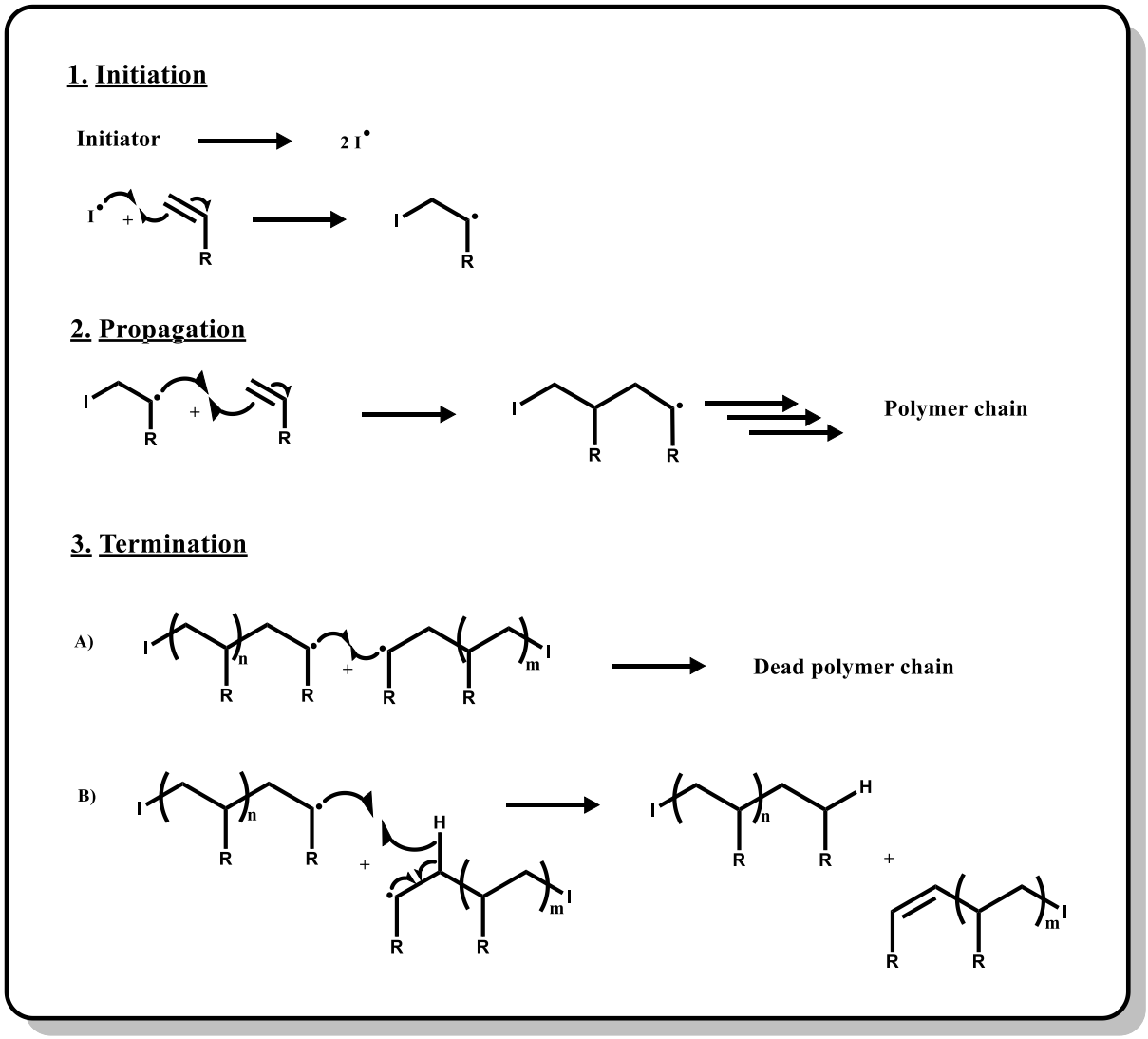

Scheme 2: Mechanism of free radical polymerisation highlighting 1. initiation, 2. propagation and 3. Termination, either by combination (A) or disproportionation (B).

Once a radical is formed, it will react with the olefin group of a monomer which leads to a new radical chain end that can subsequently continue the chain-growth polymerisation in the propagation phase (*Scheme 2*).

Termination occurs when two radical moieties react with each other. There are two main processes involved in the termination, namely combination and disproportionation. Combination implies the coupling of two radical chain ends. Since this process will lead to a doubling of the molecular weight, the presence of termination by combination can be proven by monitoring the molecular weight of the propagating species (*3.A*, *Scheme 2*). Radical disproportionation can be defined

as the abstraction of a hydrogen atom from one active chain end to another, consequently producing an unsaturation in one chain while introducing a terminal saturated group in the other (*3.B*, *Scheme 2*). An unreacted initiator molecule can also cause termination. An increase of the initiator concentration leads to an increase in the concentration of radical moieties, which influences the rate of propagation and termination. This will consequently lead to shorter chain lengths (*Equation 4*).

$$\frac{1}{DP} = \frac{2k_t\sqrt{fk_d[I]/k_t}}{k_p}\ \frac{1}{[M]} + \frac{k_{tr,M}}{k_p} + \frac{k_{tr,s}[T]}{k_p[M]} \qquad (4)$$

Equation 4: The influence on degree of polymerisation (DP) by the initiator concentration ([I]), monomer concentration ([M]), concentration of transfer reagent ([T]), efficiency factor of initiation (f) and the rate constants for initiator dissociation, propagation, termination and transfer (k_d, k_p, k_t, k_{tr}).[46]

Other sources of termination include interaction with impurities or inhibitors in the reaction vessel. A commonly known inhibitor is oxygen that will react with the growing chain leading to an oxygen radical. This significantly lowers the rate of the propagation since the oxygen radical is less reactive. As can be seen in *Equation 4,* the degree of polymerisation (DP) depends on several factors and not only on the concentration of the initiator ([I]).

A factor that also needs to be considered are transfer processes. As the name implies, the transfer step involves the transfer of a radical onto a new compound. While the termination is characterised by the destruction of two radicals, the radical count remains constant during the transfer step. Transfer reactions can be used to vary the rate of the propagation and also the molecular weight since not every radical is sufficiently reactive towards propagation. The abstraction of hydrogen plays a central role in the transfer step. There are different types of transfer reaction that

can occur. A first type involves the solvent. The radical on the propagating chain is transferred to a solvent molecule, for example by the abstraction of a hydrogen molecule from the solvent by the polymer chain (*3.A, Scheme 3*). This newly formed solvent radical will not propagate and a shortened polymer chain is obtained. This type of transfer depends significantly on the type of solvent. For instance, halogenated solvents (excluding fluorinated solvents) will readily undergo hydrogen abstraction, enhancing chain-termination.[47]

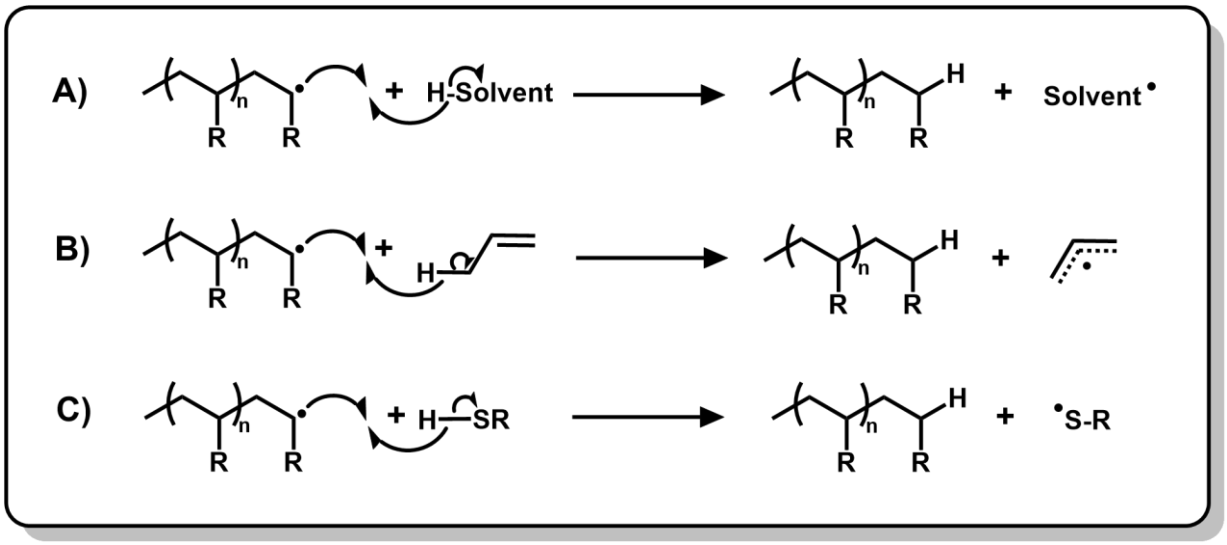

Scheme 3: Mechanism of transfer on solvent (A), monomer (B), thiol (transfer reagent) (C).

Next, transfer to monomer is also possible. This can lower the rate of propagation since this intermediate is more stabilised *via* resonance than the radical on the propagating chain (*3.B, Scheme 3*).

Further, a hydrogen molecule can be abstracted from the backbone of a vicinal polymer chain. This transfer step to the backbone of a different polymer chain leads to polymer branching.[48] Another moiety that can influence the transfer step is the initiator. In this case the transfer reaction leads to the cleavage of the sensitive bond in the initiator, forming a radical that can initiate a new chain-growth. This type of transfer depends on which initiation system that is used, for instance initiators

based on peroxides are particularly susceptible to transfer. Finally, dedicated transfer reagents such as thiols can be used to alter the rate of propagation and degree of polymerisation *(3.C, Scheme 3).*[49]

The most important effect of the transfer reactions is the decrease in the length of the polymer chains. Consequently, this can prevent the formation of chain entanglements and render the polymer material more brittle (*vide infra*). In the extreme case that the rate of transfer vastly exceeds the rate of propagation, telomerisation occurs, which yields short polymer chains up to five repeating monomers.[50] The effect of transfer has also been exploited for industrial production. This is important to circumvent specific viscosity issues arising at high conversion levels.

Free radical polymerisation generally leads to polymers with a high dispersity. However, in some cases polymers with a low dispersity are preferred. Therefore, new polymerisation methods were developed to obtain control over the molecular weight and result in polymers with extremely low dispersities. These new methods are classified as "Reversible Deactivation Radical Polymerisation" (RDRP). A dormant state of the radicals was introduced, which keeps their concentration low. This will greatly reduce termination without compromising the rate of propagation since propagation is linearly correlated to the radical concentration while termination is quadratically correlated. Several of these RDRP systems have been developed in the past three decades, examples include Atom Transfer Radical Polymerisation (ATRP),[51, 52] Nitroxide Mediated Polymerisation (NMP)[53] and Reversible Addition-Fragmentation Transfer Polymerisation (RAFT).[54]

1.3 Covalent Adaptable Networks

Covalent adaptable networks (CANs) are networks in which reversible chemistries are incorporated into the network structure. They were first described by Kloxin *et al.* in 2010 as "networks which contain a sufficient number and topology of reversible covalent bonds, so as to enable the cross-linked network structure to respond chemically to an applied stimulus".[55] The chemical response is mediated by the dynamic cross-linking exchange reactions. These will alter the network integrity and density, which will have an impact on the viscoelastic behaviour of the material. As a result, the material will be rendered more malleable and more prone to reprocessing and recycling, when compared to traditional thermosets. These networks can be divided into two classes based on the mechanism of exchange (*Scheme 4*).

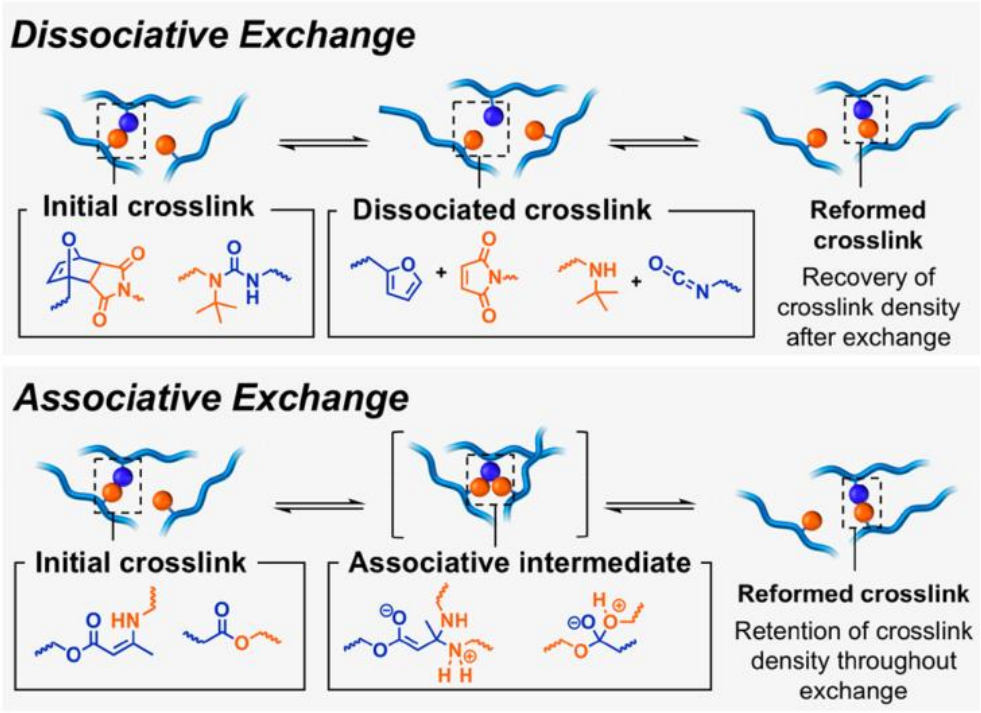

Scheme 4: Connectivity transition difference for the dissociative (top) and associative (bottom) mechanism of exchange reactions. Figure reproduced with permission from the American Chemical Society. [56]

The first class uses a dissociative mechanism and is characterised by chemical bonds that need to be broken prior to their reconnection. Upon heating, the rate of forming and breaking bonds changes and a net dissociation of bonds is induced in certain systems. Therefore, the equilibrium shifts towards depolymerisation. The reversible Diels-Alder reaction between furans and maleimides is a well-known chemical system for the design of dissociative CANs (*vide infra*).[57] The dissociative nature of this mechanism leads to a sudden drop in viscosity due to the temporary loss of cross-link density and the loss of solvent resistance. Upon cooling, the initial equilibrium is restored and the cross-links are formed to the same extent as before (*Scheme 4*).

The second class utilises an associative mechanism, which is based on a dynamic exchange reaction without a reversible bond forming step.[58] The exchange reaction often follows an addition/elimination two-step mechanism (*Scheme 4*). Therefore, this class can alter the topology of the network without losing connectivity during the exchange of the cross-links. This results in the retention of the cross-link density and keeps the network insoluble in solvent at any temperature. Upon heating, the chemical exchange reaction can become swift and results in a flow of the material, allowing reshaping and reprocessing. In the case of associative CANs, the viscosity of the material decreases gradually, due to the conservation of the network integrity (*cf.* vitreous glass), in contrast to the viscosity drop in dissociative CANs.

In summary, CANs show a trend in polymer network synthesis towards the intelligent design of structural materials having dynamic properties for specialty applications.[55]

1.3.1 Dissociative Covalent Adaptable Networks

In the field of organic chemistry, there have been a few synthetic reactions that were seminal for the development of the field. In 1928, German chemistry professor Otto Diels and his student Kurt Alder first reported their cycloaddition of a conjugated diene and an alkene.[59] This reaction has become a versatile and useful tool in the synthesis of challenging target molecules.

The intramolecular version of this reaction is remarkably resilient to obtain bridged polycyclic products with control over regio- and stereoselectivity.[60] Another useful example is the hetero Diels-Alder reaction, which can be used to synthesise heterocyclic compounds.[61] It is not surprising that Diels and Alder won the Chemistry Nobel prize in 1950 for their contributions to the field. In the next sections, this reaction will be described in more detail and the relevance of every reagent will be explained.

The reagents of a Diels-Alder reaction are a conjugated diene and an alkene, usually referred to as the dienophile. A common example of a Diels-Alder (DA) reaction is, an open-chain diene reacting with an unsaturated aldehyde, acting as the dienophile (*Scheme 5*). The reaction happens in a single step upon heating, forming a new six-membered ring with one double bond, which is often referred to as a [4+2] cycloaddition. While the mechanism is easily drawn as three rotating arrows (denoting electron pairs movement), what is occurring in reality is the formation of two new σ bonds at the same time as the loss of two former π bonds in a concerted rearrangement of the electrons from the π orbitals to the σ orbitals. Simultaneously, a new π bond is also formed.

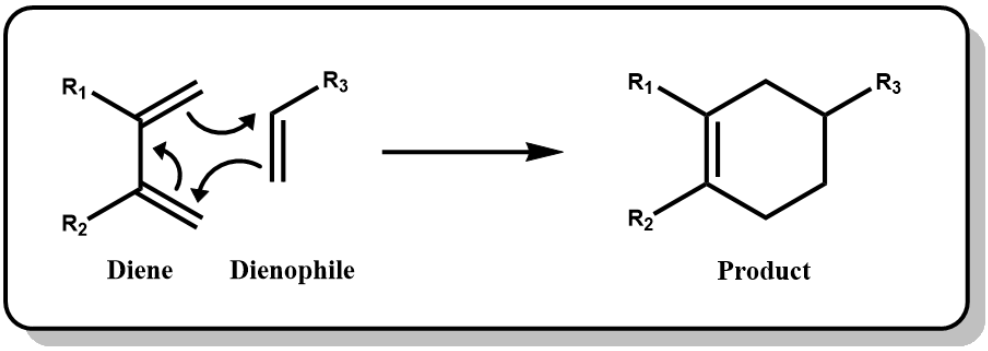

Scheme 5: General Diels-Alder reaction. Scheme adapted with permission from Oxford University Press.[62]

This reaction happens so swiftly because two σ bonds and one π bond are more stable than three π bonds. Another driving force of the reaction is the six delocalised π electrons in the transition state, rendering it aromatic and having stability (*cf.* benzene) (*Scheme 6*). Therefore, it is classified as a [4+2] cycloaddition. The specific mechanism will be discussed in detail in further sections.

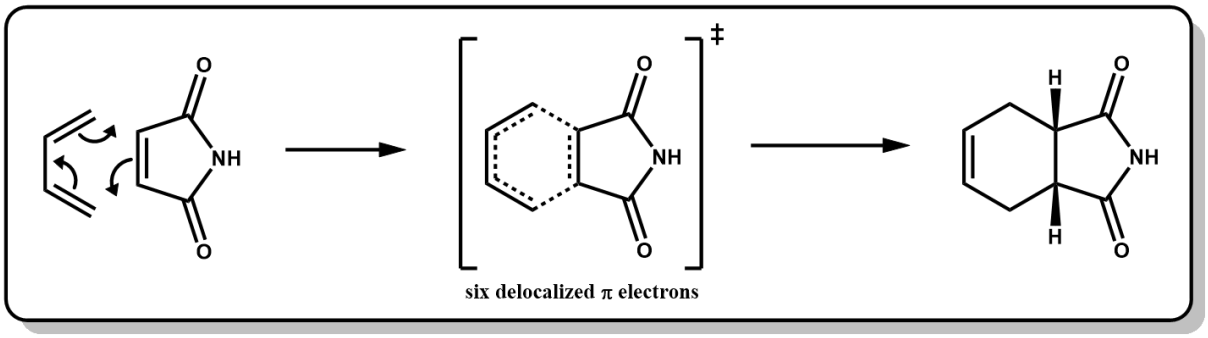

Scheme 6: [4+2] cycloaddition transition state. Scheme adapted with permission from Oxford University Press.[62]

An example of an intricate target molecule using this reaction is the synthesis of steroids.[63, 64] Here, the tetracyclic core structure is made *via* the cycloaddition (C-ring) of 1-vinylnaphthalene (A- and B-ring) with the maleic anhydride (D-ring) (*Scheme 7*). In a next step, this C-ring is isomerised to recover the aromaticity of naphthalene. In the following sections, the characteristics of both reagents are discussed in further detail.

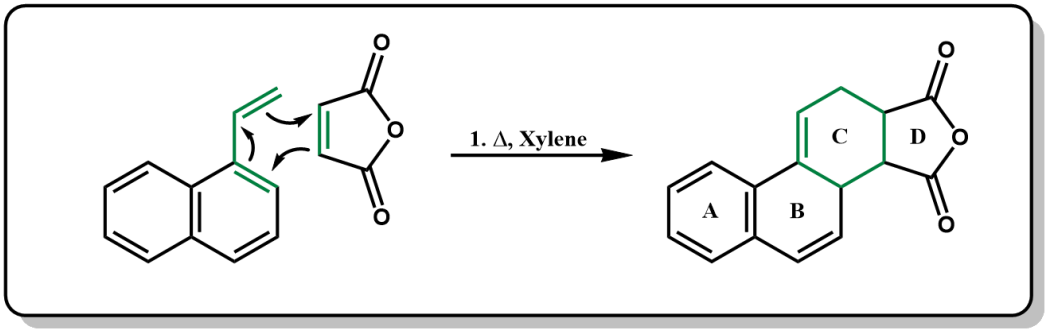

Scheme 7: First reaction step in the steroid synthesis reported by Cohen et al. in 1937. Scheme adapted with permission from the Royal Society of Chemistry.[63]

1.3.1.1 The diene

The diene in the Diels-Alder reaction can have different types of substituents and conformations (*e.g.* cyclic or open-chain). However, in order to react, the diene has to be able to arrange into the s-*cis* conformation (*Scheme 8*).

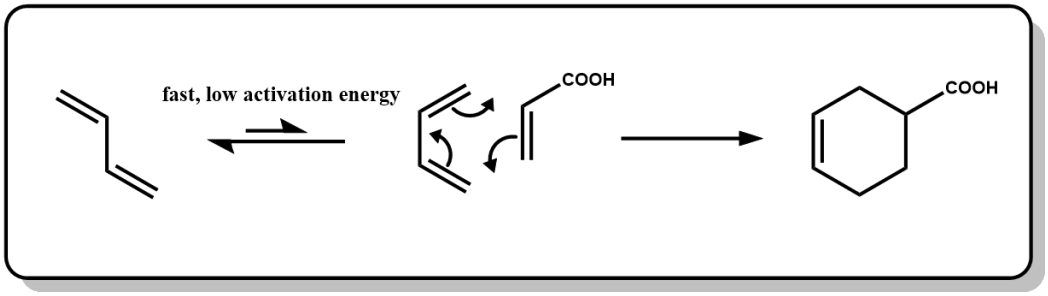

Scheme 8: Diels-Alder reaction with open-chain diene. Scheme adapted with permission from Oxford University Press.[62]

In general, for butadiene the preferred conformation is the s-*trans* conformation with the two double bonds as far away from each other as possible to reduce steric hindrance. Even though there is a thermodynamically unfavourable barrier to rotate around the central σ bond, it is small (about 30 $kJ.mol^{-1}$ at ambient temperature) and reduces upon heating. Therefore, the reactive s-*cis* conformation can be easily reached and can quickly react with the dienophile (*Scheme 8*). The conformational equilibrium follows Le Chatelier's principle, meaning only one conformer (s-*cis*) is favourable for the reaction and as it is consumed the equilibrium is skewed towards the product.[65]

On the other hand, cyclic dienes that are conformationally locked in the s-*cis* conformation are remarkably suitable for Diels-Alder reactions. One of the most widely used examples is cyclopentadiene (*Figure 6*). Cyclic dienes that are permanently in the s-*trans* conformation will evidently not participate in Diels-Alder reactions since the termini of the diene cannot both reach and react with the dienophile simultaneously (*Figure 6*). In addition, the proposed Diels-Alder adduct would contain an impossible *trans* double bond in the newly formed ring structure (the original σ bond conformation of the diene dictates the configuration of the newly formed π bond).

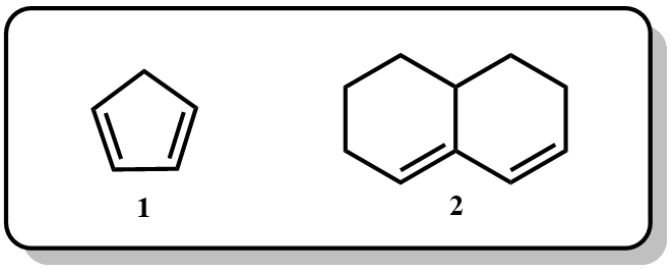

Figure 6: Structures of cyclic dienes cyclopenta-1,3-diene (1) and 1,2,3,7,8,8a-hexahydronaphthalene (2).

1.3.1.2 The dienophile

An alkene without any substituents will often have a poor reactivity.[62] In order to promote reactivity, conjugation to electron-withdrawing groups is often incorporated into the dienophile structure. Some examples include conjugated carbonyl compounds, nitro compounds, nitriles, sulfones, aryl alkenes, vinyl ethers and esters, haloalkenes and even some dienes (*Figure 7*). The molecular orbital theory behind the activation of the dienophile with an electron-withdrawing group will be discussed in more detail (*vide infra*).

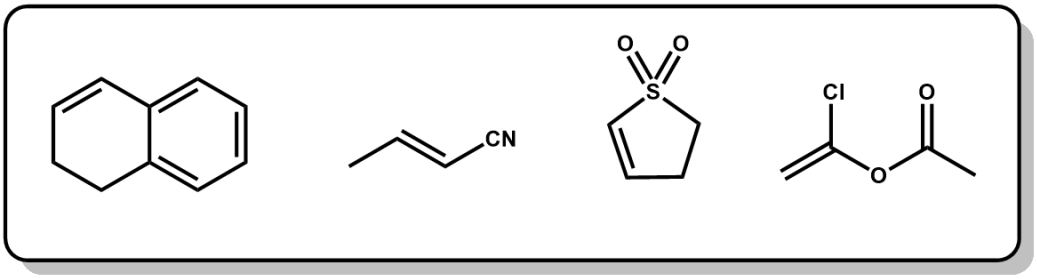

Figure 7: Examples of dienophiles.

1.3.1.3 The product

A Diels-Alder product or adduct can be recognised by a double bond inside a six-member ring with a conjugated group outside the ring opposite of the double bond. The Diels-Alder reaction is stereospecific, which means that the same stereochemistry of the dienophile can be found in the product. Different diastereoisomers are obtained when using *cis* dienophiles instead of *trans* dienophiles. This concept can be illustrated using a butadiene and diester dienophile, where the substituents, derived from the dienophile, are found in the same plane for a *cis*-alkene or in different planes for the *trans*-alkene (*Scheme 9*).

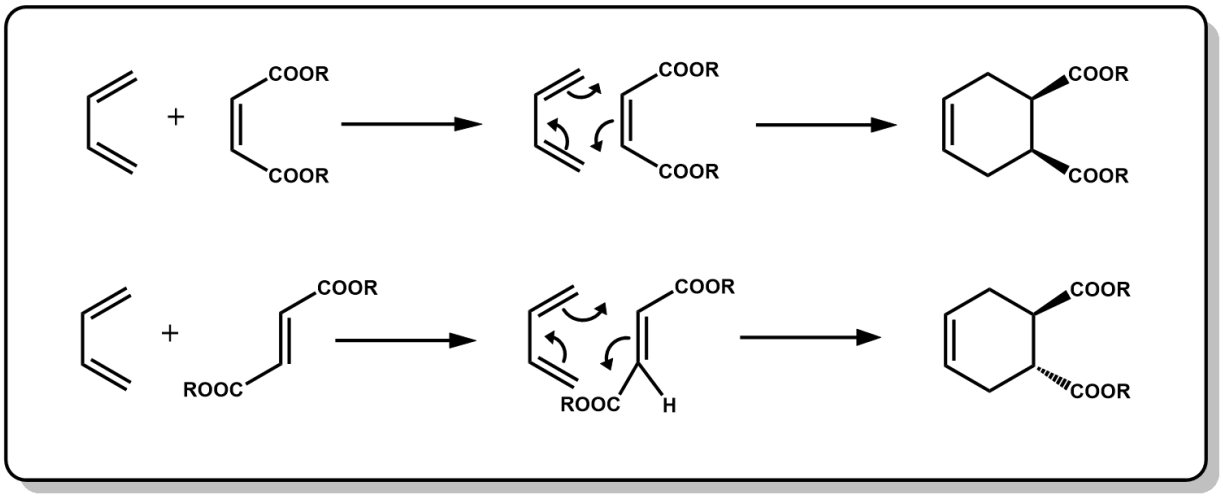

Scheme 9: Diels-Alder reaction forming diastereoisomers. Scheme adapted with permission from Oxford University Press.[62]

The stereochemistry of the diene is more complicated since it can be *cis,cis*, or *cis, trans*, or *trans,trans*. If there is no symmetry in the diene, there are even two potential *cis,trans* configurations (*Scheme 10, Scheme 11 and Scheme 12*).

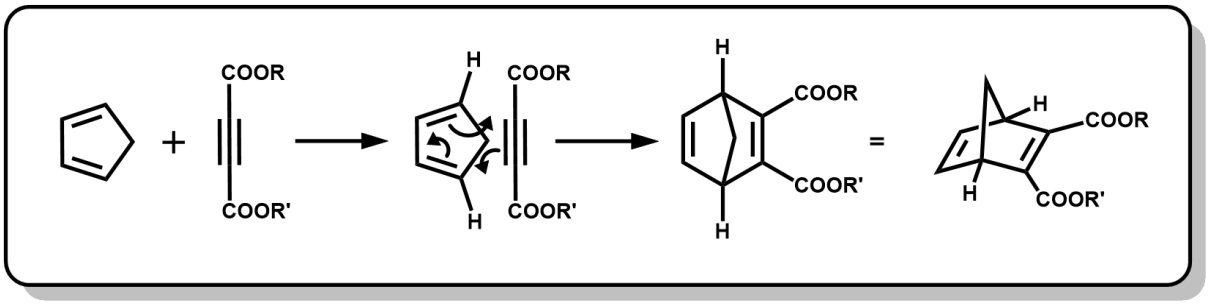

Scheme 10: Diels-Alder reaction with a cis,cis diene. Scheme adapted with permission from Oxford University Press.[62]

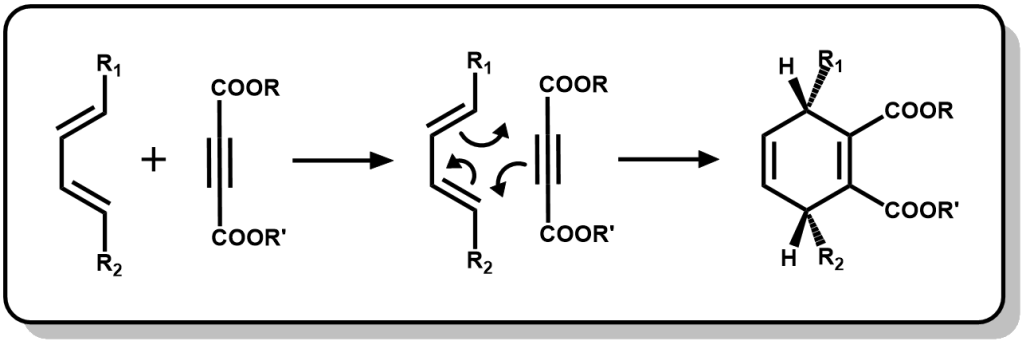

Scheme 11: Diels-Alder with a trans,trans diene. Scheme adapted with permission from Oxford University Press.[62]

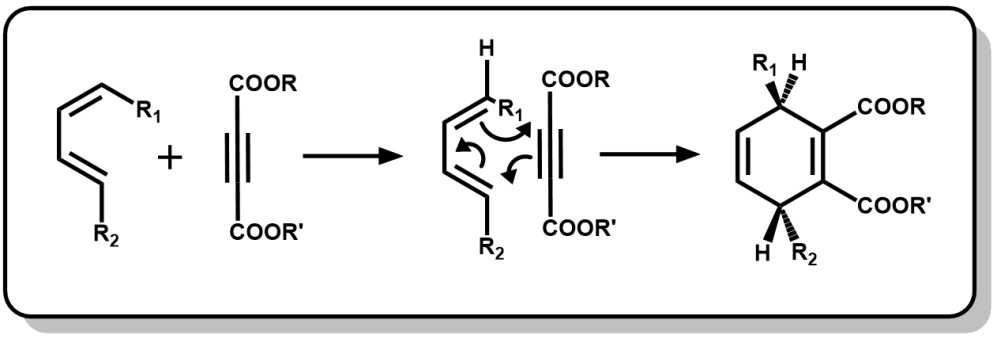

Scheme 12: Diels-Alder reaction with a cis,trans diene. Scheme adapted with permission from Oxford University Press.[62]

1.3.1.4 The frontier orbital description of cycloadditions

In a cycloaddition two new bonds are formed simultaneously. To further rationalise how this is possible, a molecular orbital energy level diagram can be used (*Scheme 13*). Two filled *p* orbitals and two empty *p* orbitals need to possess the correct symmetry and be in the correct proximity. The *p* orbitals that can overlap are the ones from the LUMO (π*) of the electron-poor anhydride (alkene) with the HOMO of the diene (ψ_2). Both orbitals have a similar symmetry with one node in the middle of the molecular orbital.

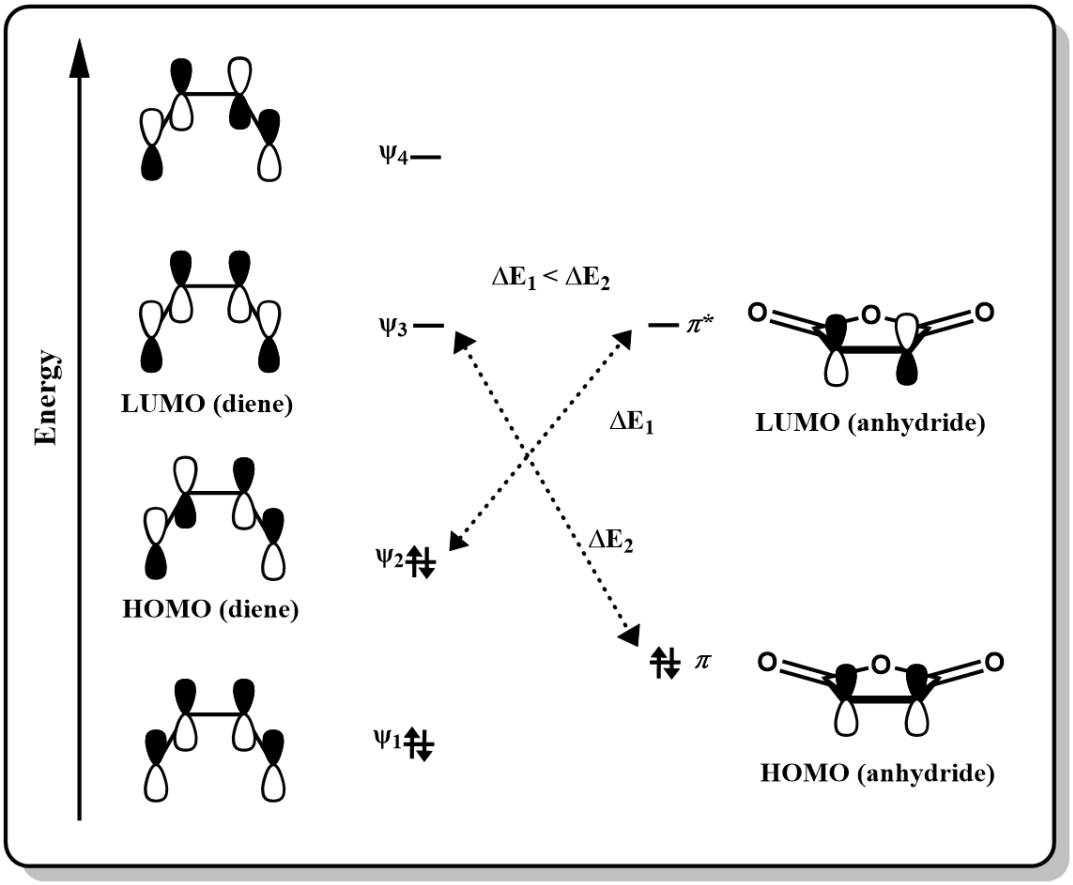

Scheme 13: The energy diagram of the frontier orbital overlap of cycloadditions. Scheme adapted with permission from Oxford University Press.[62]

Most DA reactions employ this combination of electron-poor dienophiles and electron-rich dienes, which is sometimes referred to as the normal electron demand

Diels-Alder reaction (DA_{NED}). On the contrary, it is also possible to use the rarer so-called inverse electron demand Diels-Alder reaction (DA_{INV}). This type of reaction is exactly the opposite of DA_{NED} where the HOMO (π) of the anhydride (alkene) will overlap with the LUMO of the diene (ψ_3). However, the energy gap is much larger than in the previous sample so this overlap is far less preferred (*Scheme 13*). This is only possible if the energy level of the alkene system is increased or the energy level of the diene is decreased so the energy gap between the aforementioned orbitals becomes smaller than that of the DA_{NED}. The increased energy level of the alkene can be obtained by using electron donating substituents instead of electron withdrawing ones. Similarly, the decreased energy level of the diene can be obtained by using electron withdrawing groups instead of the usual electron donating groups.

1.3.1.5 The endo rule

The *endo* rule can be easily explained if we consider the reaction between furan and maleic anhydride (*Scheme 14*). The two hydrogens on the dienophile have to be in the *cis* configuration in the product. There are two products possible that are diastereoisomers, referred to as the *endo* and *exo* product.

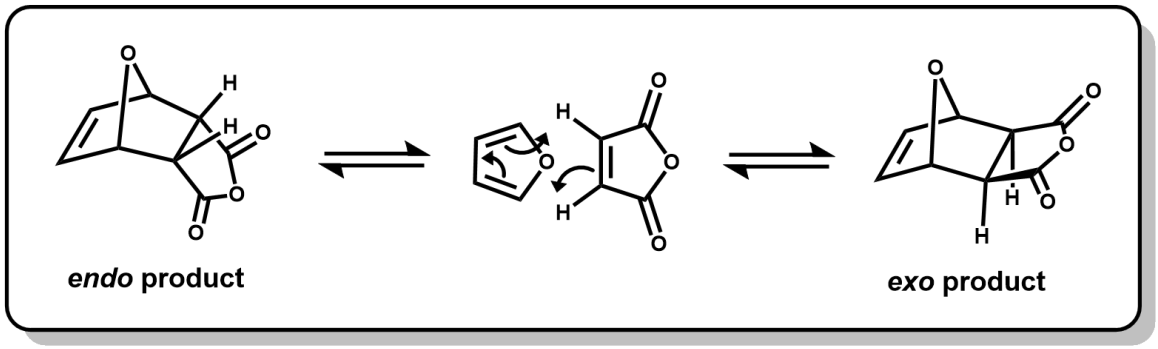

Scheme 14: Stereoselectivity of the Diels-Alder reactions. Scheme adapted with permission from Oxford University Press.[62]

The *exo* product is more stable since there is less steric hindrance present. If the reaction was completely reversible and under thermodynamic control, the *exo*

product would have the highest yield. In an irreversible Diels-Alder reaction, the *endo* product forms faster than the *exo* product, thus the *endo* adduct is the kinetic product. It forms faster because the energy of the transition state is lowered due to a bonding interaction between the electron deficient carbonyl groups and new π bond on the diene (*Scheme 15*).

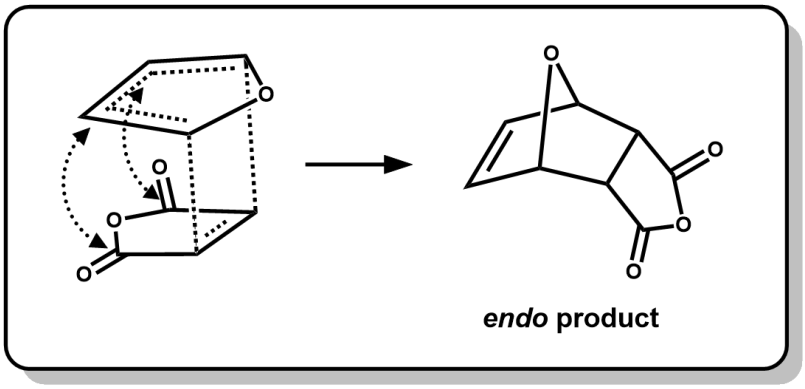

Scheme 15: Secondary orbital interactions lead to the endo product. Scheme adapted with permission from Oxford University Press.[62]

The *endo* product is also formed first when there are no electron deficient groups. This interaction can be further explained using molecular orbitals. In the dimerisation of cyclopentadiene, there is an overlap possible between the remaining *p* orbitals of the HOMO (top) and the remaining *p* orbitals of the LUMO (bottom) (*Figure 8*). This interaction only effects the stereochemistry of the reaction and will not form any new bonds.

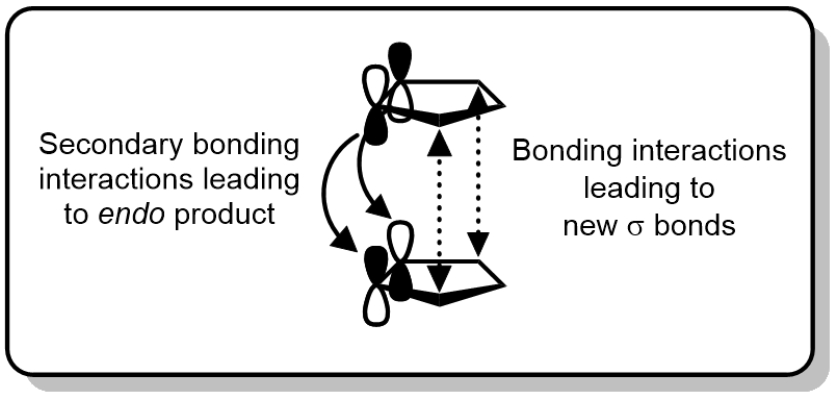

Figure 8: Secondary orbital interactions in the dimerization of cyclopentadiene. Scheme adapted with permission from Oxford University Press.[62]

1.3.1.6 Different Diels-Alder systems

1.3.1.6.1 Anthracene

Anthracene consists of three fused benzene rings (*Figure 9*). Reversible cycloadditions involving this compound have been known for a long time since it can react with a number of dienophiles to provide a range of cycloadducts.

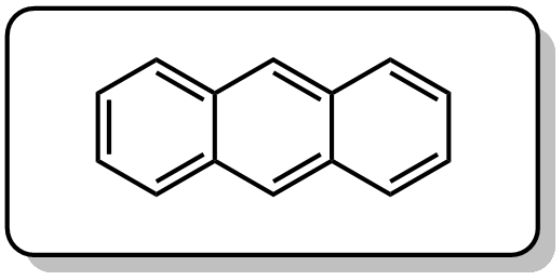

Figure 9: Structure of anthracene.

Firstly, the dimerisation of anthracene which occurs upon UV radiation ($\lambda > 300$ nm) is a typical example of a [4+4] cycloaddition since it involves the overlap of the central dienes of two anthracene molecules. Secondly, this diene can also react with a singlet oxygen in a [4+2] hetero Diels-Alder, referred to as a photooxidation.

Furthermore, anthracene can also react with other well-known dienophiles, such as maleimides. Durmaz *et al.* synthesised block copolymers by using this DA click chemistry and Gacal *et al.* grafted poly(methyl methacrylate) (PMMA) and poly(ethylene glycol) (PEG) side chains onto a polystyrene (PS) backbone, which was functionalised with anthracene.[66, 67] Kim *et al.* reported that this system can be used to functionalise several polymer matrices with chromophores.[68] Unfortunately, thermoreversibility was beyond the scope of what was researched in these papers. The DA cycloaddition for this system occurs upon heating to 125 °C and the reverse reaction occurs around 250 °C.[67, 69] These higher temperatures are one of the reasons why this system is not used for thermoreversible materials in structural

applications. For instance, if it would be incorporated in a polyester matrix, the cleaving step (at 250 °C) could cause side reactions or possible degradation in the backbone that could eventually lead to material failure.

While this system is primarily used as a modification tool, there have been a few groups researching its use for cross-linking. The first use was reported by Jones *et al.* wherein they describe the synthesis of a polyethylene terephthalate (PET) and 2,6-anthracenedicarboxylate copolymer.[70] Consequently, this copolymer was cross-linked with a bismaleimide for 15 hours at 125 °C and the cross-link density was altered by using 0.01-0.50 mol.% of anthracene. Furthermore, they determined a dissociation yield of 27% in a network with 2 mol.% anthracene at 250 °C for 7 hours. However, the thermoreversibility of these networks with higher concentrations of anthracene was not tested.

An advantage of using anthracene is the customisability of the DA and retro-DA temperature window by altering the number and type of substituents. A drawback is the unreactive nature of anthracene, which complicates the incorporation into polymer matrices.[71]

1.3.1.6.2 Cyclopentadiene

Another special example of a widely studied diene is cyclopentadiene (CPD). This compound can act as both the diene and the dienophile. Furthermore, it dimerises easily and even forms a trimer (*Scheme 16*). This moiety can be used to cross-link certain polymer systems. Kennedy *et al.* used CPD as pendant groups to cross-link isobutylene and propylene rubbers.[72] They cured these at ambient temperatures and

after 72 hours, an insoluble gel was obtained. The elastomer could be dissolved again when maleic anhydride was added and heated to 215 °C.

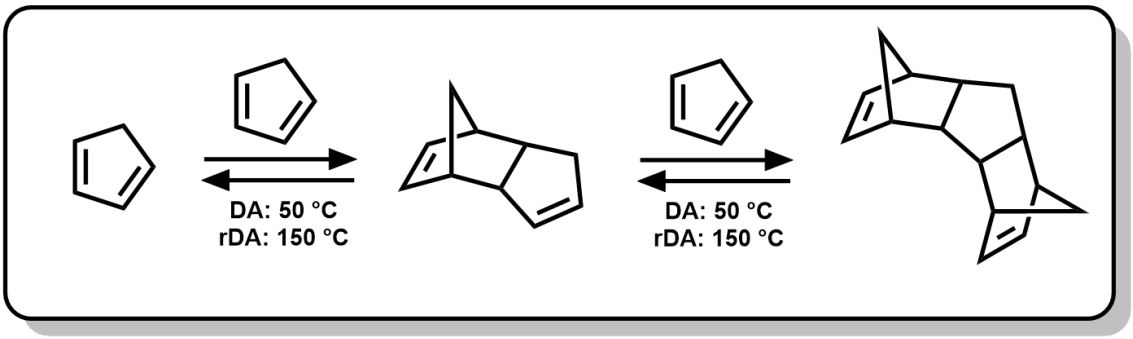

Scheme 16: Trimerisation of cyclopentadiene. Scheme adapted with permission from Oxford University Press.[62]

Furthermore, it is reported that the material can be reprocessed at high temperature (170 °C). This indicates that de-cross-linking occurs to some extent. After this initial paper, more publications have been dedicated to the use of CPD as a cross-linking group.[73, 74] Chen *et al.* reported thermoreversibility in a chlorine-containing polymer matrix at 150-170 °C. They used viscometry to monitor the reaction, namely a decrease in viscosity confirmed the presence of the retro-DA reaction. The rate of cross-linking was affected by the composition of the halogenated polymer and the polarity of the solvent.

Another study on self-healing of CPD systems was reported by Park *et al.* They used three-point bending to induce microcracks, which were healed by electrical resistive heating.[75] The reported healed strain energy for the third cycle was 94% compared to the pristine material. CPD can also be used in hetero DA reactions. Barner-Kowollik *et al.* used a tris(dithioester) to cross-link PMMA that was functionalised at the termini with CPD.[76]

1.3.1.6.3 Furan

One of the most studied Diels-Alder reaction include a furan ring as the diene moiety and a maleimide functional group as the dienophile moiety (*Scheme 17*).[77] The first reporting of this system for reversible cross-linked polymer networks was in 1969, in a patent published by Craven.[78]

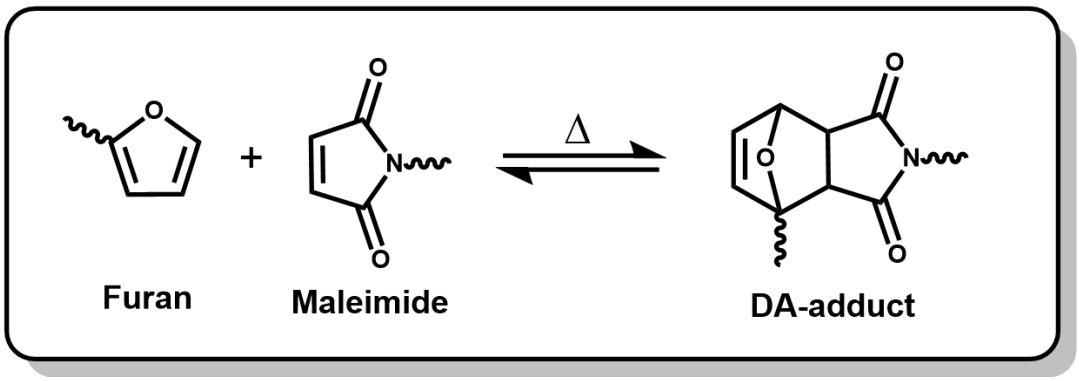

Scheme 17: Diels-Alder reaction with furan and maleimide.

The patent describes the synthesis of different matrices such as polyesters, polyureas and polyamides with pendant furan moieties. The cross-linking compounds were polyfunctional maleimides. The material samples were shaped at 140 °C and cooled to ambient temperatures to cure them. This procedure was repeated to confirm the thermoreversibility of the system. After this initial reporting of the furan-maleimide system, numerous studies have been conducted for its potential use in thermoreversible materials. In 1979, Stevens *et al.* reported the synthesis of maleimide groups which were grafted on a PS backbone using a Friedel-Crafts reaction.[79] They evaluated concentrations up to 20 mol.% of the maleimide moiety and networks were prepared by adding difurfuryl adipate. The thermoreversibility was beyond the scope of this paper and was not tested. Next, Chujo *et al.* investigated this thermoresponsive system in a new polymer matrix. Moreover, they synthesised polyoxazolines with pendant maleimide grafted on one

backbone and furfuryl groups grafted on the other.[80] This material gelled after 7 days at ambient temperature when 4 - 22 mol.% of pendant groups were incorporated. A higher degree of swelling was found for the samples with fewer cross-links. SEC and ^{1}H NMR spectroscopy were used to confirm that the molecular weight of the linear polymer did not increase after reversing the cross-linking. The heating and cooling procedures were repeated and samples with the same properties were obtained. This confirms the reversibility of the system. In 1992, Canary and Stevens reported a follow-up study on the grafted PS matrix.[81] They looked at gel formation for polymers with up to 32 mol.% of maleimide. Gelation occurred within 75 min at 64 °C when adding difurfuryl adipate as the cross-linker and de-cross-linking was observed within 2.5 minutes at 150 °C. Additionally, they looked at PS grafted with furan groups as alternative cross-linking system. Here, the polymer solution became liquid again within 15 seconds at 150 °C. The same behaviour was observed after five heating and cooling cycles, confirming the reversibility.

Goussé *et al.* synthesised statistical copolymers of styrene and furfuryl-functionalised styrene with furan content in the range of 5 to 97 mol.%.[82] They used (methylene-di-*p*-phenylene) bismaleimide to cross-link the linear polymers at 40 °C for 24 hours. De-cross-linking was achieved by heating at 130 °C for 24 hours after the addition of an excess of methylfuran. However, the thermoreversibility was only tested in one heating cycle.

In 2001, the synthesis of a styrene/furfuryl methacrylate copolymer was reported by Goiti *et al.*[83] This reaction required longer reaction times and solvent when compared to aforementioned literature since free radical polymerisation was used.

These conditions were selected to prevent side reactions with the π system of the furan groups. They also tested the same cross-linker similar to Goussé *et al.*, namely the rigid aromatic (methylene-di-*p*-phenylene) bismaleimide. A gel was obtained when a dilute solution (12%) of the copolymer of 5 mol.% furfuryl methacrylate and 95 mol.% styrene was cured at ambient temperature for 12 days. This gel could again be solubilised in toluene when heated to 110 °C.

In order to have a deeper understanding between the thermal behaviour of the system and the molecular structure, de-cross-linking in bulk instead of solution can be advantageous. This approach minimises the risk of confusing side reactions at high temperatures (*e.g.* degradation) with the retro-DA reaction. Here, bulk viscosity can be a useful, measurable parameter.

In this system the DA reaction occurs up to 60 °C, while the retro-DA becomes predominant above 110 °C.[84] These temperatures can be altered by the introduction of specific substituents.[85] Furthermore, this favourable temperature window, combined with the absence of significant side reactions, renders the furan/maleimide system exceptionally useful as a scaffold for novel thermo-responsive materials. Initially, this system was used to prepare polyaddition networks of compounds containing multifunctional furan and maleimide groups.[86, 87] Later on, other cross-linked polymers were reported based on copolymers with pendant furan/maleimide moieties.[83, 88-92] Moreover, in a chemical industry that pledges to lower its dependence on crude oil, renewable resources can be used to produce different types of furan starting material.[93]

In 2007, Kavitha *et al.* first published the synthesis of a network based on poly(furfuryl methacrylate) (PFMA).[89] Later that year, a network was reported based on poly(FMA-*co*-MMA).[89] They used ATRP as the polymerisation technique for the statistical linear prepolymer, with the furfuryl concentration being notably high in these systems, namely between 60-80 mol.%. Ye *et al.* reported a "grafted from" ATRP method where the first acrylic backbone is functionalised and acts as a macroinitiator for the next polymer chain (*Scheme 18*).[94] Another controlled radical polymerisation (CRP) technique for these systems was reported by Pramanik *et al.*[91] They used reversible addition-fragmentation chain transfer (RAFT) polymerisation to make copolymers of FMA and butyl methacrylate (BMA). The furfuryl content for these systems was between 40-60 mol.%.

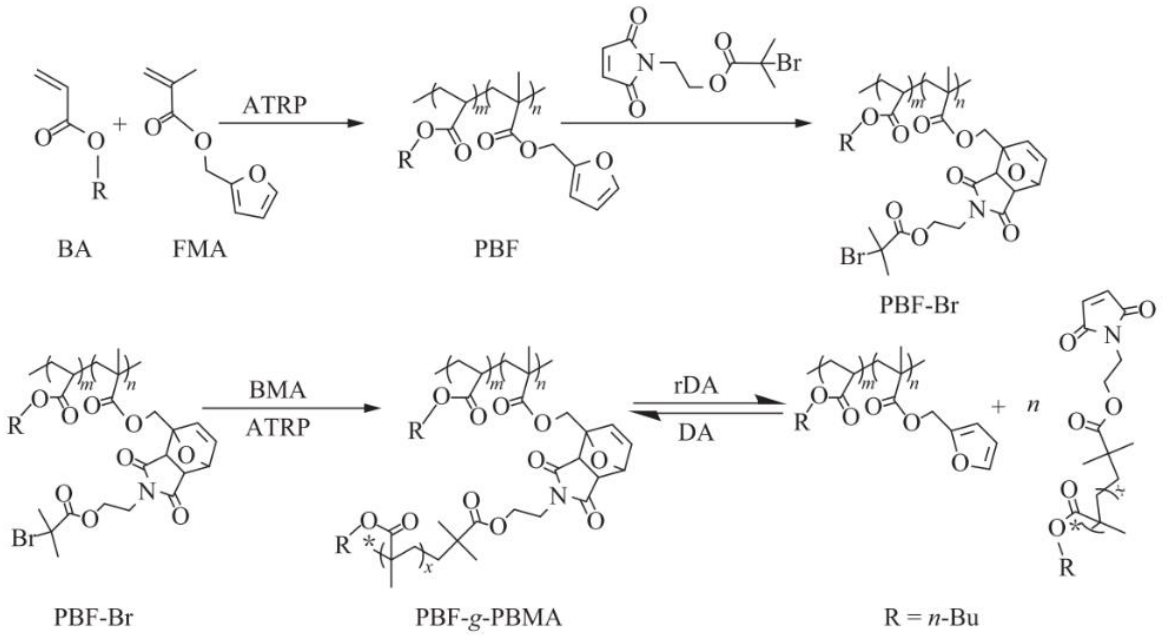

Scheme 18: Synthesis and rDA/DA reaction of thermo-reversible branched polymer (PBF-g-PBMA). Scheme reproduced with permission from the Chinese Journal of Polymer Science.[94]

Another study that focussed on the use of a methacrylate matrix is reported by Das *et al.* They copolymerised hexyl methacrylate (HMA) with 2-hydroxyethyl methacrylate (HEMA), which was functionalised in the next step with furfuryl

isocyanate, altering the furan concentration between 4 - 48 mol.%.[92] The gelation was confirmed with stress-relaxation experiments, as well as testing the adhesive properties of the system. The highest lap shear value they observed was 7.9 MPa, which combined with the fact that only cohesion failure was observed instead of adhesion failure is indicative that this system has potential as a structural adhesive.

1.3.2 Associative Covalent Adaptable Networks

1.3.2.1 Introduction

In 2005, Scott *et al.* described an associative CAN that was based on photo-mediated free radical addition-fragmentation chain transfer reactions using allyl sulphide chemical species.[95] Trithiocarbonates were later used in a similar exchange mechanism.[96-98] The stress-relaxation and flow properties were promising, however the inherent radical nature of this chemical system causes inevitable termination. This termination greatly reduces the dynamic lifetime and adaptability.

In order to circumvent this issue of radical termination, Leibler *et al.* first reported silica-like malleable materials from permanent organic networks in 2011.[99] They coined the term “vitrimers” for their materials due to the behavioural resemblance with vitreous silica (*Figure 10*).[100] Vitrimers are an associative CAN with exchange reactions that need to be thermally activated to (re)process the material. They combine the complementary advantages of thermosets and thermoplastics. Vitrimers remain insoluble even at elevated temperature, while still being processable. An important parameter for the processability is the viscosity of the polymer. Different models exist to describe the viscosity of a chosen system.[101-103] The viscosity model for inorganic materials (*e.g.* vitreous silica) is the Arrhenius model

based on the assumption that the rheological flow obeys the Arrhenius equation for molecular kinetics.[101] The model that is often used to describe fluids with a glass transition temperature is the Williams–Landel–Ferry (WLF) model.[103]

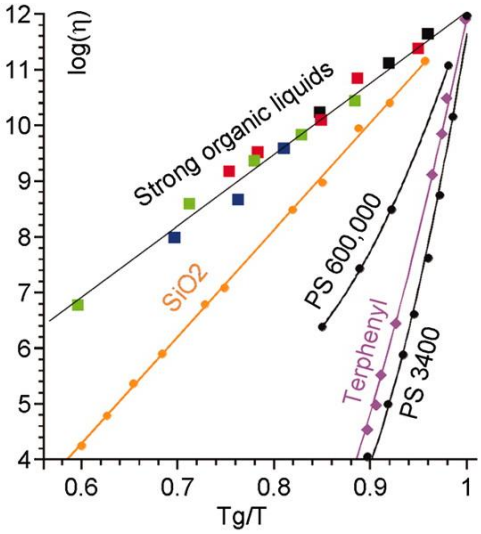

Figure 10: Angell fragility plot,[104] showing viscosity as a function of inverse temperature normalised to 1 at the glass transition temperature (T_g) for epoxy/anhydride with 5% (red squares) and 10% (black squares) $Zn(acac)_2$; for epoxy/acid with 5% (green squares) and 10% (blue squares) $Zn(ac)_2$; and for silica,[105] polystyrene,[106] and terphenyl.[107] Figure reproduced with permission from the American Association for the Advancement of Science.[99]

This model is based on empiric parameters, which enable the approximation of the temperature dependence of a polymer melt given a known viscosity at a specific temperature. The viscosity of vitrimers is often described by a combination of both models and will depend on two transition temperatures. Thus, in order to design optimal vitrimer materials, these two transition temperatures have to be considered.

The first is the glass transition temperature (T_g), where the polymer goes from the glassy state with no chain mobility to the rubbery state, where the polymer chains do show mobility. The second transition temperature that plays an important role is called the topology freezing temperature (T_v). This is the temperature at which the speed of the exchange reaction is faster than the timescale on which deformation

occurs. This reflects itself in the viscosity of the material and the T_v, which is defined as the temperature where the viscosity reaches 1×10^{12} Pa s.[104, 108]

These temperatures, T_g and T_v, can be influenced by parameters such as the exchange reaction kinetics, flexibility of the monomers and amount of exchangeable groups.[109] If the material has a $T_g < T_v$, when the temperature exceeds the T_g but not the T_v, the material will transition from the glassy state to the rubbery state and behave as an elastomer (*Figure 11*). Since the structure of the network is essentially fixed as a consequence of very slow exchange reactions.

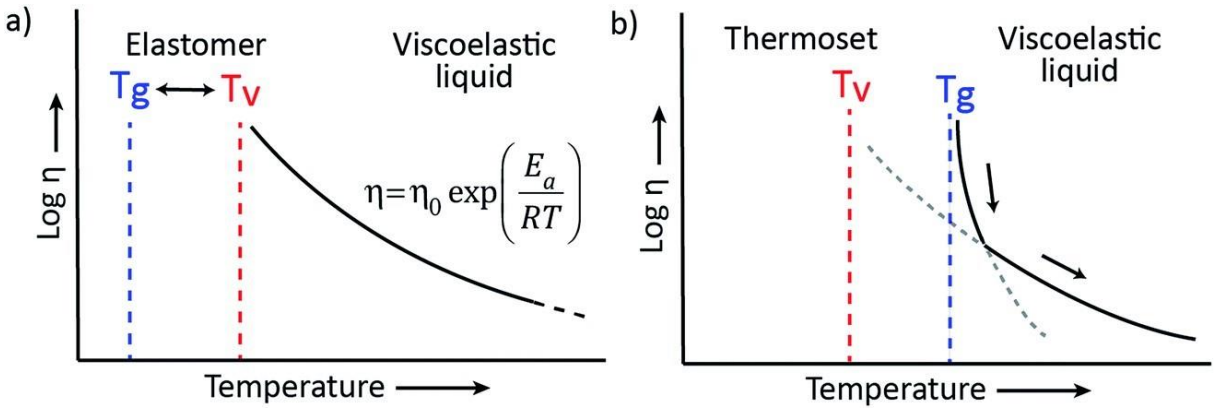

Figure 11: Viscoelastic behaviour of vitrimers with a T_g lower than T_v (a), a hypothetical T_v situated below T_g (b). Figure reproduced with permission from the Royal Society of Chemistry.[57]

Exceeding the T_v results in the rate of the exchange reactions being high enough to transform the elastomer to a viscoelastic liquid. As the flow properties are mainly controlled by the exchange kinetics, a typical Arrhenian viscosity decrease is observed (*Figure 11*). When the T_v of the material is lower than the T_g, the T_v can be calculated *via* extrapolation of stress-relaxation or creep tests.[57] The aforementioned transition is in this case hypothetical, since the network is now fixed due to the absence of motion of the polymer chains in the glassy state, rather than by slow exchange kinetics.

Above the T_g, polymeric segments start to show motion, the rate of exchange reactions greatly exceeds this motion and network topological rearrangements are only restricted by the mobility of the polymer chains. This results in a diffusion controlled flow behaviour according to the WLF model.[103, 110] At higher temperatures, the behaviour changes to an Arrhenian flow controlled by exchange kinetics. When used in an application, vitrimers should maintain mechanical strength and should not exhibit creep at service temperature. Only in the case of sufficient heating should the material show a macroscopic flow that is significant. To facilitate the commercial implementation of these new materials on an industrial scale, numerous challenges have to be addressed. Finding new chemistries for CANs that do not require a catalyst and that are simple to perform is still necessary.[111] Other issues, such as scalability and optimisation of the viscoelastic behaviour for convenient extrusion or injection moulding, also need to be considered before large scale usage is economically feasible.[99, 112] Since the first report, new alternative chemistries have been explored by numerous researchers to design and synthesise vitrimer type materials.

1.3.2.2 Exchange chemistries

1.3.2.2.1 Transesterification

Vitrimers based on the transesterification reaction were initially described by Leibler *et al.*[99] These materials were epoxy/carboxylic acid networks (*Scheme 19*). They were synthesised using diglycidyl ether of bisphenol A (DGEBA) and a mixture of fatty dicarboxylic and tricarboxylic acids. A zinc acetate [$Zn(ac)_2$] or zinc acetyl acetonate [$Zn(acac)_2$] catalyst was used to promote the reaction.

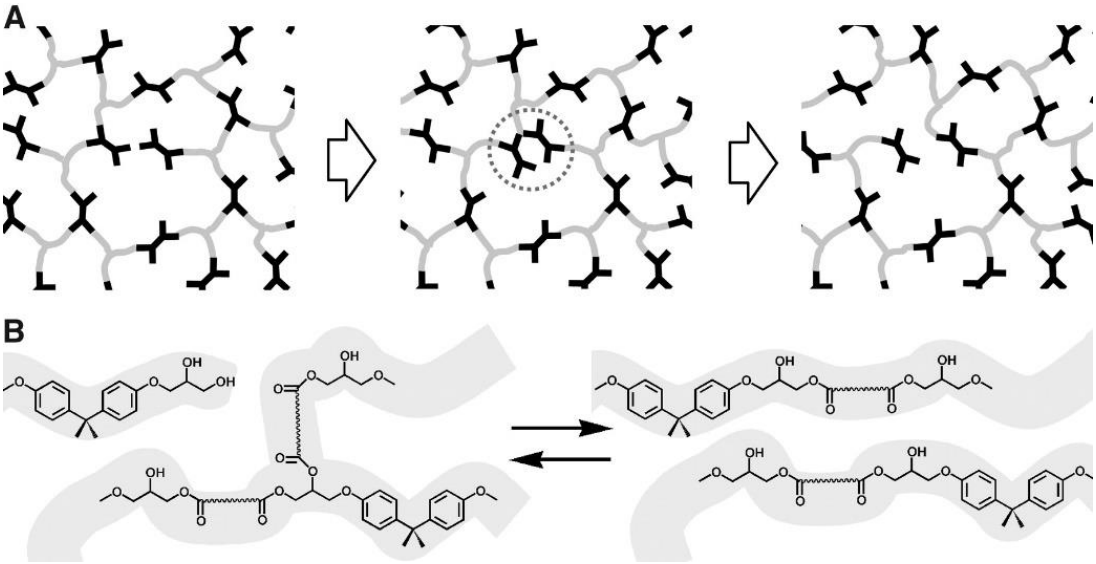

Scheme 19: Transesterification reaction used in the first vitrimers. Scheme reproduced with permission from the American Association for the Advancement of Science.[99]

The viscosity showed the typical Arrhenian viscosity decrease and an activation energy of approximately 80 kJ.mol^{-1} was reported. The relaxation time was around 58 hours at 100 °C. Extrapolation of this value towards 40 °C leads to a relaxation time of 1 year and at ambient temperature to roughly 6 years.[99] The exchange reaction kinetics can be controlled through the rational selection of the catalysts. In 2019, Niu *et al.* reported a method to circumvent the problem of catalyst leaching at high loadings.[113] Instead of using small molecules as a catalyst, they copolymerised acrylonitrile with zinc methacrylate. This polymer catalyst, namely poly(acrylonitrile-*co*-zinc methacrylate) (Zn-PAM), was incorporated in the epoxy matrix during curing and the transesterification catalysis efficiency was systematically investigated. More recently, Cuminet *et al.* even report a catalyst-free approach, where the exchange reaction is accelerated due to the activation *via* α-difluoroesters.[114]

The transesterification chemistry can also be implemented in elastomers. Imbernon *et al.* described the use of associative CANs in the design and production of

reprocessable elastomers, which were inherently not malleable after vulcanisation.[115] At ambient temperature, this new type of elastomers do not show creep due to the slow exchange reaction, but can be reprocessed at elevated temperatures. These recyclable elastomers can have tremendous economic value since rubbers are widely used. Since these methods use a catalyst, stability can become an issue on the long term as a consequence of the susceptibility of catalysts to ageing, leaching or hydrolysis.

In summary, vitrimers based on the transesterification chemistry show great potential for industrial implementation (*e.g.* reactive extrusion).[99, 116] This is possible due to availability of the monomers and robust synthesis. Recently, Demongeot *et al.* reported the preparation of poly(butylene terephthalate) (PBT) vitrimers *via* reactive extrusion from industrial PBT thermoplastics.[116] However, in order to obtain a meaningful processability, high catalyst loadings and temperatures are needed in most systems, which can be considered industrially disadvantageous.[99, 115]

1.3.2.2.2 Transalkylation

Another approach to recyclable cross-linked materials is the use of transalkylation involving triazolium salts.[117] Mudraboyina *et al.* reported networks containing 1,2,3-triazolines and pendant halide chains (*Scheme 20*). A one-pot polyaddition of α-azide-ω-alkyne monomers was performed involving a thermal azide-alkyne Huisgen 1,3-dipolar cycloaddition. The curing was done simultaneously using dibromo and diiodo alkanes or alkyl mesylates as bifunctional alkylating moieties. Using bromide as a counter-ion, stress-relaxation with an activation energy of 140 $kJ.mol^{-1}$ was observed. Relaxation times varied between 30 minutes at 130 °C to a couple of

seconds at 200 °C. The adequate selection of the counter-ion dictates the viscoelastic and rheological properties of this type of material. The impact of this selection on properties, such as ionic conductivity and thermal stability, which are considered crucial for most applications of polymerised ionic liquids (PILs), was thoroughly investigated.[118]

Despite major advantages, such as the solvent- and catalyst-free character of this chemical system and the convenient one-pot polymerisation, the scalability of the costly and hazardous reagents is the main drawback for large scale usage. An interesting development in this field was reported by Hendriks *et al.,* exploring the transalkylation of less activated aliphatic sulfonium salts and thioethers (*Scheme 20C*).[119] These poly(thioether) networks were prepared by the photoinduced thiol-ene reaction of thiol and alkene monomers in bulk.

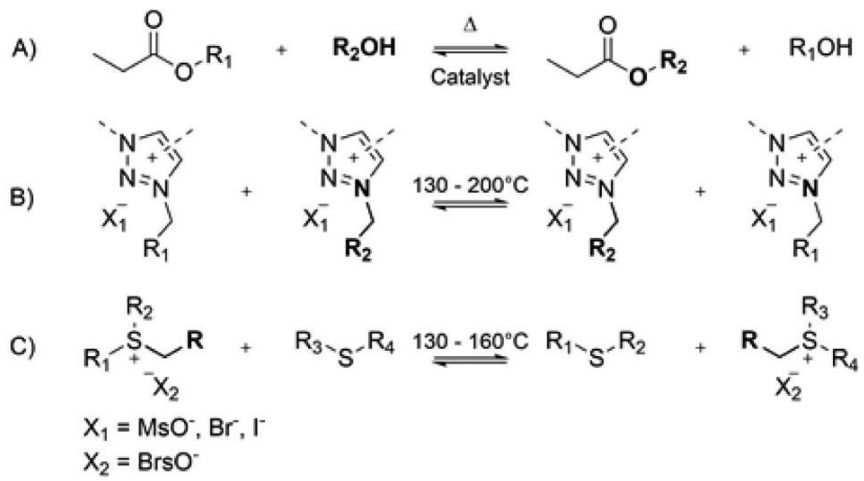

Scheme 20: Overview of the transesterification reaction (A), the C–N transalkylation reaction (B), and the transalkylation reaction of sulfonium salts (C) used for the design of vitrimer materials. Scheme adapted with permission from the American Chemical Society.[119]

1.3.2.2.3 Metathesis

The olefin metathesis reaction has proved itself in modern organic synthesis as a potent methodology with various applications.[120, 121] Lu *et al.* implemented this methodology in the design of a new type of CAN.[122] They used a second-generation Grubbs' Ru metathesis catalyst to ensure the rapid exchange reactions on the poly(butadiene) (PBD) backbone through a metallocyclobutane intermediate.[123]

More recently, Röttger *et al.* reported a catalyst-free approach using dioxaborolanes.[112] Dioxaborolanes participate in a rapid metathesis reaction at moderate temperatures. This moiety is resistant and tolerant towards multiple functional groups. They demonstrated that the mechanical properties of commercial thermoplastics can be enhanced by the implementation of dioxaborolane cross-links (*Scheme 21*). Reversible addition-fragmentation chain transfer polymerisation (RAFT) was used to synthesise these copolymers. The obtained networks showed improved properties in terms of melt strength, solvent and environmental stress cracking resistance, dimensional stability at high temperatures and bulk adhesion compared to generic thermoplastics. An activation energy of only 15.9 ± 0.5 $kJ.mol^{-1}$ was reported. Furthermore, despite the cross-linked nature of the material, processing of the material was feasible with extrusion at 180 °C.[112]

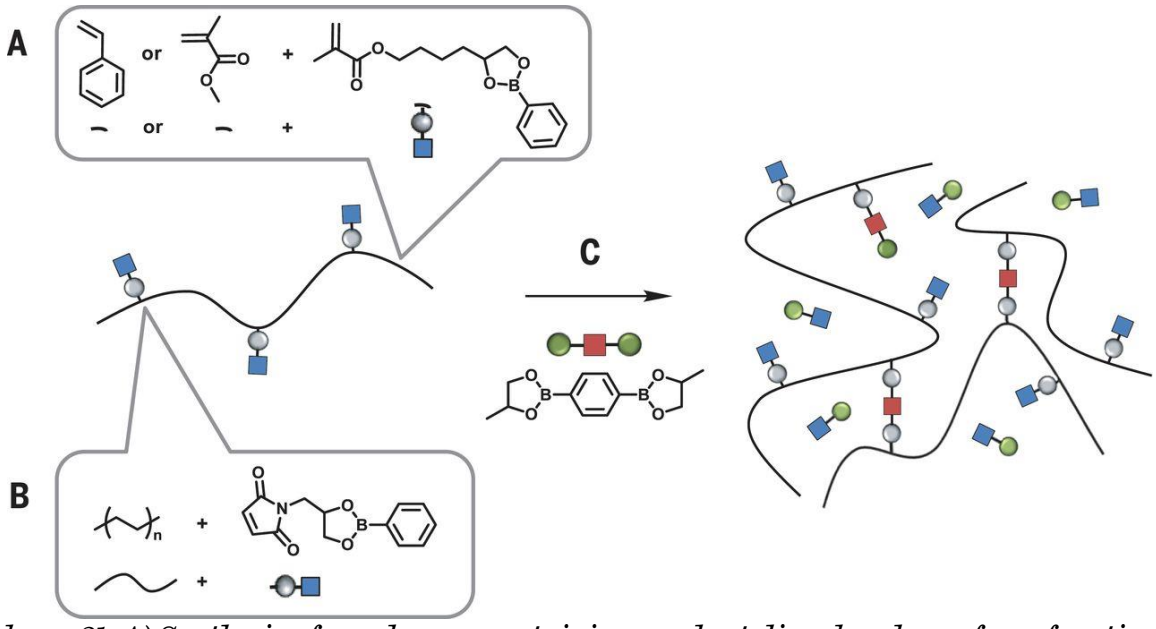

Scheme 21: A) Synthesis of copolymers containing pendant dioxaborolanes from functional monomers. (B) Grafting of dioxaborolanes onto thermoplastic polymers by means of reactive processing. (C) Cross-linking of functional polymers containing pendant dioxaborolane units by means of metathesis with a bis-dioxaborolane. Free dioxaborolanes formed during the cross-linking process can be kept in the system as plasticisers or removed through evaporation. Scheme reproduced with permission from the American Association for the Advancement of Science.[112]

1.3.2.2.4 Transamination

In order to obtain catalyst-free vitrimer materials and thereby circumvent the issues posed by general catalyst usage, alternative chemistries were investigated by Denissen *et al.*[124]

The first chemical platform that was considered as an alternative for the transesterification was the well-known transamidation. However, the rate of transamidation can typically only be altered by catalysts that are often accompanied with sensitivity issues towards air or moisture. These catalysts are also not always compatible with other functional groups.[125, 126] Urea was also considered as a candidate for the substitution of the transesterification reaction. However, these compounds are thermodynamically very stable, which implies that regular urea

functionalities do not participate in exchange reactions. Moreover, a dissociation reaction can occur similar to the one in amides that yields the corresponding amine and isocyanate (*Scheme 22*). In a next step, this isocyanate can react with water and lead to the release of CO_2.

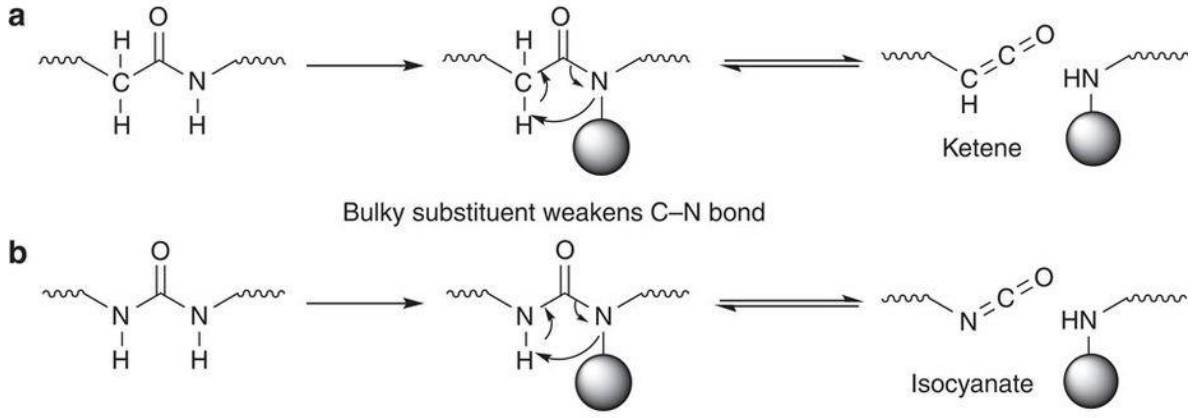

Scheme 22: Mechanism of the dissociation reaction that can occur with a) amides b) urea. Scheme reproduced with permission from Springer Nature.[127]

Urethanes, at the interface between amides and esters, were the next possible alternative. These species do participate in exchange reactions, however, a Lewis acid catalyst is required.[128] At higher temperatures, the risk of the dissociation side reaction increases as well.[129] Together with the rather low rate of the reversible exchange reactions, this limits the practical use in vitrimer materials.

As a last candidate the enaminone was considered. The general structure is (N—C=C—C(=O) —X). These vinylogous acyl moieties have the possibility to contain amides (X = C), urethanes (X = O) or urea (X = N) depending on the identity of the vicinal carbonyl group X. The vinylic bond between the carbonyl group and the nitrogen atom is of tremendous importance for the reactivity of this species (*Scheme 23*). Chemically, these vinylogous moieties resemble their non-vinylogous versions because of the mesomeric electron withdrawing effect of the carbonyl.[130-132] Due to

the efficient N to C *p*-bonding, these chemical species resemble the thermodynamic stability of ureas, urethanes and esters.

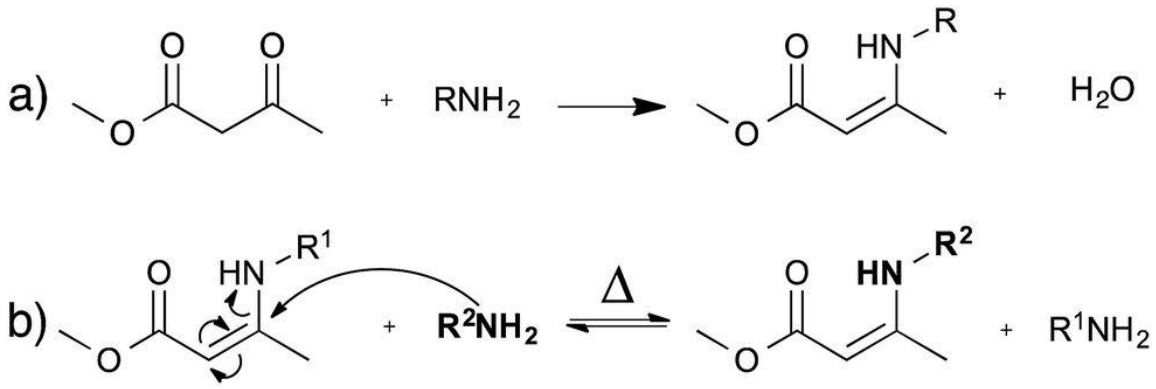

Scheme 23: a) Condensation reaction of an acetoacetate and an amine, b) Schematic representation of the exchange reaction involving vinylogous urethanes. Scheme reproduced with permission from the Royal Society of Chemistry.[57]

The rate of the exchange depends strongly on the nature of the enaminone. Vinylogous amides show the lowest exchange kinetics and thus longer relaxation times, even at elevated temperatures. Vinylogous urethanes exhibit fast exchange kinetics, however, the rate of exchange in the vinylogous urea systems are even higher.[133] This difference in exchange kinetics can be explained by the additional mesomeric donating effect on top of the inductive withdrawing effect.[134] These vinylogous acyl containing compounds can easily be obtained *via* the spontaneous condensation reaction between acetoacetate groups and amines with the release of water. Besides temperature, the presence of an acid or a base also displayed an influence on the kinetics of the reaction. Denissen *et al.* reported the acceleration of the exchange reaction upon the addition of *p*-toluene sulfonic acid (*p*-TsOH) and sulfuric acid (H_2SO_4).[135] They also observed that the addition of a base, such as triazabicyclodecene (TBD), slows down the exchange rate. Therefore, they proposed a reaction mechanism where the presence of a proton is of importance.[135]

Initial studies of the vinylogous urethane system showed an agreement between the activation energy (E_a) obtained by analysis of a model system on the one hand and rheological stress-relaxation experiments on the other.[133] However, Guerre *et al.* observed a considerable shift in E_a when investigating longer chain systems, which depended on temperature besides the stoichiometry.[136] In the past, this dependence was only reported for catalyst- or additive modified vinylogous urethane material.[135] They hypothesised that the dependence is related to the dynamic exchange mechanism since the shear modulus was unchanged for all of these vitrimer materials. Thus, the influence of chain mobility and cross-linking density has been ruled out. Furthermore, the different slopes in the Arrhenius plots were rationalised by two distinct pathways of the same dynamic bond exchange process.

A first one under neutral or acidic conditions involves a protic pathway *via* an activated iminium intermediate (*Scheme 24*). This leads to an enthalpic barrier E_a of roughly 70-76 kJ.mol^{-1}. The second pathway predominates upon addition of a strong base. This base inhibits the iminium intermediates and promotes the direct Michael-type addition between the free amine and the neutral vinylogous urethane moiety (*Scheme 24*). This reaction occurs much slower with a significantly higher E_a ranging from 99-141 kJ.mol^{-1}. Guerre *et al.* also observed a stronger dependence on the free amine species for this pathway, which could be explained by the rate-determining nature of the deactivated Michael-addition in that mechanism.

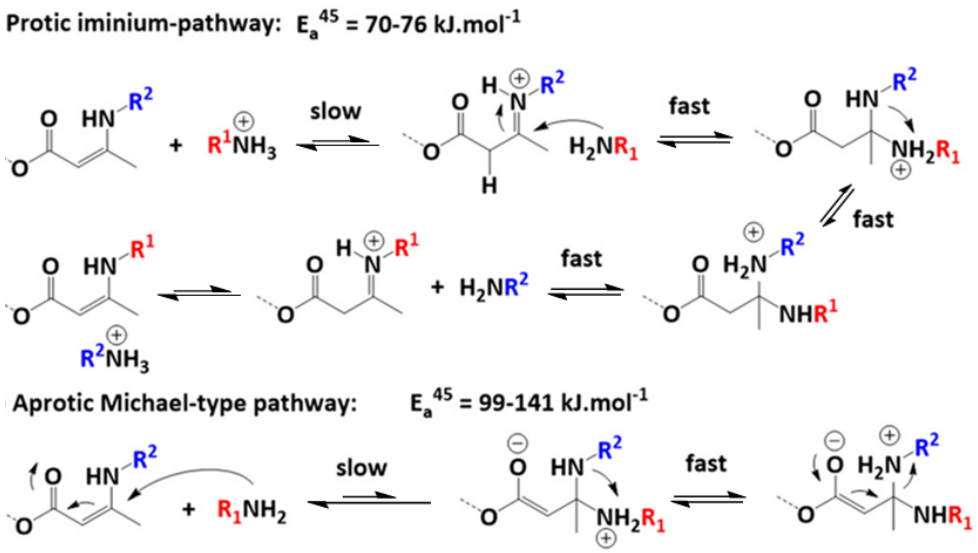

Scheme 24: Different mechanisms for the transamination of vinylogous urethanes. Scheme adapted with permission from the American Chemical Society.[136]

In summary, the higher E_a mechanism will become the dominant exchange reaction at high temperature due to its enthalpic dependence. In contrast, the iminium pathway will proceed at low temperatures. The high E_a mechanism was only reported for the fluorinated vinylogous urethane vitrimers so far. It was rationalised by the presence of longer chain fragments between the dynamic cross-links since it was also observed for similar molecular architecture.

Denissen *et al.* prepared this type of network from the condensation reaction of cyclohexane dimethanol bisacetoacetate (CDM-AA) with *m*-xylylene diamine and tris(2-aminoethyl)amine (TREN).[124] Here, free amines are necessary for swift exchange reactions, which are obtained by using a slight offset in the stoichiometry of the condensation reaction. Kinetically, vinylogous urethanes have the same reactive behaviour as a typical Michael acceptor through a conjugated nucleophilic addition of an amine, which preferably reacts with the less stable C-C double bond instead of the robust carbonyl double bond. Hydrolysis is a problem that needs to be considered when working with urea as previously mentioned. However, this should

not pose an issue since it is reported that these enaminone bonds can be formed in an aqueous solvent.[137-140]

The obtained materials showed shorter relaxation times when compared to the epoxy-based vitrimers (approx. 3 min. at 150 °C).[135] Finally, they reported the possible application of these enaminone-based vitrimers in fibre-reinforced composites.[141] One issue that has to be mitigated for long-term use is the possible oxidative damage that might occur involving the amines present in the network. In this case, stabilisers could be added to the material.

1.4 Neighbouring Group Participation (NGP)

In the last decade, there have been a lot of new developments in the field of vitrimers.[142-144] There is a recent new trend towards catalyst-free systems.[142-144] Here, researchers try to address the drawbacks of an added external catalyst. These drawbacks include the toxic and corrosive properties of strong bases and organic salts.[145, 146] Moreover, solubility issues may arise at high loadings, leading to heterogeneous systems. Also, the catalyst can be susceptible to ageing and leaching, which will limit the recyclability of the material.[147, 148]

A possible solution to these drawbacks in vitrimer systems, where catalysis is necessary and the catalyst-free approach is not technically available, is the use of an internal catalyst. Internal catalysis, also known as Neighbouring Group Participation (NGP), can circumvent most of the issues arising from using external catalysis. In the case of the latter, the catalyst is added to the system as an additive (*e.g.* a metal complex). The case of the former will be discussed in more detail (*vide infra*).

The International Union of Pure and Applied Chemistry (IUPAC) defines neighbouring group participation as: " The direct interaction of the reaction centre (usually, but not necessarily, an incipient carbenium centre) with a lone pair of electrons of an atom or with the electrons of a σ- or π-bond contained within the parent molecule but not conjugated with the reaction centre."[149] An example of π-bond stabilisation in an NGP reaction is shown in *Scheme 25*. Here, the acetylation of the norbornene system goes *via* the carbenium intermediate. This intermediate is stabilised by the π-system in the norbornene backbone, facilitating the loss of the tosylate group and subsequent acetylation.[150]

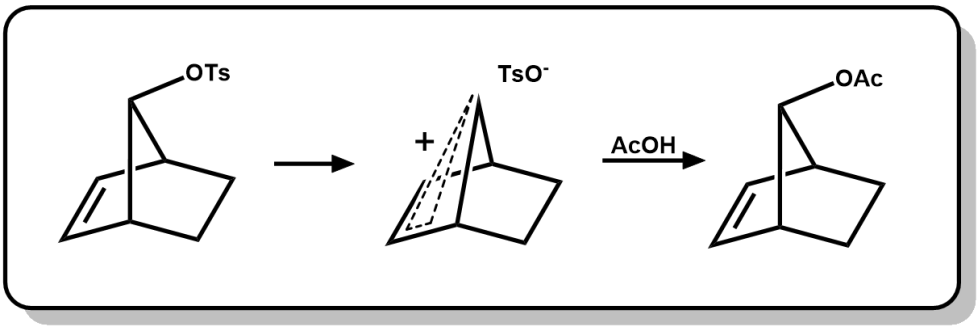

Scheme 25: Carbenium centre stabilised by π-bond. Scheme adapted with permission from the Royal Society of Chemistry.[150]

In the field of organic chemistry, there are a few parameters that can significantly change the rate of the reactions or the final product. Two important effects are dependent on the enthalpy and entropy on the reaction. The former involves the changes in stability of participating electrons. Examples of this effect can be seen when introducing electron donating or electron withdrawing groups, namely they can accelerate or decelerate the reaction, respectively. Moreover, not only the rate of reaction can be altered but also the preferred reactive position (*e.g. ortho/para*) (*Scheme 26*).[151]

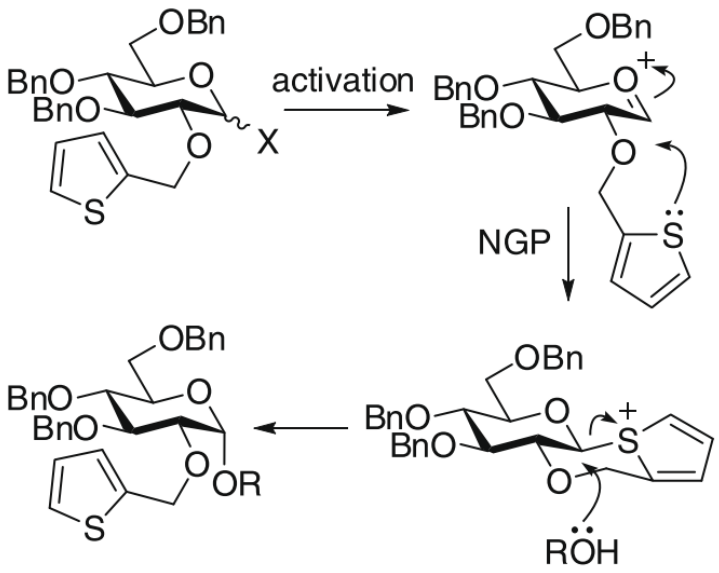

Scheme 26: α-selective glycosylation process involving neighbouring group participation (NGP) via an intermediate ß-thiophenium ion. Scheme reproduced with permission from Elsevier.[151]

The latter effect deals with the statistical probabilities on the molecular level. In order for a chemical reaction to occur, a number of requirements needs to be fulfilled. The relevant reagents need to collide in a particular fashion. This collision does not only require a specific rate, but also distinct orientation. Therefore, the reaction is dependent on the probability of the preferred orientation of the reagents. Again, this orientation can be altered by the introduction of substituents.

In the above examples, the proximity of a given functional group to the reactive site can be seen to have a substantial influence on the reaction outcome, dictating rate, regioselectivity or chirality. This effect is often referred to as the Neighbouring Group Participation (NGP) or internal catalysis if it leads to an increase in reaction rate. The name anchimeric assistance can also be used when chiral reactions are discussed.

In a number of cases, NGP often proceeds with the formation of a cyclic intermediate or transition state. There are several factors that can influence the formation and

size of these intermediate species. One of them is the ring strain, which decreases from 28 kcal.mol^{-1} for 3-membered rings to 0 kcal.mol^{-1} for 6-membered rings and increases again to 11 kcal.mol^{-1} to a 9-membered ring.[152] Another factor is the entropic loss upon ring closure compared to the linear chain, with formation of a larger ring species leading to a greater reduction in entropy. A third factor that can affect the ring size is the electronic effect of the leaving group (*Scheme 27*).

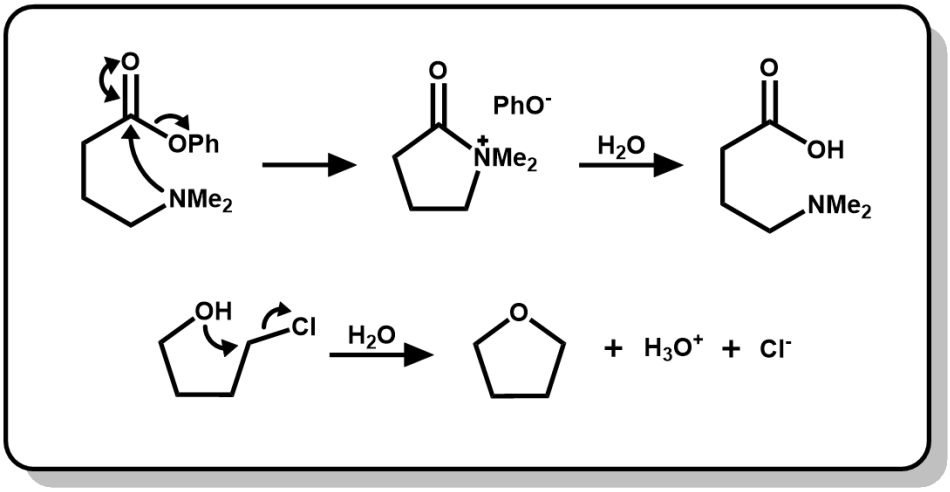

Scheme 27: Examples of intramolecular catalysis (neighbouring group participation). Scheme adapted with permission from the Royal Society of Chemistry.[150]

1.4.1 Examples

This neighbouring group effect has been observed and reported numerous times throughout the years in different reactions in the field of organic synthesis. For instance, in the halogenation of olefins,[153] solvolysis of cyclic compounds,[154] the hydrolysis of halohydrins[155] and the stereoselective synthesis of α-glucosides.[151]

Capon *et al.* describe the influence of different substituent groups (methoxyl, hydroxyl, amino etc.) on the reaction rate.[156] They also look into factors influencing the ease of ring-closure. Further, Page *et al.* compared some inter- and intramolecularly catalysed reactions in water.[150] They comprehensively investigated the energetics of NGP. Moreover, Gibson *et al.* use NGP for their synthesis of α-

lithiated thioacetals, which are useful organic compounds since they are synthetic equivalents of carbonyl anions.[157] The NGP effect is also extensively used in the field of glucosides. Here, it greatly facilitates the substitution on the 6-membered ring *via* activation with a fused ring transition state. Next, Gierer *et al.* described the use of NGP in the field of natural products such as lignin.[158] Furthermore, Morrison *et al.* demonstrated the use of NGP in the epoxide migration within steroids.[159]

In more recent years, the NGP is even extended to the field of vitrimers.[160] For instance, Delahaye *et al.* employ a double NGP effect to facilitate the exchange reactions in phthalate monoester networks made from multifunctional diols, a ß-amino diol and a diphthalic anhydride with an aliphatic core (*Scheme 28*).[161]

They propose a mechanism where an initial internal proton transfer occurs with consequent zwitterion formation. This in turn catalyses the ring closure and formation of the anhydride intermediate, which ultimately increases the rate of the transesterification reaction (*Scheme 28*). This acceleration led to a 500-fold decrease in the relaxation times. Furthermore, these very short relaxation times ($\tau \approx 1$ s) enabled processing with a double-screw mini-extruder at 150 °C.

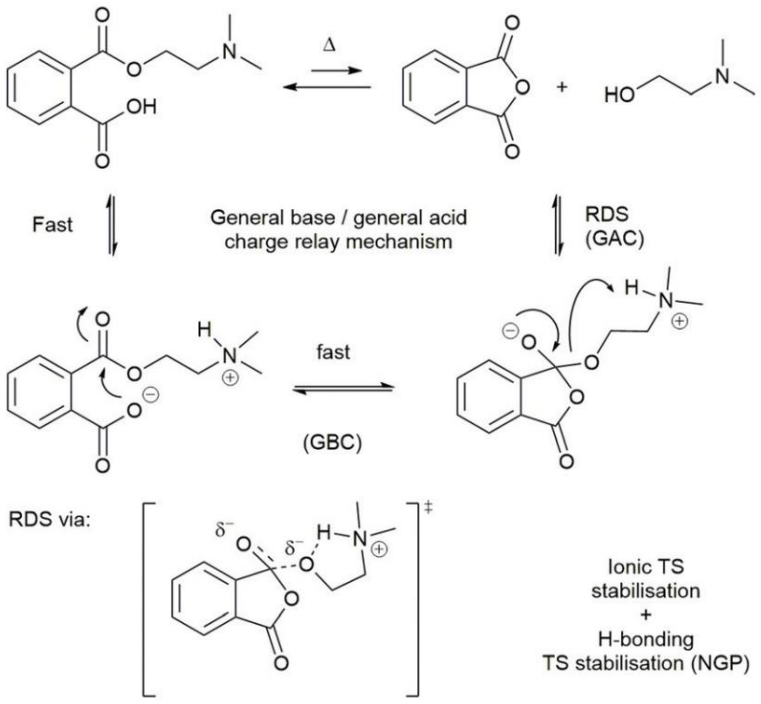

Scheme 28: Proposed mechanism for the rapid transesterification of the β-amino ester, via a stabilisation of the transition state (TS) during the rate determining step (RDS). Reaction proceeds via a general base catalysis (GBC)/general acid catalysis (GAC) charge relay mechanism. Scheme reproduced with permission from the Royal Society of Chemistry.[161]

1.5 Aims

The field of covalent adaptable networks (CANs) is very young when compared to classic thermoplastics and thermosets. A number of different chemistries have been developed. However, at the beginning of this project the material properties of different CAN systems had not been compared on the same polymer backbone.

The aim of this work is to conduct a comprehensive comparison of CANs based on three different types of dynamic covalent chemistry incorporated in the same acrylic polymer backbone. The materials are potentially useful as novel recyclable/self-healing acrylic adhesives. The dynamic behaviour of these CANs can be divided into a dissociative mechanism, an associative mechanism and a hybrid between these two. The dissociative type will be based upon Diels-Alder chemistry

with a furan moiety as the diene and a maleimide as the dienophile. The associative type, also referred to as a vitrimer, will be based upon the transamination of vinylogous urethanes and the hybrid will be based on the transesterification of phthalate monoesters. All systems avoid the use of an external catalyst.

In the first system, an acrylic monomer will be copolymerised with furfuryl methacrylate (FMA) to introduce a pendant diene functionality (*Scheme 29A*).

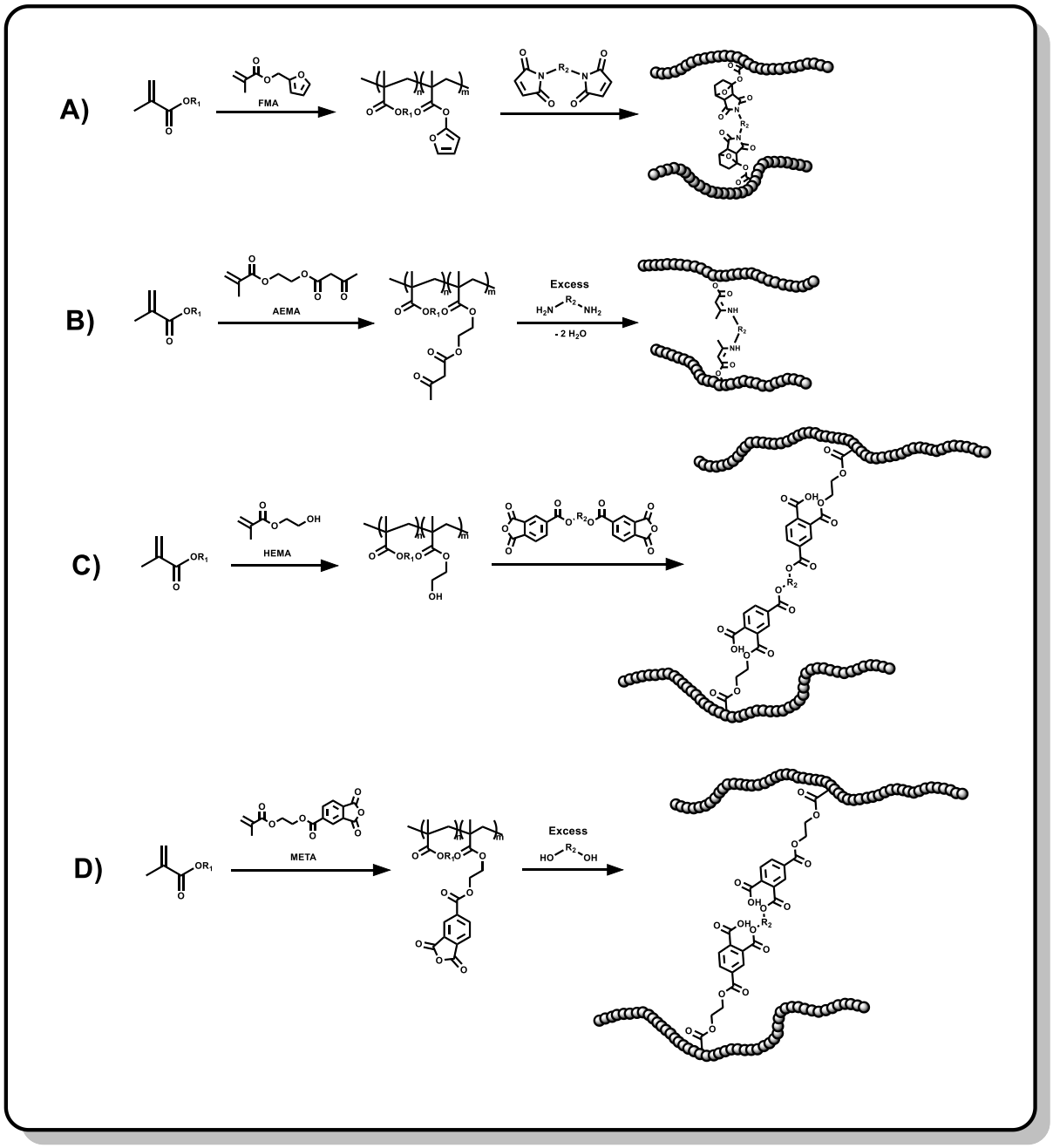

Scheme 29: Schematic overview of the objectives of this work.

Moreover, a bismaleimide cross-linker will be added in next step to obtain the final reversible network. In the second system, the acrylic starting material will be copolymerised with acetoacetoxyethyl methacrylate (AEMA) to build in an acetoacetoxy moiety (*Scheme 29B*). Furthermore, a diamine will be added to form the vinylogous urethanes cross-links in a spontaneous condensation reaction with the liberation of water. In a third system, the acrylic monomer will be copolymerised with 2-hydroxyethyl methacrylate (HEMA) to incorporate a pendant hydroxyl group (*Scheme 29C)*. This hydroxyl group can then be reacted with a phthalic anhydride to form the phthalate monoester. This third type of network can also be synthesised in an inverse manner. Here, the acrylic monomer is copolymerised with a methacrylate that is functionalised with a phthalic anhydride (*Scheme 29D*). Consequently, this functional copolymer can be cured with a simple commercial diol.

Conventional free radical polymerisation has been chosen deliberately to provide functional copolymers that are potentially scalable. In order to moderate the molecular weight of the copolymers, a chain transfer agent (CTA) will be added. Controlled radical polymerisation techniques such as reversible addition-fragmentation chain transfer polymerisation (RAFT) or atom transfer radical polymerisation (ATRP) have not been considered since they often require longer reaction times and more stringent reaction conditions; there are few examples of commercialisation using these methods.

The initial work consists of the optimisation of the copolymerisation reaction between the (meth)acrylic monomer and the appropriate functionalised (meth)acrylic monomer to prepare prepolymers for cross-linking comprising

different comonomer contents and molecular weights. Subsequently, the prepared copolymers will be cross-linked with various types of complementary cross-linkers. The formed networks will be tested for recyclability and will be characterised *via* different techniques such as differential scanning calorimetry (DSC), thermogravimetric analysis (TGA), rheology tests, DMTA, solubility tests and tensile testing. Ultimately, the aim is to generate a full mechanical and chemical characterisation for different types of dynamic chemistry on the same acrylic backbone in order to directly compare their relative performance.

Chapter 2 presents the results for the dissociative networks based on Diels-Alder chemistry. Chapter 3 describes the results for the vitrimers based on transamination of vinylogous urethanes and chapter 4 reviews the results of the hybrid system based on the transesterification of phthalate monoesters. The advantages and disadvantages of the different approaches are reviewed and critically compared in Chapter 5.

Chapter 2 Diels-Alder – Dissociative type

2.1 Functional copolymers

In order to synthesise the envisaged acrylic networks, an appropriate acrylic monomer has to be selected that fulfils all the requirements as a backbone. Firstly, a relatively low glass-transition temperature (T_g) was targeted to provide flexibility in order to facilitate the dynamic reactions in the networks at elevated temperatures, the sample preparation at room temperature and the measurement of the mechanical properties. (Meth)acrylic monomers with different alkyl substituents provide significant versatility with respect to targeting a range of T_g's varying from -65 °C for poly(lauryl methacrylate) (PLMA) to -10 °C for poly(2-ethylhexyl methacrylate) (PEHMA) (*Figure 12*). Secondly, most of these types of monomers are commercially available and used for industrial applications in large quantities (*e.g.* poly(methyl methacrylate)-based adhesive industry).[9]

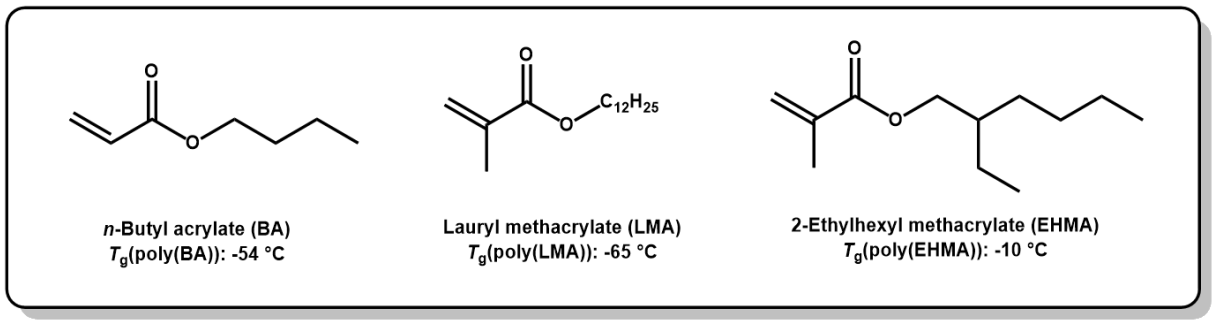

Figure 12: Structures of (meth)acrylic monomers considered for the copolymer backbone.

Initially, *n*-butyl acrylate (BA) was evaluated as the monomer is used commercially for the manufacture and application of pressure sensitive adhesives. These monomers are susceptible to back-biting of the radicals on the growing polymer

chain (*Scheme 30*).[162, 163] This back-biting leads to the formation of a mid-chain radical (MCR), which can disproportionate on either the longer or shorter side of the backbone (A or B) or propagate, thus causing the formation of a secondary propagating radical (SPR). Further, these SPRs cause short and long chain branching. As a result, the preliminary polymerisations of *n*-butyl acrylate in toluene yielded polymers with a relatively high dispersity *Đ* of 3.2-6.6.

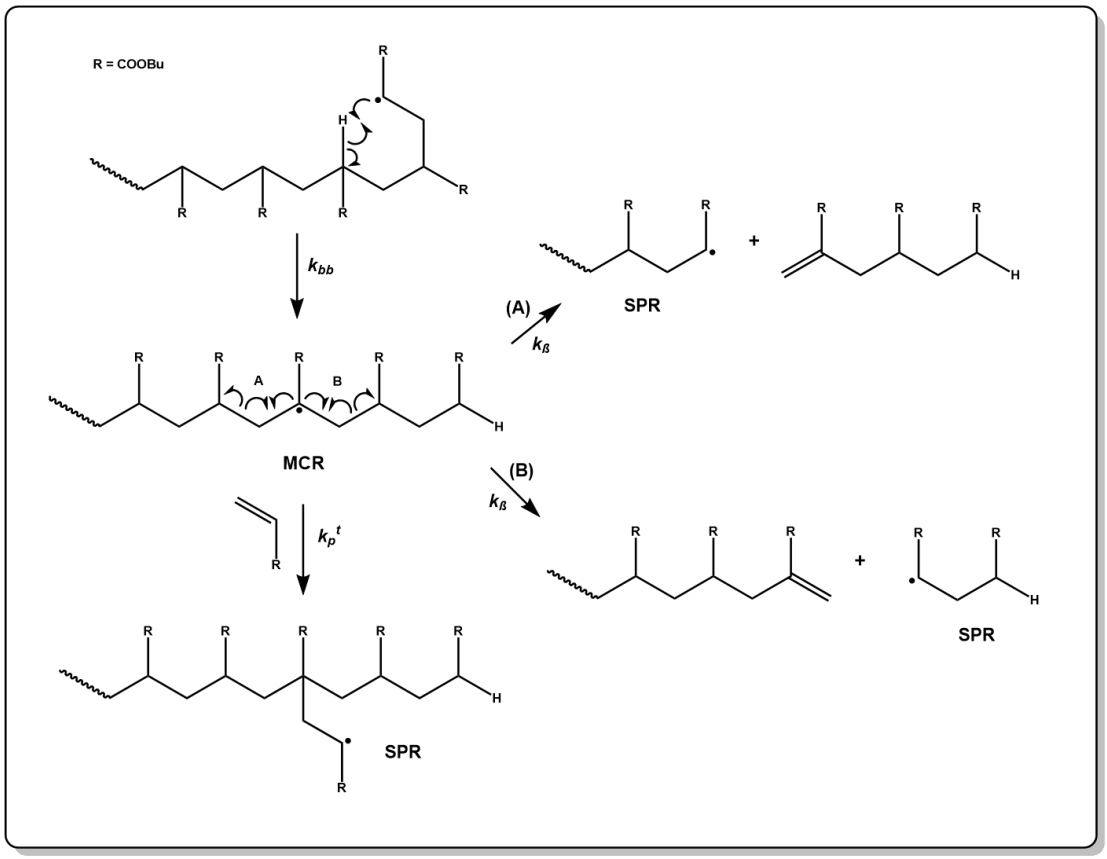

Scheme 30: The mechanism of back-biting during the free-radical polymerisation of acrylate monomers showing the formation of mid-chain radicals and the consequent side reactions.

A possible method of circumventing this side reaction could be the use of a controlled radical polymerisation technique such as reversible addition/fragmentation chain transfer (RAFT) polymerisation.[164] Here, a chain transfer agent (CTA), usually a dithioester, is used to protect and deprotect the

growing radical polymer chains that quickly alternate between their dormant and active state.[165] Ultimately, the use of this technique was not implemented as a consequence of the odour and thermal stability of the CTA, discolouration of the obtained polymer and lack of control at high conversion. Moreover, these factors prevent wider exploitation of RAFT on an industrial basis.[166]

A second method to suppress adverse back-biting side reactions was reported by Liang *et al.* through the implementation of acrylic polymerisations in the presence of protic solvents, such as *n*-butanol.[167, 168] However, the reaction should be ideally feasible in bulk or a minimal volume of readily available and benign solvents. Thus, to ensure the aforementioned robustness and scalability of the synthesis, this method was not pursued.

In order to avoid the broadening of dispersity, the focus was changed to methacrylates. Lauryl methacrylate (LMA) was firstly evaluated as the long alkyl chain produces a very low T_g of the homopolymer (-65 °C) with some crystallinity that exhibits a melting temperature (T_m) of -34 °C (*Figure 12*). Hence, this monomer is suitable for polymerisations in bulk without the risk of solidifying. Ultimately, it was not an ideal candidate as a consequence of its crystallinity and complicated work-up. The extremely low T_g requires the solvents to be cooled with liquid nitrogen or a dry ice bath during precipitation to easily isolate the product. The next candidate that was tested was 2-ethylhexyl methacrylate (EHMA), with the shorter, branched alkyl chain, the T_g is higher than LMA but still below ambient, which facilitates the work-up significantly. This monomer has been widely reported in

literature as a consequence of the commercial availability and compatibility with other methacrylate comonomers. [169-173]

Therefore, EHMA was copolymerised with furfuryl methacrylate (FMA) to incorporate a pendant furan ring in the polymer backbone (*Figure 13*). This furan group can then react with a maleimide group *via* Diels-Alder cycloaddition reactions to form the cross-linked polymer networks. Different functional copolymers were synthesised in order to assess the influence of molecular weight and composition.

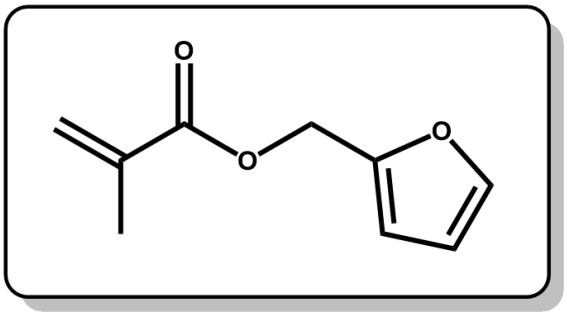

Figure 13: The structure of furfuryl methacrylate (FMA) used as functional comonomer.

Initially, different molecular weights were targeted to determine the influence of the molecular weight on the properties of the copolymers and resulting networks. The number average molecular weights M_n of 10, 25 and 40 kg.mol^{-1} were selected to determine the influence of chain entanglements on the material properties. As polymer chains grow, there is a critical molecular weight (M_c) at which the chains start to form a statistical random coil and entangle.[174, 175] These entanglements have a significant impact on the viscosity and structural properties of the polymer material (*Figure 14*). Since viscosity is the resistance to flow, polymers with a molecular weight above their M_c will show a sharp increase in their viscosity. These entanglements consequently reinforce the material and will render it more tough and ductile as a result.

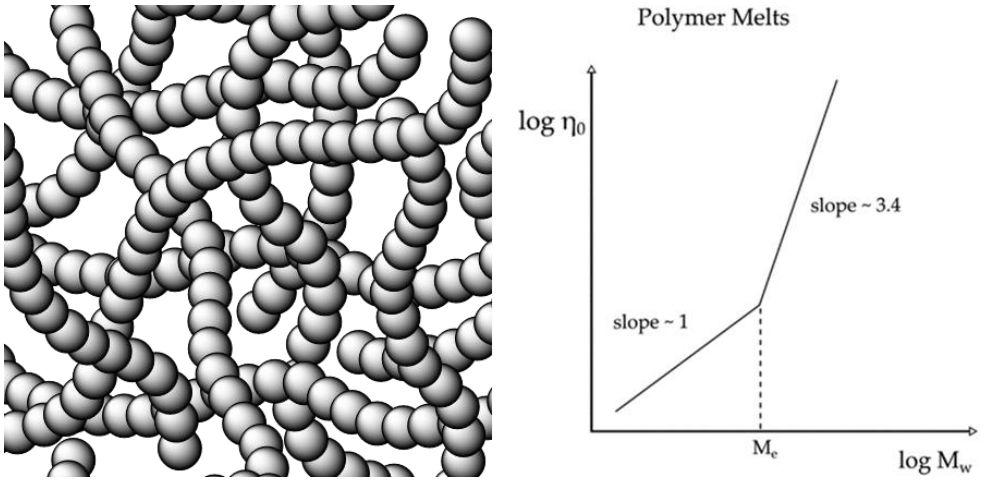

Figure 14: Illustration of chain entanglements (left), schematic showing the melt viscosity of a linear polymer in function of the molecular weight (right). A change in the slope is observed when M_w exceeds M_e, where sufficient chain entanglements occur.[176]

The relation between molecular weight (M) and intrinsic viscosity (η) is described by the Mark-Houwink empirical equation (*Equation 5*):

$$\eta = KM^a \qquad (5)$$

The entanglement molecular weight (M_e) of poly(EHMA) has been extrapolated from the values reported on poly(*n*-hexyl methacrylate) and poly(*n*-octyl methacrylate), namely 33.8 kg.mol^{-1} and 47.5 kg.mol^{-1}, respectively.[175] Therefore, a value of roughly 40 kg.mol^{-1} was approximated for the M_e and consequently the M_c is approximately half that value, namely 20 kg.mol^{-1}.[174] Therefore, the lower targeted molecular weight is below M_e whereas the higher targeted molecular weight is around M_e. Additionally, a mid-range molecular weight of M_n = 25 kg.mol^{-1} was also targeted, however, this work was stopped due to time constraints.

In order to control the molecular weight, a chain transfer agent (CTA) was added to the reaction mixture (*Table 1*). *N*-dodecyl mercaptan (DDM) was selected due to its commercial availability, high boiling point and low odour (*Figure 15*). It is routinely used in industry on a large scale in commercial products.[177]

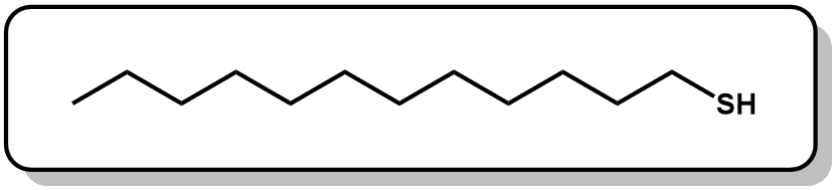

Figure 15: The structure of n-dodecyl mercaptan (DDM), used as chain transfer agent to control molecular weight.

Different concentrations of initiator azobisisobutyronitrile (AIBN) and DDM were investigated to obtain the targeted molecular weights (*Table 1*). The initial scale of the reaction was approximately 4 g and was stepwise increased up to 100 g. Further scale-up is possible, however, in order to preserve reagents and ensure multiple experiments were feasible, 100 g was selected as the largest experimental scale. This scale-up minimised the weighing error and as a result the weight differences of AIBN and DDM between different batches in addition to providing enough material from one batch for subsequent material evaluation.

The nomenclature for the functional copolymers comprises of an initial number referring to the targeted molecular weight in $kg.mol^{-1}$ (*e.g.* 10), followed by the name of the incorporated functional comonomer (*e.g.* FMA) and ending in the targeted composition of this comonomer in mol.% (*e.g.* 5) (*vide supra*). For example, 10FMA5 is a 10 $kg.mol^{-1}$ PEHMA with 5 mol.% incorporation of FMA. This nomenclature was employed to facilitate the discussion of the experimental results.

In most cases, the molecular weights achieved were close to those targeted (*i.e.* M_n = 10 $kg.mol^{-1}$ and 40 $kg.mol^{-1}$), the exception being **40FMA2**. This may be the result of a sub-optimal initiation or inefficient action of the CTA. All copolymers were made to high conversion (70-90%) within 3.5-4 hours and unlike poly(*n*-butyl acrylate), dispersities obtained were typically in the region of 1.8-2.2, the exception being **40FMA20**. Again, this could have been cause by an inefficient initiation or CTA.

Table 1: Free-radical copolymerisation of poly(EHMA-co-FMA) using different concentrations of I and CTA to control molecular weight.

Name	$f_{\%EHMA}$[a]	$f_{\%FMA}$[a]	*[I]* (mol.L^{-1})	*[CTA]* (mol.L^{-1})	*[CTA]/[M]*	M_n (kg.mol^{-1})[b]	$Đ_M$[b]
10FMA3	**97**	**3**	**0.003**	**0.062**	**0.014**	**11.6**	**1.7**
40FMA2	**98**	**2**	**0.001**	**0.008**	**0.002**	**58.8**	**2.2**
10FMA5	**95**	**5**	**0.003**	**0.062**	**0.014**	**9.8**	**1.8**
40FMA5	**95**	**5**	**0.001**	**0.008**	**0.002**	**44.9**	**2.1**
10FMA10	**90**	**10**	**0.003**	**0.060**	**0.013**	**10.6**	**1.8**
40FMA10	**90**	**10**	**0.002**	**0.015**	**0.003**	**38.2**	**2.0**
10FMA20	**80**	**20**	**0.003**	**0.055**	**0.012**	**12.7**	**2.0**
40FMA20	**80**	**20**	**0.001**	**0.010**	**0.002**	**40.4**	**2.9**

[a]*Feed ratio in mol.%.* [b]*Measured via SEC ($CHCl_3$, PMMA standards).*

The molecular weights were determined with size exclusion chromatography (SEC) in $CHCl_3$ using PMMA standards (*Figure 16, Figure 17*). The SEC chromatograms for copolymers within both molecular weight ranges targeted (M_n = 10 kg.mol^{-1} and 40 kg.mol^{-1}) are mostly uniform, apart from **40FMA20**, which shows a slight shoulder on the high molecular weight end of the distribution. This may be the result of inefficient chain transfer or radical termination by combination (*vide supra*).

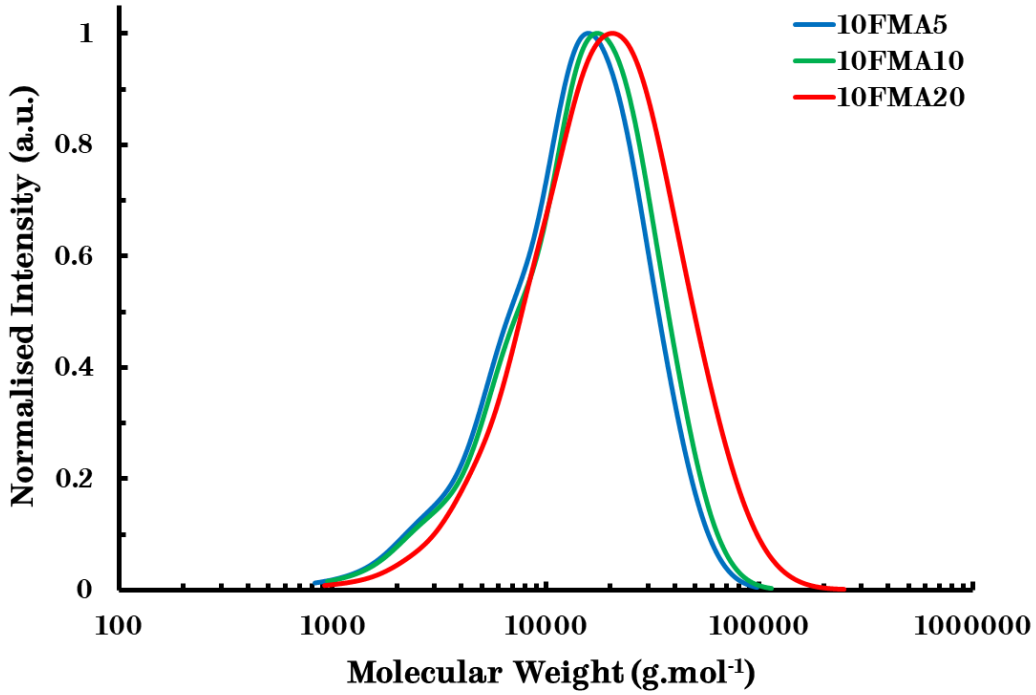

Figure 16: SEC chromatogram of poly(EHMA-co-FMA) with a targeted molecular weight M_n = 10 kg.mol^{-1} and different FMA concentrations ($CHCl_3$, PMMA standards).

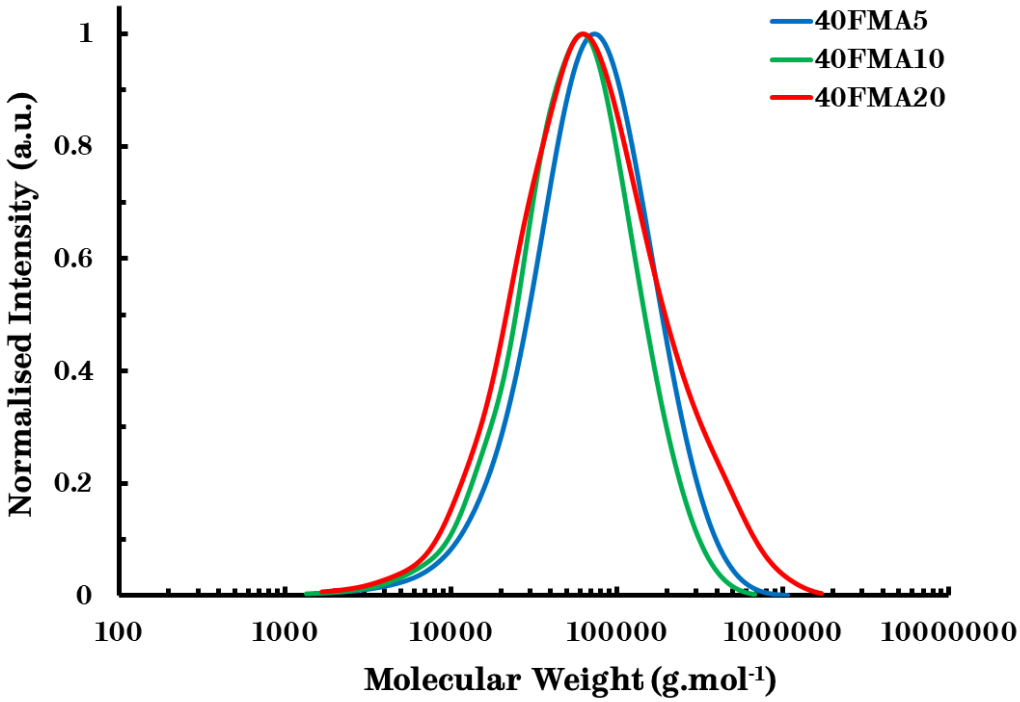

Figure 17: SEC chromatogram of poly(EHMA-co-FMA) with a targeted molecular weight M_n = 40 kg.mol^{-1} and different FMA concentrations ($CHCl_3$, PMMA standards).

Initially, different chemical compositions were targeted to determine the influence of the prepolymer composition and resulting network cross-link density on their performance. Copolymers were targeted with 2, 5 and 10 mol.% of comonomer. After the initial experiments, the 2 mol.% composition was eliminated for future study as a consequence of the cross-link density of the resultant networks being too low and the network completely dissolved in solvent (*vide infra*). New copolymers with 20 mol.% FMA comonomer were made in order to gain insight into the effect of increased cross-linking in the subsequent networks. Highly cross-linked systems generally have a higher structural strength (Young's modulus), but they are usually more brittle. Lightly cross-linked systems can be more ductile and will likely require less extensive curing at the expense of cohesive strength.

^{1}H NMR spectroscopy was used to determine the content of furfuryl methacrylate incorporated into the backbone (*Figure 18*). The relevant resonances used for this calculation were the methylene proton resonances adjacent to the ester at chemical shifts δ = 3.9-4.04 ppm for copolymerised EHMA and δ = 4.9 ppm corresponding to copolymerised FMA. Both of these resonances correspond to the same number of protons, namely 2 (-OCH_2-), so the relative ratio of the integration of these resonances can be used directly to determine the composition. Furthermore, this relative ratio can be converted into a percentage ratio using $Ratio_{Rel}/(1 + Ratio_{Rel})$ (*Table 2*). This percentage can then be used to calculate the average number of functional groups per chain (functionality).

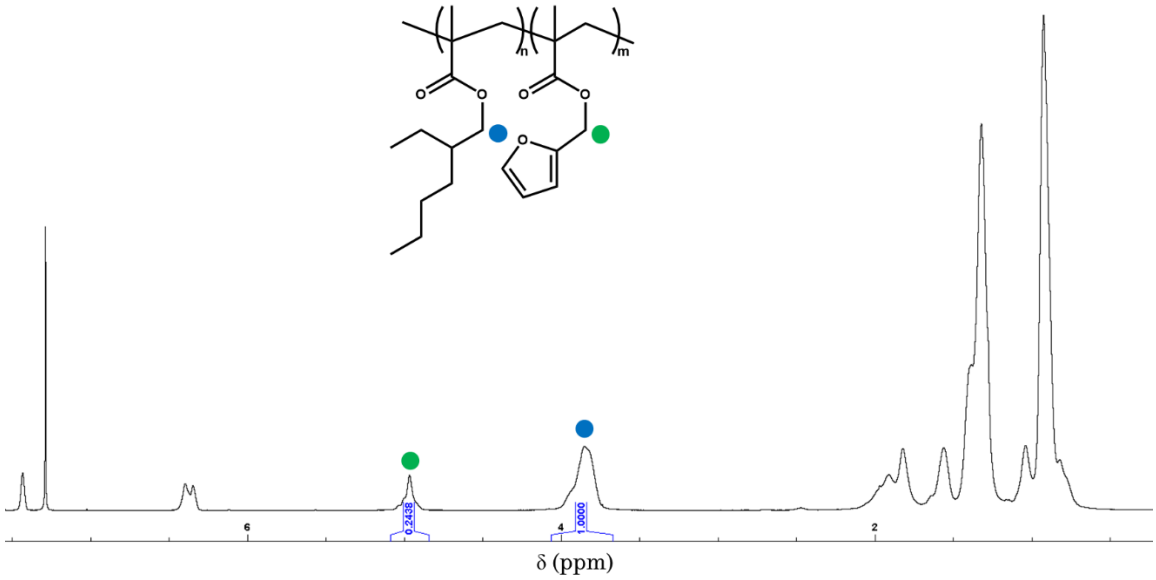

*Figure 18: ^{1}H NMR spectrum of **10FMA20** (400 MHz, $CDCl_3$, 298 K).*

The data show that the copolymer compositions ($F_{\%FMA}$) obtained were similar to the molar feed ratios of the comonomers, indicating a good compatibility between the comonomers (*Table 2*).

Table 2: Monomer feed vs. composition and molecular weight of poly(EHMA-co-FMA).

Name	$f_{\%EHMA}$[a]	$f_{\%FMA}$[a]	M_n (kg mol^{-1})[b]	$Đ_M$[b]	$F_{\%FMA}$[c]
10FMA3	97	3	11.6	1.7	3.1
40FMA2	98	2	58.8	2.2	1.9
10FMA5	95	5	9.8	1.8	5.1
40FMA5	95	5	44.9	2.1	5.4
10FMA10	90	10	10.6	1.8	10.1
40FMA10	90	10	38.2	2.0	9.9
10FMA20	80	20	12.7	2.0	19.6
40FMA20	80	20	40.4	2.9	22.2

[a]Feed ratio in mol.%. [b]Measured via SEC ($CHCl_3$, PMMA standards). [c]Calculated from ^1H NMR spectroscopy.

Differential scanning calorimetry (DSC) was used to determine the glass-transition temperature (T_g) of the copolymers (*Figure 19, Figure 20*).

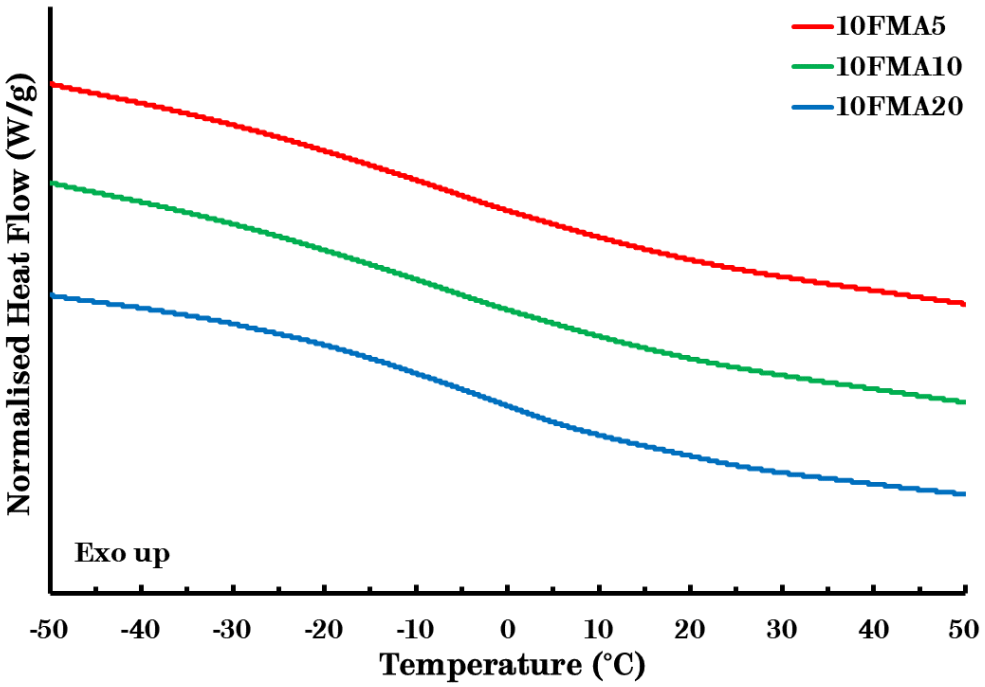

Figure 19: DSC thermograms of poly(EHMA-co-FMA) with a targeted molecular weight M_n = 10 kg.mol^{-1} and different FMA concentrations (Second heating curve, heating rate 10 °C.min^{-1}).

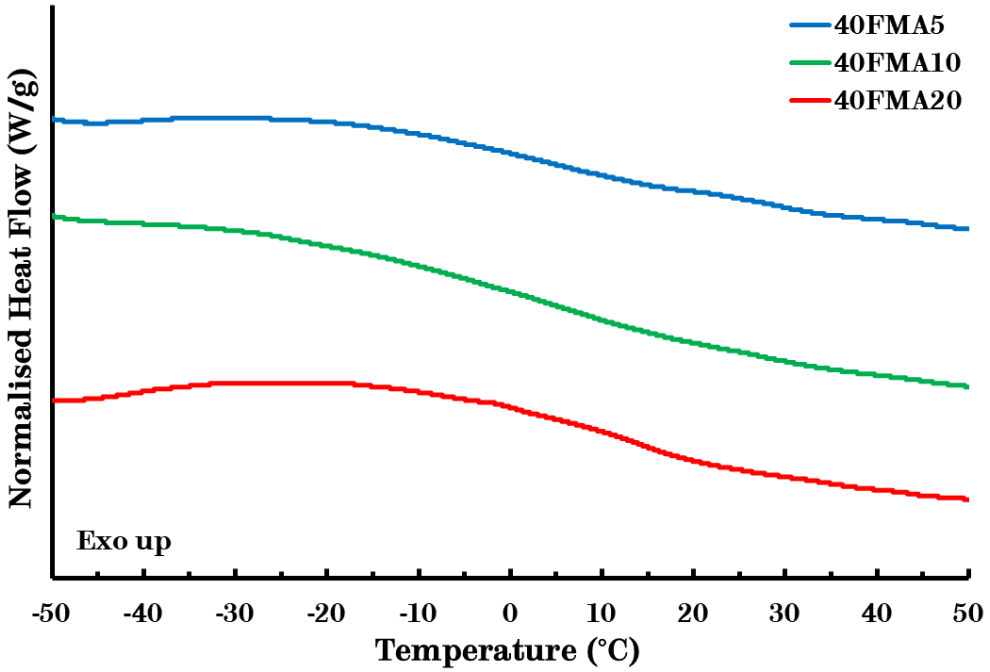

Figure 20: DSC thermograms of poly(EHMA-co-FMA) with a targeted molecular weight M_n = 40 kg.mol^{-1} and different FMA concentrations (Second heating curve, heating rate 10 °C.min^{-1}).

The T_g values were calculated from the second heating curve. The T_g of homogeneous blends of homopolymers or statistical copolymers follow a simple additive rule, commonly referred to as the Flory-Fox equation (*Equation 6*).

$$\frac{1}{T_g} = \frac{w_1}{T_{g1}} + \frac{w_2}{T_{g2}} \qquad (6)$$

Here, w_1 and w_2 are the weight percentages of monomers 1 and 2 in the copolymer and T_{g1} and T_{g2} are the glass transition temperatures of monomers 1 and 2, respectively. The T_g of the copolymers is dependent on the composition and ranges from -1 to 10 °C, which lies between the T_g of PEHMA (-10 °C) and the T_g of PFMA (39 °C) (*Table 3*).[170, 178]

Table 3: DSC results of poly(EHMA-co-FMA) comparing the theoretical T_g with the experimental T_g for different concentrations of FMA.

Name	M_n (kg.mol^{-1})[a]	$F_{\%FMA}$[b]	T_g (°C) Th.[c]	T_g (°C) Exp.[d]
10FMA5	**9.8**	**5.1**	**-7.9**	**-0.5**
10FMA10	**10.6**	**10.1**	**-5.8**	**-0.7**
10FMA20	**12.7**	**19.6**	**-1.5**	**1.7**
40FMA5	**44.9**	**5.4**	**-7.9**	**1.2**
40FMA10	**38.2**	**9.9**	**-5.8**	**3.2**
40FMA20	**40.4**	**22.2**	**-1.5**	**9**

[a] Measured via SEC ($CHCl_3$, PMMA standards). [b] Calculated from ^1H NMR spectroscopy. [c] Calculated from Flory-Fox equation. [d] Measured via DSC (heating rate 10 °C.min^{-1}).

2.2 Network synthesis

After the synthesis of the functional copolymers, cross-linked networks were made using a solvent casting method (*Figure 21*). This involved dissolving the functional copolymer and mixing with the appropriate amount of cross-linker followed by removal of the solvent and curing of the sample. Mixing was carried out manually as a consequence of the small scale (5 – 20 g). The reaction mixture was poured into a PTFE-lined Petri dish to ensure easy removal of the sample. For the removal of the solvent, the duration, temperature and vacuum were determined to minimise spillage and bubble formation (*Table 4*).

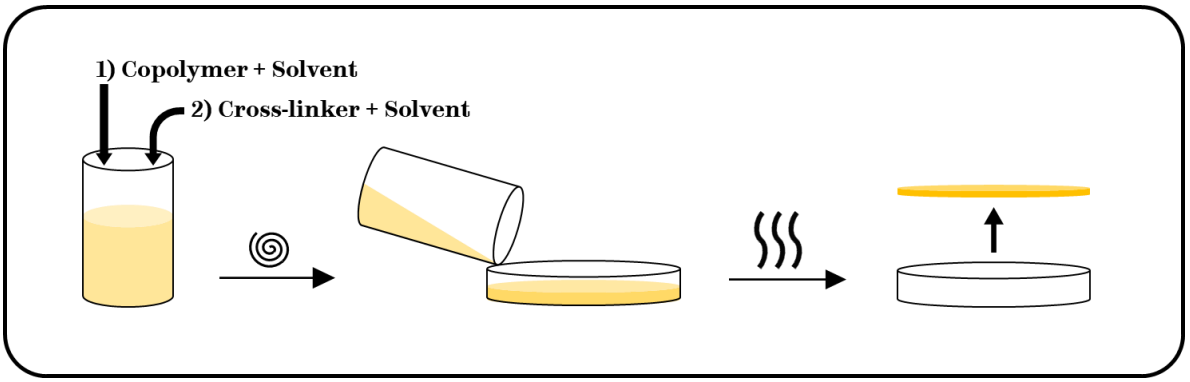

Figure 21: Illustration of the process of solvent-casting a mixture of functional prepolymer and cross-linker followed by drying and curing to obtain cross-linked networks.

Table 4: Drying/curing methods during solvent casting.

	Method 1	Method 2
Step 1	**ambient overnight no vacuum**	**30 min at 80 °C no vacuum**
Step 2	**30 min at 90 °C no vacuum**	**1 h at 100 °C 50% vacuum**
Step 3	**2 h at 90 °C full vacuum**	**2 h at 100 °C full vacuum**

The initial curing step was then followed by compression moulding to obtain homogenous, defect-free samples with a constant thickness. Rapid prototyping of the networks was performed using vacuum compression moulding, which avoids the risk of wasting material and gave initial parameters for the reprocessing of the material. Furthermore, different geometries (*e.g.* discs, bars and plate) could be made for rheological and thermal analysis. The three parameters that were systematically altered were temperature, time and pressure. For vacuum compression moulding, the pressure was fixed at 1 atm. Custom aluminium moulds were used to ensure fast heating and cooling of the material. All Diels-Alder networks were post-cured at ambient temperature for 7 days before performing any characterisation to ensure a good network formation.

Initially, an aromatic crosslinker was tested, namely 1,1′-(methylenedi-4,1-phenylene)-bismaleimide (**BMI1**) (yellow solid, *m.p.* = 156-158 °C) (*Figure 22*). This crosslinker was selected since aromatic compounds are more rigid and improve the overall strength of the polymer network. Additionally, **BMI1** has often been used as a cross-linker in Diels-Alder systems reported in literature and would serve as a useful reference.[179] However, making uniform samples using **BMI1** was challenging.

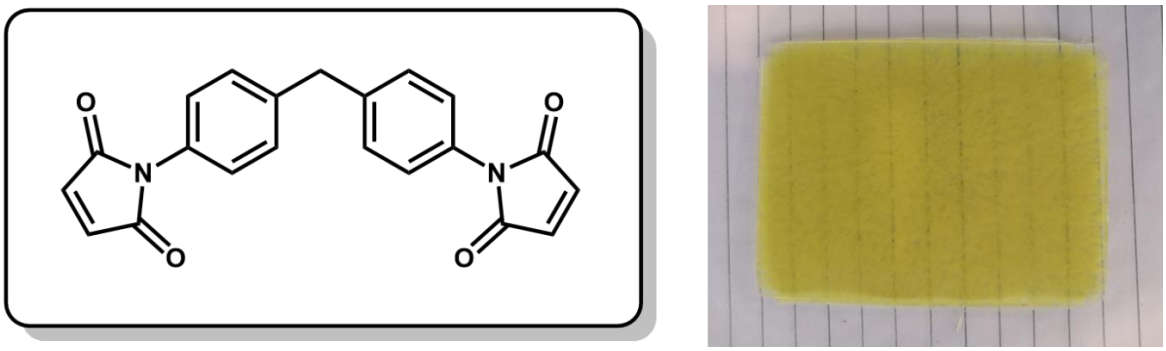

*Figure 22: The structure of 1,1'-(Methylenedi-4,1-phenylene)-bismaleimide (**BMI1**) (left) and a picture of a typical cross-linked network obtained from poly(EHMA-co-FMA) cured with **BMI1** (right).*

Despite a large range of processing conditions being attempted, phase separation was observed after incorporating **BMI1**, which may be the result of the significant difference in polarity between **BMI1** and the PEHMA matrix (*Figure 22*). The material is not transparent and pale-yellow particles are evident typically a few mm in diameter. After extensive experimentation with the processing conditions, suitable homogeneous materials could not be realised. Since this would likely affect the rheological and thermal properties, an aliphatic C_{36} dimer diol hexyl ester bismaleimide (**BMI2**) was selected to ensure good compatibility with the acrylic polymer matrix (*Figure 23*). In contrast to the previous networks, there was no phase separation and the final networks were homogeneous and transparent as a consequence of the long aliphatic chains of the C_{36} core of this bismaleimide.

The nomenclature of the networks will be the same as the copolymers, followed by the name of the incorporated cross-linker. For example, **10FMA5-BMI2** is a network based on 10 $kg.mol^{-1}$ PEHMA with 5 mol.% incorporation of FMA, which is cross-linked with **BMI2**.

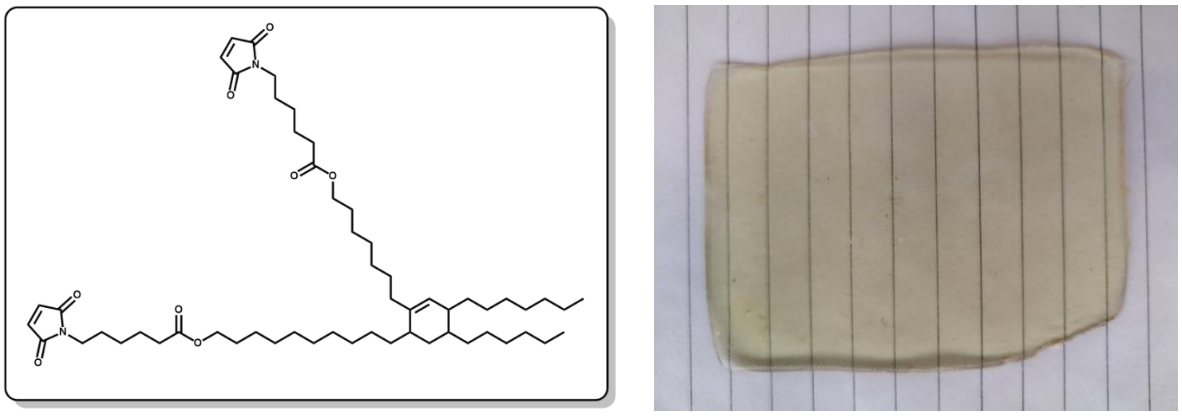

*Figure 23: The structure of the flexible hexyl ester bismaleimide cross-linker **BMI2** (left) and a picture of a typical cross-linked network obtained from poly(EHMA-co-FMA) cured with **BMI2** (right).*

Further, **BMI2** is a liquid and miscible in most organic solvents. As a consequence of poor compatibility of the PEHMA matrix and **BMI1**, networks containing both components were not tested further and attention was focused on the networks comprising the flexible aliphatic **BMI2**. Since the furan-maleimide chemistries have a retro-Diels-Alder temperature in the range of 110-135 °C, the processing temperatures and pressures could not be too high, otherwise the material would dissociate and flow from the moulds (*Table 5*). High temperatures and long reprocessing times should also be avoided to minimise the risk of possible maleimide side reactions occurring above 150 °C (*e.g.* Michael addition reactions, thermal radical homopolymerisations).[180-185]

Table 5: Processing parameters of the Diels-Alder networks based on poly(EHMA-co-FMA) with different molecular weights and concentration of FMA.

Name	***M_n*** **(kg.mol^{-1})[a]**	***$F_{\%FMA}$*** **[b]**	***P*** **(bar)**	***Temp.*** **(°C)**	***Time*** **(min)**
10FMA5-BMI2	**9.8**	**5.1**	**20**	**125**	**5**
10FMA10-BMI2	**10.6**	**10.1**	**30**	**135**	**1**
10FMA20-BMI2	**12.7**	**19.6**	**40**	**150**	**5**
40FMA5-BMI2	**44.9**	**5.4**	**25**	**145**	**2**
40FMA10-BMI2	**38.2**	**9.9**	**30**	**140**	**5**
40FMA20-BMI2	**40.4**	**22.2**	**40**	**160**	**20**

[a]Measured via SEC ($CHCl_3$, PMMA standards). [b]Calculated from ^{1}H NMR spectroscopy.

There were two trends visible in the processing of the samples. Firstly, more demanding processing parameters were necessary for the networks based on the higher molecular weight poly(EHMA-*co*-FMA) as a consequence of the reduced chain mobility due to the presence of chain entanglements when compared to the networks based on the lower molecular weight copolymers. Secondly, as the FMA concentration increases, higher processing temperatures and time were required. Thus, a combination of both effects was apparent for the challenging processing of **40FMA20-BMI2**.

2.3 Characterisation of the networks

2.3.1 Thermal Properties

Thermogravimetric analysis (TGA) was performed to investigate the thermal stability of the materials. The 5% mass degradation temperature ($T_{deg5\%}$) of the copolymers with the lower molecular weight were in the range of 305-315 °C, which is slightly higher than the previously reported 300 °C for a comparable poly(EHMA-*co*-FMA) (M_n = 5.4 kg.mol^{-1}).[173] However, it is lower than the value of 375 °C reported for high molecular weight PEHMA.[186] The $T_{deg5\%}$ did not increase after cross-linking and even decreased for **10FMA5-BMI2**, which may be the result of residual solvent due to insufficient drying (*Figure 24*). In the 400-500 °C region, an increased stability with higher composition (more crosslinks) was observed. The shoulder in that range could be explained by the presence of a higher percentage of residual **BMI2**.

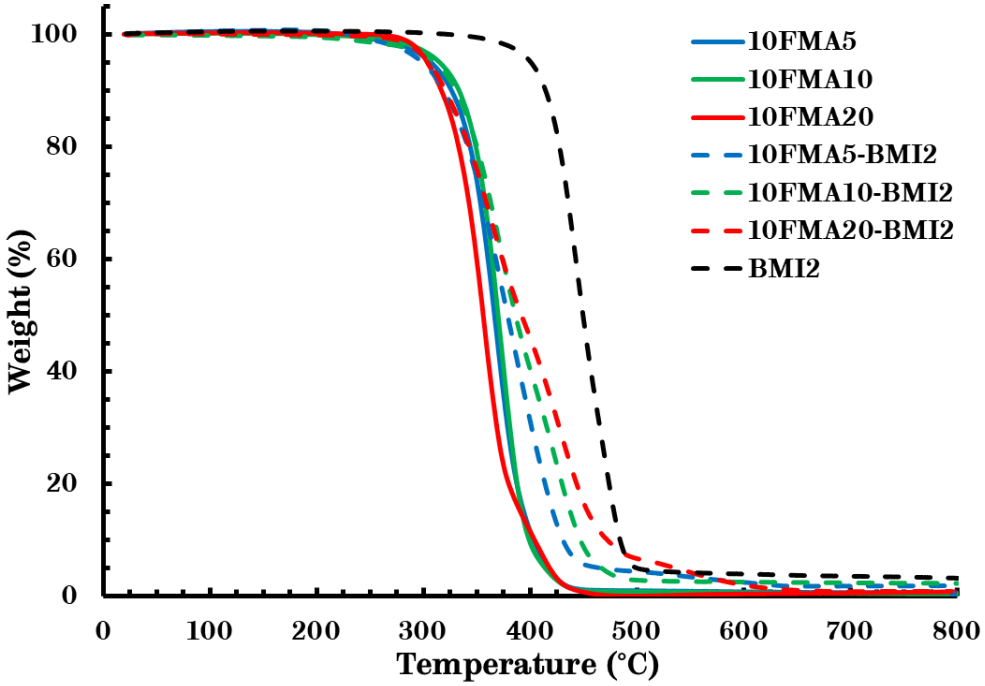

Figure 24: TGA thermograms of poly(EHMA-co-FMA) with a targeted molecular weight M_n = 10 kg.mol^{-1} and their corresponding networks, comprising different FMA concentrations (N_2, heating rate 10 °C.min^{-1}).

The results for poly(EHMA-*co*-FMA) with the higher molecular weight (40 kg.mol^{-1}) were similar, namely the $T_{deg5\%}$ was in the range of 280-310 °C (*Figure 25*). Furthermore, this range approximates the previously reported value of 300 °C of equivalent poly(EHMA-*co*-FMA).[173] Further, an overall increase in stability was found after cross-linking (297-303 °C). Again, the shoulder that can be observed in the range of 350-500 °C may be the result of a higher percentage of residual cross-linker. Thus, all acrylic materials involving the dissociative Diels-Alder chemistry are thermally stable up to at least 280 °C and the cured networks are more stable than their respective prepolymers. Cross-linking using the flexible aliphatic **BMI2** seems to reinforce the thermal stability of the copolymers. This trend aligns with previously reported furan-maleimide networks based on PEHMA.[172]

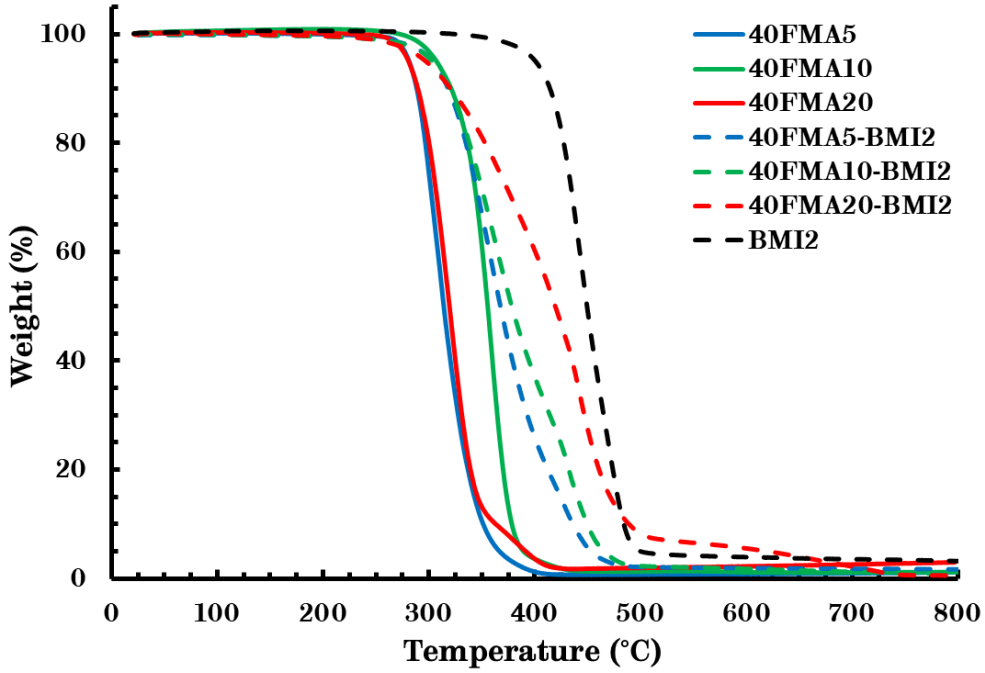

Figure 25: TGA thermograms of poly(EHMA-co-FMA) with a targeted molecular weight M_n = 40 kg.mol^{-1} and their corresponding networks, comprising different FMA concentrations (N_2, heating rate 10 °C.min^{-1}).

DSC was used to determine the T_g of the networks and determine the Diels-Alder and retro-Diels-Alder (rDA) reaction in this acrylic matrix (*Figure 26, Figure 27*).

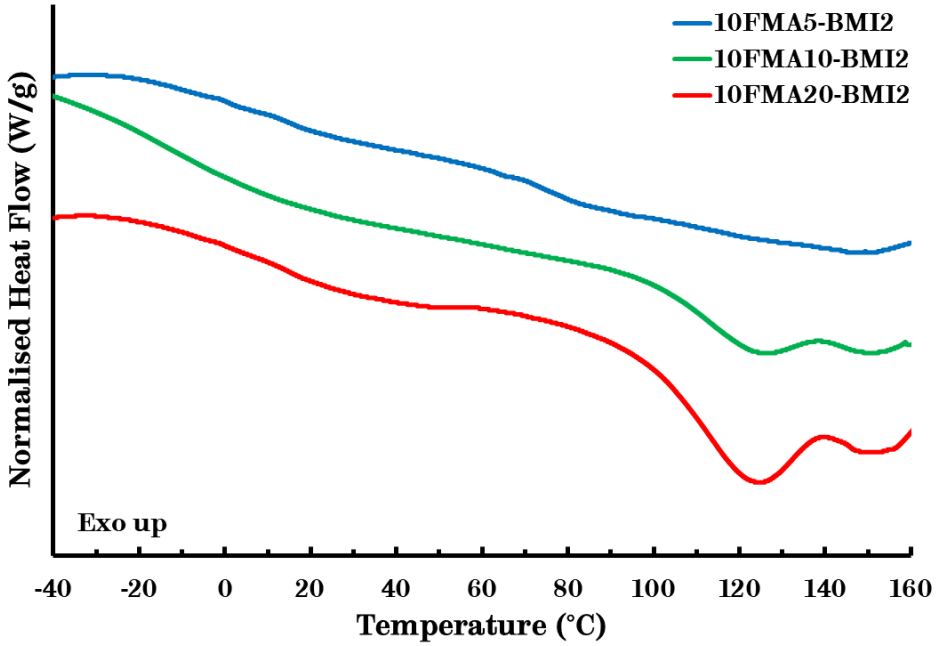

Figure 26: DSC thermograms of the networks based on poly(EHMA-co-FMA) with a targeted molecular weight M_n = 10 kg.mol^{-1} and different FMA concentrations (First heating curve, heating rate 10 °C.min^{-1}).

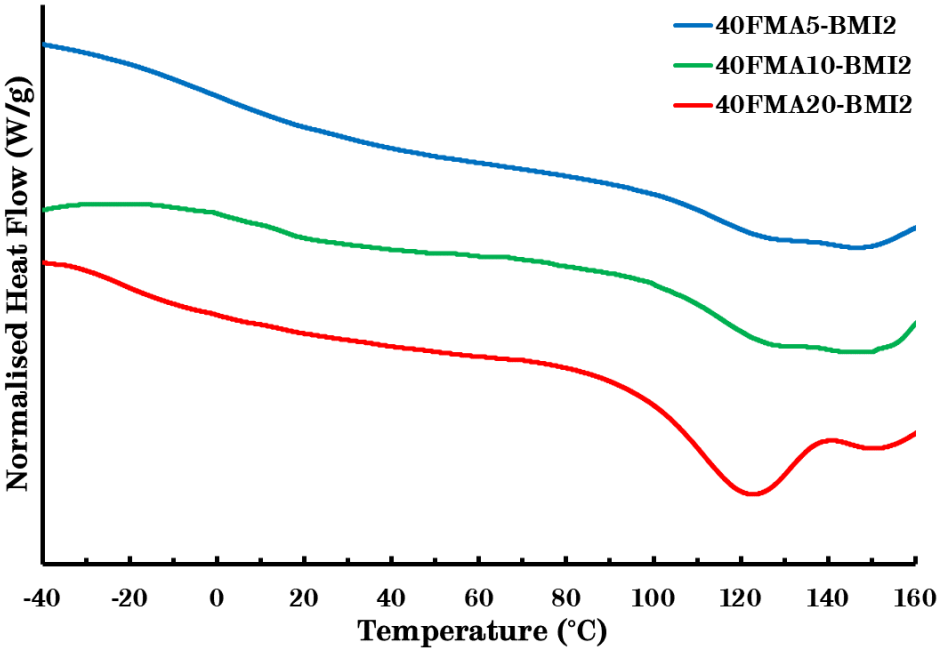

Figure 27: DSC thermograms of the networks based on poly(EHMA-co-FMA) with a targeted molecular weight M_n = 40 kg.mol^{-1} and different FMA concentrations (First heating curve, heating rate 10 °C.min^{-1}).

The data show that the cross-linked networks have a lower T_g when compared to the respective prepolymers (*Table 6*). The difference in T_g increases with higher concentrations of FMA as a consequence of the higher concentrations of more flexible cross-linker that are required for the stoichiometry of maleimide-furan to be equivalent. The flexible cross-linker has a significantly lower T_g (-55 °C) than the copolymer and has a plasticising effect on the polymer, thus decreasing the T_g. Thus, this effect was positively correlated with the composition of the networks. Generally, the rDA reaction of this furan-maleimide systems occurs in the range of 110-135 °C. The range of the rDA reaction in all the networks is slightly upshifted to 125-150 °C, which may be the result of the reduced chain mobility and high heating rate of 10 °C.min^{-1}. Furthermore, a clear trend is visible of an increasing endothermic change due to more rDA reactions occurring with higher FMA incorporation in the PEHMA backbone. Moreover, the kinetic *endo* adduct is more predominant than the

thermodynamic *exo* adduct due to the short processing times. Moreover, the *endo/exo* adduct ratio can be influenced with curing time.[187]

Table 6: The T_g of poly(EHMA-co-FMA) prepolymers and resulting networks.

Name	M_n (kg.mol^{-1})[a]	$F_{\%FMA}$[b]	T_g (°C)[c]
10FMA5	**9.8**	**5.1**	**-0.5**
10FMA5-BMI2			**-17.7**
10FMA10	**10.6**	**10.1**	**-0.7**
10FMA10-BMI2			**-24.0**
10FMA20	**12.7**	**19.6**	**1.7**
10FMA20-BMI2			**-26.0**
40FMA5	**44.9**	**5.4**	**1.2**
40FMA5-BMI2			**-16.7**
40FMA10	**38.2**	**9.9**	**3.2**
40FMA10-BMI2			**-22.1**
40FMA20	**40.4**	**22.2**	**9.0**
40FMA20-BMI2			**-23.5**

[a]Measured via SEC ($CHCl_3$, PMMA standards). [b]Calculated from ^{1}H NMR spectroscopy. [c]Measured via DSC (heating rate 10 °C.min^{-1}).

2.3.2 Solubility

Solubility experiments using Soxhlet extraction were conducted in order to assess the extent of the network formation. The selection of a suitable solvent is important for solubility experiments since the soluble fraction usually increases if the extraction is performed at a higher temperature. Thus, an extraction in a high boiling solvent (*e.g.* toluene) yields the upper limit of the possible values of the soluble fraction. However, due to the rDA reaction that typically occurs above 100 °C for the maleimide-furan system, a different solvent is required. Otherwise, it is difficult to distinguish between the soluble fraction caused by the rDA reaction on the one hand and the absence of network integrity on the other. Furthermore, previously reported furan-maleimide networks based on methacrylates completely dissolve in toluene at 100-130 °C.[91, 188] Therefore, ethyl acetate (EtOAc) was selected

because of its moderate boiling point of 77 °C. This value seemed low enough not to trigger the rDA but high enough to obtain accurate values for the soluble fraction.

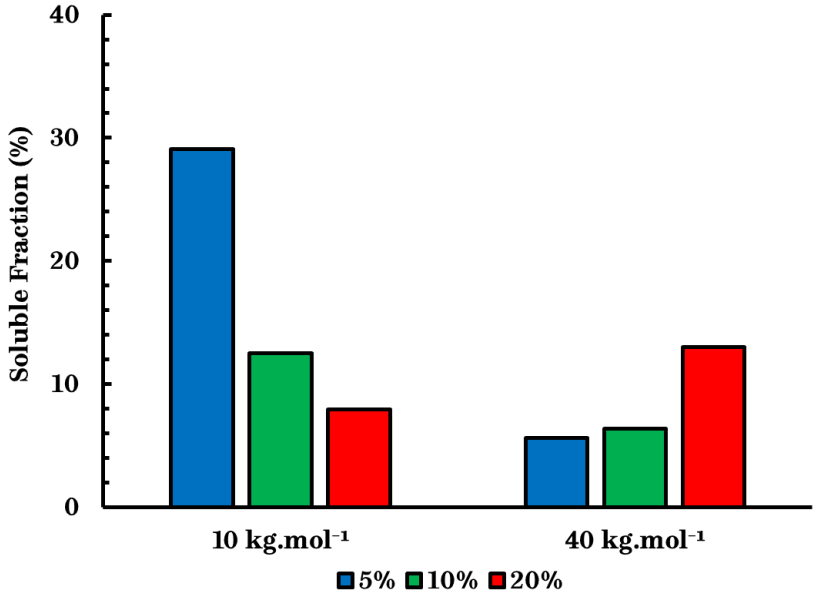

Figure 28: Soluble fractions of both sets of Diels-Alder networks at different concentration of FMA (5, 10, 20 mol.%) after extraction in EtOAc.

DMTA data shows that a plateau modulus is retained above T_g at this temperature (*vide infra*). Due to this reasoning, other solvents like $CHCl_3$, THF or diethyl ether were not considered. For the networks based on the lower molecular weight copolymers, there is a clear trend visible between the soluble fraction and the composition, with the lowest cross-link density giving the highest soluble fraction (*Figure 28, Table 7).* This results from the low average number of functional groups per chain for this material (2.5). Although the average number of functional groups per chain is > 2.0 and the network has gelled, there is likely to be a significant population of chains with lower functionality as a consequence of free-radical copolymerisation producing statistical copolymers. Moreover, the functionality of **10FMA5-BMI2** is below the minimum threshold to form good networks (approx. 3-5 functional groups per chain). The soluble fractions of **10FMA10-BMI2** and

10FMA20-BMI2 are 13% and 8%, respectively. Furthermore, these values align with the soluble fraction of 11% in THF at ambient temperatures reported for comparable furan/maleimide networks based on PEHMA.[171]

For the networks based on the higher molecular weight copolymers, the soluble fraction ranges between 6-13% (*Table 7*). The slightly higher soluble fraction of **40FMA20-BMI2** may result from insufficient curing of the sample and the consequent leaching of the residual cross-linker. As previously discussed in *2.2 Network synthesis*, the slow curing process of **40FMA20-BMI2** can be rationalised by the reduced chain mobility at high molecular weights. The data shows an inverse correlation between degree of swelling and cross-link density for both sets of networks (*Figure 29, Table 7*).

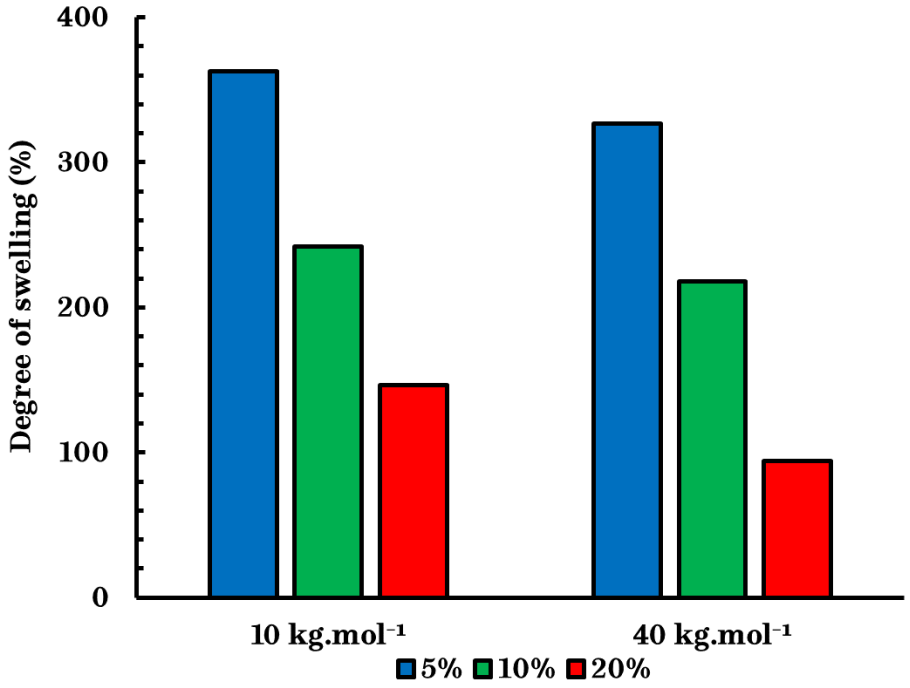

Figure 29: Degree of swelling of both sets of Diels-Alder networks at different concentration of FMA (5, 10, 20 mol.%) after extraction in EtOAc.

The correlation between degree of swelling and M_c (cross-link density) is described by the Flory-Rehner theory with the degree of swelling decreasing with decreasing M_c and thus increasing cross-link density.[189] The solubility data is indicative that the degree of swelling of the networks is only depends on the M_c (cross-link density), not the molecular weight of the functional copolymers.

Table 7: Results of the solubility experiments of both sets of Diels-Alder networks at different FMA concentrations compared to the functionality of the functional prepolymers.

Name	M_n **(kg.mol^{-1})[a]**	$F_{\%FMA}$[b]	***Sol. Fr.*** **(%)[c]**	***Swell.*** **(%)[c]**	***Funct.***[a,b]
10FMA5-BMI2	**9.8**	**5.1**	**29**	**363**	**2.5**
10FMA10-BMI2	**10.6**	**10.1**	**13**	**242**	**5.5**
10FMA20-BMI2	**12.7**	**19.6**	**8**	**146**	**13.0**
40FMA5-BMI2	**44.9**	**5.4**	**6**	**327**	**12.3**
40FMA10-BMI2	**38.2**	**9.9**	**6**	**218**	**19.4**
40FMA20-BMI2	**40.4**	**22.2**	**13**	**94**	**46.7**

[a] Measured via SEC ($CHCl_3$, PMMA standards). [b] Calculated from ^{1}H NMR spectroscopy. [c] Measured via Soxhlet extraction.

2.3.3 Rheology

Understanding the rheology of the material is extremely helpful for the manufacturing phase (processing), the use phase (material failure such as creep) and the end-of-life phase (disassembly and recycling). The rheology was tested both with a rheometer and dynamic mechanical thermal analysis (DMTA). Initially, an amplitude sweep was performed on one of the networks, namely **40FMA10-BMI2**, to determine the linear viscoelastic region (LVR) of the material (*Figure 30*).

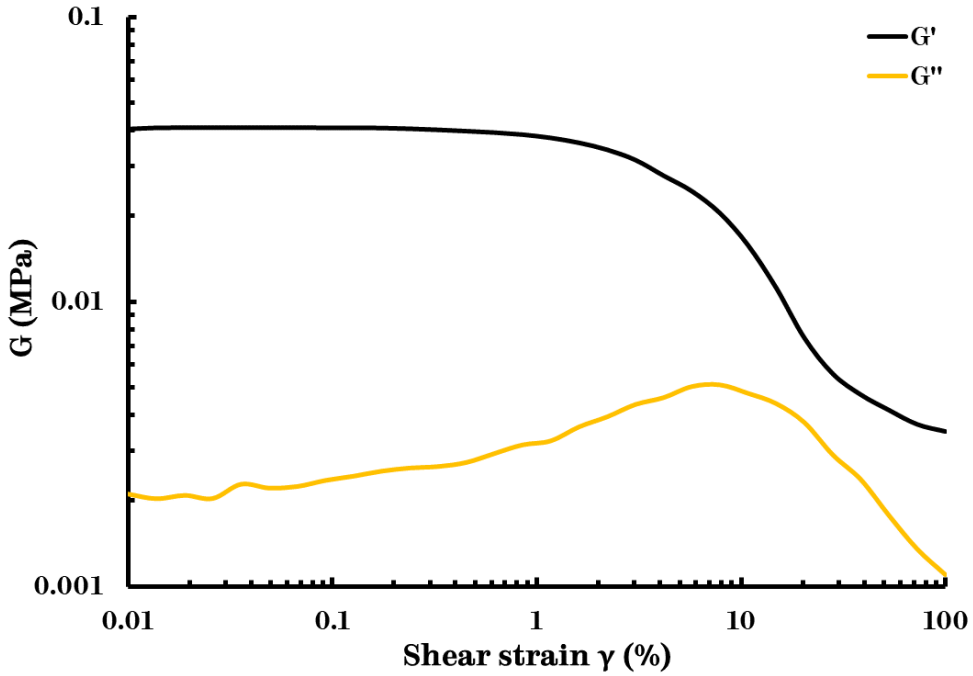

*Figure 30: Amplitude sweep of **40FMA10-BMI2** at 100 °C and 10 Hz*

This LVR can be observed as a plateau at 0.01-1% strain, where the storage modulus (*G'*) exceeds the loss modulus (*G"*). This plateau depends on the temperature and the frequency of the strain sweep experiments, which were 100 °C and 10 Hz, respectively. Furthermore, higher temperatures were not investigated to minimise the risk of dissociating the networks. In order to compare the rheology of all the different chemistries adequately, the value 1% for shear strain was selected for all consequent stress-relaxation experiments since this value lies optimally in the LVR of all networks (*vide infra*). For a dissociative mechanism, the material is expected to have a sol-gel transition and above the rDA temperature (125-150 °C) the viscosity would drop significantly with increasing temperature (*vide supra*).

Initially, stress-relaxation experiments were performed on all the Diels-Alder networks at one temperature, namely 130 °C. The relaxation modulus (*G)* was normalised against the apparent plateau value (G_0) at t = 1 s, after the initial step strain of 1%. The intersections of the horizontal dashed lines with the stress

relaxation curves indicate where $G/G_0 = 1/e$ and $t = \tau$. Thus, the relaxation time τ can be defined as the time it takes for the system to relax to a value of $1/e$ (approximately 37%).

For the networks based on the lower molecular weight copolymers, similar fast relaxation time were found for all compositions in the range of 58 - 83 s (*Figure 31*). Thus, (re)processing of the material at this temperature is possible and the service temperature in a specific application should be significantly lower than this value to avoid material failure. For the networks based on the higher molecular weight copolymers, the relaxation times are slightly longer (82 - 137 s), but in the same order of magnitude when compared to the previously discussed networks (*Figure 32*). The longer relaxation times may be the result of reduced chain mobility as a consequence of the chain entanglements.

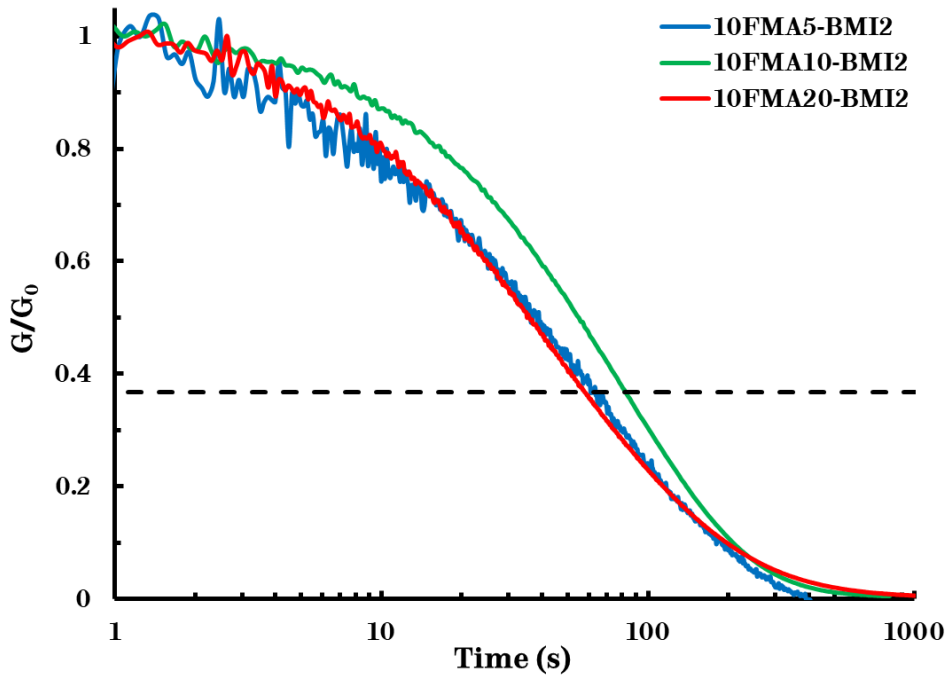

Figure 31: Stress-relaxation data at 130 °C for polymer networks made from poly(EHMA-co-FMA) prepolymers with a targeted molecular weight M_n = 10 kg.mol^{-1} and different FMA concentrations.

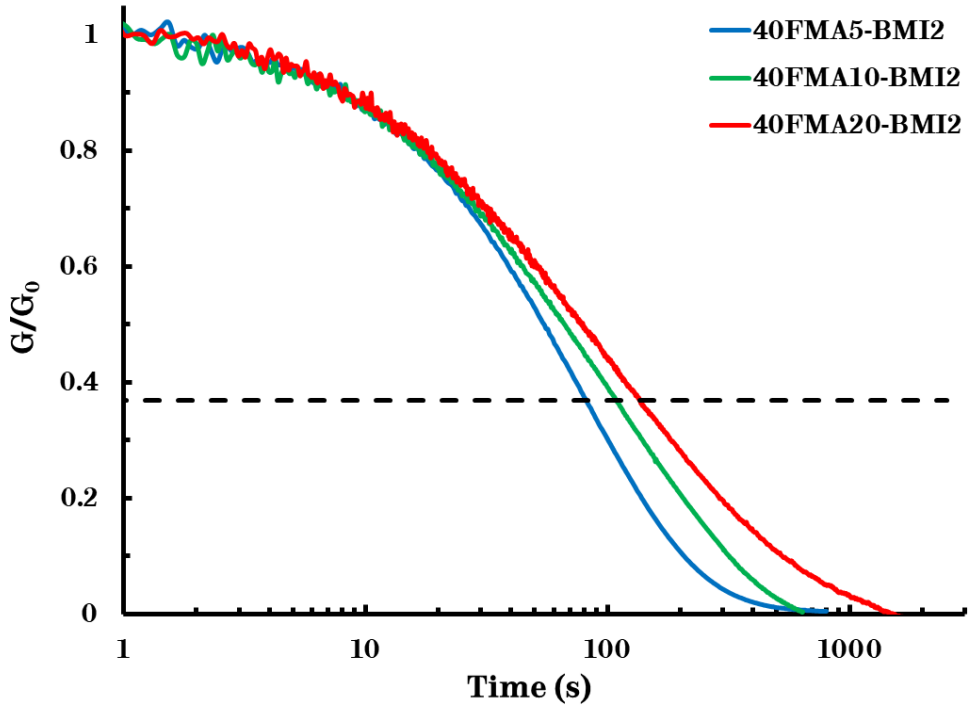

Figure 32: Stress-relaxation data at 130 °C for polymer networks made from poly(EHMA-co-FMA) prepolymers with a targeted molecular weight M_n = 40 kg.mol^{-1} and different FMA concentrations.

Next, stress relaxation experiments were performed on **10FMA20-BMI2** at different temperatures since previous data suggest that this is one of the more robust networks (lowest soluble fraction). The relaxation time τ can be defined as the time it takes the system to relax to a value of 1/*e* (approximately 37%) and is dependent on temperature. Relaxation times (τ) clearly decrease with increasing temperature (*Figure 33*). Between 130 - 150 °C, the relaxation times are quite short, in the range 10 - 100 seconds. For comparison, the relaxation time of an uncross-linked copolymer at these temperatures is usually ≤ 5 seconds. Further, Das *et al.* reported a τ of 7 seconds at 140 °C for their Diels-Alder networks based on furfuryl functionalised poly(HMA-*co*-HEMA) ($F_{\%HEMA}$ = 18 mol.%, M_n = 15.4 kg.mol^{-1}), cross-linked with **BMI1**.[92] At this temperature, **10FMA20-BMI2** exhibits a slightly longer τ of 23 seconds, which may be the result of a slightly shorter equilibration before the experiment.

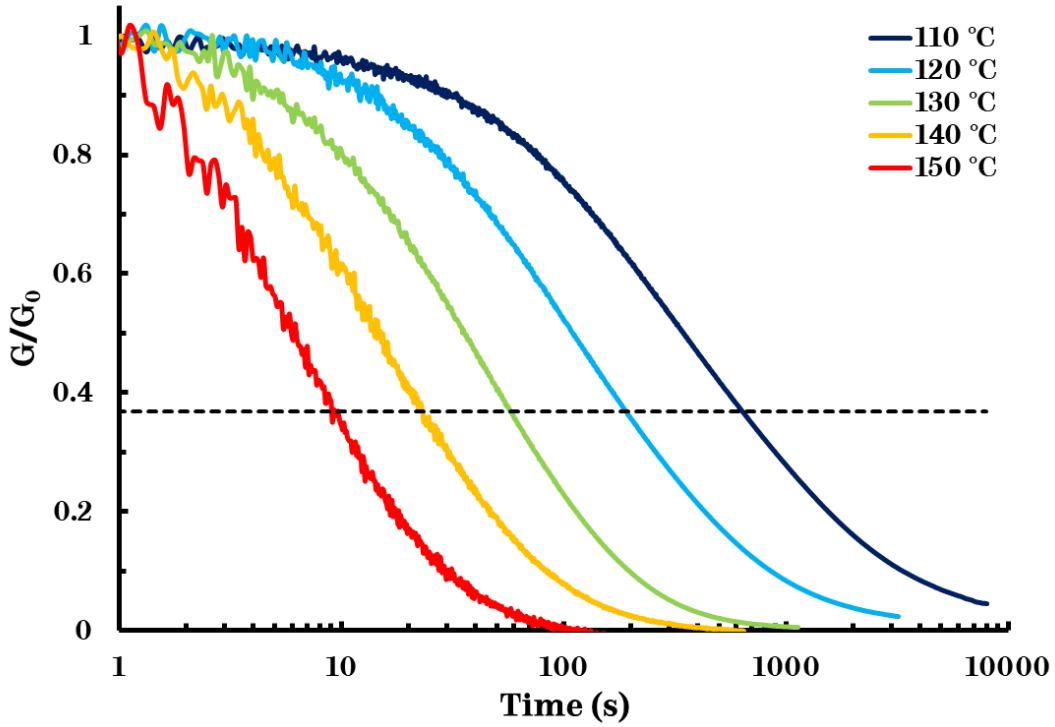

*Figure 33: Stress-relaxation data of **10FMA20-BMI2** at different temperatures.*

DMTA was also performed on both **10FMA20-BMI2** and **40FMA20-BMI2** (*Figure 34, Figure 35*). For both networks, the storage modulus (*G'*) remains >1 GPa below 0 °C. The T_g can be defined as the midpoint of the *G'* inflection and was significantly higher for both networks when compared to the values obtained using DSC analysis. This is expected since the T_g depends on the measuring technique and heating rate. Moreover, a lower heating rate generally yields a higher T_g (10 °C.min^{-1} *vs.* 3 °C.min^{-1}). Another finding worth mentioning is the plateau of the storage modulus in the range of 55-95 °C. This rubbery plateau storage modulus (G'_{rubber}) approximated 3.5 MPa for **10FMA20-BMI2** and 4.0 MPa for **40FMA20-BMI2**.

Above this range, a clear dissociation of the network become apparent which ultimately leads to a significant drop in *G'* and decreased signal-to-noise ratio in *G"*. Furthermore, the decrease in *G'* above 100 °C is less pronounced in **40FMA20-BMI2**

as a consequence of the additional chain entanglements resulting from the higher molecular weight prepolymers. This G'_{rubber} can be used to calculate M_c *via Equation 7:*

$$M_c = \frac{\rho RT}{G'_{rubber}} \quad (7)$$

Where ρ is the density of the PEHMA matrix (approx. 0.9 g.mL^{-1}), R is the gas constant (8.314 J.mol^{-1} .K^{-1}) and T is the average temperature at which G'_{rubber} was measured (approx. 75 °C).[174, 190, 191] Using *Equation 7*, a similar M_c of 744 g.mol^{-1} and 651 g.mol^{-1} was found for **10FMA20-BMI2** and **40FMA20-BMI2**, respectively. Moreover, the small difference in G'_{rubber} and consequently M_c can be rationalised by the small difference in $F_{\%FMA}$ and thus cross-link density of both networks (*Table 7*).

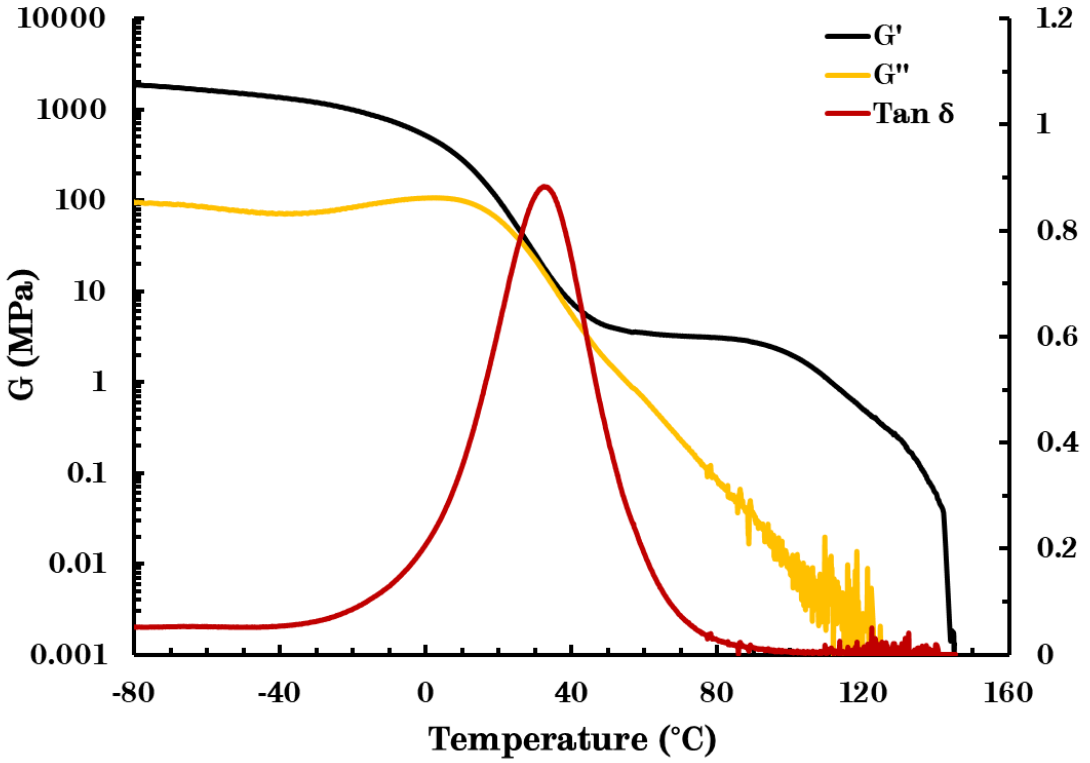

*Figure 34: Storage modulus, loss modulus and tan δ of results of **10FMA20-BMI2** measured via DMTA (Heating rate 3 °C.min^{-1}).*

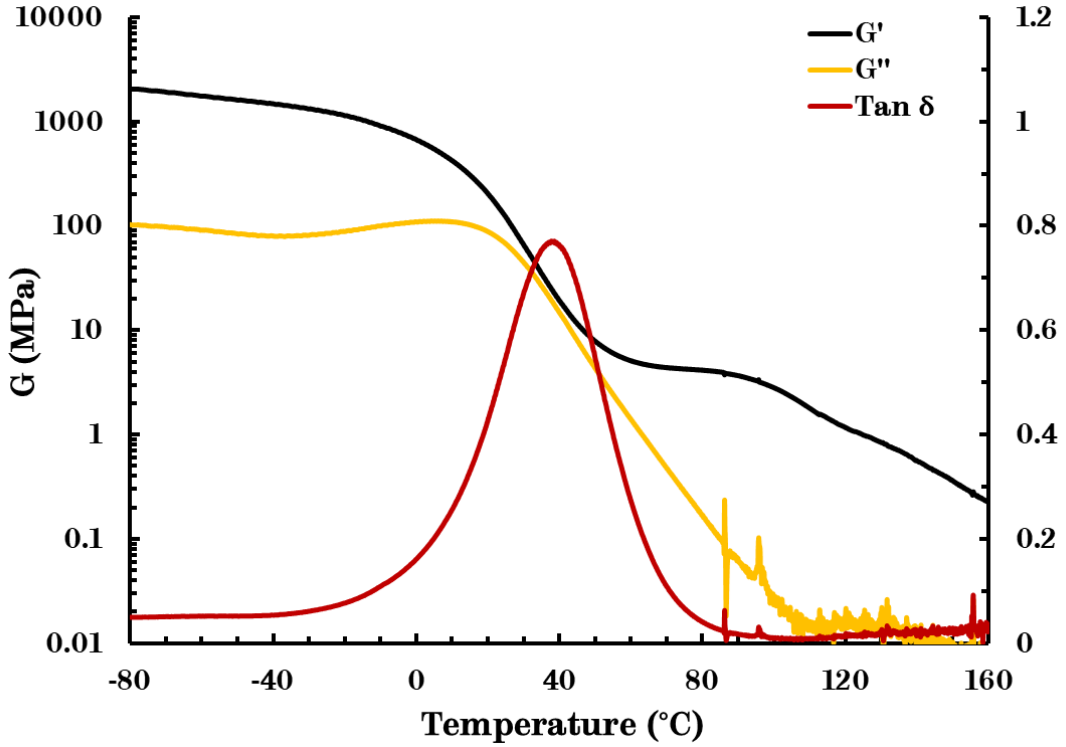

*Figure 35: Storage modulus, loss modulus and tan δ of results of **40FMA20-BMI2** measured via DMTA (Heating rate 3 °C.min^{-1}).*

2.3.4 Mechanical Properties

Tensile testing was performed to assess the mechanical properties of the prepared networks. Furthermore, the properties that were investigated were the Young's modulus (E), the stress at break (σ_b) and elongation at break (ε_b). The data suggest an approximate linear correlation between E and composition together with an approximate inverse correlation between ε_b and composition (*Table 8*, *Figure 36*). Thus, the stiffness of the material increases linearly with cross-link density (composition). Moreover, the σ_b range of 1-3 MPa is lower and the ε_b range of 155-441% is higher than the reported values of 8 MPa and 30% of furan/maleimide networks based on low molecular weight PEHMA (M_n = 5.9 kg.mol^{-1}), which may be the result of the significantly higher incorporation of functional groups (50 mol.%).[172]

Cross-referencing the tensile properties with the results of the previously discussed solubility experiments (cross-link density) leads to the conclusion that the network integrity of **10FMA5-BMI2** is partially lost as a consequence of a significant fraction of material not cross-linked due to the low average number of functional groups on the prepolymer chains, which is apparent in the lower σ_b and higher ε_b. However, **10FMA5-BMI2** does not show an identical elastic behaviour as homopolymer PEHMA (ε_b > 1100%).[170]

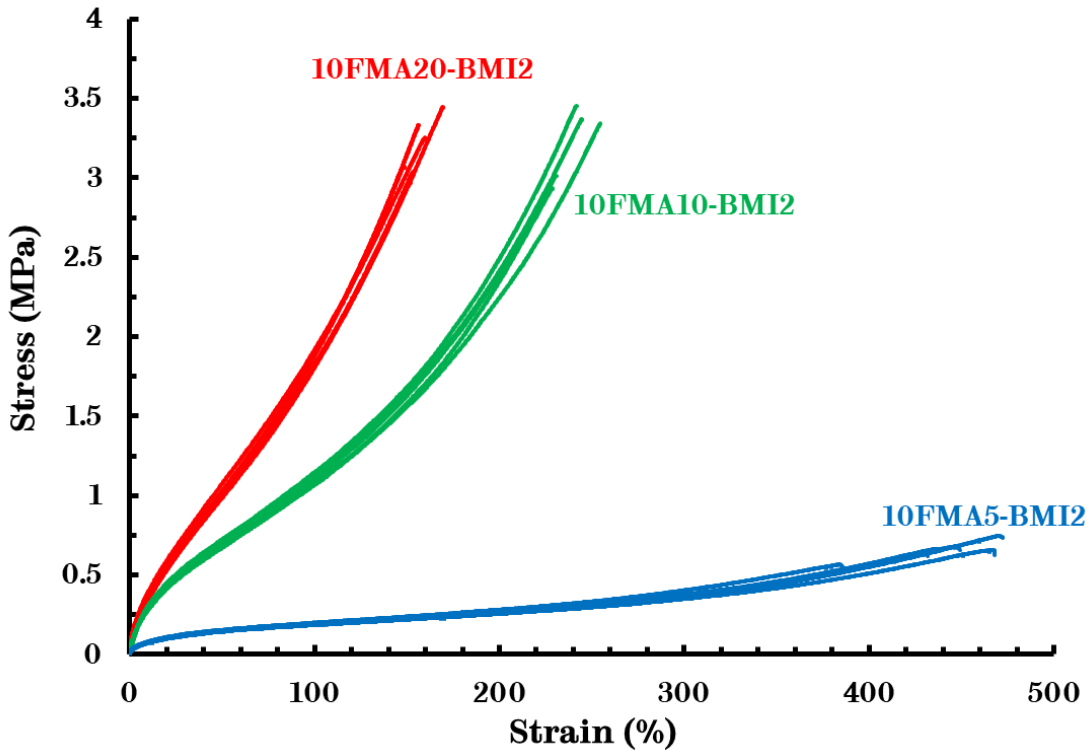

Figure 36: Stress-strain curves of the networks based on poly(EHMA-co-FMA) with a targeted molecular weight M_n = 10 kg.mol^{-1} and different FMA concentrations.

A similar linear trend between stiffness and cross-link density (composition) is observed for the networks based on the higher molecular weight copolymers (*Figure 37*). Furthermore, the networks based on the higher molecular weight copolymers exhibit an increased *E* range of 16-67 MPa when compared to the networks based on the lower molecular weight copolymers, which may result from the reinforcement

of the chemical cross-links by the physical chain entanglements (*Table 8*). Further, this is a significant improvement over the value of $E = 5 \pm 1$ MPa, reported for the homopolymer PEHMA (M_n = 53 kg.mol^{-1}).[170] However, these tensile properties are exceeded by the values reported by Kavitha *et al.* for their furan/maleimide system based on a poly(furfuryl methacrylate)-*b*-poly-(2-ethylhexyl acrylate)-*b*-poly(furfuryl methacrylate) (FEF) triblock copolymers (M_n = 27.7–52.9 kg.mol^{-1}), cross-linked with the aromatic **BMI1**.[192] These Diels-Alder networks exhibit a E range of 8.2-265.7 MPa, a σ_b range of 3.0-35.4 MPa and a ε_b range of 42.8-15.9%. This difference in tensile properties can be rationalised by the difference in used cross-linker (aliphatic **BMI2** *vs.* aromatic **BMI1**) and the significantly higher FMA content (32-64 mol.%).

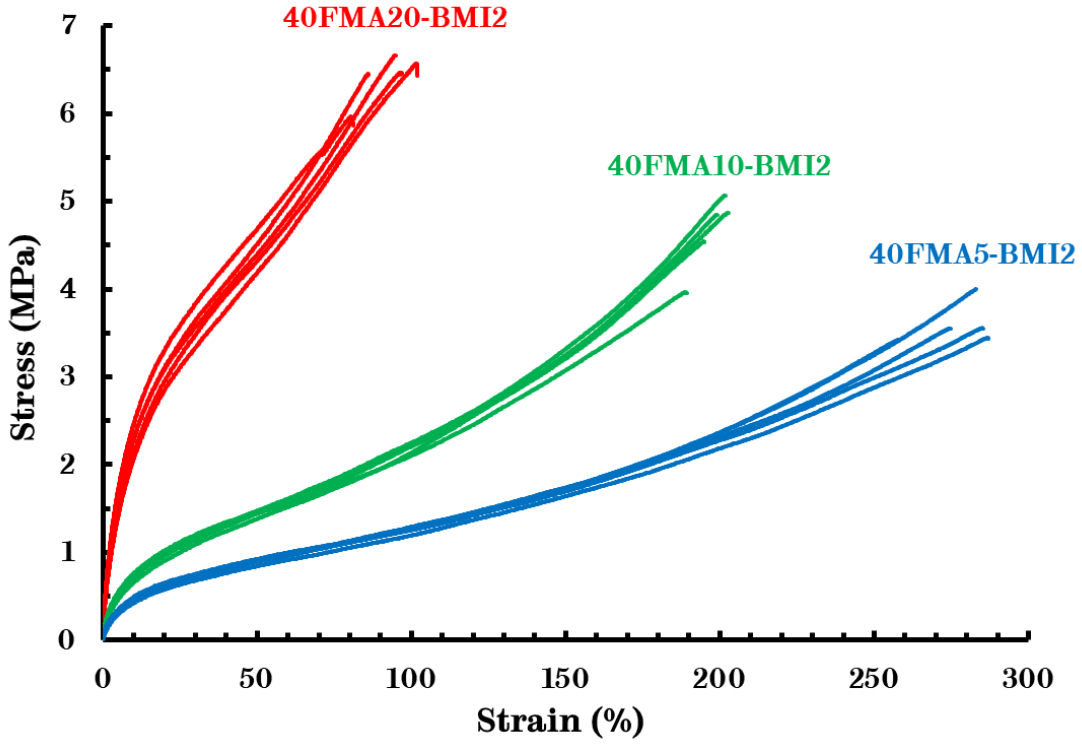

Figure 37: Stress-strain curves of the networks based on poly(EHMA-co-FMA) with a targeted molecular weight M_n = 40 kg.mol^{-1} and different FMA concentrations.

Table 8: Tensile testing results of the networks based on poly(EHMA-co-FMA) with different targeted molecular weights and concentrations of FMA.

Name	M_n (kg.mol^{-1})[a]	$F_{\%FMA}$[b]	E (MPa)	σ_b (MPa)	ε_b (%)
10FMA5-BMI2	**9.8**	**5.1**	**4.13 ± 0.16**	**0.64 ± 0.02**	**441 ± 13**
10FMA10-BMI2	**10.6**	**10.1**	**6.96 ± 0.52**	**3.22 ± 0.10**	**240 ± 5**
10FMA20-BMI2	**12.7**	**19.6**	**13.16 ± 0.48**	**3.16 ± 0.09**	**155 ± 4**
40FMA5-BMI2	**44.9**	**5.4**	**16.16 ± 0.11**	**3.59 ± 0.11**	**278 ± 5**
40FMA10-BMI2	**38.2**	**9.9**	**27.99 ± 1.01**	**4.65 ± 0.20**	**198 ± 2**
40FMA20-BMI2	**40.4**	**22.2**	**66.52 ± 2.86**	**6.02 ± 0.48**	**92 ± 4**

[a]Measured via SEC ($CHCl_3$, PMMA standards). [b]Calculated from ^{1}H NMR spectroscopy.

2.3.5 Ageing

Weathering experiments were conducted on both **10FMA20-BMI2** and **40FMA20-BMI2** to investigate the long-term stability of the material. The samples were aged at 80 °C for 3 weeks and their tensile properties were tested again. It should be highlighted that at this temperature the storage modulus (*G'*) is in the plateau region from DMTA and below the temperature where the rDA reaction occurs (*vide supra*). For both networks, mechanical properties appear to be enhanced after ageing, namely the *E* of **10FMA20-BMI2** and **40FMA20-BMI2** increased by 136% and 112%, respectively (*Table 9*). Further, a clear trend is visible where both networks become stiffer (higher *E*, lower ε_b) (*Figure 38, Figure 39*). This effect can be rationalised by a post-cure occurring in the Diels-Alder networks at 80 °C.

FTIR spectroscopy of both **10FMA20-BMI2** and **40FMA20-BMI2** was performed before and after ageing to investigated possible side reaction or degradation. The IR spectra of **10FMA20-BMI2** are nearly identical, indicating no degradation of the sample (*Figure 40*). The IR spectra of **40FMA20-BMI2** are also similar although there is a small difference in the region 500-700 cm^{-1} (*Figure 41*), which may relate to

changes in the furan ring due to the side reaction that can occur at elevated temperatures (*vide supra*).[180-185]

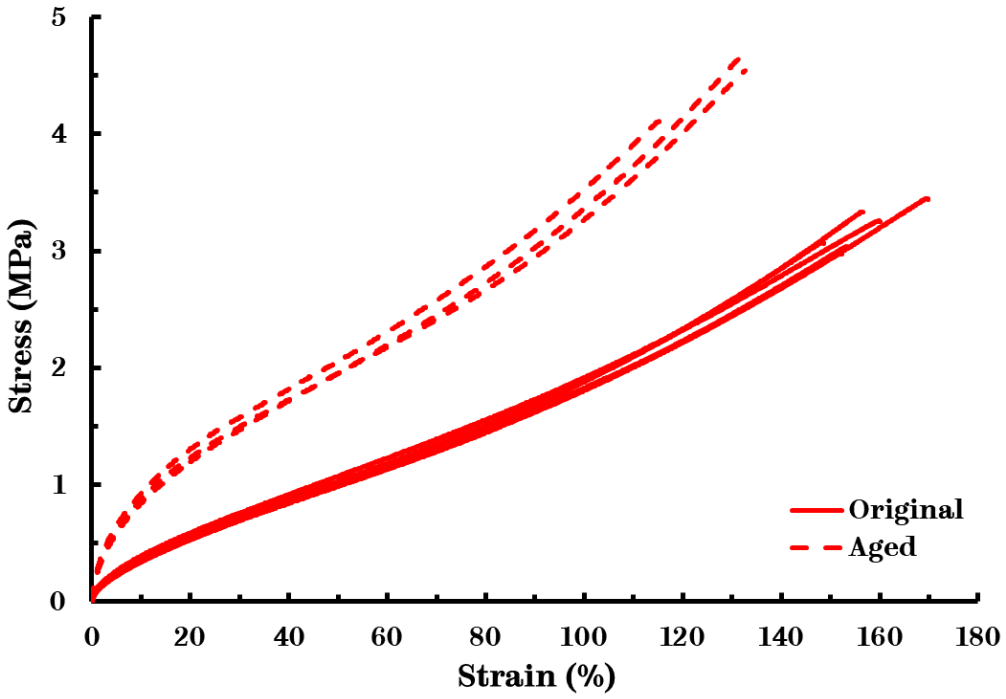

*Figure 38: Stress-strain curves of **10FMA20-BMI2** before and after ageing at 80 °C for 3 weeks.*

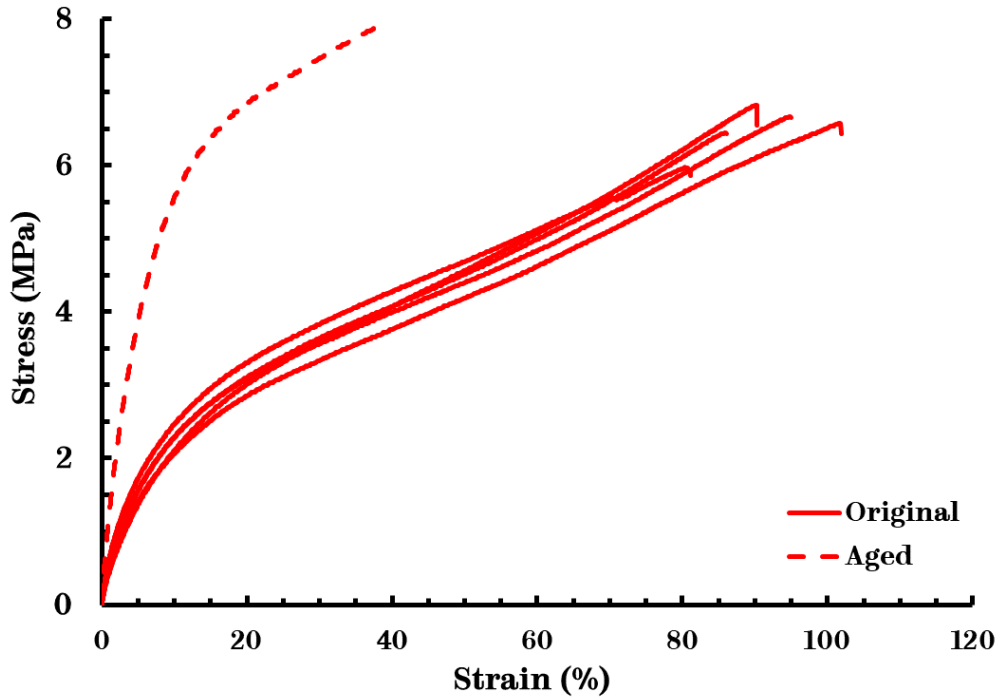

*Figure 39: Stress-strain curves of **40FMA20-BMI2** before and after ageing at 80 °C for 3 weeks.*

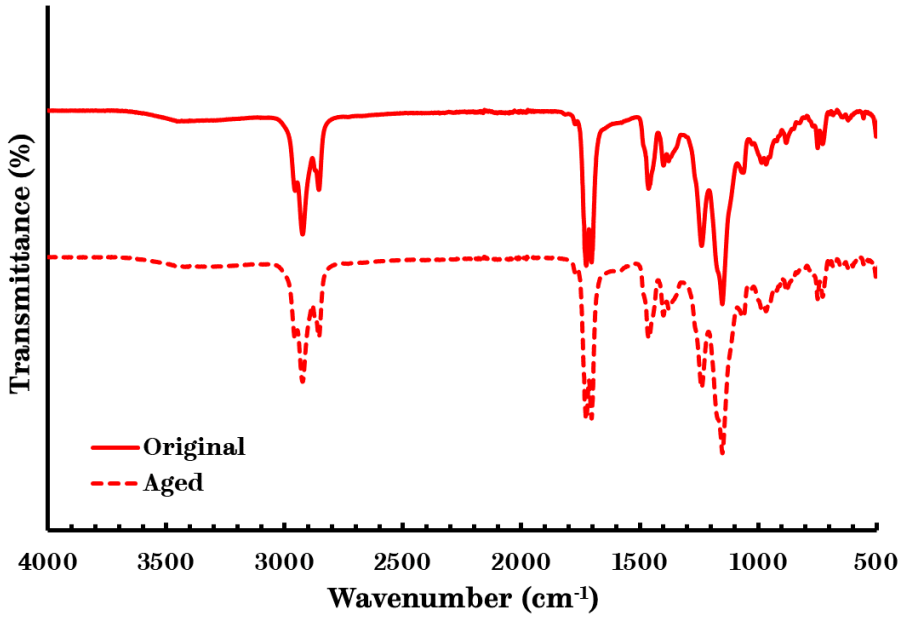

*Figure 40: IR spectrum of **10FMA20-BMI2** before and after ageing at 80 °C for 3 weeks.*

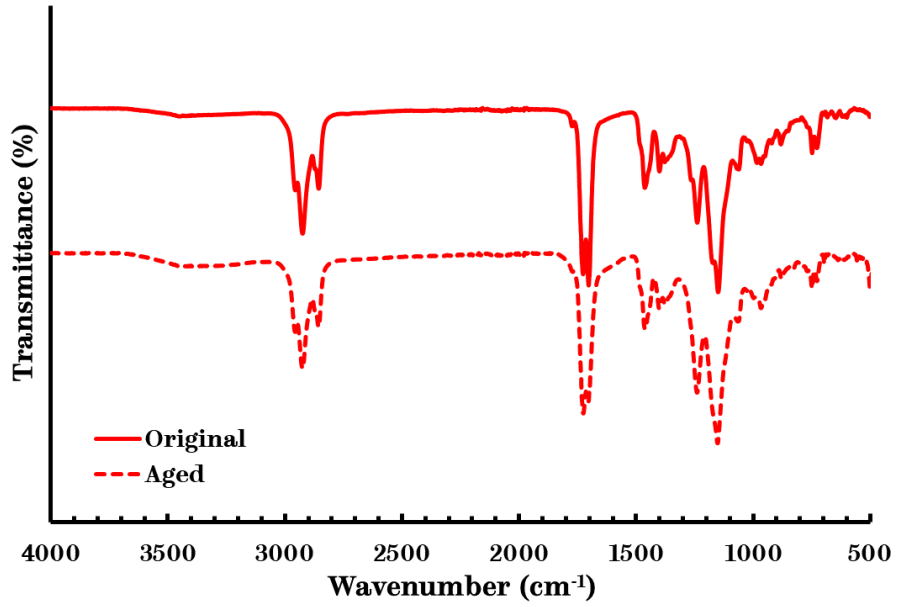

*Figure 41: IR spectrum of **40FMA20-BMI2** before and after ageing at 80 °C for 3 weeks.*

Table 9: Tensile testing results of the networks based on poly(EHMA-co-FMA) before and after ageing at 80°C for 3 weeks.

	Name	***M_n*** **(kg.mol^{-1})[a]**	***$F_{\%FMA}$*** **[b]**	***E*** **(MPa)**	**σ_b (MPa)**	**ε_b (%)**
Original	**10FMA20-BMI2**	**12.7**	**19.6**	**13.16 ± 0.48**	**3.16 ± 0.09**	**155 ± 4**
Aged				**31.00 ± 1.25**	**4.43 ± 0.17**	**127 ± 6**
Original	**40FMA20-BMI2**	**40.4**	**22.2**	**66.52 ± 2.86**	**6.02 ± 0.48**	**92 ± 4**
Aged				**141.18**	**7.82**	**38**

[a]Measured via SEC ($CHCl_3$, PMMA standards). [b]Calculated from ^{1}H NMR spectroscopy.

2.3.6 Recyclability

In order to test the recyclability of the prepared networks, tensile testing was performed on repeatedly reprocessed samples (recycles) and the results were compared to the pristine material (Original) (*Figure 42*).

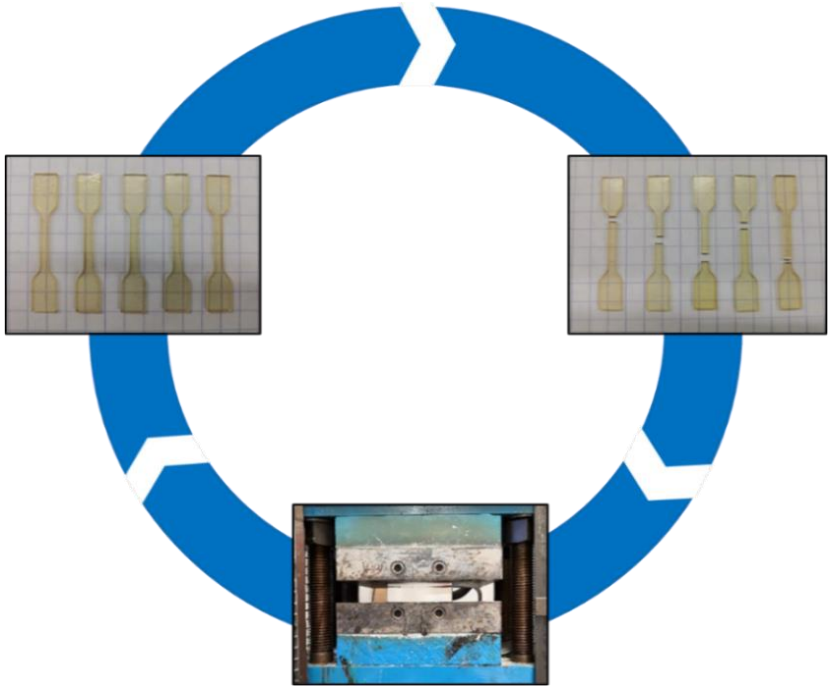

Figure 42: Schematic of the recycling process.

Due to time constraints towards the end of the project, only one recycle (R1) was performed on **10FMA20-BMI2** and **40FMA20-BMI2** and two recycles (R2) on **40FMA10-BMI2** (*Table 10*).

Table 10: Reprocessing parameters of the Diels-Alder networks based on poly(EHMA-co-FMA) with different molecular weights and concentration of FMA.

	Name	***M_n*** **(kg.mol^{-1})[a]**	***$F_{\%FMA}$*** **[b]**	***P*** **(bar)**	***Temp.*** **(°C)**	***Time*** **(min)**
Original	**10FMA20-BMI2**	**12.7**	**19.6**	**40**	**150**	**5**
R1				**40**	**150**	**3**
Original	**40FMA10-BMI2**	**38.2**	**9.9**	**30**	**140**	**5**
R1				**30**	**150**	**10**
R2				**30**	**150**	**12**
Original	**40FMA20-BMI2**	**40.4**	**22.2**	**40**	**160**	**20**
R1				**40**	**150**	**20**

[a]Measured via SEC ($CHCl_3$, PMMA standards). [b]Calculated from ^{1}H NMR spectroscopy.

The reprocessing parameters of **10FMA20-BMI2** and **40FMA20-BMI2** were approximately the same as the original processing parameters, indicating a good recyclability of the samples. After R1, the *E* of **10FMA20-BMI2** and **40FMA20-BMI2** increased by 352% and 76%, respectively. After R1, the *E* of **40FMA10-BMI2** increased by 13%. However, after R2, the *E* remained the same (*Table 11*).

Table 11: Results of the tensile testing of the networks based on poly(EHMA-co-FMA) with different targeted molecular weights and with different concentrations of FMA before and after recycling.

	Name	M_n (kg.mol^{-1})[a]	$F_{\%FMA}$[b]	***E*** (MPa)	σ_b (MPa)	ε_b (%)
Original	**10FMA20-BMI2**	**12.7**	**19.6**	**13.16 ± 0.48**	**3.16 ± 0.09**	**155 ± 4**
R1				**59.53 ± 2.12**	**6.41 ± 0.50**	**134 ± 7**
Original	**40FMA10-BMI2**	**38.2**	**9.9**	**27.99 ± 1.01**	**4.65 ± 0.20**	**198 ± 2**
R1				**31.69 ± 1.47**	**3.87 ± 0.13**	**175 ± 5**
R2				**28.02 ± 0.61**	**3.89 ± 0.18**	**199 ± 4**
Original	**40FMA20-BMI2**	**40.4**	**22.2**	**66.52 ± 2.86**	**6.02 ± 0.48**	**92 ± 4**
R1				**116.85 ± 9.53**	**7.88 ± 0.28**	**84 ± 4**

[a]Measured via SEC ($CHCl_3$, PMMA standards). [b]Calculated from ^1H NMR spectroscopy.

A clear trend is visible with the samples showing an increased *E* in a similar fashion to the aged samples (*Figure 43, Figure 44*). However, the ε_b is largely maintained for the recycled materials in contrast to the aged samples indicating the material became tougher rather than stiffer. This toughening could again be a consequence of a post-curing effect during recycling.

Recyclability was also tested for **40FMA10-BMI2**, but in this case the material was recycled twice. Contrary to **40FMA20-BMI2**, the recycled material was nearly identical to the pristine material after two recycles (*Figure 45*). This may be a result of the less stringent processing parameters (lower temperature and shorter time) required for these materials. Furthermore, FTIR spectroscopy of **40FMA10-BMI2** confirmed little degradation occurred during recycling (*Figure 46*).

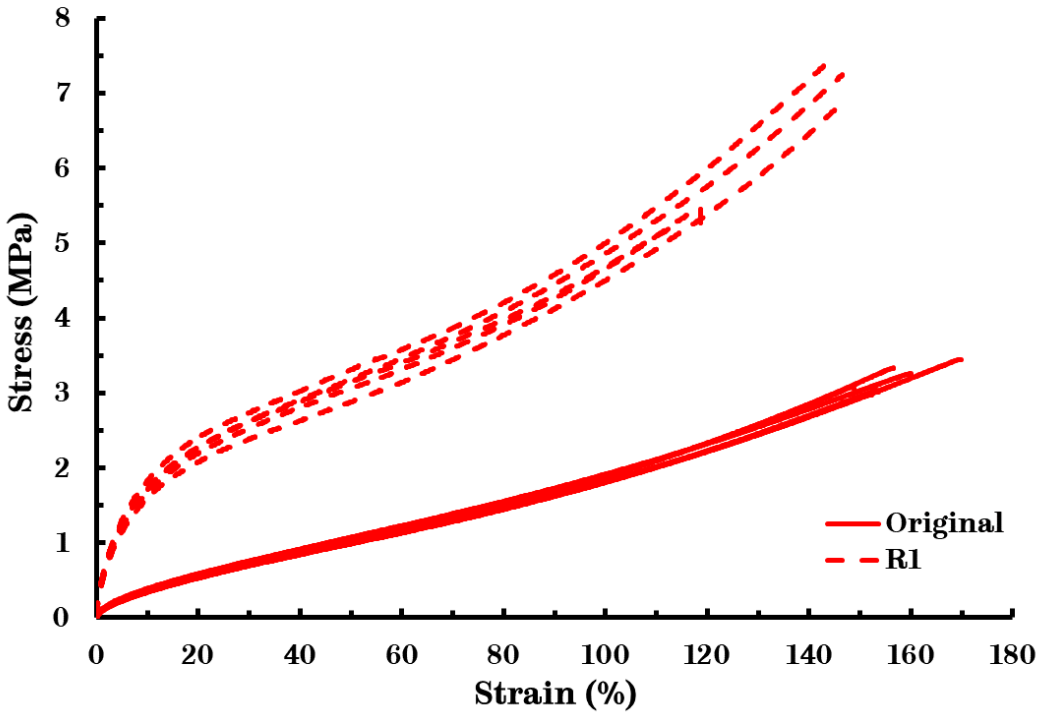

*Figure 43: Stress-strain curves of **10FMA20-BMI2** before and after recycling.*

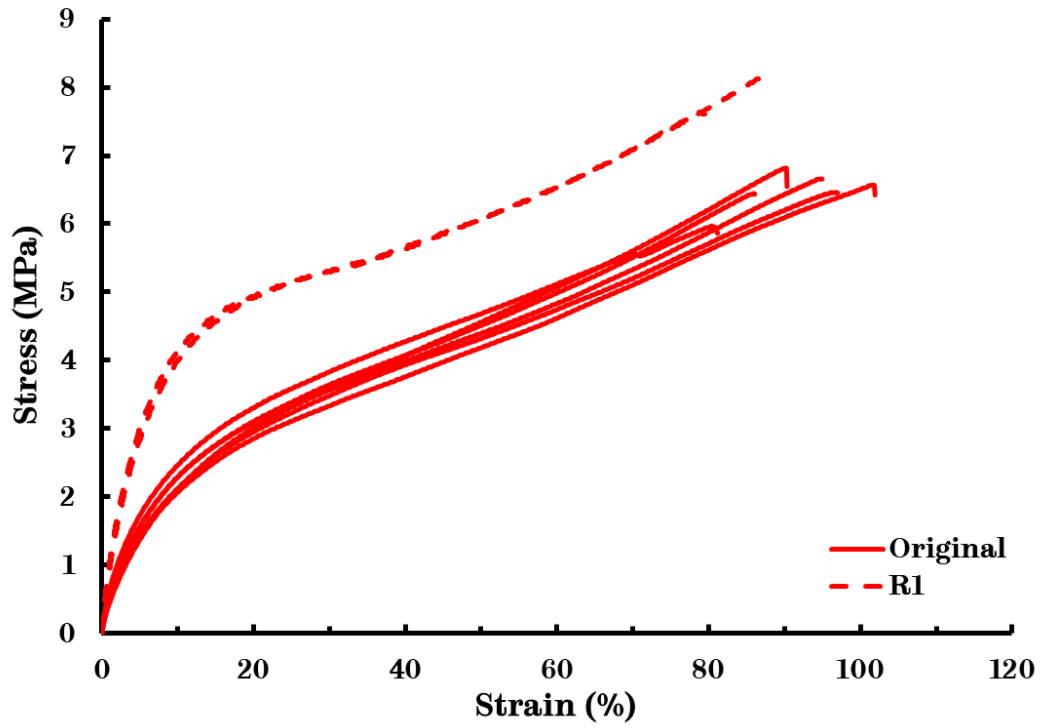

*Figure 44: Stress-strain curves of **40FMA20-BMI2** before and after recycling.*

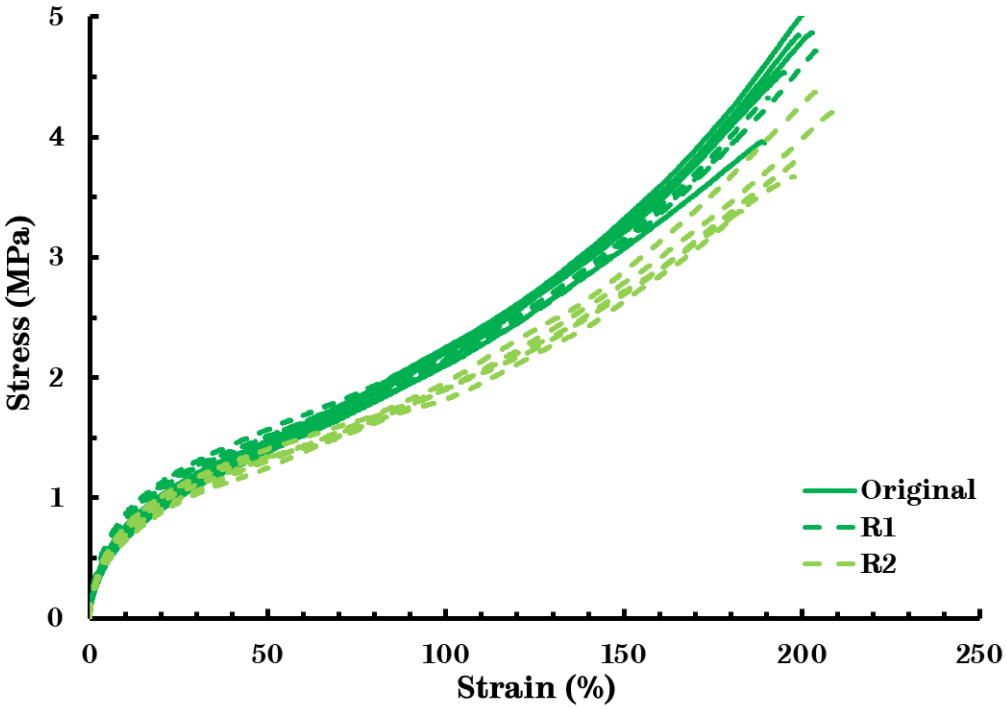

*Figure 45: Stress-strain curves **40FMA10-BMI2** before and after recycling.*

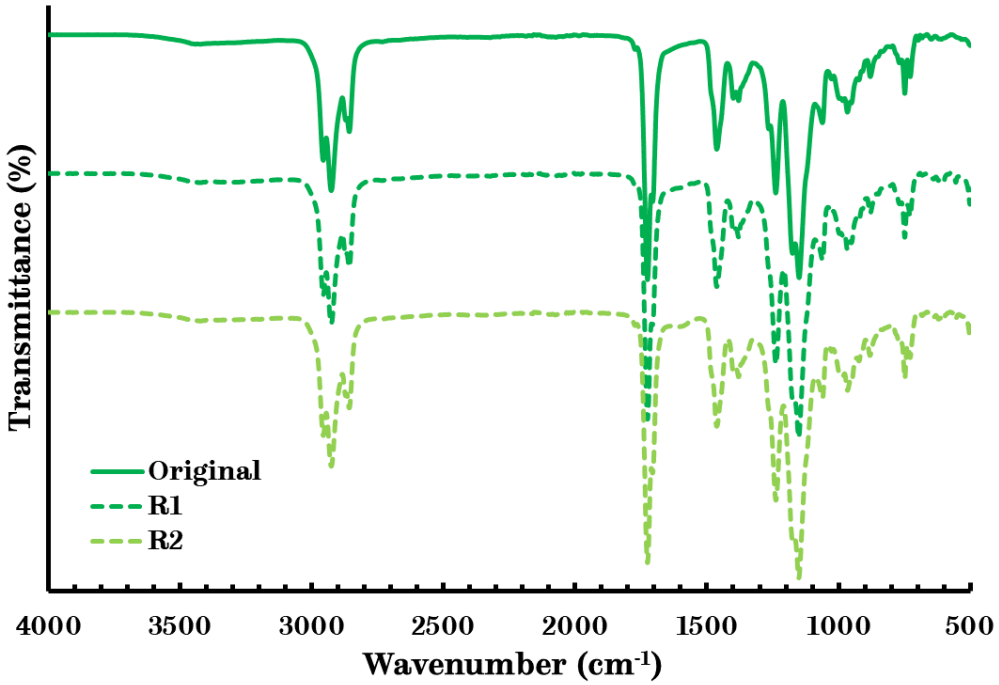

*Figure 46: IR spectrum of **40FMA10-BMI2** before and after recycling.*

2.4 Conclusion

Functional copolymers were synthesised based on EHMA and varying concentrations of FMA (5-20 mol.%). Next, these copolymers were cross-linked with a flexible aliphatic cross-linker BMI2 to obtain homogeneous networks comprising Diels-Alder adducts. Compression moulding was used to prepare different geometries by varying the processing parameters (temperature, time and pressure). Further, the different material properties of these networks were characterised. An increased thermal stability above 300 °C was found and the cross-linker moiety lowered the T_g compared to the prepolymers. The obtained low soluble fractions (6-13%) are indicative of good network formation, unless the average number of functional groups per chain was below the threshold value for this type of chemistry. Next, the solubility data suggested that the degree of swelling is only dependent on the number of cross-links per unit volume (cross-link density). Further, the thermoreversibility of the cycloaddition reaction was confirmed *via* rheological experiments. Finally, the tensile properties were tested on the pristine samples (E = 4-67 MPa), after ageing at 80 °C for 3 weeks (E = 31-141 MPa) and after recycling (E = 28-117 MPa). Here, an increased stiffness was observed, which may be the result of a post-cure effect.

Chapter 3 Vinylogous Urethane – Associative type

3.1 Functional copolymers

As previously discussed in *Chapter 2 Diels-Alder – Dissociative type*, *n*-butyl acrylate (BA) and lauryl methacrylate (LMA) were initially tested as the main comonomers. However, for the same reasons explained in *Chapter 2 Diels-Alder – Dissociative type*, these were no longer investigated and 2-ethylhexyl methacrylate was employed for all experiments to facilitate the comparison between the different functional copolymers and resulting networks.

EHMA was copolymerised with acetoacetoxyethyl methacrylate (AEMA) to incorporate a pendant acetoacetoxy moiety in the polymer backbone (*Figure 47*). This functional group can then undergo a condensation reaction with a primary amine to form a vinylogous urethane as a cross-linking bond in the network. Different functional copolymers were synthesised in order to assess the influence of both molecular weight and composition.

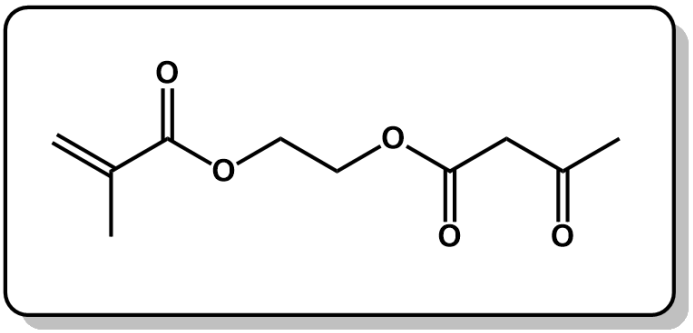

Figure 47: Structure of functional comonomer acetoacetoxyethyl methacrylate (AEMA).

Different number average molecular weights (M_n) of 10 and 40 kg.mol^{-1} were targeted in order to determine the influence of the molecular weight on the properties of the

copolymers and resulting networks. These values are the same as the functional copolymers comprising furfuryl methacrylate (FMA), which allows for an optimal comparison of the copolymers and resulting networks. Since EHMA was incorporated as the main comonomer, the same influence of chain entanglements was expected. In order to control the molecular weight, the same chain transfer agent, *n*-dodecyl mercaptan (DDM), was used as in the copolymerisation of EHMA and FMA.

The nomenclature for the functional copolymers comprises of an initial number referring to the targeted molecular weight in kg.mol^{-1} (*e.g.* 10), followed by the name of the incorporated functional comonomer (*e.g.* AEMA) and ending in the targeted composition of this comonomer in mol.% (*e.g.* 5) (*vide supra*). For example, 10AEMA5 is a 10 kg.mol^{-1} PEHMA with 5 mol.% incorporation of AEMA. This nomenclature was employed to facilitate the discussion of the experimental results.

Table 12: Free-radical copolymerisation of poly(EHMA-co-AEMA) using different concentrations of I and CTA to control molecular weight.

Name	$f_{\%EHMA}$[a]	$f_{\%AEMA}$[a]	***[I]*** **(mol.L^{-1})**	***[CTA]*** **(mol.L^{-1})**	***[CTA]/[M]***	M_n **(kg.mol^{-1})**[b]	$Đ_M$[b]
10AEMA3	**97**	**3**	**0.003**	**0.057**	**0.014**	**10.3**	**1.7**
40AEMA2	**98**	**2**	**0.001**	**0.008**	**0.002**	**48.8**	**2.1**
10AEMA5	**95**	**5**	**0.003**	**0.062**	**0.014**	**10.5**	**1.8**
40AEMA5	**95**	**5**	**0.001**	**0.010**	**0.002**	**39.0**	**2.2**
10AEMA10	**90**	**10**	**0.003**	**0.059**	**0.013**	**11.3**	**1.8**
40AEMA10	**90**	**10**	**0.001**	**0.010**	**0.002**	**43.8**	**2.2**
10AEMA20	**80**	**20**	**0.003**	**0.053**	**0.012**	**10.1**	**2.2**
40AEMA20	**80**	**20**	**0.002**	**0.009**	**0.002**	**68.5**	**2.9**

[a]*Feed ratio in mol.%.* [b]*Measured via SEC ($CHCl_3$, PMMA standards).*

Different concentrations of initiator azobisisobutyronitrile (AIBN) and DDM were tested to obtain the targeted molecular weights (*Table 12*). The same stepwise scale-up was performed as for the copolymerisation reaction of poly(EHMA-*co*-FMA),

namely from approximately 6 g to over 100 g. In most cases, the molecular weight achieved were close to those targeted (*i.e.* 10-40 kg.mol^{-1}), the exception being **40AEMA2** and **40AEMA20**. This may be the result of a weighing error of AIBN, sub-optimal initiation or inefficient CTA as a consequence of the higher bulk viscosity at higher conversions. Most copolymers were made to high conversion (approx. 70-90%) within 3-4 hours and dispersities ($Đ_M$) obtained were typically in the range of 1.7-2.2.

The molecular weights were determined with size exclusion chromatography (SEC) using $CHCl_3$ as an eluent. The SEC chromatograms of both copolymers with different molecular weight targets (M_n = 10-40 kg.mol^{-1}) were mostly monomodal and close to Gaussian distribution (*Figure 48, Figure 49*).

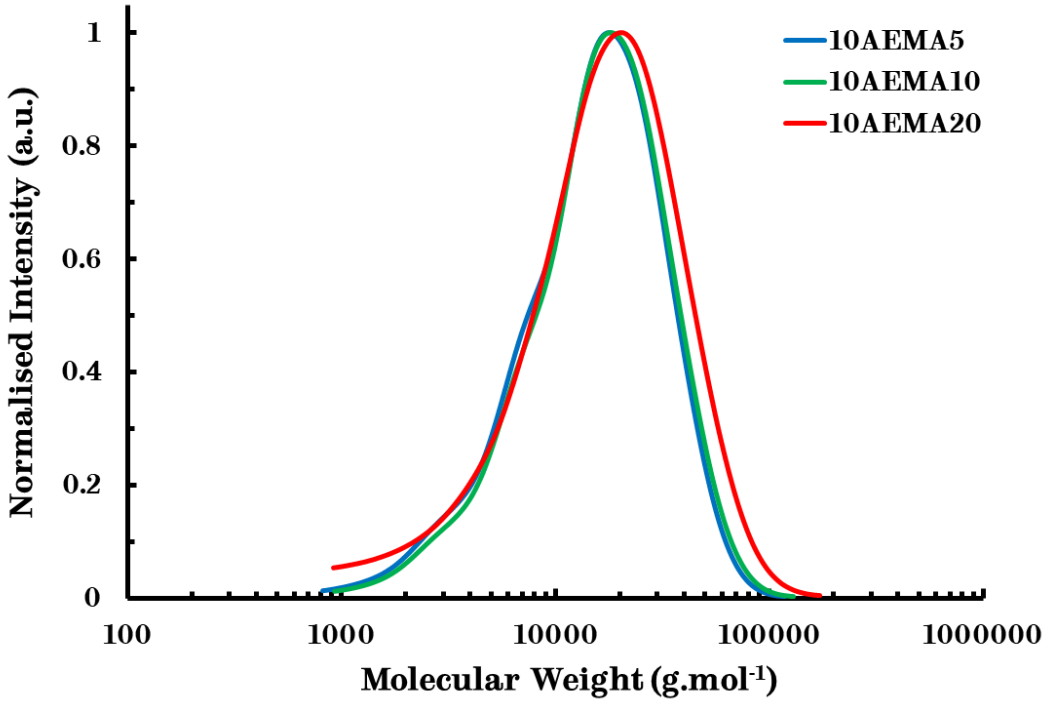

Figure 48: SEC chromatogram of poly(EHMA-co-AEMA) with a targeted molecular weight M_n = 10 kg.mol^{-1} and different AEMA concentrations ($CHCl_3$, PMMA standards).

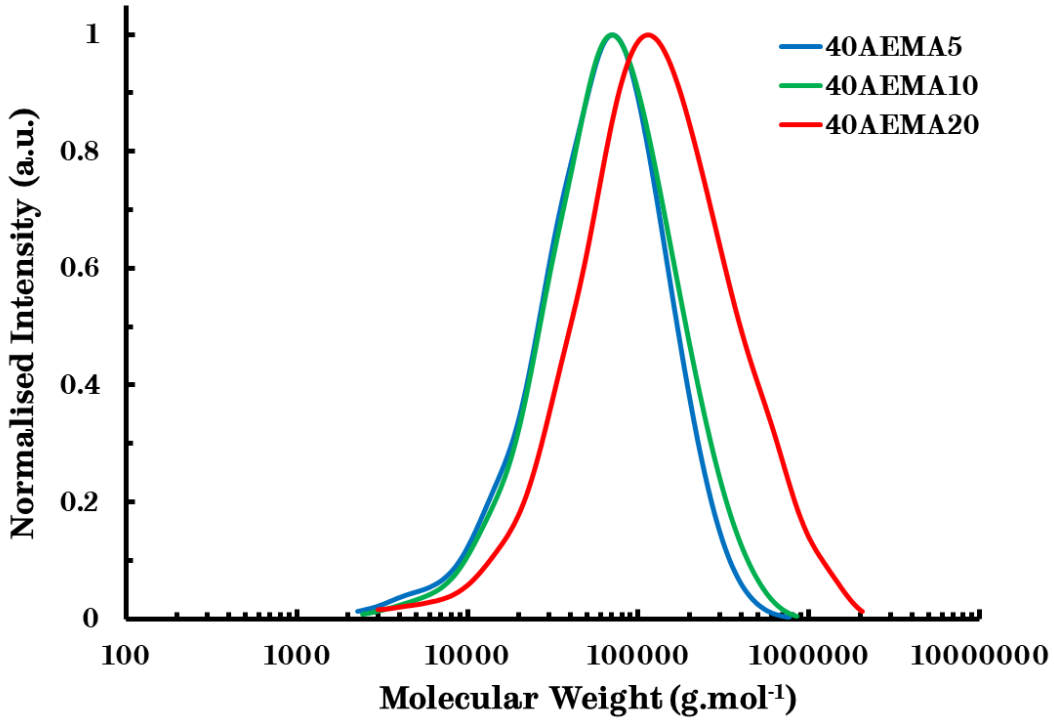

Figure 49: SEC chromatogram of poly(EHMA-co-AEMA) with a targeted molecular weight M_n = 40 kg.mol^{-1} and different AEMA concentrations ($CHCl_3$, PMMA standards).

Initially, the same chemical composition of the previously discussed poly(EHMA-*co*-FMA) were selected, namely 2, 5 and 10 mol.%, to determine the influence of the prepolymer composition and resulting network cross-link density on their performance. The 2 mol.% composition was not used for further experiments as a consequence of the cross-link density of the resultant network being too low and the network completely dissolving in solvent. 20 mol.% AEMA copolymers were synthesised in order to gain more information on the effect of increased cross-linking in the networks.

^{1}H NMR spectroscopy was used to determine the content of AEMA incorporated into the backbone (*Figure 50*). The relevant resonances used for this calculation were the methylene proton resonances adjacent to the ester at chemical shifts δ = 3.9-4.04 ppm for copolymerised EHMA and the signals at δ = 4.2-4.4 ppm corresponding to copolymerised AEMA. Both of these resonances correspond to the same number of

protons, namely 2 (-OCH_2-), so the relative ratio of the integration of these resonances can be used directly to determine the composition. Furthermore, this relative ratio can be converted into a percentage ratio using $Ratio_{Rel}/(1 + Ratio_{Rel})$ (*Table 13*). This percentage can then be used to calculate the average number of functional groups per chain (functionality). Comparable to the poly(EHMA-*co*-FMA) copolymerisation, the data shows that the copolymer compositions ($F_{\%AEMA}$) obtained were similar to the feed ratios with the AEMA content varying in the range of 2.0-20.2 mol.% (*Table 13*).

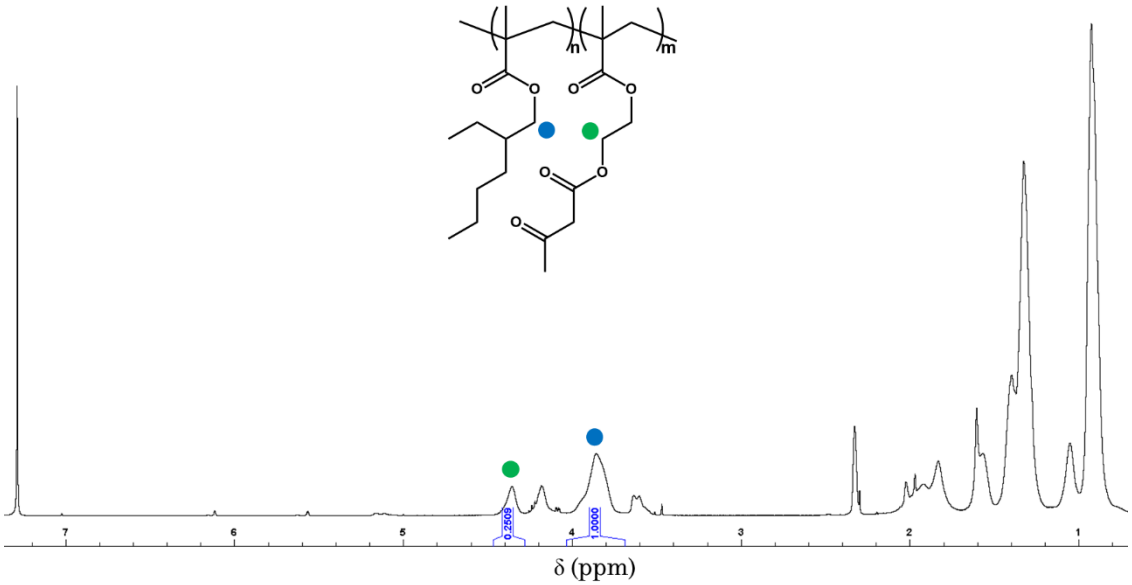

*Figure 50: ^{1}H NMR spectrum of **40AEMA20** (400 MHz, $CDCl_3$, 298 K).*

Table 13: Monomer feed vs. composition and molecular weight of poly(EHMA-co-AEMA).

Name	$f_{\%EHMA}$[a]	$f_{\%AEMA}$[a]	M_n (kg.mol^{-1})[b]	$Đ_M$[b]	$F_{\%AEMA}$[c]
10AEMA3	**97**	**3**	**10.3**	**1.7**	**3.4**
40AEMA2	**98**	**2**	**48.8**	**2.1**	**2.0**
10AEMA5	**95**	**5**	**10.5**	**1.8**	**3.4**
40AEMA5	**95**	**5**	**39**	**2.2**	**3.7**
10AEMA10	**90**	**10**	**11.3**	**1.8**	**9.1**
40AEMA10	**90**	**10**	**43.8**	**2.2**	**10.3**
10AEMA20	**80**	**20**	**10.1**	**2.2**	**17.6**
40AEMA20	**80**	**20**	**68.5**	**2.9**	**20.2**

[a]Feed ratio in mol.%. [b]Measured via SEC ($CHCl_3$, PMMA standards). [c]Calculated from ^{1}H NMR spectroscopy.

Differential scanning calorimetry (DSC) was used to determine the glass transition temperature of the copolymers. The values were calculated from the second heating curve (*Figure 51*, *Figure 52*).

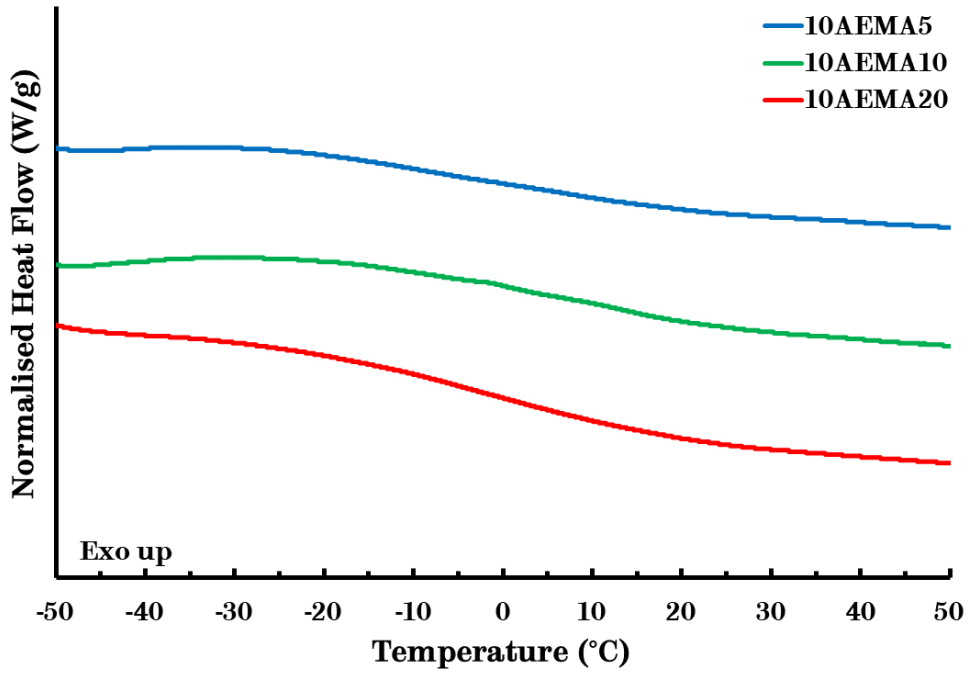

Figure 51: DSC thermograms of poly(EHMA-co-AEMA) with a targeted molecular weight M_n = 10 kg.mol^{-1} and different AEMA content (Second heating curve, heating rate 10 °C.min^{-1}).

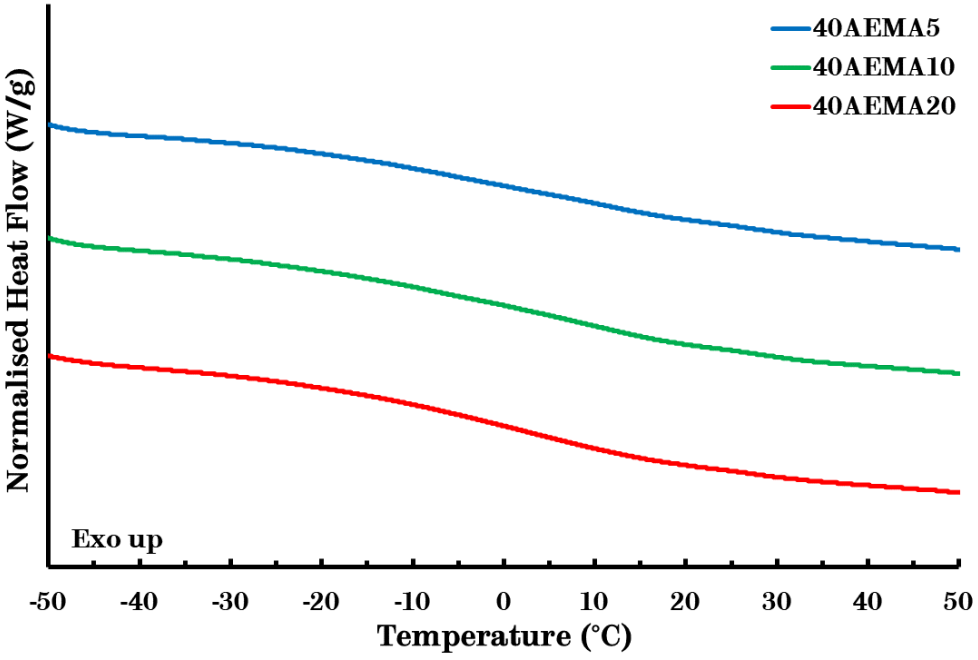

Figure 52: DSC thermograms of poly(EHMA-co-AEMA) with a targeted molecular weight M_n = 40 kg.mol^{-1} and different AEMA content (Second heating curve, heating rate 10 °C.min^{-1}).

The data shows that the T_g of the copolymers is dependent on the composition of the comonomers and increased with AEMA concentration (*Table 14)*.

Table 14: DSC results of poly(EHMA-co-AEMA) comparing the theoretical T_g with the experimental T_g for different concentrations of AEMA.

Name	M_n **(kg.mol^{-1})[a]**	$F_{\%AEMA}$**[b]**	T_g **(°C) Th.[c]**	T_g **(°C) Exp.[d]**
10AEMA5	**10.5**	**3.4**	**-8.7**	**-4.6**
10AEMA10	**11.3**	**9.1**	**-7.4**	**-0.7**
10AEMA20	**10.1**	**17.6**	**-4.8**	**0.6**
40AEMA5	**39.0**	**3.7**	**-8.7**	**3.7**
40AEMA10	**43.8**	**10.3**	**-7.4**	**4.6**
40AEMA20	**68.5**	**20.2**	**-4.8**	**5.7**

[a]Measured via SEC ($CHCl_3$, PMMA standards). [b]Calculated from ^{1}H NMR spectroscopy. [c]Calculated from Flory-Fox equation. [d]Measured via DSC (heating rate 10 °C.min^{-1}).

3.2 Network synthesis

Solvent casting was used to form the cross-linked networks on the same scale of 5 – 20 g as in the synthesis of the dissociative Diels-Alder networks (*vide supra*). Initially, both aromatic and aliphatic cross-linkers were considered to assess the influence of the rigidity of the cross-linker on the material properties. The aromatic *m*-xylylenediamine (**DAM1**) was first investigated as a cross-linker (*Figure 53*). Unlike in the dissociative Diels-Alder networks, these associative vinylogous urethane networks showed no compatibility issues between the cross-linker and the copolymer. Hence, homogeneous, uniform samples were obtained (*Figure 53*). For the aliphatic cross-linkers, different candidates were tested. Initially, either 1,4-diaminopentane, Jeffamine® D400 or Priamine™ 1075 were added to the functional copolymers.

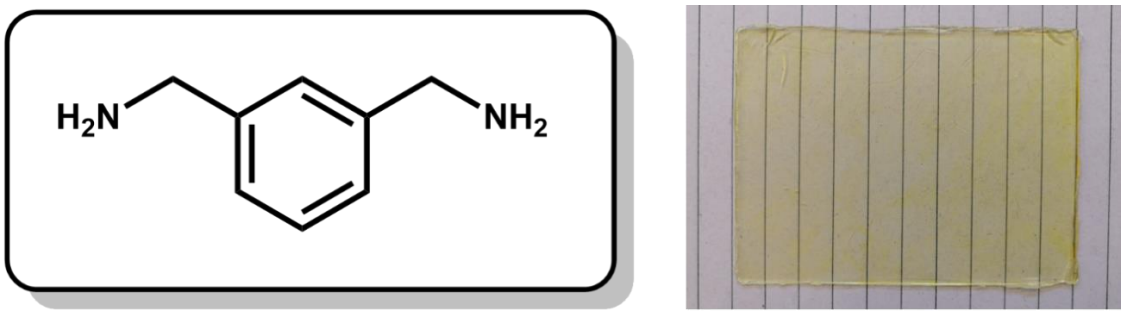

*Figure 53: The structure of m-xylylene diamine (**DAM1**) (left) and a picture of a typical cross-linked network obtained from poly(EHMA-co-AEMA) cross-linked with **DAM1** (right).*

After these preliminary experiments, Priamine™ 1075 (**DAM2**) was selected as the best candidate as a consequence of the cross-linker having the same C_{36} dimer core structure as **BMI2** used with the poly(EHMA-*co*-FMA) copolymers (*Figure 54*). In order to compare the different networks adequately, **DAM2** was employed for all further experiments. This comparison could not be made with the same fidelity for the aromatic cross-linker given the aforementioned compatibility issues with the dissociative networks (*Network Synthesis, Diels-Alder – Dissociative type*). The nomenclature of the networks will be the same as the copolymers, followed by the name of the incorporated cross-linker.

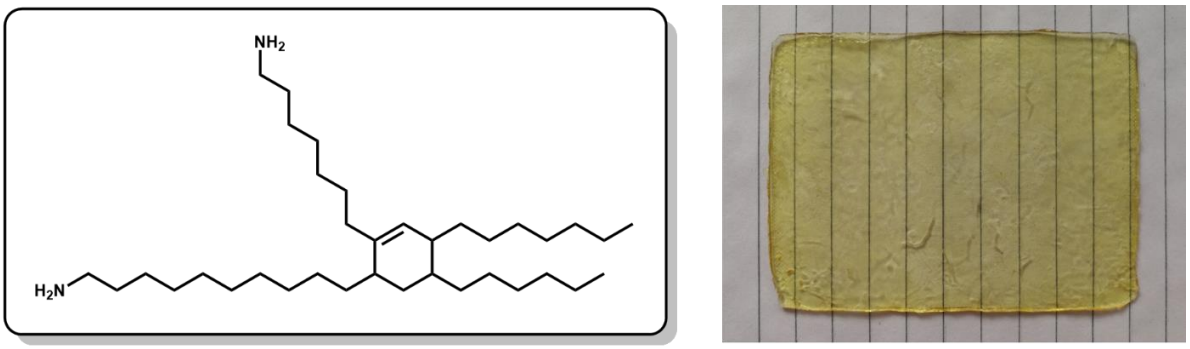

*Figure 54: The structure of Priamine™ 1075 (**DAM2**) (left) and a picture of a typical cross-linked network obtained from poly(EHMA-co-AEMA) cross-linked with **DAM2** (right).*

Contrary to the Diels-Alder networks where only equimolar amounts of cross-linker and incorporated pendant functional groups are required, an excess of amines is necessary for the exchange mechanism of the transamination of vinylogous urethanes (*vide supra*). Initially, 5 and 10 mol.% excess with respect to the

acetoacetoxy groups were tested, similar to the step-growth networks in the seminal work of Denissen *et al.*[124] This enabled the synthesis of the networks based on poly(EHMA-*co*-AEMA) comprising 2, 5 and 10 mol.% AEMA. However, processing of the networks based on the functional copolymers with 20 mol.% AEMA was not feasible (*Figure 55*).

*Figure 55: Inhomogeneous compression moulded plate of **40AEMA20** cross-linked with 10 mol.% of **DAM2**.*

In order to ensure that all networks are prepared with the same amount of cross-linker and to validate their comparison, a larger excess of amine was evaluated. Thus, the excess of cross-linker that was selected to prepared all the networks was 50 mol.% with respect to the acetoacetoxy moieties, similar to the previously reported networks based on poly(methyl methacrylate) (PMMA), which were cross-linked with a triamine tris(2-aminoethyl)amine (TREN).[193] For the removal of the solvent, the duration, temperature and vacuum were determined to minimise spillage and bubble formation (*Table 15*).

Table 15: Drying/curing methods during solvent casting.

	Method 1	Method 2
Step 1	**ambient overnight no vacuum**	**30m at 80 °C no vacuum**
Step 2	**30m at 90 °C 50% vacuum**	**1h at 110 °C 50% vacuum**
Step 3	**1h at 110 °C full vacuum**	**1h at 110 °C full vacuum**

The initial curing step was then followed by compression moulding to obtain homogenous, defect-free samples with a constant thickness. Again, rapid prototyping was done using vacuum compression moulding. This avoided the risk of wasting material and gave initial parameters for the reprocessing of the material. Moreover, the same geometries (*e.g.* disc, bar and plate) could be made for rheological and thermal analysis as in the previously discussed Diels-Alder networks. The three parameters that were systematically altered were temperature, time and pressure. In the case of vacuum compression moulding the pressure was fixed at 1 atm. Custom aluminium moulds were used to ensure fast heating and cooling of the material. Unlike the dissociative Diels-Alder networks, these materials are vitrimers. In this case, processing temperatures influence the exchange kinetics and viscosity gradually according to an Arrhenian model (*vide supra*). During the compression moulding of the previously cured networks based on the lower molecular weight poly(EHMA-*co*-AEMA), the processing temperatures are slightly lower and the processing time is slightly shorter (*Table 16*).

A significantly lower processing pressure, temperature and shorter processing time was found for **10AEMA5-DAM2** and **10AEMA10-DAM2**. This might suggest that the network formation is incomplete, which was later confirmed with solubility

experiments (*vide infra*). For the networks based on the higher molecular weight, the processing temperatures were higher and the processing times longer. These could be optimised to minimise the probability of side reactions and degradation.

Table 16: Compression moulding parameters of plate geometries of the cured transamination networks based on poly(EHMA-co-AEMA) with different molecular weights and concentration of AEMA.

Name	M_n **(kg.mol^{-1})[a]**	$F_{\%AEMA}$[b]	***P*** **(bar)**	***Temp.*** **(°C)**	***Time*** **(min)**
10AEMA5-DAM2	**10.5**	**3.4**	**20**	**80**	**1**
10AEMA10-DAM2	**11.3**	**9.1**	**40**	**150**	**5**
10AEMA20-DAM2	**10.1**	**17.6**	**50**	**180**	**20**
40AEMA5-DAM2	**39.0**	**3.7**	**50**	**190**	**7**
40AEMA10-DAM2	**43.8**	**10.3**	**50**	**190**	**10**
40AEMA20-DAM2	**68.5**	**20.2**	**40**	**185**	**35**

[a]Measured via SEC ($CHCl_3$, PMMA standards). [b]Calculated from ^1H NMR spectroscopy.

Ideally, a comparative assessment in terms of degradation has to be made between shorter processing times at higher processing temperatures or longer processing times at lower processing temperatures. The processing pressures were moderate in the range of 40 to 50 bar, which was significantly higher than the pressure in vacuum compression moulding (approx. 1 bar) but low enough to avoid spillage from the mould.

3.3 Characterisation of the networks

3.3.1 Thermal Properties

Thermogravimetric analysis was performed to investigate the thermal stability of the materials. The lower molecular weight copolymers are thermally stable in the range of 280-300 °C. Further, the resultant networks had a 5% mass degradation temperature ($T_{deg5\%}$) of 325-343 °C, which is a slight improvement of the reported value range of 273-335 °C in a similar network based on PMMA with a comparable M_n (*Figure 56, Figure 57*).[193] However, it is exceeded by the $T_{deg5\%}$ = 375 °C of high molecular weight PEHMA.[186] In the 400-500 °C region, an increased stability with higher composition (more cross-links) was observed. Thus, the thermal stability of the copolymers is structurally reinforced by the flexible aliphatic cross-linker **DAM2**.

A similar $T_{deg5\%}$ range was found for the higher molecular weight copolymers (275-300 °C) and the resultant networks (320-330 °C) (*Figure 57*). Again, there is an overall increase in stability found after cross-linking, which is more pronounced for the higher compositions (higher cross-link density).

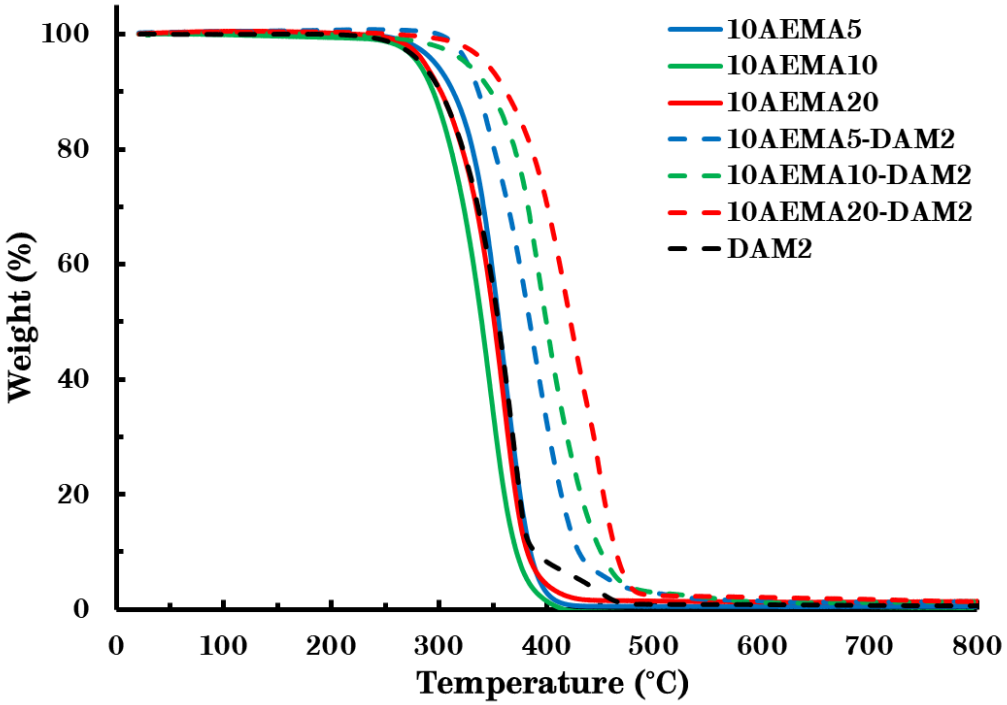

Figure 56: TGA thermograms of poly(EHMA-co-AEMA) with a targeted molecular weight M_n = 10 kg.mol^{-1} and their corresponding networks, comprising different AEMA concentrations (N_2, heating rate 10 °C.min^{-1}).

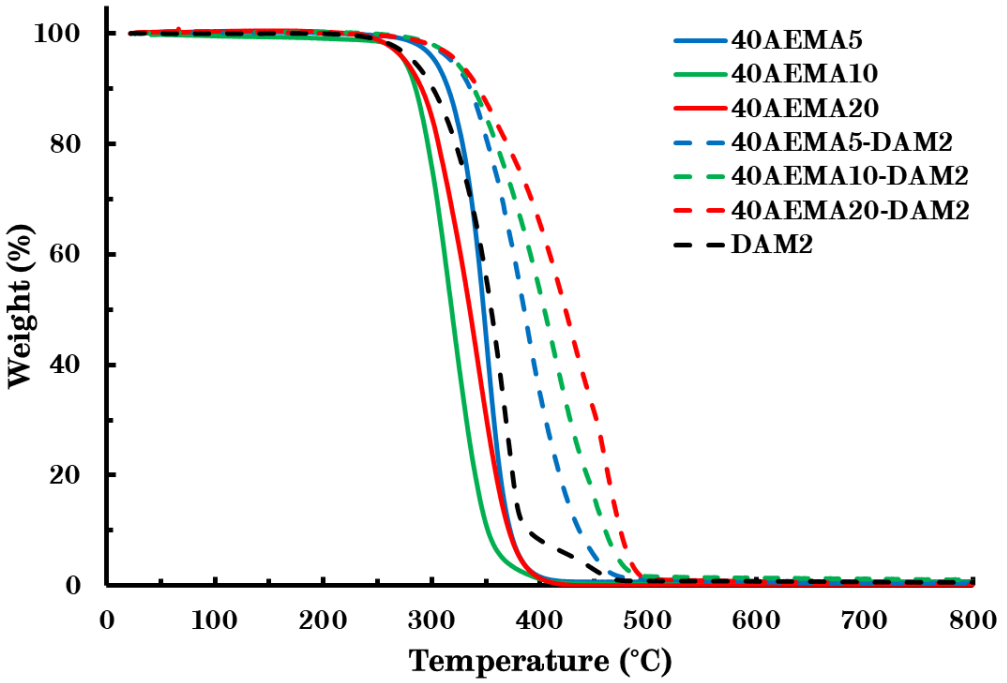

Figure 57: TGA thermograms of poly(EHMA-co-AEMA) with a targeted molecular weight M_n = 40 kg.mol^{-1} and their corresponding networks, comprising different FMA concentrations (N_2, heating rate 10 °C.min^{-1}).

DSC was used to determine the glass transition temperature (T_g) of the networks (*Table 17*). The data shows that the cross-linked networks have a lower T_g when compared to the respective prepolymers (*Figure 58, Figure 59*). This decrease could be rationalised by the introduction of the flexible cross-linker, which has a significantly lower T_g (-77 °C) than the copolymers.

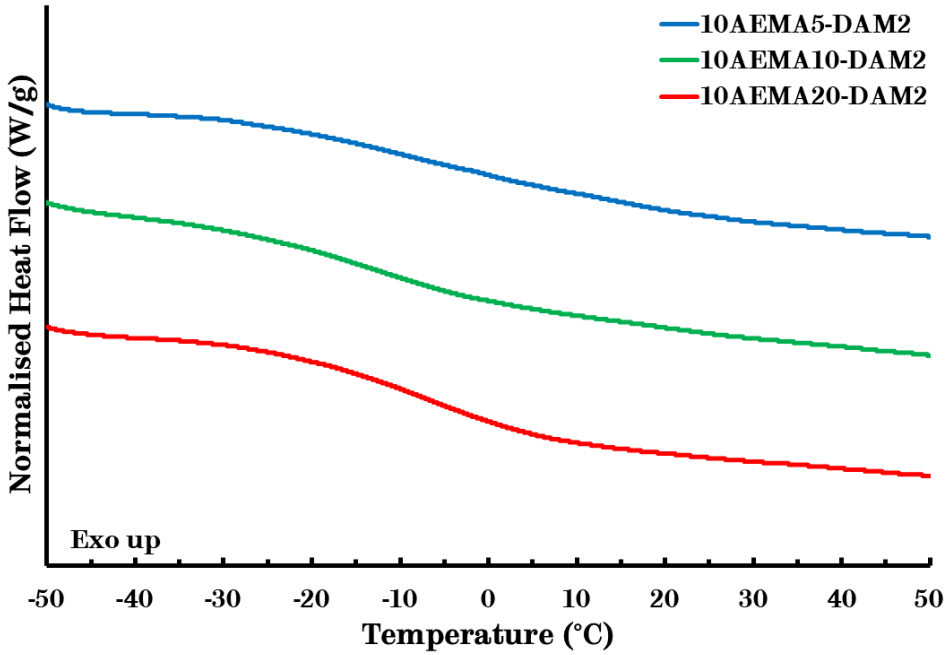

Figure 58: DSC thermograms of the networks based on poly(EHMA-co-AEMA) with a targeted molecular weight M_n = 10 kg.mol^{-1} and different AEMA concentrations (Second heating curve, heating rate 10 °C.min^{-1}).

Further, a similar decrease in T_g could be observed at each composition, regardless of the molecular weight, of approximately 2 °C for the 5 mol.% AEMA composition, 12 °C for the 10 mol.% AEMA composition and 5 °C for the 20 mol.% AEMA composition. Thus, the decrease reaches a maximum for the 10 mol.% AEMA composition. This may be the result of an increase in T_g for the highest compositions as a consequence of the increase of the cross-link density above a certain threshold value ($10 < F_{\%AEMA} < 20$).

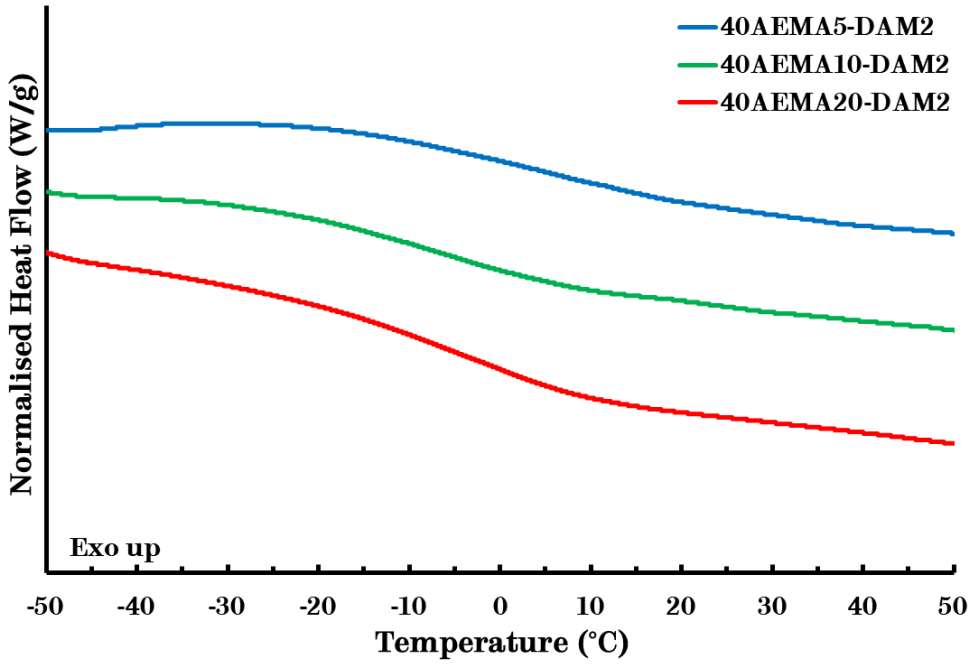

Figure 59: DSC thermograms of the networks based on poly(EHMA-co-AEMA) with a targeted molecular weight M_n = 40 kg.mol^{-1} and different AEMA concentrations (Second heating curve, heating rate 10 °C.min^{-1}).

Table 17: The T_g of poly(EHMA-co-AEMA) and resulting networks.

Name	***M*n (kg.mol^{-1})[a]**	***F*%AEMA[b]**	***T*g (°C)[c]**
10AEMA5	**10.5**	**3.4**	**-4.6**
10AEMA5-DAM2			**-6.6**
10AEMA10	**11.3**	**9.1**	**-0.7**
10AEMA10-DAM2			**-12.2**
10AEMA20	**10.1**	**17.6**	**0.6**
10AEMA20-DAM2			**-5.7**
40AEMA5	**39.0**	**3.7**	**3.7**
40AEMA5-DAM2			**1.8**
40AEMA10	**43.8**	**10.3**	**4.6**
40AEMA10-DAM2			**-7.2**
40AEMA20	**68.5**	**20.2**	**5.7**
40AEMA20-DAM2			**-2.8**

[a]Measured via SEC ($CHCl_3$, PMMA standards). [b]Calculated from ^{1}H NMR spectroscopy. [c]Measured via DSC (heating rate 10 °C.min^{-1}).

3.3.2 Solubility

Solubility experiments were conducted in order to assess the extent of the network formation *via* Soxhlet extraction. The solubility of a sample depends on the polarity and boiling point of the extraction solvent. Hence, toluene was selected for its high boiling point of 110 °C (*Table 18)*. For the networks based on poly(EHMA-*co*-AEMA) with a targeted molecular weight M_n = 10 kg.mol^{-1}, the soluble fractions decreased with increasing AEMA content (higher cross-link density) (*Figure 60*).

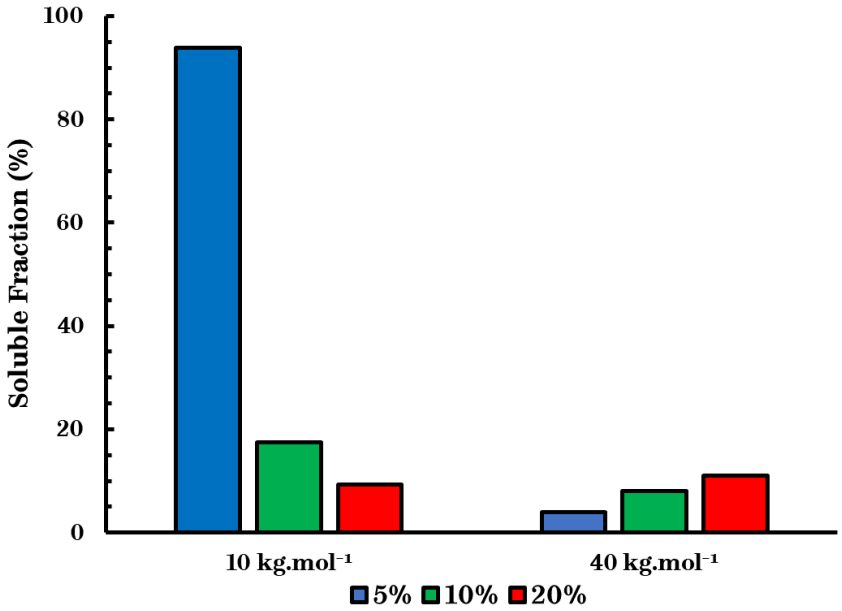

Figure 60: Soluble fractions of both sets of transamination networks at different concentrations of AEMA (5, 10, 20 mol.%) after extraction in toluene.

10AEMA5-DAM2 had a soluble fraction of nearly 95%, indicating that the network formation (gelation) failed. This is the result of the low average number of AEMA groups per chain (1.8). Using *Equation 2* previously described in *1.2.1 Polymer Networks,* a theoretical value of p_{Bg} can be calculated > 1, which shows that 1.8 functional groups per chain is not sufficiently high enough for network formation to occur. For the networks based on poly(EHMA-co-AEMA) with the higher targeted molecular weight, the soluble fractions were in the range of 4-11% (*Table 18*). Here, an

increase of the soluble fraction was observed with composition, which could be rationalised by the large excess of cross-linker in these networks (50 mol.% excess). A comparable influence of excess amine on soluble fraction has been reported for step-growth networks based on cyclohexane dimethanol bisacetoacetate (CDM-AA), diamine **DAM1** and triamine TREN.[124] Thus, this could explain the slightly higher range of soluble fractions compared to the preferred <5% range. Moreover, this was confirmed by follow-up experiments with a small excess of cross-linker (5 mol.% excess), where the soluble fractions were in the 4-5% range.

The degree of swelling was consistent for all transamination networks in the range of 340-450% with the exception of **10AEMA5-DAM2** (*Figure 61).*

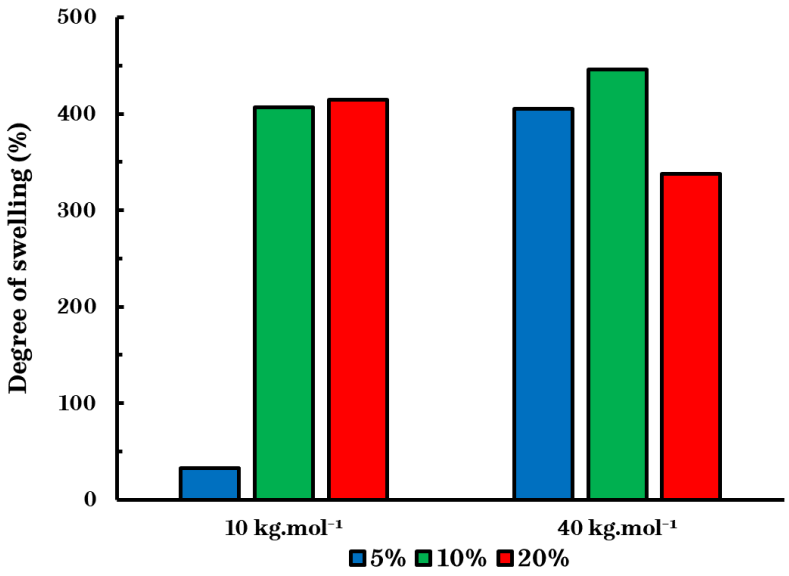

Figure 61: Degree of swelling of both sets of transamination networks at different concentrations of AEMA (5, 10, 20 mol.%) after extraction in toluene.

Here, the low swelling degree (33%) after extraction could be explained by the low gel fraction of the remaining network (6%) rather than being a highly cross-linked sample. As previously discussed, these similar degrees of swelling are indicative that the experimental M_c (cross-link density) of these networks are comparable.

Moreover, these degrees of swelling are lower than the value reported for the extraction of step-growth transamination networks in *N*-methyl-2-pyrrolidone (NMP) at 100 °C (750%).[124]

Table 18: Results of the solubility experiments of both sets of transamination networks at different AEMA concentrations compared to the functionality of the functional prepolymers.

Name	M_n **(kg.mol^{-1})[a]**	$F_{\%AEMA}$[b]	***Sol. Fr.*** **(%)[c]**	***Swell.*** **(%)[c]**	***Funct.***[a,b]
10AEMA5-DA2	**10.5**	**3.4**	**94**	**33**	**1.8**
10AEMA10-DA2	**11.3**	**9.1**	**17**	**406**	**5.1**
10AEMA20-DA2	**10.1**	**17.6**	**9**	**414**	**8.9**
40AEMA5-DA2	**39**	**3.7**	**4**	**405**	**7.2**
40AEMA10-DA2	**43.8**	**10.3**	**8**	**446**	**22.5**
40AEMA20-DA2	**68.5**	**20.2**	**11**	**338**	**69**

[a] Measured via SEC ($CHCl_3$, PMMA standards). [b] Calculated from ^{1}H NMR spectroscopy. [c] Measured via Soxhlet extraction.

3.3.3 Rheology

The rheology of the transamination networks was tested both with a rheometer and dynamic mechanical thermal analysis (DMTA). Initially, amplitude sweeps (strain sweeps) were performed to determine the linear viscoelastic region (LVR) of the material. This LVR can be observed as a plateau, where the storage modulus (*G'*) exceeds the loss modulus (*G"*) (*Figure 62*). This region depends on the temperature and the frequency of the strain sweep experiments, which in this case was 200 °C and 10 Hz. This temperature is the highest of all the temperatures at which the stress-relaxation experiments were performed (*vide infra*). Moreover, this ensured that the observed LVR at this temperature was the most stringent and the LVR at all other temperatures would encompass this range. The experiments were performed on one network per set (*i.e.* **40AEMA20-DAM2**) and afterwards the

selected strain value of 1% was kept the same for all consequent stress-relaxation experiments.

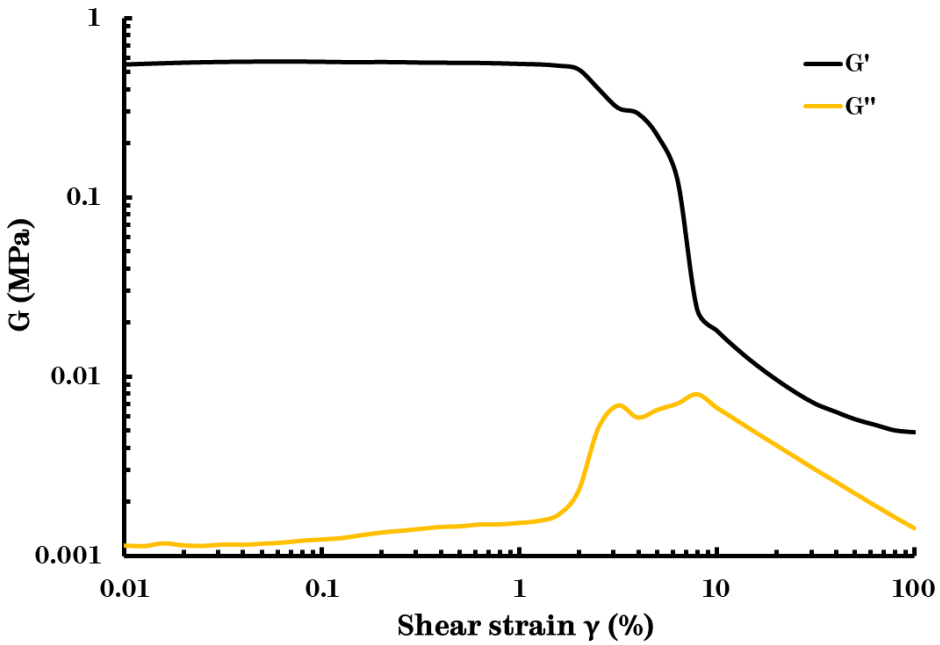

*Figure 62: Amplitude sweep of **40AEMA20-DAM2** at 200 °C and 10 Hz.*

Stress-relaxation experiments were performed to validate the dynamic behaviour of the vitrimers. Initially, stress-relaxation experiments were performed on all the transamination networks, except the networks based on the lowest composition copolymers as a consequence of the poor network integrity of **10AEMA5-DAM2** (*vide supra*). The relaxation modulus (*G)* was normalised against the apparent plateau value (G_0) at t = 1 s, after the initial step strain of 1%. The intersections of the horizontal dashed lines with the stress relaxation curves indicate where $G/G_0 = 1/e$ and $t = \tau$ since the relaxation time τ of a vitrimer can be defined as the time it takes for the system to relax to a value of $1/e$ (approximately 37%) and depends on temperature.[135] Higher temperatures generally reduce the relaxation time. Thus, in order to reduce experimental time, an elevated temperature of 200 °C was selected to obtain a comparison between the networks.

A relaxation time of 75 s and 102 s was found for **10AEMA10-DAM2** and **10AEMA20-DAM2**, respectively. These values were lower than the values observed for the networks with similar composition, but with additional chain entanglements, namely **40AEMA10-DAM2** and **40AEMA20-DAM2** (270 s and 308 s, respectively) (*Figure 63*). Thus, the transamination reaction, which governs the relaxation of this vitrimer, may be facilitated by the higher chain mobility of the networks based on the lower molecular weight copolymers. This indicates that the relaxation of the material is mainly diffusion controlled. Moreover, this effect has also been reported for transamination vitrimers in a PMMA matrix.[193] Generally, diffusion control is not investigated as a limiting factor when the vinylogous urethane networks are synthesised *via* step-growth polymerisation of low molecular weight monomers. Furthermore, this could explain the lower activation energies (26 – 60 $kJ.mol^{-1}$) that are usually reported for step-growth based vitrimers compared to chain-growth based vitrimers within the same dynamic transamination chemistry.[124, 194, 195]

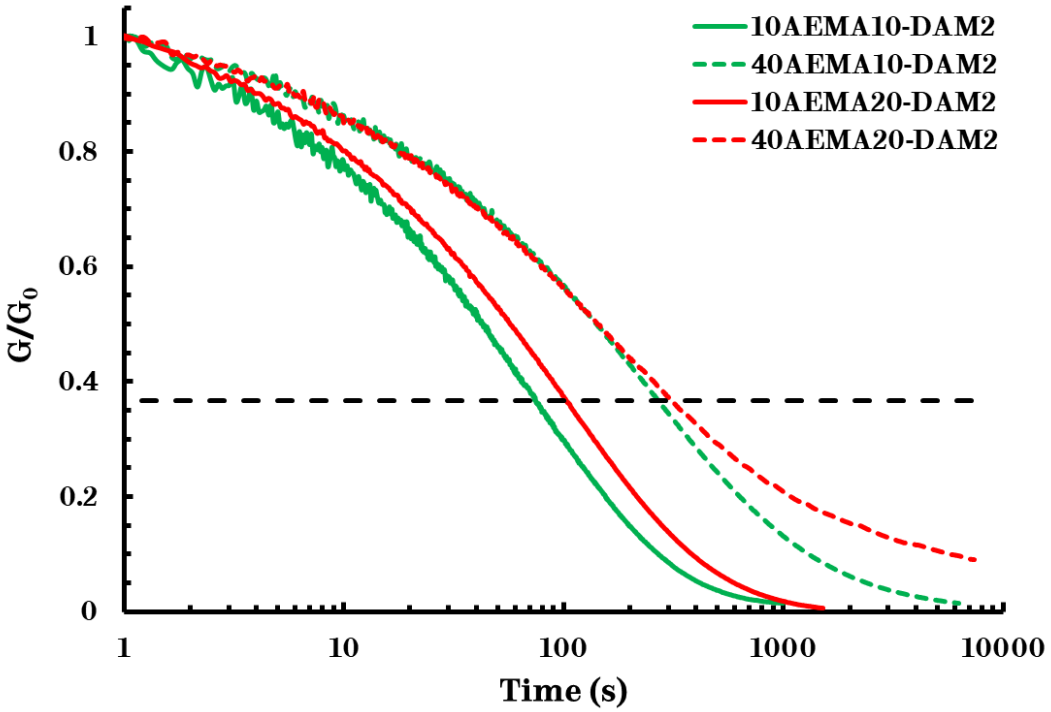

Figure 63: Comparison of stress-relaxation data at 200 °C of networks based on poly(EHMA-co-AEMA) prepolymers with different targeted molecular weights and concentrations of AEMA.

Next, a comprehensive rheological study was done on one of these networks, namely **40AEMA10-DAM2**, in order to calculate the activation energy E_a of this type of network and compare this value to the literature. The temperature range 160-200 °C was selected to reduce experimental time. There is a clear trend visible of increasing relaxation times with decreasing temperature (*Figure 64*). This relaxation time ranges from 269 s at 200 °C to 5080 s at 160 °C. The constant intervals between the stress-relaxation curves indicates a homogeneous sample.

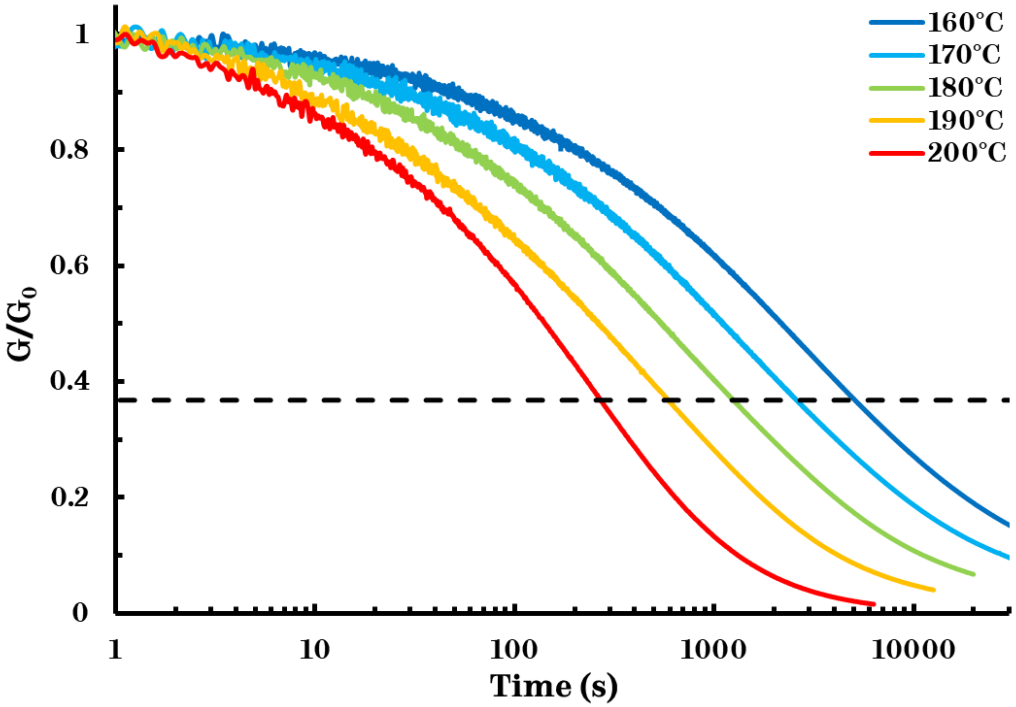

*Figure 64: Stress-relaxation curves of **40AEMA10-DAM2** at different temperatures.*

The relaxation times can be plotted against inverse temperature (T^{-1}) in an Arrhenius plot (*Figure 65*). Here, the activation energy E_a can be calculated from the slope of the trendline. For this type of network, a value of 125 ± 4 kJ.mol^{-1} was found, which is in line with the range of reported values of 102-165 kJ.mol^{-1} for chain-growth networks based on vinylogous urethane bonds.[193, 196, 197] This value is higher than the reported values of the comparable step-growth networks (26 – 60 kJ.mol^{-1}), where the cross-link density is significantly higher.[124, 194, 195]

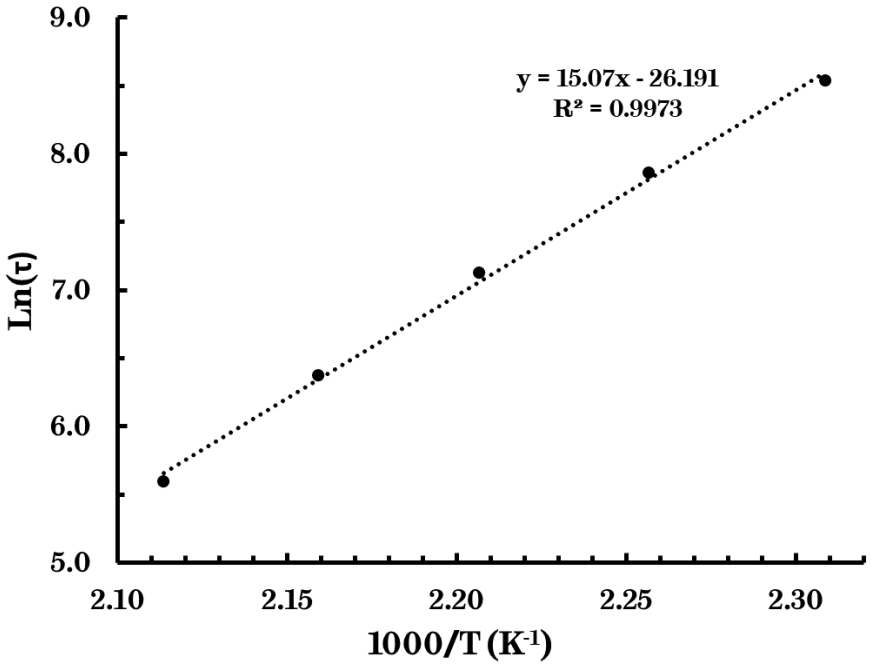

*Figure 65: Arrhenius plot of **40AEMA10-DAM2** showing the different relaxation times at different temperatures.*

DMTA was also performed on **10AEMA20-DAM2** and **40AEMA20-DAM2**. **10AEMA20-DAM2** and **40AEMA20-DAM2** exhibit a glassy plateau storage modulus (*G'*) of 1.9 and 1.6 GPa, respectively, and rubbery plateau storage modulus (G'_{rubber}) of 2.5 MPa, which extends to 200 °C (*Figure 66, Figure 67*). As previously discussed in *2.3.3 Rheology*, M_c = 1192 g.mol^{-1} can be calculated (*Equation 7*).

These values resemble the reported *G'* = 1.8 GPa and G'_{rubber} = 4 MPa of the transamination vitrimers based on low molecular weight PMMA with an AEMA content of 10 mol.%.[193] Furthermore, they are an improvement when compared to the reported *G'* = 0.8 GPa and G'_{rubber} = 0.2 MPa of the transamination vitrimers based on methacrylic block copolymers with an AEMA content of 20 mol.%.[198] However, they are lower than the *G'* = 2.8 GPa and G'_{rubber} = 10 MPa of the vitrimers based on polystyrene with a high AEMA concentration of 43 mol.%.[197] Further, the T_g can be

defined as the midpoint of the *G'* inflection and was significantly higher for both networks compared to the values obtained using DSC analysis.

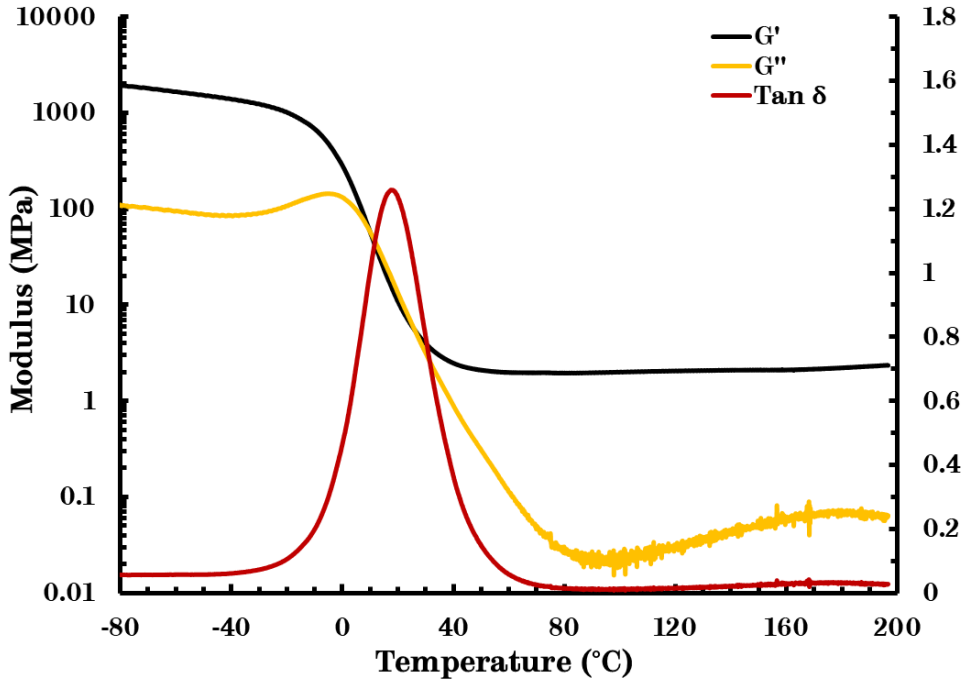

*Figure 66: Storage modulus, loss modulus and tan δ of **10AEMA20-DAM2** measured via DMTA (Heating rate 3 °C.min^{-1}).*

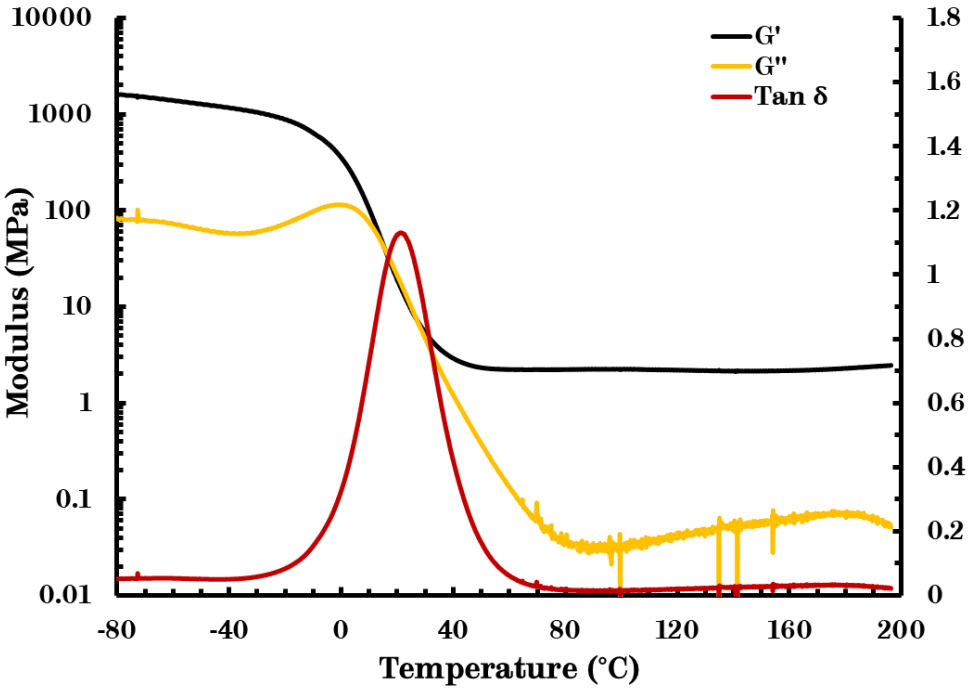

*Figure 67: Storage modulus, loss modulus and tan δ of **40AEMA20-DAM2** measured via DMTA (Heating rate 3 °C.min^{-1}).*

3.3.4 Mechanical properties

Tensile testing was performed to assess the mechanical properties of the prepared networks. The most important properties to consider were the Young's modulus (*E*), stress at break (σ_b) and elongation at break (ε_b). For the networks based on the lower molecular weight copolymers, an identical trend was found as in the Diels-Alder equivalent networks, namely as the AEMA content increases (cross-link density), material with higher stiffness and lower elongation at break are obtained (*Figure 68, Table 19*). However, the moduli are in the range of 1.9-2.4 MPa, which is slightly lower than E = 5 ± 1 MPa, reported for the homopolymer PEHMA (M_n = 53 kg.mol^{-1}).[170] Furthermore, this low E may be the result of the large excess of cross-linker incorporated in the matrix, which can act as a plasticiser. Moreover, **10AEMA5-DAM2** was highly elastic, with the final ε_b unable to be measured using the available experimental set-up. This elastic behaviour resembles the tensile properties of PEHMA (ε_b > 1100%).[170] Cross-referencing this data with the results from the solubility experiments, the poor network formation is confirmed again as a consequence of the large fraction of material not being cross-linked as a result of the low average number of functional groups on the prepolymer chains.

The networks based on poly(EHMA-*co*-AEMA) with the higher targeted molecular weights exhibit an increased E range of 2.2-4.4, comparable to PEHMA (M_n = 53 kg.mol^{-1}) (*Table 19*). A distinction can be made between **40AEMA20-DAM2** and the other two compositions, namely **40AEMA20-DAM2** exhibited a higher σ_b and lower ε_b, confirming the increased stiffness of the material (*Figure 69*).

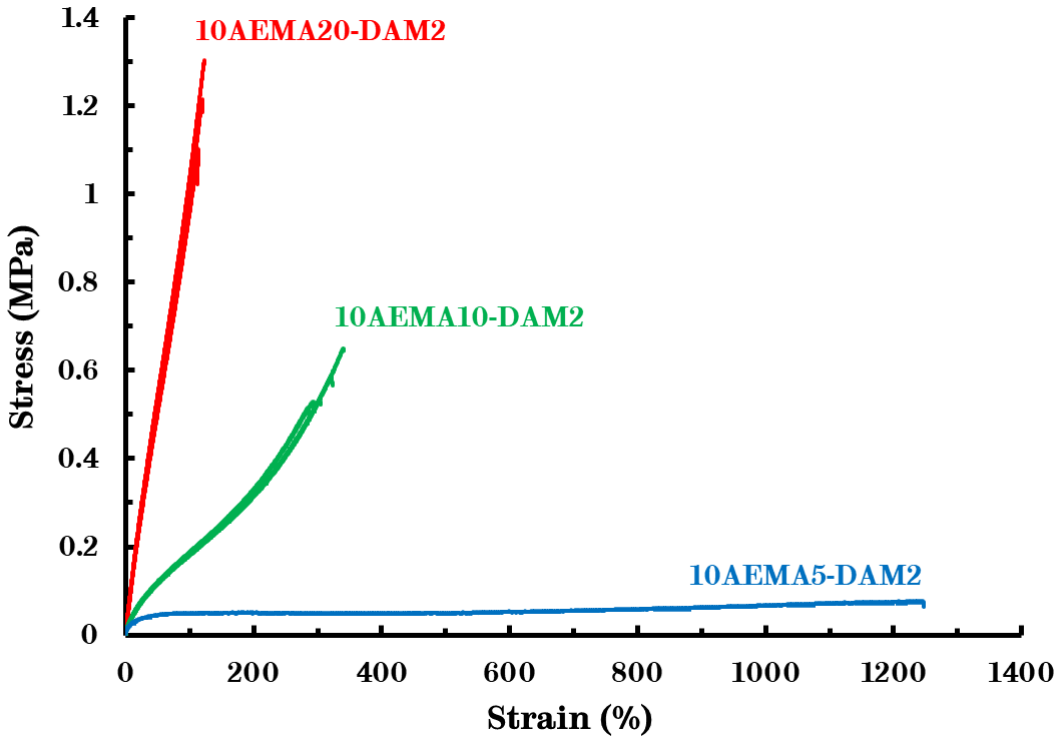

Figure 68: Stress-strain curves of the networks based on poly(EHMA-co-AEMA) with a target molecular weight M_n = 10 kg.mol^{-1} and different AEMA concentrations.

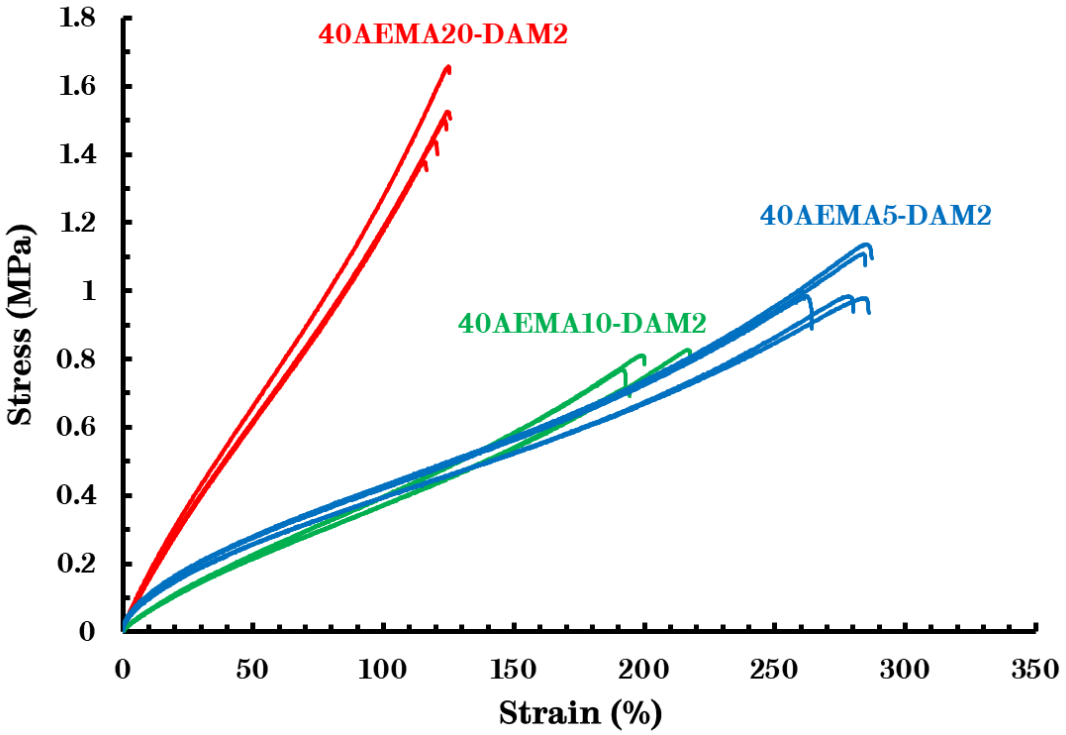

Figure 69: Stress-strain curves of the networks based on poly(EHMA-co-AEMA) with a targeted molecular weight M_n = 40 kg.mol^{-1} and different FMA concentrations.

Table 19: Tensile properties of the networks based on poly(EHMA-co-AEMA) with different targeted molecular weights and with different concentrations of AEMA.

Name	M_n (kg.mol^{-1})[a]	$F_{\%AEMA}$[b]	E (MPa)	σ_b (MPa)	ε_b (%)
10AEMA5-DAM2	**10.5**	**3.4**	**2.12**	**N/a**	**N/a**
10AEMA10-DAM2	**11.3**	**9.1**	**1.89 ± 0.06**	**0.55 ± 0.03**	**310 ± 10**
10AEMA20-DAM2	**10.1**	**17.6**	**2.36 ± 0.19**	**1.12 ± 0.05**	**116 ± 2**
40AEMA5-DAM2	**39.0**	**3.7**	**4.43 ± 0.25**	**0.99 ± 0.04**	**280 ± 4**
40AEMA10-DAM2	**43.8**	**10.3**	**2.24 ± 0.10**	**0.75 ± 0.03**	**201 ± 6**
40AEMA20-DAM2	**68.5**	**20.2**	**3.56 ± 0.14**	**1.47 ± 0.05**	**122 ± 2**

[a]*Measured via SEC ($CHCl_3$, PMMA standards).* [b]*Calculated from ^{1}H NMR spectroscopy.*

3.3.5 Ageing

Weathering experiments were conducted on the networks comprising 20% AEMA to investigate the longer-term stability of the material (*Figure 70, Figure 71*). The samples were aged at 80 °C for 3 weeks and their tensile properties were tested again. At this temperature, G' is in the plateau region observed *via* DMTA (*vide supra*).

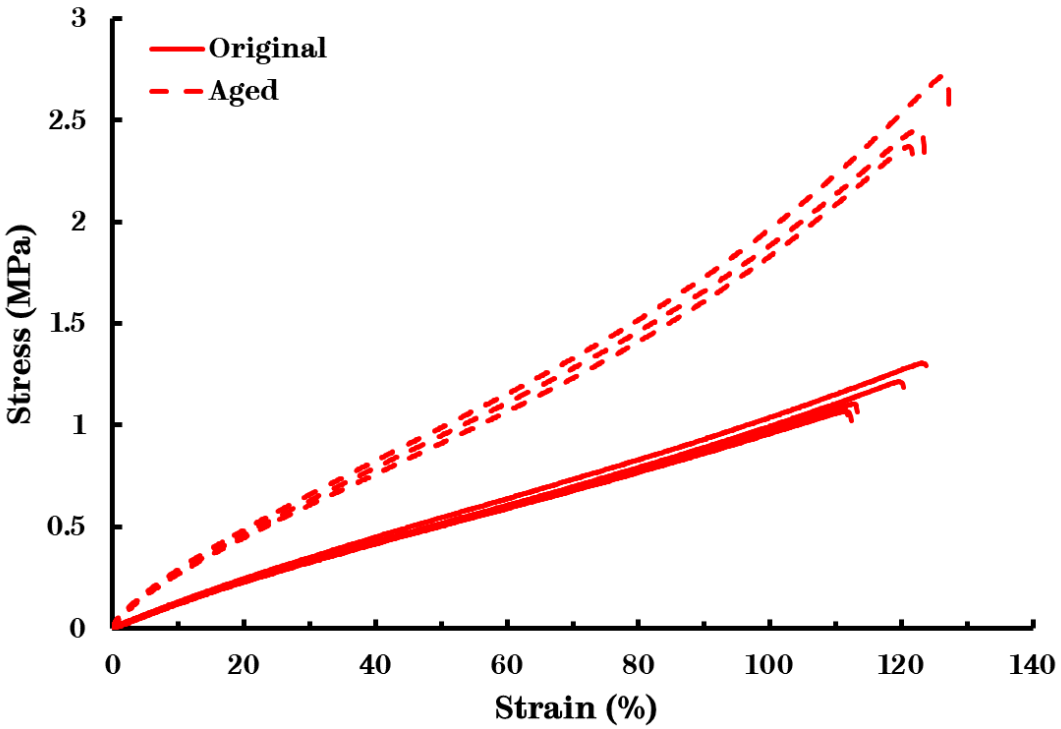

*Figure 70: Stress-strain curves of **10AEMA20-DAM2** before and after ageing at 80 °C for 3 weeks.*

The E of **10AEMA20-DAM2** and **40AEMA20-DAM2** increased by 190% and 155%, respectively. Further, a similar trend is visible as in the Diels-Alder networks,

namely that the stiffness of the samples is increased (higher σ_b and lower ε_b), which may be the result of a post-cure occurring in the material.

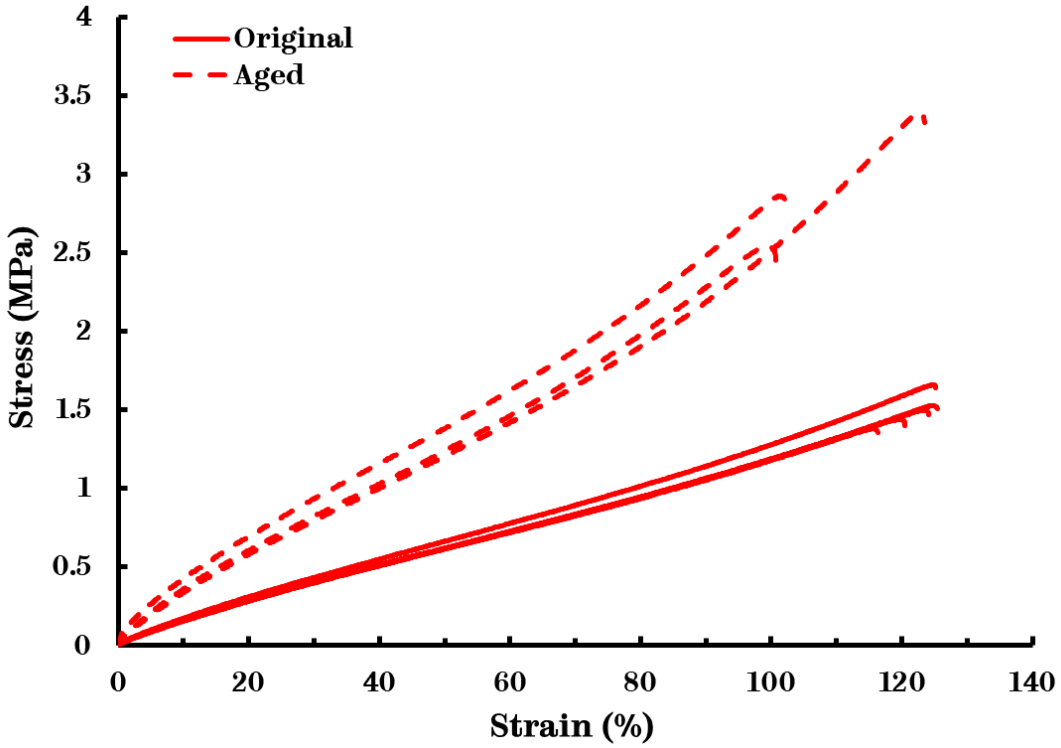

*Figure 71: Stress-strain curves of **40AEMA20-DAM2** before and after ageing at 80 °C for 3 weeks.*

Table 20: Tensile properties of the networks based on poly(EHMA-co-AEMA) with 20% of AEMA before and after ageing at 80°C for 3 weeks.

	Name	M_n (kg.mol^{-1})[a]	$F_{\%AEMA}$[b]	E (MPa)	σ_b (MPa)	ε_b (%)
Original	**10AEMA20-DAM2**	**10.1**	**17.6**	**2.36 ± 0.19**	**1.12 ± 0.05**	**116 ± 2**
Aged				**6.84 ± 0.56**	**2.40 ± 0.08**	**124 ± 2**
Original	**40AEMA20-DAM2**	**68.5**	**20.2**	**3.56 ± 0.14**	**1.47 ± 0.05**	**122 ± 2**
Aged				**9.09 ± 1.28**	**2.84 ± 0.26**	**109 ± 7**

[a]*Measured via SEC ($CHCl_3$, PMMA standards).* [b]*Calculated from ^1H NMR spectroscopy.*

FTIR spectroscopy of both **10AEMA20-DAM2** and **40AEMA20-DAM2** was performed before and after ageing to investigated possible side reaction or degradation. The IR spectra of **10AEMA20-DAM2** before and after ageing are nearly identical, suggesting no apparent degradation of the sample (*Figure 72*). The IR

spectra of **40AEMA20-DAM2** before and after ageing are also similar, which is indicative of the absence of detrimental side reactions (*Figure 73*).

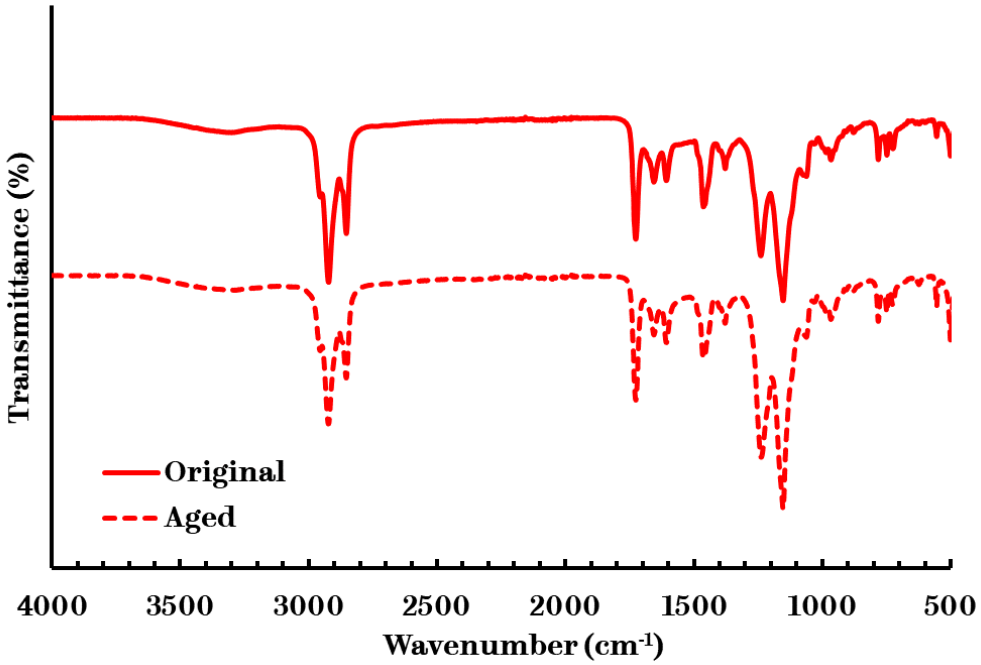

*Figure 72: IR spectrum of **10AEMA20-DAM2** before and after ageing at 80 °C for 3 weeks.*

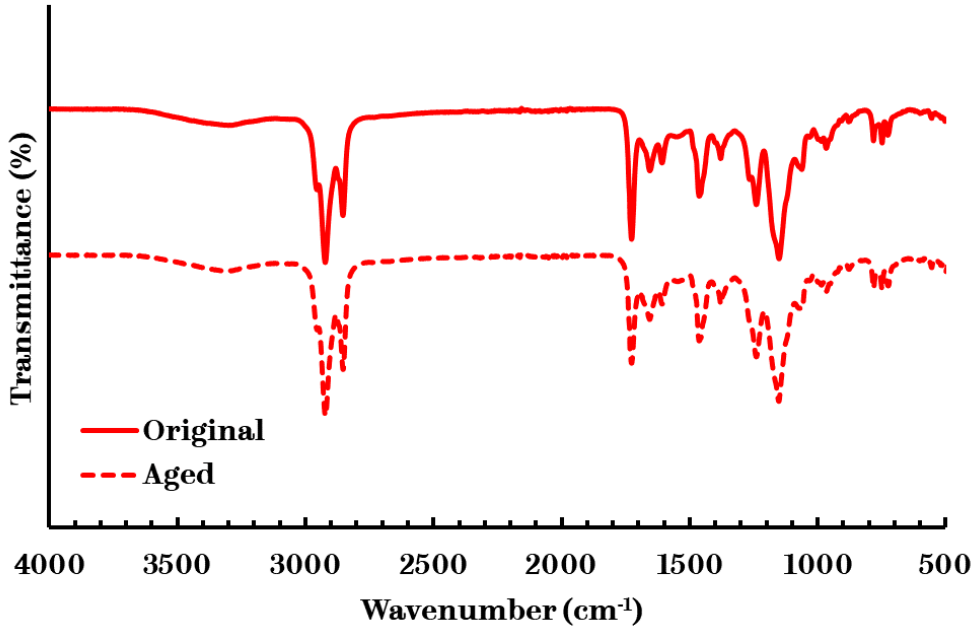

*Figure 73: IR spectrum of **40AEMA20-DAM2** before and after ageing at 80 °C for 3 weeks.*

3.3.6 Recyclability

In order to evaluate the recyclability of the prepared networks, tensile testing was performed on repeatedly reprocessed samples (recycles) and the results were compared to the pristine material (Original). Due to time constraints towards the end of the project, only one recycle (R1) was performed on **10AEMA20-DAM2** and **40AEMA20-DAM2**, but two recycles (R2) were performed on **40AEMA10-DAM2** (*Table 21*). It is important to highlight that the reprocessing parameters of **10AEMA20-DAM2** and **40AEMA20-DAM2** were approximately the same as the original processing parameters, indicating a good recyclability of the samples.

Table 21: Reprocessing parameters of the transamination networks based on poly(EHMA-co-AEMA) with different molecular weights and concentration of AEMA.

	Name	***M_n*** **(kg.mol^{-1})[a]**	***$F_{\%AEMA}$*** **[b]**	***P*** **(bar)**	***Temp.*** **(°C)**	***Time*** **(min)**
Original	**10AEMA20-DAM2**	**10.1**	**17.6**	**50**	**180**	**20**
R1				**50**	**180**	**20**
Original	**40AEMA10-DAM2**	**43.8**	**10.3**	**50**	**190**	**10**
R1				**40**	**180**	**20**
R2				**50**	**180**	**35**
Original	**40AEMA20-DAM2**	**68.5**	**20.2**	**40**	**185**	**35**
R1				**50**	**180**	**35**

[a]Measured via SEC ($CHCl_3$, PMMA standards). [b]Calculated from ^{1}H NMR spectroscopy.

After R1, the *E* of **10AEMA20-DAM2** and **40AEMA20-DAM2** increased by 194% and 237%, respectively. After R1 and R2, the *E* of **40AEMA10-DAM2** increased by 85% and 268%, respectively (*Table 22*). Thus, a clear trend is visible comparable to the aged samples having an increased *E* (*Figure 74, Figure 75 and Figure 76*). For all samples the ε_b also slightly increased, indicating that the materials have an improved ductility rather than stiffness. This may be the result of a post-cure during recycling.

FTIR spectroscopy of **40AEMA10-DAM2** was performed before and after recycling to investigated possible side reactions (*e.g.* hydrolysis, oxidation of the free amines) or degradation (*Figure 77*). A slight decrease was observed of the vinylogous urethane stretches (1604-1640 cm^{-1}), while the primary aliphatic amine stretch (3300 cm^{-1}) was unchanged. This indicates minimal oxidation of the free amines.

Table 22: Results of the tensile testing of the networks based on poly(EHMA-co-AEMA) with different targeted molecular weights and with different concentrations of AEMA before and after recycling.

	Name	M_n (kg.mol^{-1})[a]	$F_{\%AEMA}$[b]	*E* (MPa)	σ_b (MPa)	ε_b (%)
Original	**10AEMA20-DAM2**	**10.1**	**17.6**	**2.36 ± 0.19**	**1.12 ± 0.05**	**116 ± 2**
R1				**6.95 ± 0.42**	**1.76 ± 0.24**	**128 ± 10**
Original	**40AEMA10-DAM2**	**43.8**	**10.3**	**2.24 ± 0.10**	**0.75 ± 0.03**	**201 ± 6**
R1				**4.15 ± 0.15**	**1.34 ± 0.10**	**253 ± 13**
R2				**8.24 ± 0.72**	**1.55 ± 0.12**	**210 ± 10**
Original	**40AEMA20-DAM2**	**68.5**	**20.2**	**3.56 ± 0.14**	**1.47 ± 0.05**	**122 ± 2**
R1				**12.0 ± 0.60**	**2.45 ± 0.15**	**148 ± 7**

[a]*Measured via SEC ($CHCl_3$, PMMA standards).* [b]*Calculated from ^1H NMR spectroscopy.*

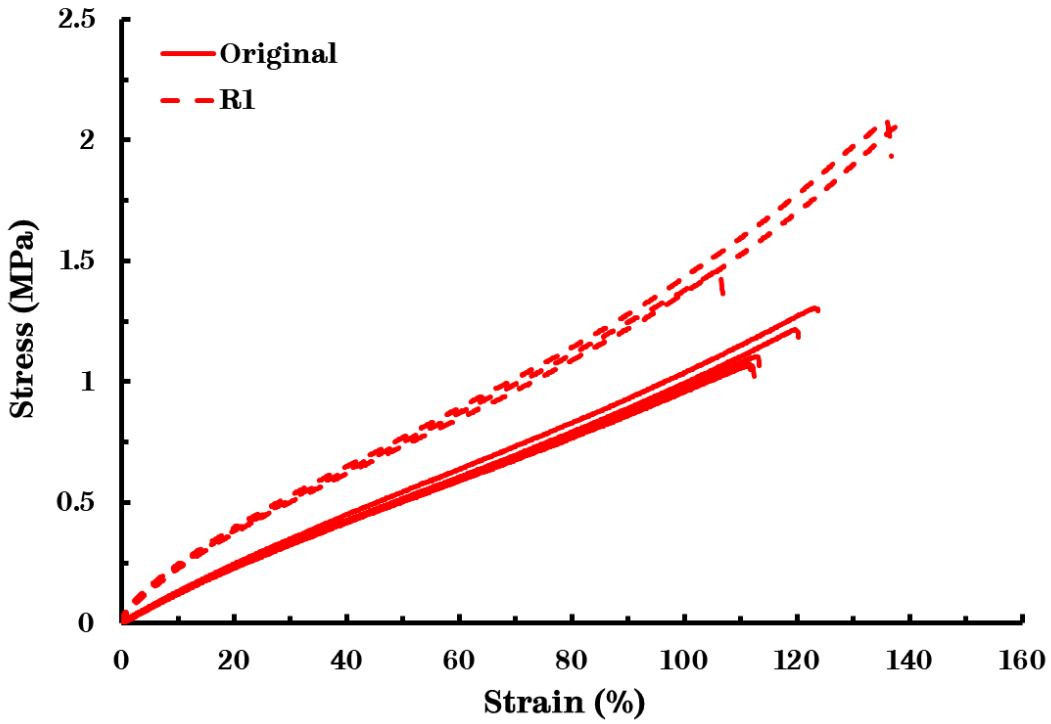

*Figure 74: Stress-strain curves of **10AEMA20-DAM2** before and after recycling.*

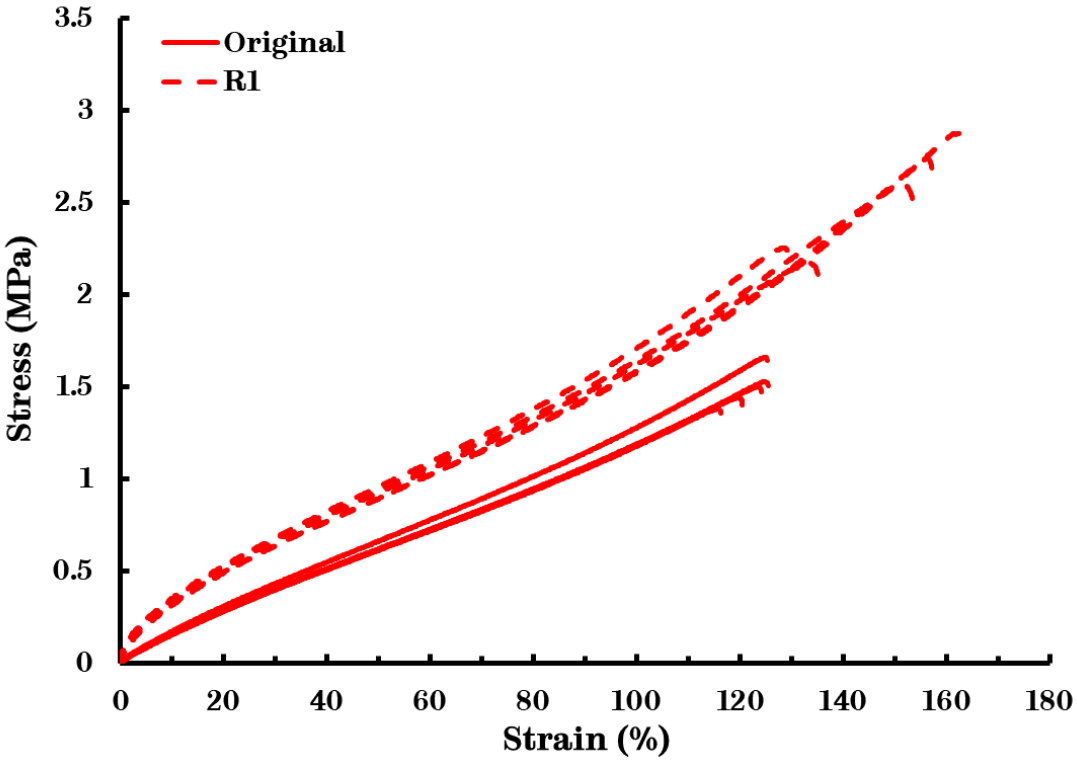

*Figure 75: Stress-strain curves of **40AEMA20-DAM2** before and after recycling.*

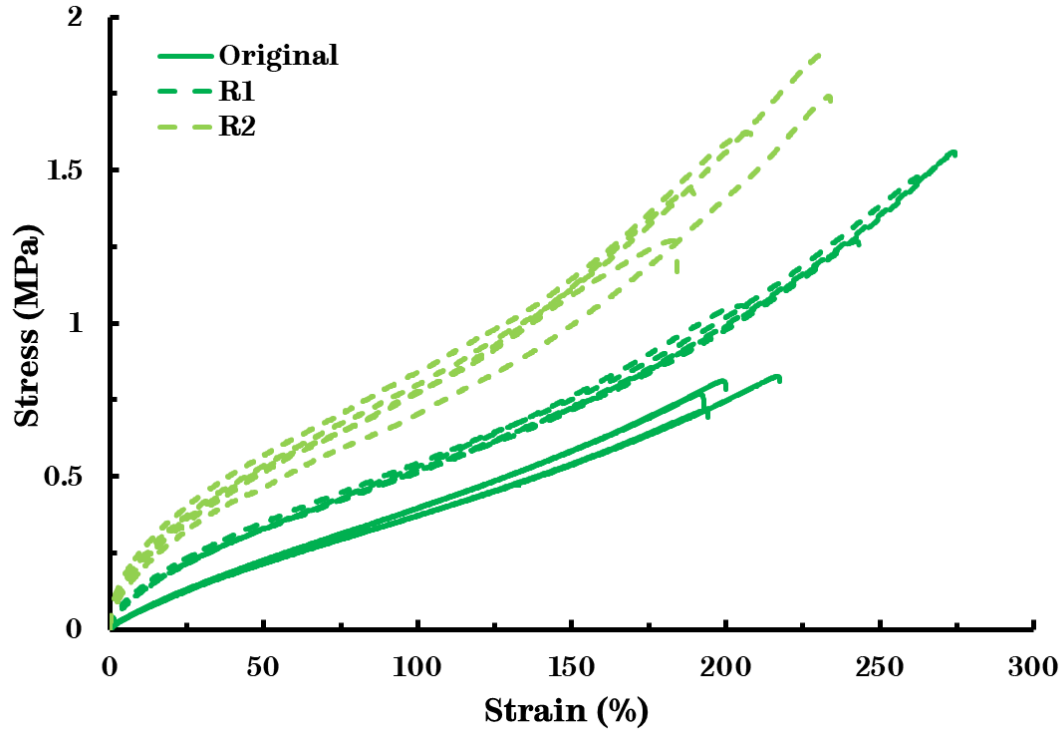

*Figure 76: Stress-strain curves of **40AEMA10-DAM2** before and after recycling.*

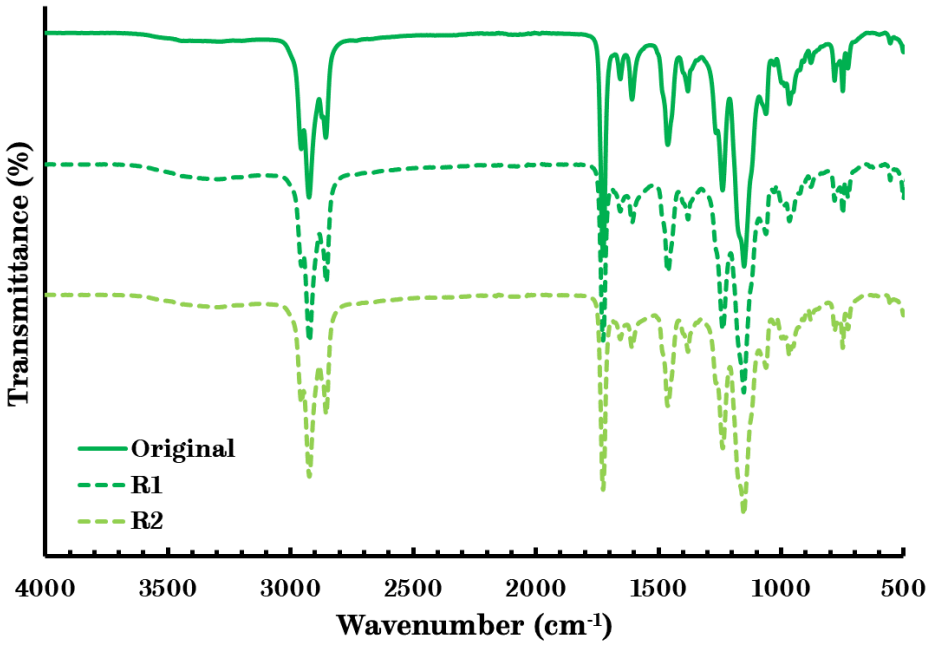

*Figure 77: IR spectrum of **40AEMA10-DAM2** before and after recycling.*

3.4 Conclusion

Functional copolymers were synthesised based on EHMA and varying concentrations of comonomer AEMA (5 – 20 mol.%). Next, these copolymers were cross-linked with a flexible aliphatic cross-linker **DAM2** (50 mol.% excess) to obtain homogeneous networks comprising vinylogous urethane bonds. Different geometries were prepared by altering the processing parameters (temperature, time and pressure). These networks were characterised to investigate the material properties. They exhibit an improved thermal stability above 300 °C and lower T_g compared to the prepolymers. They also possess low soluble fraction (4-17%) indicating good network formation, unless the average number of functional groups per chain was below the threshold value for this type of chemistry. Further, the dynamic behaviour of the material was confirmed *via* stress-relaxation experiments (E_a = 125 ± 4 kJ.mol^{-1}). The tensile properties were tested on the pristine samples (E =

2-4 MPa), after ageing at 80 °C for 3 weeks (E = 7-9 MPa) and after recycling (E = 7-12 MPa). Furthermore, an increased stiffness of the material was observed, which may be the result of a post-cure effect.

Chapter 4 Phthalate monoester – Hybrid type

4.1 Functional copolymers

After the aforementioned preliminary experiments with *n*-butyl acrylate (BA) and lauryl methacrylate (LMA) as the main monomers in *Chapter 2 Diels-Alder – Dissociative type* and *Chapter 3 Vinylogous Urethane – Associative type*, these monomers were not investigated for the synthesis of the networks of a third dynamic chemistry, namely the transesterification of phthalate monoesters (PMEs). 2-Ethylhexyl methacrylate (EHMA) was selected as the main monomer in order to facilitate the comparison with the previously discussed functional copolymers and resulting networks. Initially, EHMA was copolymerised with 2-hydroxethyl methacrylate (HEMA) as the functional comonomer (*Figure 78*). This introduces a primary alcohol functionality that in the next step can react with a *meta*-substituted phthalic anhydride to form the envisaged PMEs.

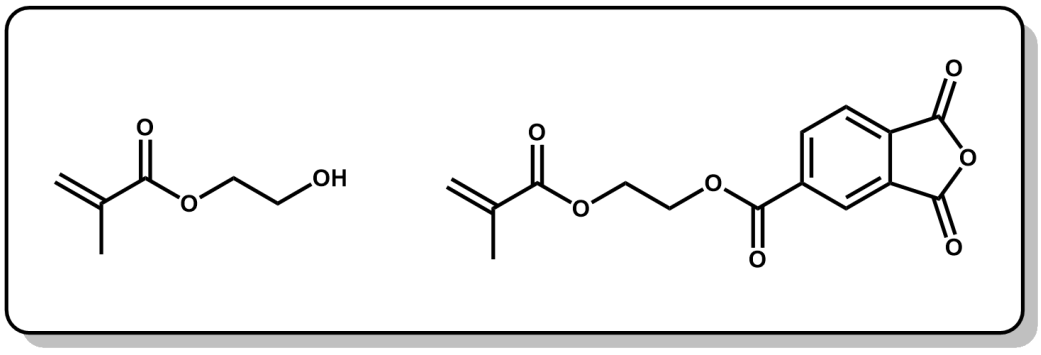

Figure 78: Structure of functional comonomers 2-hydroxyethyl methacrylate (HEMA) (left) and 4-methacryloxyethyl trimellitic anhydride (META) (right).

Later, in order to make the networks in the inverse way, EHMA was copolymerised with 4-methacryloxyethyl trimellitic anhydride (META) (*Figure 78*). The incorporated phthalic anhydride could then be reacted with a diol to form similar PMEs to the aforementioned materials.

Different functional copolymers were synthesised in order to assess the influence of both molecular weight and composition. Different molecular weights were targeted to determine the influence of the molecular weight on the properties of the copolymers and resulting networks. The number-average molecular weight M_n of 10 kg.mol^{-1} and 40 kg.mol^{-1} were selected. These values are the same as the functional copolymers comprising FMA and AEMA (*Chapter 2 Diels-Alder – Dissociative type* and *Chapter 3 Vinylogous Urethane – Associative type*), which allows for a better comparison of the influence on the properties of the copolymers and resultant networks. Further, the same influence of chain entanglements was expected due to the incorporation of a majority of the same comonomer EHMA. In order to control the molecular weight, the same chain transfer agent *n*-dodecyl mercaptan (DDM) as in the previously discussed copolymerisations of EHMA was added. Different concentrations of initiator azobisisobutyronitrile (AIBN) and DDM were tested to obtain the targeted molecular weights (*Table 23*). Again, the same stepwise scale-up was performed as for the previous copolymerisations of EHMA, namely from approximately 6 g to over 100 g.

The nomenclature for the functional copolymers comprises an initial number referring to the targeted molecular weight in kg.mol^{-1} (*e.g.* 10), followed by the name of the incorporated functional comonomer (*e.g.* HEMA) and ending in the targeted

composition of this comonomer in mol.% (*e.g.* 5) (*vide supra*). For example, 10HEMA5 is a 10 kg.mol^{-1} PEHMA with a targeted 5 mol.% incorporation of HEMA. This nomenclature was employed to facilitate the discussion of the experimental results.

Table 23: Free-radical copolymerisation of EHMA and HEMA using different concentration of I and CTA to control molecular weight.

Name	$f_{\%EHMA}$[a]	$f_{\%HEMA}$[a]	[I] (mol.L^{-1})	[CTA] (mol.L^{-1})	[CTA]/[M]	M_n[b] (kg.mol^{-1})	$Đ_M$[b]
10HEMA2	**98**	**2**	**0.003**	**0.064**	**0.014**	**9.8**	**1.8**
40HEMA2	**98**	**2**	**0.001**	**0.008**	**0.002**	**64.4**	**1.9**
10HEMA5	**95**	**5**	**0.003**	**0.063**	**0.014**	**11.4**	**1.8**
40HEMA5	**95**	**5**	**0.001**	**0.008**	**0.002**	**38.7**	**2.2**
10HEMA10	**90**	**10**	**0.003**	**0.061**	**0.013**	**9.5**	**1.8**
40HEMA10	**90**	**10**	**0.002**	**0.015**	**0.003**	**38.1**	**1.8**
10HEMA20	**80**	**20**	**0.003**	**0.057**	**0.012**	**8.4**	**2.0**
40HEMA20	**80**	**20**	**0.014**	**0.007**	**0.001**	**47.9**	**2.4**

[a]*Feed ratio in mol.%.* [b]*Measured via SEC ($CHCl_3$, PMMA standards).*

Table 24: Free-radical copolymerisation of EHMA and META using different concentration of I and CTA to control molecular weight.

Name	$f_{\%EHMA}$[a]	$f_{\%META}$[a]	[I] (mol.L^{-1})	[CTA] (mol.L^{-1})	[CTA]/[M]	M_n[b] (kg.mol^{-1})	$Đ_M$[b]
10META5	**95**	**5**	**0.001**	**0.010**	**0.003**	**9.3**	**1.8**
40META5	**95**	**5**	**0.005**	**0.002**	**0.001**	**40.5**	**2.5**
10META10	**90**	**10**	**0.004**	**0.002**	**0.001**	**12.7**	**1.5**

[a]*Feed ratio in mol.%.* [b]*Measured via SEC ($CHCl_3$, PMMA standards).*

In most cases, the molecular weight achieved were close to those targeted (*i.e.* 10-40 kg.mol^{-1}), the exception being **40HEMA2** and **40HEMA20**. Again, this may be the result of a weighing error of AIBN, a sub-optimal initiation or inefficient CTA. Most copolymers were made to high conversion (approx. 70-90%) within 3-4 hours and dispersities ($Đ_M$) obtained were typically in the range of 1.5-2.0, the exception being **40HEMA20** and **40META5**. Moreover, this may be the result of a sub-optimal initiation or inefficient CTA.

The molecular weights were determined with size exclusion chromatography (SEC) in $CHCl_3$. The SEC chromatograms of both copolymers with molecular weight ranges targeted (M_n = 10 kg.mol^{-1} and 40 kg.mol^{-1}) are mostly uniform (*Figure 79, Figure 80*).

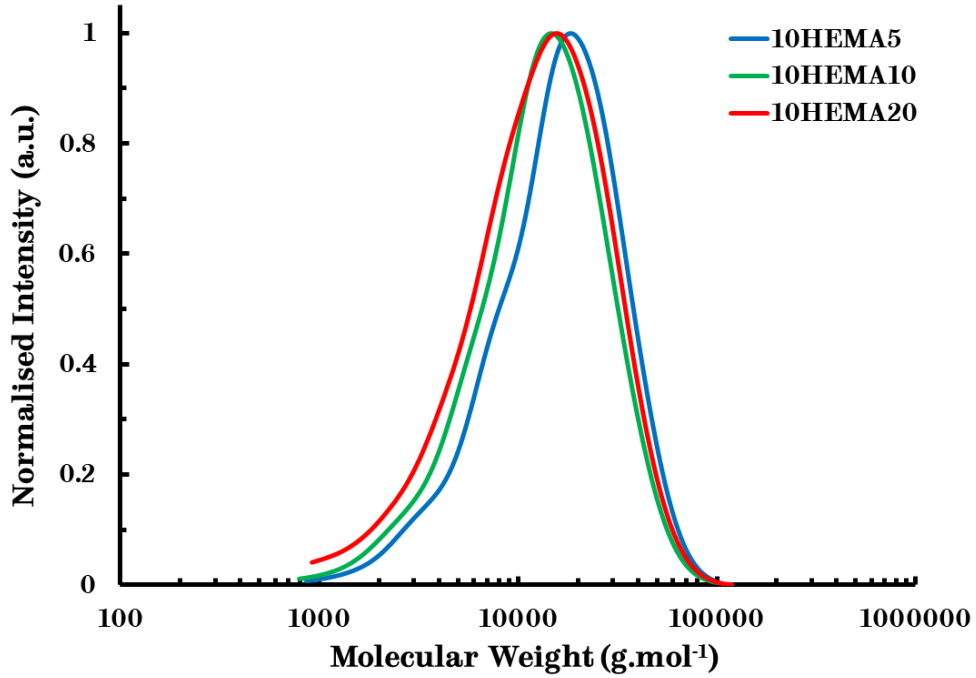

Figure 79: SEC chromatograms of poly(EHMA-co-HEMA) with a targeted molecular weight M_n = 10 kg.mol^{-1} and different HEMA concentrations ($CHCl_3$, PMMA standards).

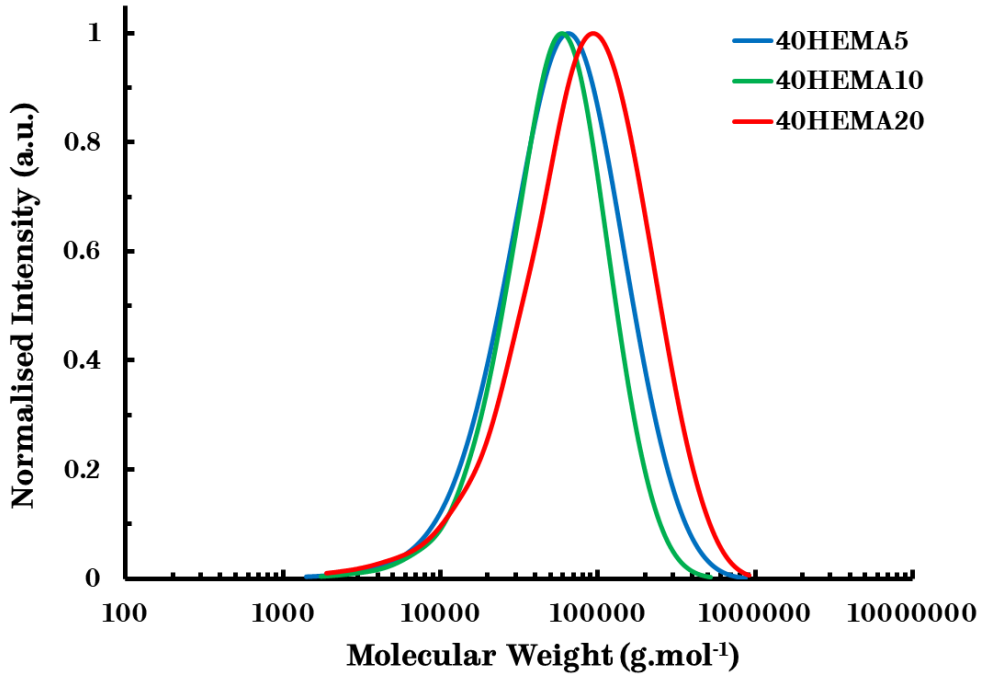

Figure 80: SEC chromatograms of poly(EHMA-co-HEMA) with a targeted molecular weight M_n = 40 kg.mol^{-1} and different HEMA concentrations ($CHCl_3$, PMMA standards).

As previously discussed, different chemical compositions were targeted to determine the influence of the prepolymer composition and resulting network cross-link density on their performance. After the initial experiments, the 2 mol.% composition was not further investigated since the cross-link density of the consequent networks was too low and the networks completely dissolved (*vide infra*). 20 mol.% HEMA copolymers were synthesised in order to gain insight in the effect of increased cross-linking in the networks.

For poly(EHMA-*co*-META), only the 5% META copolymers were initially synthesised as a consequence of the limited commercial availability of META. Fine-tuning was required to the polymerisation parameters to synthesise **10META10** and **40META5**. The 20 mol.% META copolymers were not synthesised due to time constraints and the limited commercial availability of META. Furthermore, the SEC chromatograms of **10META5**, **10META10** and **40META5** are mostly uniform (*Figure 81*).

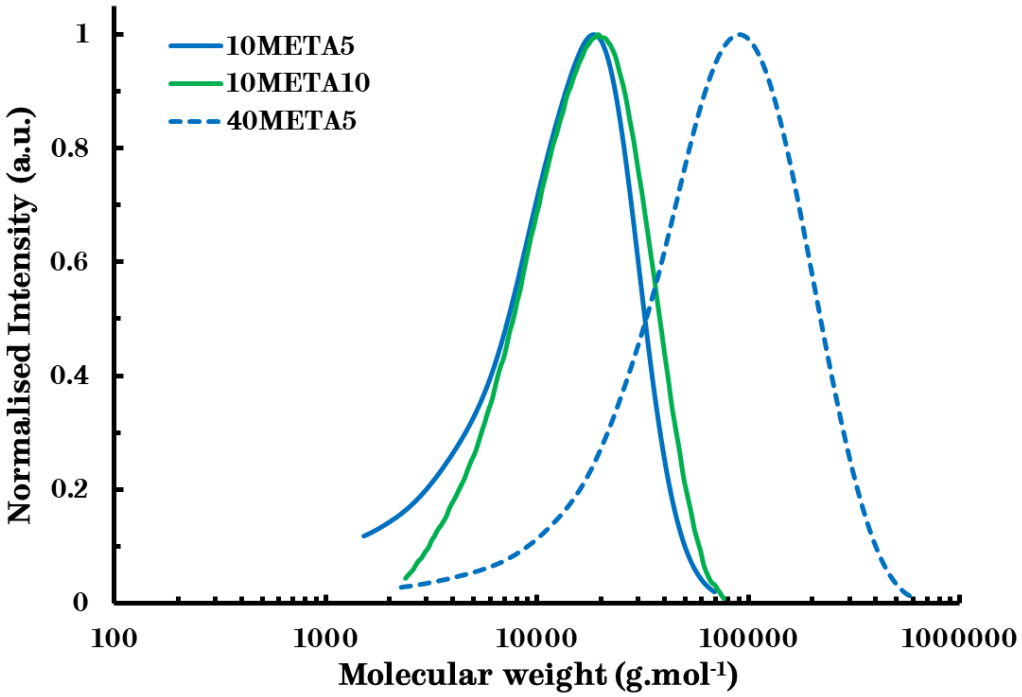

Figure 81: SEC chromatograms of poly(EHMA-co-META) with a different targeted molecular weights and different META concentrations ($CHCl_3$, PMMA standards).

The composition was determined using ^{1}H NMR spectroscopy. The relevant resonances, required for the calculation of the HEMA content, were the methylene proton resonances adjacent to the ester group of EHMA at chemical shifts δ = 3.75-4.00 ppm, which overlap with the methylene proton resonances adjacent to ester group of HEMA and the signals at δ = 4.00-4.25 ppm corresponding to the methylene proton resonances adjacent to the hydroxyl group of copolymerised HEMA (*Figure 82*). Furthermore, due to the resonance overlap at δ = 3.75-4.00, the relative ratio of the integrated resonance peaks at δ = 4.00-4.25 ppm and δ = 3.75-4.00 ppm is the same as the previously discussed percentage ratio (*Table 25*). This percentage can then be used to calculate the average number of functional groups per chain (functionality).

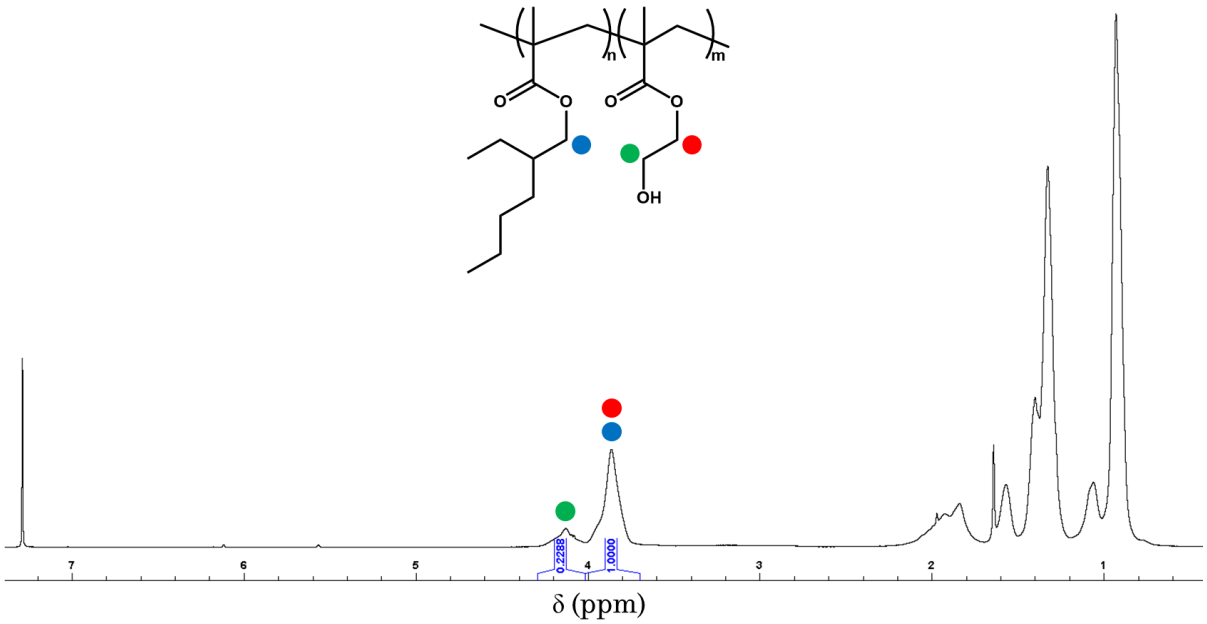

*Figure 82: ^{1}H NMR spectrum of **40HEMA20** (400 MHz, $CDCl_3$, 298 K).*

For the inverse method, the composition was also determined using ^{1}H NMR spectroscopy. The relevant resonances, required for the calculation of the META content, were the methylene proton resonances adjacent to the ester at chemical

shifts δ = 3.75-4.00 ppm for copolymerised EHMA and the signals at δ = 4.50-4.70 ppm corresponding to copolymerised META (*Figure 83*). Both of these resonances correspond to the same number of protons, namely 2 (-OCH_2-), so the relative ratio of the integration of these resonances can be used directly to determine the composition. Furthermore, this relative ratio can be converted into a percentage ratio using $Ratio_{Rel}/(1 + Ratio_{Rel})$ (*Table 26*). This percentage can then be used to calculate the average number of functional groups per chain (functionality).

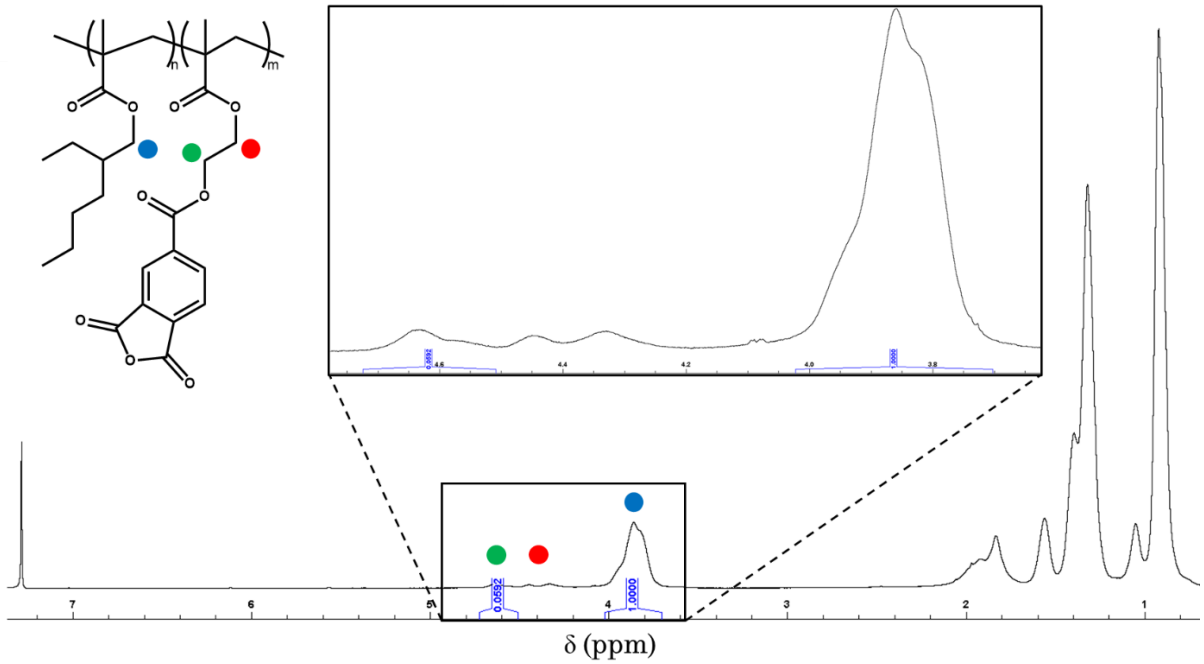

*Figure 83: ^{1}H NMR spectrum of **10META5** (400 MHz, $CDCl_3$, 298 K).*

Comparable to the previously discussed copolymerisations, the data shows that the copolymer composition obtained were similar to the feed composition with the HEMA and META content varying in the range of 1.2-22.9 mol.% and 5.4-9.2 mol.%, respectively (*Table 25, Table 26*).

Table 25: Monomer feed vs. Composition and molecular weight of poly(EHMA-co-HEMA).

Name	$f_{\%EHMA}$[a]	$f_{\%HEMA}$[a]	M_n (kg.mol^{-1})[b]	$Đ_M$[b]	$F_{\%HEMA}$[c]
10HEMA2	**98**	**2**	**9.8**	**1.8**	**1.2**
40HEMA2	**98**	**2**	**64.4**	**1.9**	**1.6**
10HEMA5	**95**	**5**	**11.4**	**1.8**	**7.8**
40HEMA5	**95**	**5**	**38.7**	**2.2**	**6.4**
10HEMA10	**90**	**10**	**9.5**	**1.8**	**12.1**
40HEMA10	**90**	**10**	**38.1**	**1.8**	**12.8**
10HEMA20	**80**	**20**	**8.4**	**2.0**	**21.7**
40HEMA20	**80**	**20**	**47.9**	**2.4**	**22.9**

[a]Feed ratio in mol.%. [b]Measured via SEC ($CHCl_3$, PMMA standards). [c]Calculated from ^1H NMR spectroscopy.

Table 26: Monomer feed vs. Composition and molecular weight of poly(EHMA-co-META).

Name	$f_{\%EHMA}$[a]	$f_{\%META}$[a]	M_n (kg.mol^{-1})[b]	$Đ_M$[b]	$F_{\%META}$[c]
10META5	**95**	**5**	**9.3**	**1.8**	**5.4**
40META5	**95**	**5**	**40.5**	**2.5**	**5.4**
10META10	**90**	**10**	**12.7**	**1.5**	**9.2**

[a]Feed ratio in mol.%. [b]Measured via SEC ($CHCl_3$, PMMA standards). [c]Calculated from ^1H NMR spectroscopy.

Differential scanning calorimetry (DSC) was used to determine the glass transition temperature of the copolymers. The values were calculated from the second heating curve (*Figure 84, Figure 85 and Figure 86*). Comparable to the previously discussed functional copolymers, the data shows that the T_g of the copolymers is dependent on the composition of the comonomers and increased proportionally with HEMA or META concentration (*Table 27, Table 28*).

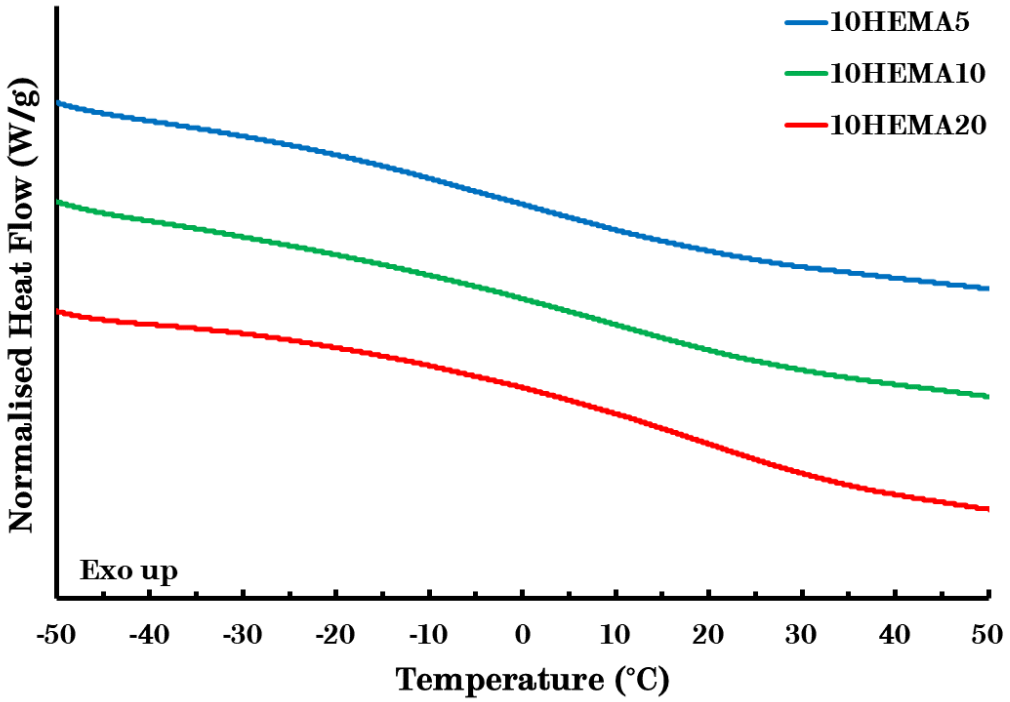

Figure 84: DSC thermograms of poly(EHMA-co-HEMA) with a targeted molecular weight M_n = 10 kg.mol^{-1} and different HEMA concentrations (Second heating curve, heating rate 10 °C.min^{-1}).

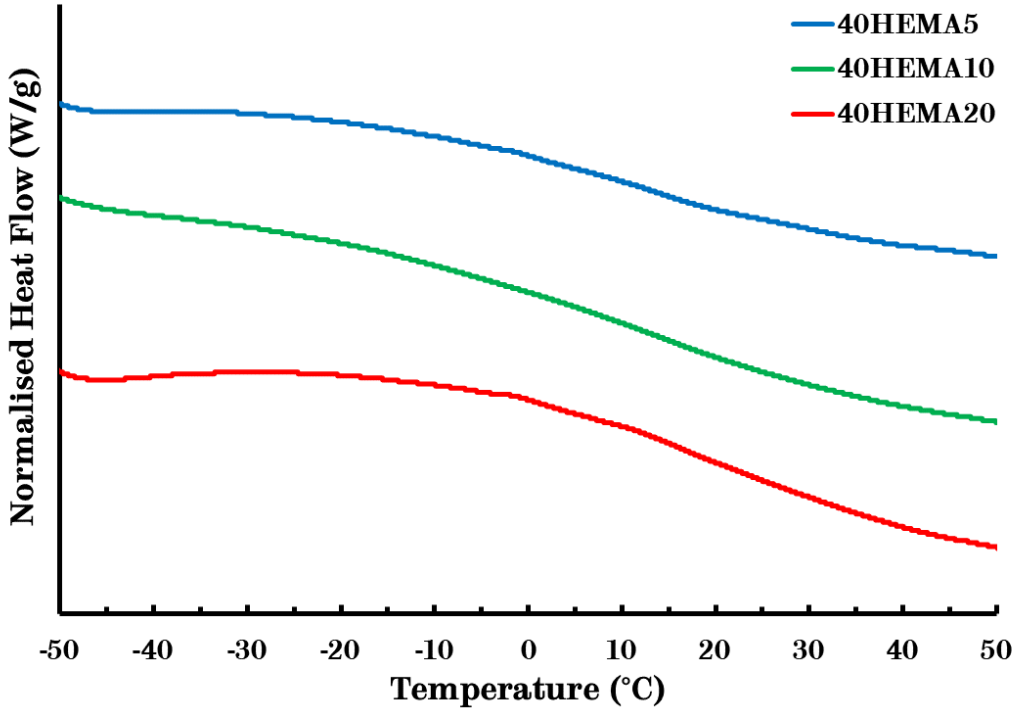

Figure 85: DSC thermograms of poly(EHMA-co-HEMA) with a targeted molecular weight M_n = 40 kg.mol^{-1} and different HEMA concentrations (Second heating curve, heating rate 10 °C.min^{-1}).

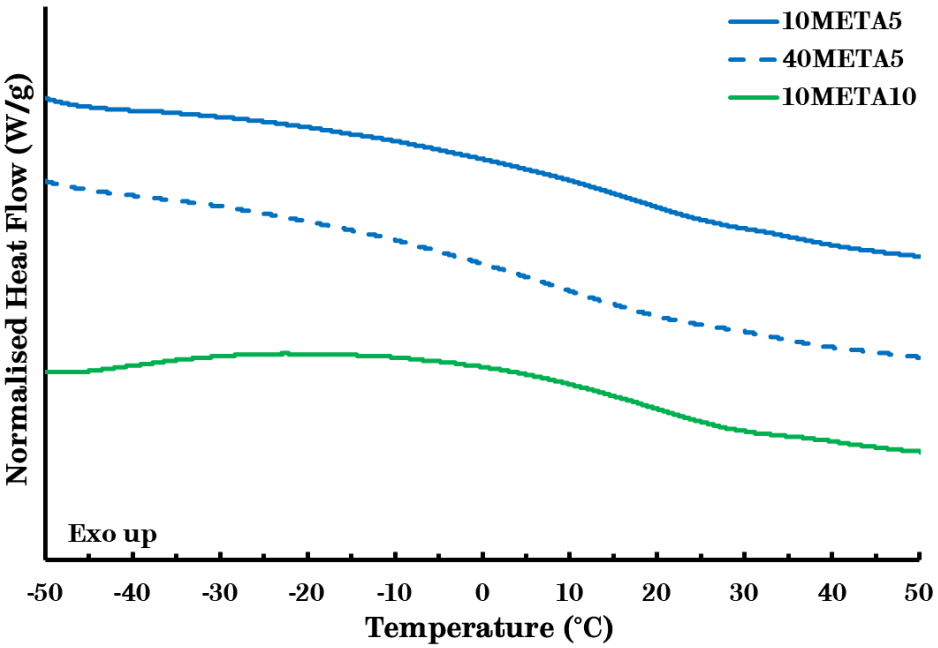

Figure 86: DSC thermograms of poly(EHMA-co-META) with both targeted molecular weights and different META concentrations (Second heating curve, heating rate 10 °C.min^{-1}).

Table 27: DSC results of the functional copolymers comparing the theoretical T_g with the experimental T_g for different concentrations of HEMA comonomer.

Name	***M*$_n$ (kg.mol^{-1})[a]**	***F*$_{\%HEMA}$[b]**	***T*$_g$ (°C) Th.[c]**	***T*$_g$ (°C) Exp.[d]**
10HEMA5	**11.4**	**7.8**	**-7.3**	**-2.3**
10HEMA10	**9.5**	**12.1**	**-4.6**	**11.4**
10HEMA20	**8.4**	**21.7**	**1.1**	**17.8**
40HEMA5	**38.7**	**6.4**	**-7.3**	**6.0**
40HEMA10	**38.1**	**12.8**	**-4.6**	**13.4**
40HEMA20	**47.9**	**22.9**	**1.1**	**21.6**

[a]Measured via SEC ($CHCl_3$, PMMA standards). [b]Calculated from ^{1}H NMR spectroscopy. [c]Calculated from Flory-Fox equation. [d]Measured via DSC (heating rate 10 °C.min^{-1}).

Table 28: DSC results of the functional copolymers comparing the theoretical T_g with the experimental T_g for different concentrations of META comonomer.

Name	***M*$_n$ (kg.mol^{-1})[a]**	***F*$_{\%META}$[b]**	***T*$_g$ (°C) Th.[c]**	***T*$_g$ (°C) Exp.[d]**
10META5	**9.3**	**5.4**	**N/a**	**15.5**
10META10	**12.7**	**9.2**	**N/a**	**17.4**
40META5	**40.5**	**5.4**	**N/a**	**8.7**

[a]Measured via SEC ($CHCl_3$, PMMA standards). [b]Calculated from ^{1}H NMR spectroscopy. [c]T_g of poly(META) not reported in literature. [d]Measured via DSC (heating rate 10 °C.min^{-1}).

4.2 Network synthesis

As previously discussed, cross-linked networks were obtained from the functional copolymers *via* solvent casting. The same scale of 5 – 20 g was used as in the synthesis of the aforementioned dissociative and associative networks (*vide supra*). Initially, an aromatic cross-linker pyromellitic dianhydride (**DAH1**) was considered for the previously mentioned reasons, namely that aromatic compounds are more rigid and could improve the overall strength of the polymer network (*Figure 87*). However, in a similar fashion to the Diels-Alder networks, compatibility issues occurred and phase separation was observed (*Figure 87*).

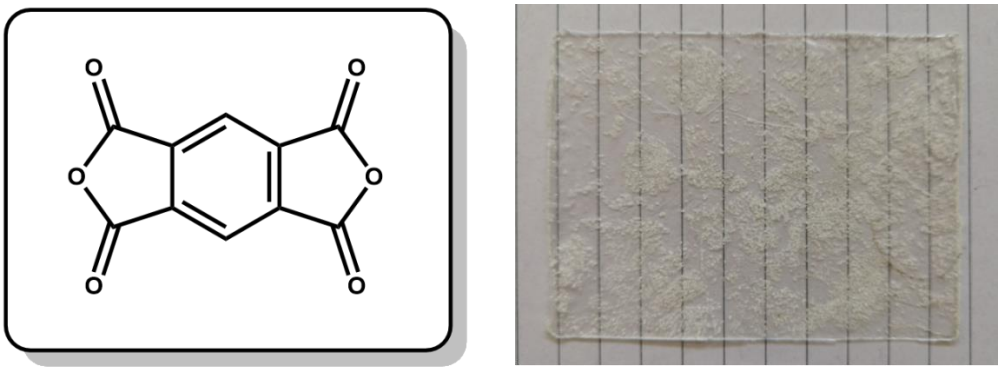

*Figure 87: The structure of pyromellitic dianhydride (**DAH1**) (left) and a picture of a typical cross-linked network obtained from poly(EHMA-co-HEMA) cross-linked with **DAH1** (right).*

In order to ensure good compatibility, aliphatic phthalic anhydride cross-linkers were synthesised. This synthesis involved the reaction of trimellitic anhydride chloride (TMAC) with a series of diols. The first two diols that were tested were 1,10-decanediol and 1,12-dodecanediol. These are crystalline solids with a melting point of 70-73 °C and 79-81 °C, respectively. Due to their crystallinity and polarity, the work-up was complicated as a consequence of the difficult separation from the unreacted TMAC. Therefore, more aliphatic and apolar diols were investigated, namely poly(ethylene glycol) (PEG), poly(tetrahydrofuran) (PTHF) and Pripol™ 2033 (**POL**).

These exhibited a better solubility in toluene and were easier to separate during work-up. Ultimately, **POL** was selected as the most relevant diol due to the identical C_{36} dimer core unit as in **BMI2** and **DAM2** for the other types of networks (*vide supra*) (*Figure 88*). Hence, this would allow for a better comparison of the chemistries without significant differences in the core structure of the cross-linker. Furthermore, **POL** functionalised with TMAC will be referred to as **DAH2**. No phase separation was observed in the networks cross-linked with **DAH2** (*Figure 88*).

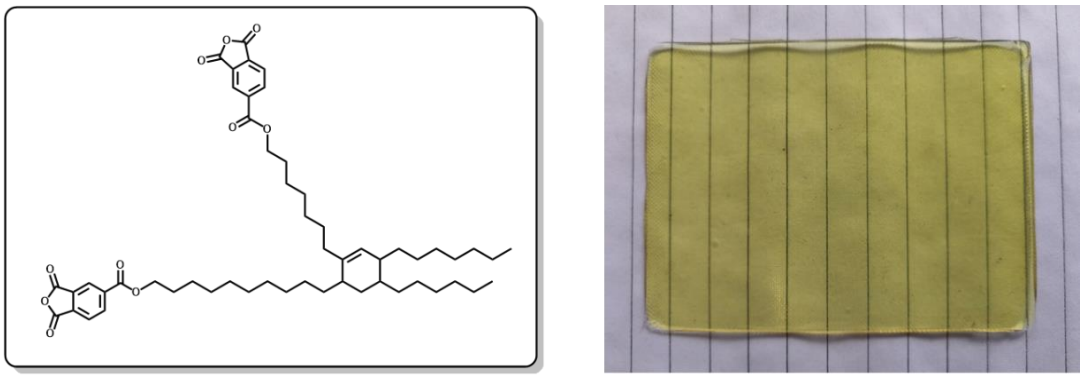

*Figure 88: The structure of phthalic anhydride cross-linker **DAH2** and a picture of a typical cross-linked network obtained from poly(EHMA-co-HEMA) cross-linked with **DAH2***

For the inverse method, poly(EHMA-*co*-META) was cross-linked with **POL** itself (*Figure 89*). This would result in an almost identical network as the original method, which facilitates the comparison with the other chemistries.

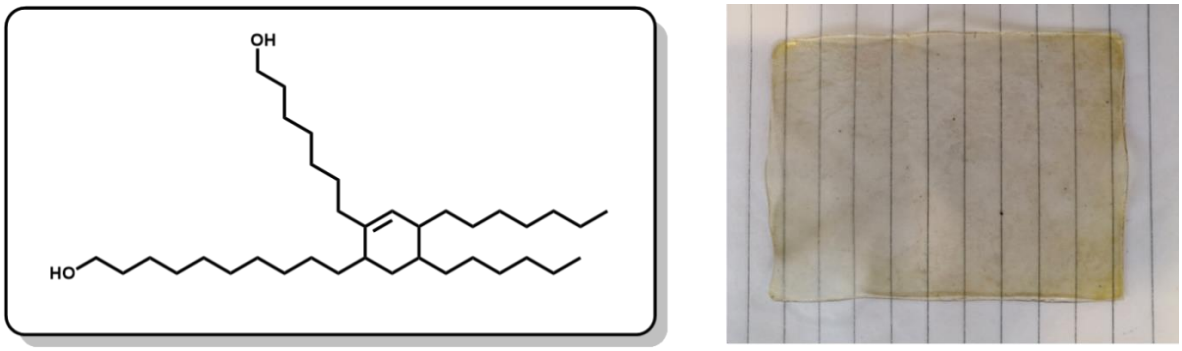

*Figure 89: The structure of flexible bifunctional cross-linker **POL** and a picture of a typical cross-linked network obtained from poly(EHMA-co-META) cross-linked with **POL***

Technically, the transesterification of PMEs should occur *via* a dissociative mechanism, comparable to the Diels-Alder networks, involving the formation of the cyclic anhydride.[199] Here, the relaxation of the material is independent of an excess of free hydroxyl groups. For example, Zhang *et al.* reported relaxation of their transesterification networks in the absence of an excess of hydroxyl groups.[200] However, it can also occur *via* the less preferred direct transesterification reaction upon heating above 200 °C resulting in an associative mechanism, which suggests partial vitrimeric behaviour.[199] An excess of hydroxyl groups was employed in this type of hybrid material as a compromise between these two mechanisms.

Initially, 20 mol.% of excess hydroxyl groups was selected, which was increased to 25 mol.% and ultimately 35 mol.% after the preliminary results of the synthesis of the aforementioned transamination networks, where 50 mol.% excess of cross-linker was incorporated. Thus, in order to cross-link poly(EHMA-*co*-HEMA), 0.65 - 0.80 eq. of phthalic anhydrides were added with respect to the hydroxyl moieties. Moreover, for the removal of the solvent, the duration, temperature and vacuum were determined to minimise spillage and bubble formation (*Table 29*).

Table 29: Drying/curing methods during solvent casting.

	Method 1	**Method 2**
Step 1	**1 h at 90 °C no vacuum**	**45 min at 110 °C no vacuum**
Step 2	**2 h at 100 °C 50% vacuum**	**1 h at 110 °C 50% vacuum**
Step 3	**2 h at 115 °C full vacuum**	**overnight at 60 °C full vacuum**

As previously discussed, the initial curing step was followed by compression moulding to obtain homogenous samples. Again, vacuum compression moulding of

the cured samples was performed to investigate initial processing parameters without wasting material. Further, geometries were prepared for rheological and thermal analysis, namely discs, bars and plates, by systematically varying the processing temperature, time and pressure (*Table 30, Table 31*). **10HEMA5-DAH2**, **10HEMA10-DAH2** and **40HEMA5-DAH2** required significantly lower processing temperatures and times, when compared to the previously reported PCL based PMEs (100 bar, 180 °C and 15 minutes) and step-growth PMEs based on triol trimethylolpropane (TMP), diol diethyl-1,5-pentanediol (DEPD) and dianhydride **DAH2** (100 bar, 150 °C and 1 hour).[199, 200] Thus, this suggests thermoplastic behaviour and poor network formation, which was later confirmed by solubility experiments (*vide infra*). Moreover, the networks based on poly(EHMA-*co*-META) required high processing temperatures indicating slow dynamic exchange kinetics of the transesterification.

Table 30: Compression moulding parameters of plate geometries of the cured transesterification networks based on poly(EHMA-co-HEMA) with different molecular weights and concentration of HEMA.

Name	M_n **(kg.mol^{-1})[a]**	$F_{\%HEMA}$[b]	***P*** **(bar)**	***Temp.*** **(°C)**	***Time*** **(min)**
10HEMA5-DAH2	**11.4**	**7.8**	**20**	**60**	**1**
10HEMA10-DAH2	**9.5**	**12.1**	**40**	**80**	**6**
10HEMA20-DAH2	**8.4**	**21.7**	**40**	**170**	**20**
40HEMA5-DAH2	**38.7**	**6.4**	**20**	**110**	**2**
40HEMA10-DAH2	**38.1**	**12.8**	**50**	**190**	**5**
40HEMA20-DAH2	**47.9**	**22.9**	**40**	**170**	**30**

[a]Measured via SEC ($CHCl_3$, PMMA standards). [b]Calculated from ^{1}H NMR spectroscopy.

Table 31: Compression moulding parameters of plate geometries of the cured transesterification networks based on poly(EHMA-co-META) with different molecular weights and concentration of META.

Name	M_n **(kg.mol^{-1})[a]**	$F_{\%META}$[b]	***P*** **(bar)**	***Temp.*** **(°C)**	***Time*** **(min)**
10META5-POL	**9.3**	**5.4**	**50**	**190**	**30**
10META10-POL	**12.7**	**9.2**	**50**	**190**	**35**
40META5-POL	**40.5**	**5.4**	**50**	**200**	**35**

[a]Measured via SEC ($CHCl_3$, PMMA standards). [b]Calculated from ^{1}H NMR spectroscopy.

4.3 Characterisation of the networks

4.3.1 Thermal properties

Thermogravimetric analysis was performed to investigate the thermal stability of the materials. The lower molecular weight copolymers are thermally stable in the range of 280-310 °C, similar to the lower molecular weight poly(EHMA-*co*-AEMA) copolymers. Furthermore, the resultant networks had a 5% mass degradation temperature ($T_{deg5\%}$) of around 285-335 °C (*Figure 90*). Comparable trends were observed as in previously discussed networks, namely in the 400-500 °C region, an increased stability with higher composition (more crosslinks). Thus, the thermal stability of the copolymers is structurally reinforced by the flexible aliphatic cross-linker **DAH2**.

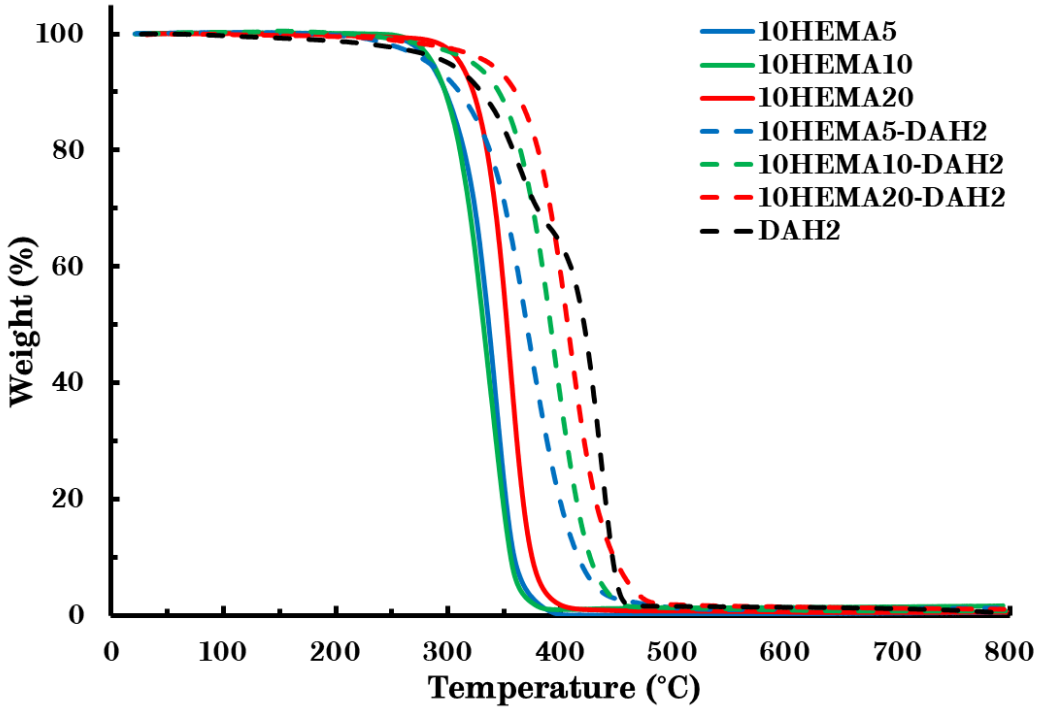

Figure 90: TGA thermograms of poly(EHMA-co-HEMA) with a targeted molecular weight M_n = 10 kg.mol^{-1} and their corresponding networks, comprising different HEMA concentrations (N_2, heating rate 10 °C.min^{-1}).

A similar $T_{deg5\%}$ range was found for the higher molecular weight copolymers (290-300 °C) and the resultant networks (300-325 °C) (*Figure 91*). Again, there is an overall increase in stability found after cross-linking, which is more pronounced for the higher compositions (higher cross-link density). Finally, the $T_{deg5\%}$ range of the poly(EHMA-*co*-META) was 250-290 °C (*Figure 92*). Similar to the previously discussed transesterification networks, the resulting networks exhibited an increased thermal stability ($T_{deg5\%}$ range of 277-312 °C). Thus, the observed stability lies between the reported $T_{deg5\%}$ = 253 °C for the step-growth PMEs based on trifunctional polycaprolactone (PCL, M_n = 2 kg.mol^{-1}, T_g = −63 °C) and aromatic cross-linker **DAH1** and the reported $T_{deg5\%}$ = 311 °C for the step-growth PMEs based on triol TMP, diol 1,6-hexanediol and aliphatic cross-linker **DAH2**.[161, 200]

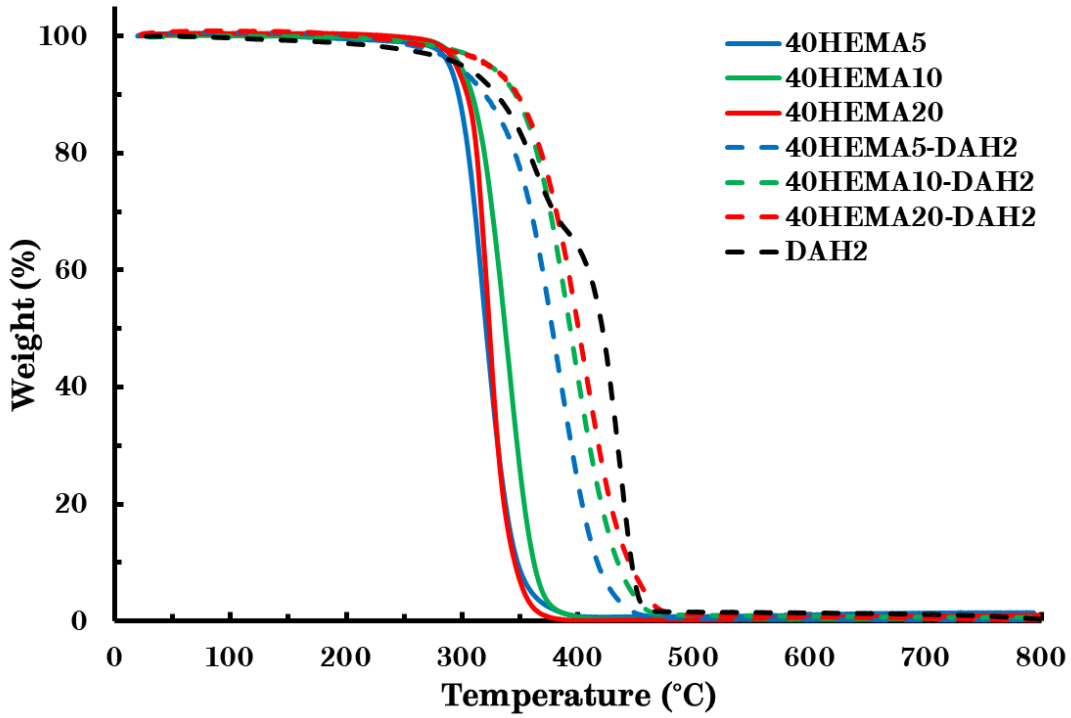

Figure 91: TGA thermograms of poly(EHMA-co-HEMA) with a targeted molecular weight M_n = 40 kg.mol^{-1} and their corresponding networks, comprising different HEMA concentrations (N_2, heating rate 10 °C.min^{-1}).

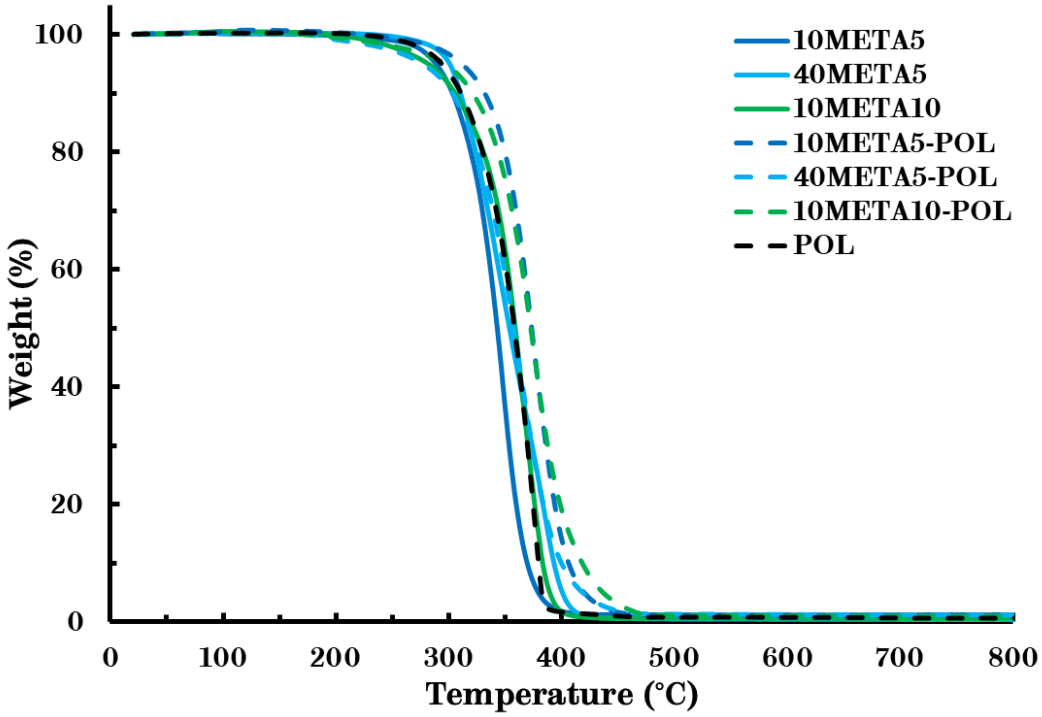

Figure 92: TGA thermograms of poly(EHMA-co-META) with different targeted molecular weights and their corresponding networks, comprising different META concentrations (N_2, heating rate 10 °C.min^{-1}).

DSC was performed to determine the glass transition temperature of the networks (*Table 32, Table 33*). A similar trend was found compared to the Diels-Alder and transamination networks, namely that the cross-linked networks have a lower T_g when compared to the respective prepolymers (*Figure 93, Figure 94, Figure 95*). This decrease could be rationalised by the introduction of the flexible cross-linkers **DAH2** and **POL**, which have a significantly lower T_g than the copolymers (-17 °C and -63 °C, respectively). Similar to the Diels-Alder networks, this plasticising effect is inversely correlated with the composition of the networks based on the higher molecular weight copolymers, namely larger decreases in T_g were observed for networks with a higher HEMA content (*Table 32*).

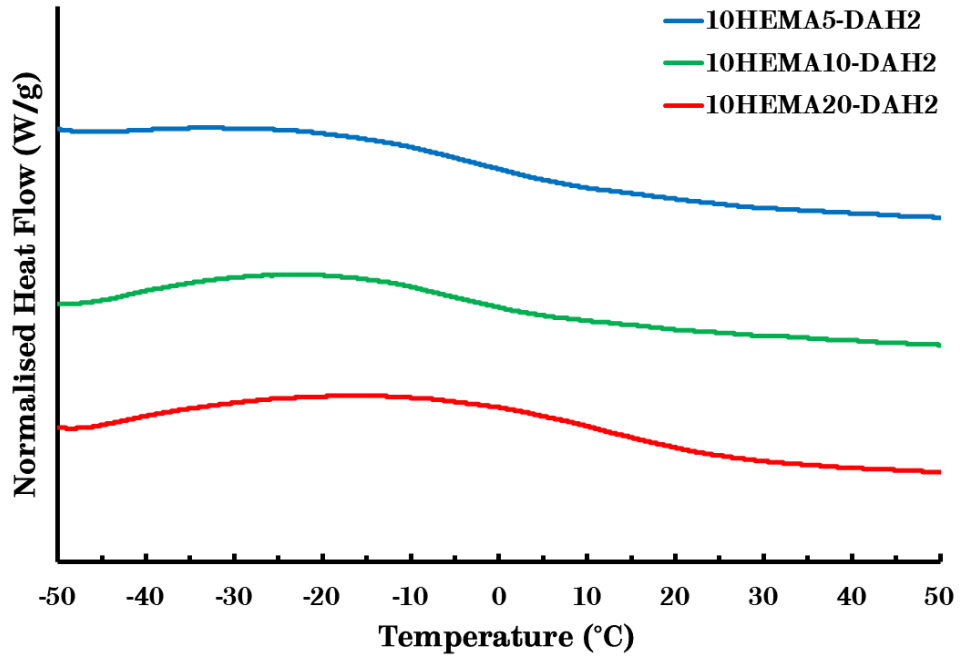

Figure 93: DSC thermograms of the networks based on poly(EHMA-co-HEMA) with a targeted molecular weight M_n = 10 kg.mol^{-1} and different HEMA concentrations (Second heating curve, heating rate 10 °C.min^{-1}).

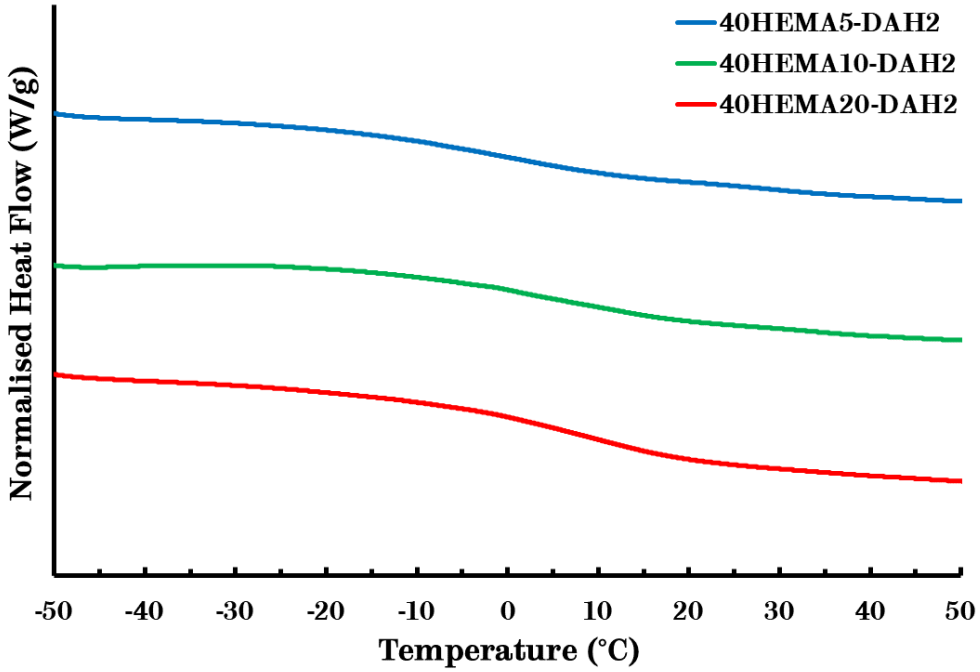

Figure 94: DSC thermograms of the networks based on poly(EHMA-co-HEMA) with a targeted molecular weight M_n = 40 kg.mol^{-1} and different HEMA concentrations (Second heating curve, heating rate 10 °C.min^{-1}).

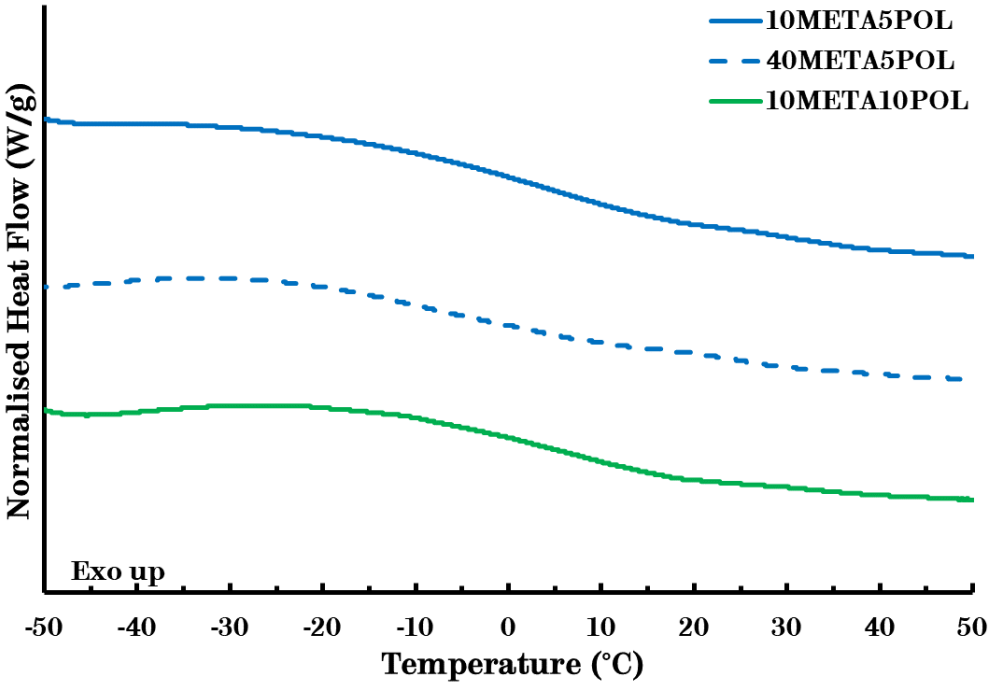

Figure 95: DSC thermograms of the networks based on poly(EHMA-co-META) with different targeted molecular weights and different META concentrations (Second heating curve, heating rate 10 °C.min^{-1}).

Table 32: T_g of poly(EHMA-co-HEMA) and resulting networks.

Name	M_n (kg.mol^{-1})[a]	$F_{\%HEMA}$[b]	T_g (°C)[c]
10HEMA5	**11.4**	**7.8**	**-2.3**
10HEMA5-DAH2			**-2.9**
10HEMA10	**9.5**	**12.1**	**11.4**
10HEMA10-DAH2			**-5.1**
10HEMA20	**8.4**	**21.7**	**17.8**
10HEMA20-DAH2			**12.1**
40HEMA5	**38.7**	**6.4**	**6.0**
40HEMA5-DAH2			**0.4**
40HEMA10	**38.1**	**12.8**	**13.4**
40HEMA10-DAH2			**2.9**
40HEMA20	**47.9**	**22.9**	**21.6**
40HEMA20-DAH2			**7.2**

[a] Measured via SEC ($CHCl_3$, PMMA standards). [b] Calculated from ^{1}H NMR spectroscopy. [c] Measured via DSC (heating rate 10 °C.min^{-1}).

Table 33: T_g of poly(EHMA-co-META) and resulting networks.

Name	M_n **(kg.mol^{-1})[a]**	$F_{\%META}$[b]	T_g **(°C)[c]**
10META5	**9.3**	**5.4**	**15.5**
10META5-POL			**3.7**
10META10	**12.7**	**9.2**	**17.4**
10META10-POL			**2.5**
40META5	**40.5**	**5.4**	**6.9**
40META5-POL			**-5.3**

[a]Measured via SEC ($CHCl_3$, PMMA standards). [b]Calculated from ^1H NMR spectroscopy. [c]Measured via DSC (heating rate 10 °C.min^{-1}).

4.3.2 Solubility

Solubility experiments were conducted in order to assess the extent of the network formation *via* Soxhlet extraction. The high boiling solvent toluene was selected to facilitate comparison with the results of the previously discussed networks (*Table 34, Table 35*). Additionally, there should be no interference of the dissociative mechanism at the boiling point of toluene as a consequence of the ring closure reaction resulting in the formation of the phthalic anhydride moieties only occurring at temperatures above 170 °C.[199] For the networks based on poly(EHMA-*co*-HEMA) with a targeted molecular weight M_n = 10 kg.mol^{-1}, all soluble fractions were nearly 100%, except for **10HEMA20-DAH2** (*Figure 96*).

As previously discussed, this suggests that the network formation in those samples failed. Cross-referencing these results with the functionality indicates that the theoretical average number of hydroxyl groups per chain (4.5 – 6.0) is too low to form a network in this type of material (*Table 34*). Furthermore, due to the aforementioned excess of hydroxyl groups, the experimental average number of hydroxyl groups that can actually form a cross-linking bond with the phthalic anhydrides is 20 - 35% lower (3.6 to 4.5).

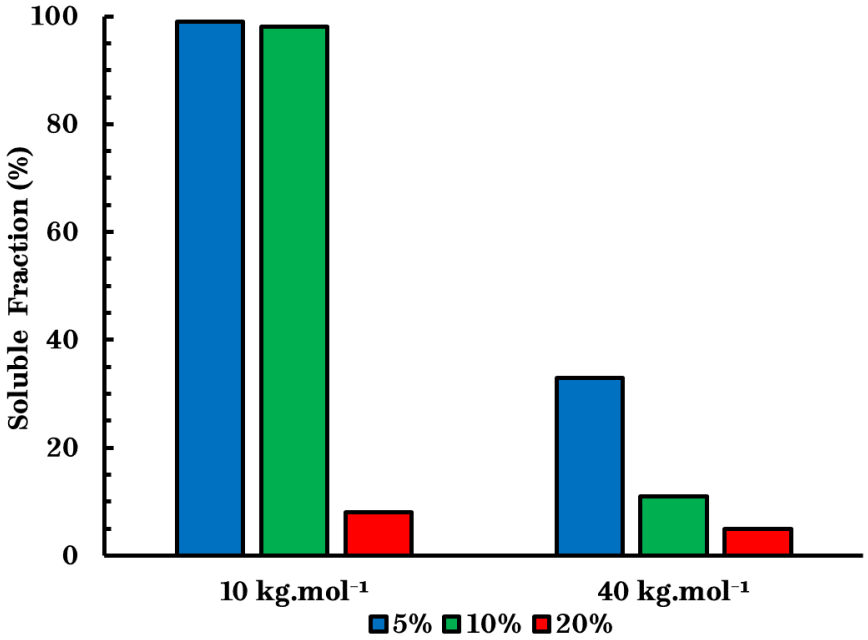

Figure 96: Soluble fractions of both sets of transesterification networks at different concentrations of HEMA (5, 10, 20 mol.%) after extraction in toluene.

For the networks based on poly(EHMA-*co*-HEMA) with the higher targeted molecular weight, the soluble fraction were in the range of 5-33% (*Table 34*). Here, a decrease was observed of the soluble fractions with composition (cross-link density), indicating a poor network formation for **40HEMA5-DAH2** (*Figure 96*). Moreover, a post-cure might be necessary to improve the formation of the networks.

Further, the degrees of swelling for the networks based on poly(EHMA-*co*-HEMA) with the higher targeted molecular weight decreased with increasing cross-link density and ranged from 370-690% (*Figure 97*). **10HEMA5-DAH2** and **10HEMA10-DAH2** exhibit low degrees of swelling (35-77%) after the extraction and can be explained by the exceptionally low gel fraction (1-2%) of the remaining network rather than being highly cross-linked samples, similar to the previously discussed **10AEMA5-DAM2** (*Table 34*).

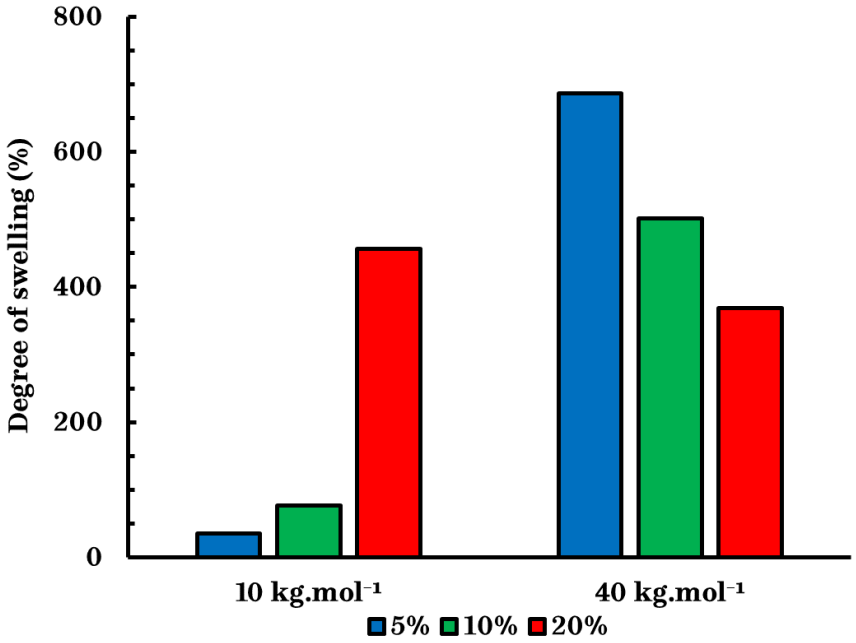

Figure 97: Degree of swelling of both sets of transesterification networks at different concentrations of HEMA (5, 10, 20 mol.%) after extraction in toluene.

For the networks based on poly(EHMA-*co*-META), the soluble fractions were in the range of 2-9%, which indicated a good network formation (*Figure 98, Table 35*). This may be the result of the experimental average number of phthalic anhydride groups closely approximating the theoretical average number. Furthermore, the degree of swelling was in the range of 315-425%, which is consistent with **10HEMA20-DAH2** and **40HEMA20-DAH2** (*Figure 99*). Thus, they show soluble fractions and degrees of swelling comparable to step-growth PMEs based on triol TMP, DEPD and **DAH2** extracted in THF at 25 °C (6.4% and 416%, respectively).[199]

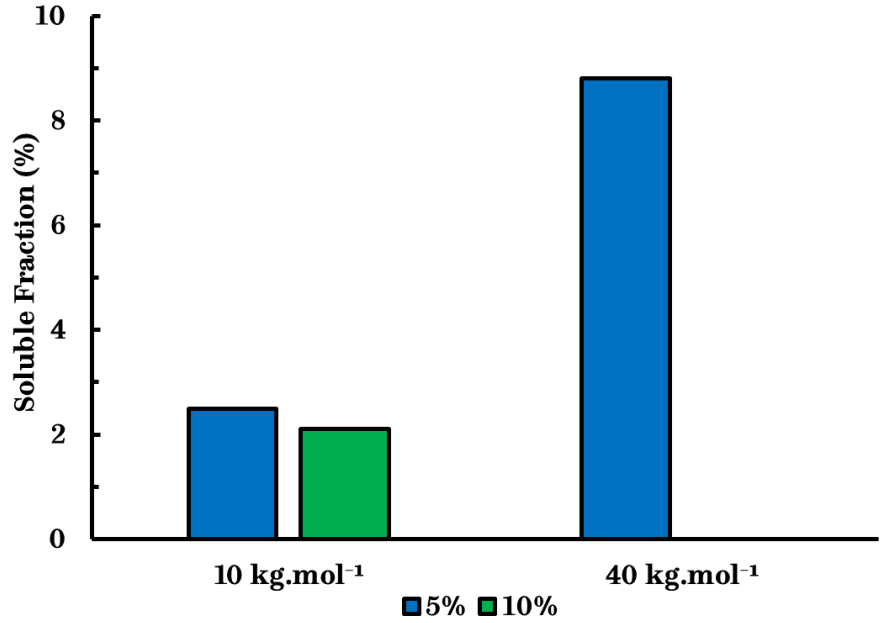

Figure 98: Soluble fractions of both sets of transesterification networks at different concentrations of META (5, 10 mol.%) after extraction in toluene.

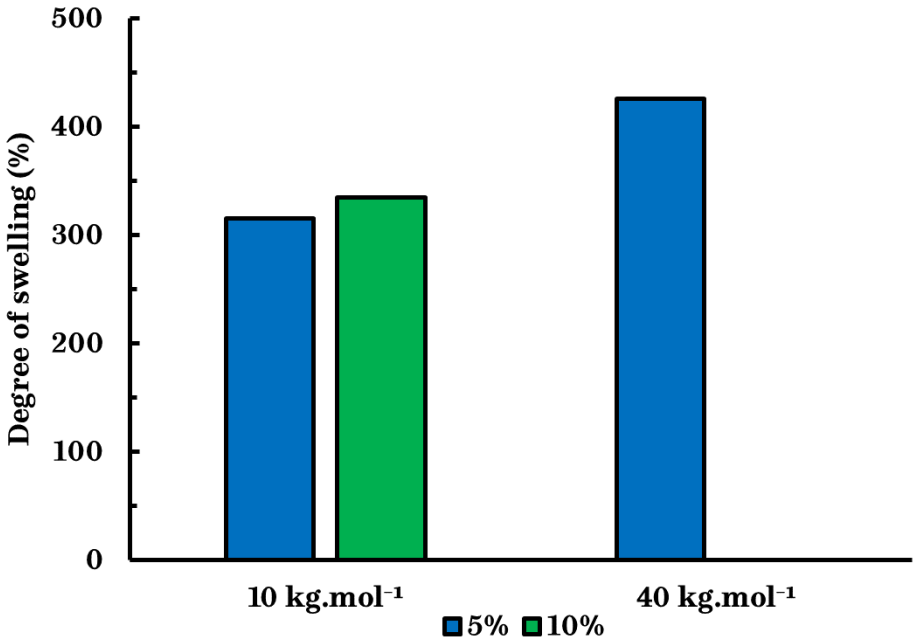

Figure 99: Degree of swelling of both sets of transesterification networks at different concentrations of META (5, 10 mol.%) after extraction in toluene.

Table 34: Results of the solubility experiments of both sets of transesterification networks at different HEMA concentrations compared to the functionality of the functional prepolymers.

Name	M_n **(kg.mol^{-1})[a]**	$F_{\%HEMA}$[b]	***Sol. Fr.*** **(%)[c]**	***Swell.*** **(%)[c]**	***Funct.***[a,b]
10HEMA5-DAH2	**11.4**	**7.8**	**99**	**35**	**4.5**
10HEMA10-DAH2	**9.5**	**12.1**	**98**	**77**	**6.0**
10HEMA20-DAH2	**8.4**	**21.7**	**8**	**456**	**9.9**
40HEMA5-DAH2	**38.7**	**6.4**	**33**	**686**	**12.7**
40HEMA10-DAH2	**38.1**	**12.8**	**11**	**501**	**25.5**
40HEMA20-DAH2	**47.9**	**22.9**	**5**	**369**	**59.4**

[a] *Measured via SEC ($CHCl_3$, PMMA standards).* [b] *Calculated from ^{1}H NMR spectroscopy.* [c] *Measured via Soxhlet extraction.*

Table 35: Results of the solubility experiments of both sets of transesterification networks at different META concentrations compared to the functionality of the functional prepolymers.

Name	M_n **(kg.mol^{-1})[a]**	$F_{\%META}$[b]	***Sol. Fr.*** **(%)[c]**	***Swell.*** **(%)[c]**	***Funct.***[a,b]
10META5-POL	**9.3**	**5.4**	**2.5**	**315**	**2.5**
10META10-POL	**12.7**	**9.2**	**2.1**	**335**	**5.6**
40META5-POL	**40.5**	**5.4**	**8.8**	**426**	**10.7**

[a] *Measured via SEC ($CHCl_3$, PMMA standards).* [b] *Calculated from ^{1}H NMR spectroscopy.* [c] *Measured via Soxhlet extraction.*

4.3.3 Rheology

The rheology of the transesterification networks was tested both with a rheometer and dynamic mechanical thermal analysis (DMTA). Initially, amplitude sweeps (strain sweeps) were performed to determine the linear viscoelastic region (LVR) of the material. Again, this LVR can be observed as a plateau, where the storage modulus G' exceeds the loss modulus G" (*Figure 100*). This region depends on the temperature and the frequency of the strain sweep experiments, which in this case was 200 °C and 10 Hz. Similar to the rheological experiments on the transamination networks, this temperature is the highest of all the temperatures at which the stress-relaxation experiments were performed (*vide infra*). Moreover, this ensured that the LVR that was found at this temperature was the most stringent and the LVR at all

other temperatures would encompass this range. Again, the experiments were performed on one network per set (*i.e.* **40HEMA20-DAH2**) and afterwards the selected strain value of 1% was kept the same for all consequent stress-relaxation experiments.

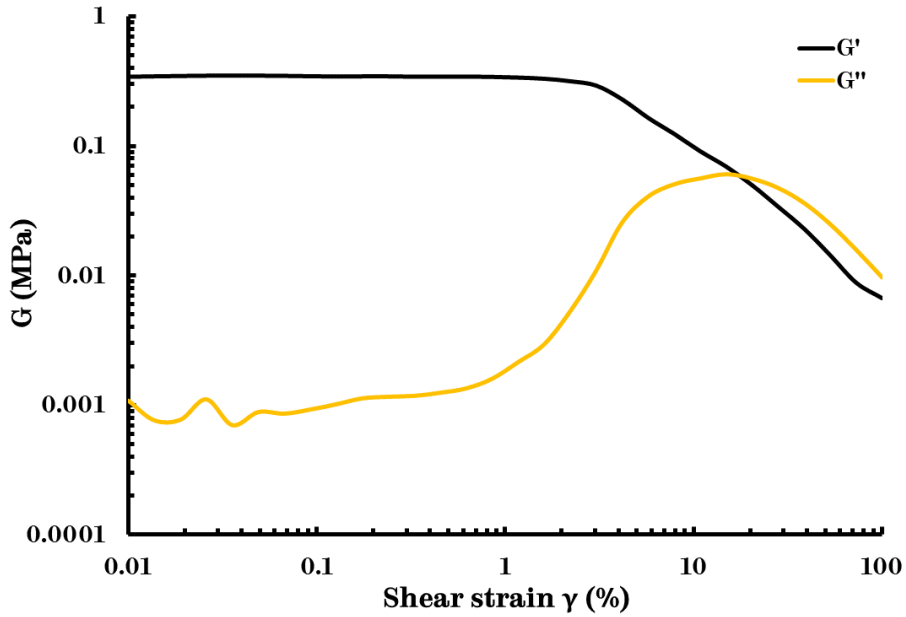

*Figure 100: Amplitude sweep of **40HEMA20-DAH2** at 200 °C and 10 Hz.*

Stress-relaxation experiments were performed to validate the dynamic behaviour of the transesterification networks. Only the networks with a good network integrity that exhibited a low soluble fraction were investigated, namely **40HEMA10-DAH2**, **10HEMA20-DAH2** and **40HEMA20-DAH2**. The same temperature that was employed with the transamination networks, namely 200 °C, was selected to gain insight into the differences between the sets of networks as well as the differences within the sets (*Figure 101*). Again, the relaxation modulus (G) was normalised against the apparent plateau value (G_0) at t = 1 s, after the initial step strain of 1%. The intersections of the horizontal dashed lines with the stress relaxation curves indicate where $G(t)/G_0 = 1/e$ and $t = \tau$.

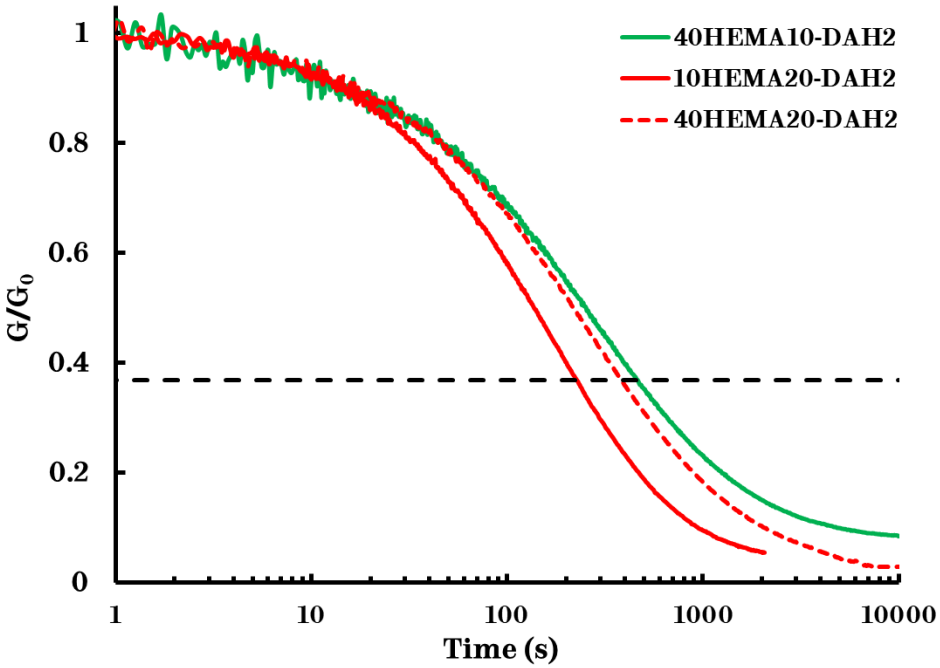

Figure 101: Comparison of stress-relaxation data of networks based on poly(EHMA-co-HEMA) prepolymers with different targeted molecular weights and concentrations of HEMA, measured at 200 °C.

The relaxation time τ ranged from 227 s for **10HEMA20-DAH2** to 464 s for **40HEMA10-DAH2**. Thus, a similar trend is observed as in the transamination networks, namely that the transesterification reaction, which governs the relaxation of this vitrimer, may be facilitated by the higher chain mobility of the networks based on the lower molecular weight copolymers. Again, this suggests that the relaxation of the material is mainly diffusion controlled.

Next, a comprehensive rheological study was done on one of these networks, namely **10HEMA20-DAH2**, in order to calculate the apparent activation energy (E_a) of this type of network and compare this value to the literature. The same temperature range as in the rheological experiments on **40AEMA10-DAM2** (160-200 °C) was selected to adequately compare the data and to reduce experimental time. Similar to the aforementioned rheological experiments, there is a clear trend visible of increasing τ with decreasing temperature (*Figure 102*).

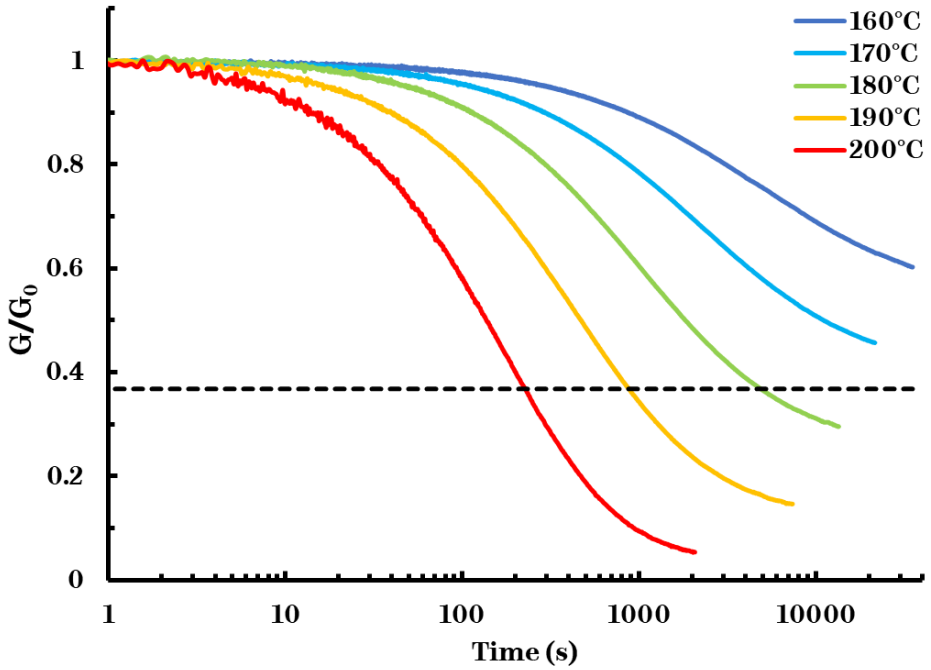

*Figure 102: Stress-relaxation data of **10HEMA20-DAH2** at different temperatures.*

The τ ranges from 227 s at 200 °C to 4879 s at 180 °C. Below 180 °C, stress-relaxation becomes extremely slow. Similar to the rheological experiments on **40AEMA10-DAM2**, there are constant intervals between the stress-relaxation curves. However, the curves do not relax back to baseline with decreasing temperature, which might be the result of a build-up of stress. This stress might be caused by additional esterification reactions of **DAH2** at higher temperatures, which could yield irreversible phthalic 1,2-diesters, triesters or tetra-esters.[200] These esters can only undergo direct transesterification *via* the associative mechanism, which generally requires catalyst and additional free hydroxyl groups in this temperature range.

The τ at 180-200 °C can be plotted against inverse temperature (T^{-1}) in an Arrhenius plot (*Figure 103*). Here, the E_a can be calculated from the slope of the trendline of the three data points. For this type of network, a value of 274 ± 2 kJ.mol^{-1} was found, which is significantly higher than the reported values of step-growth PMEs (75-123 kJ.mol^{-1}).[161, 199, 200]

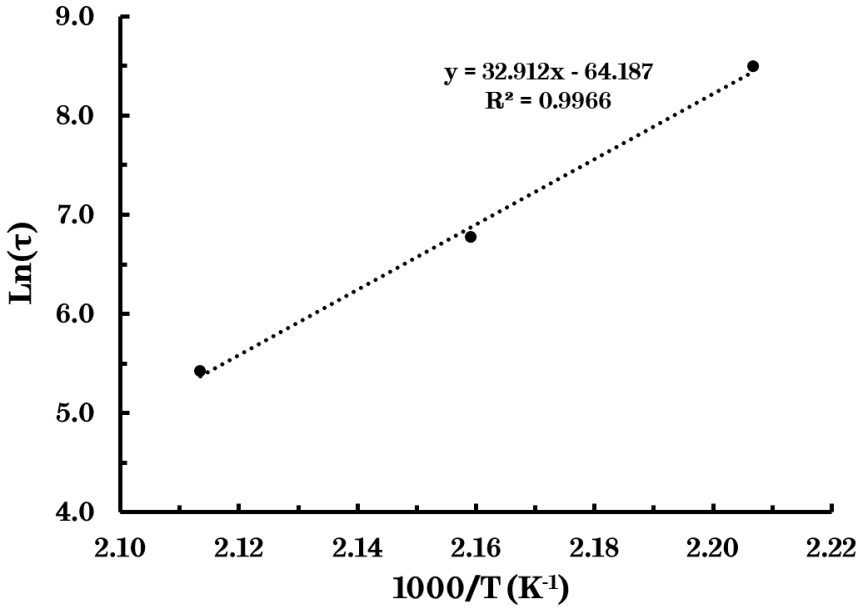

*Figure 103: Arrhenius plot of **10HEMA20-DAH2** showing the different relaxation times at different temperatures.*

A rheological study was also performed on one of the networks based on poly(EHMA-*co*-META), namely **10META5-POL**. Again, the same temperature range of 160-200 °C was selected as in the previously discussed rheological experiments to adequately compare the data and to reduce experimental time (*Figure 104*).

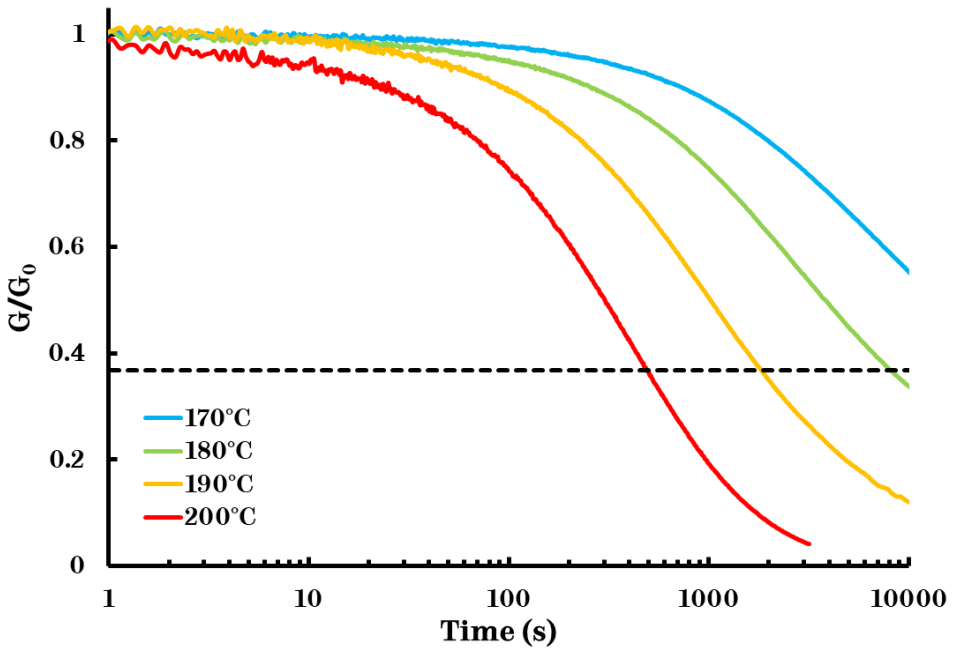

*Figure 104: Stress-relaxation data of **10META5-POL** at different temperatures.*

Similar trends were observed as in the results of **10HEMA20-DAH2**, namely increasing relaxation times and stress build-up with decreasing temperature. An E_a of 248 ± 1 kJ.mol^{-1} was calculated from the trendline of the Arrhenius plot, which is in a similar range as **10HEMA20-DAH2** (*Figure 105*).

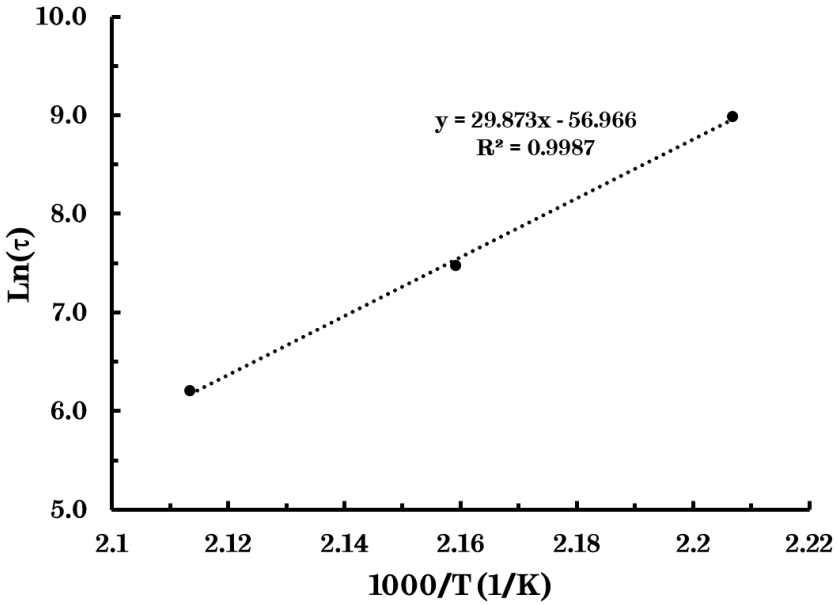

*Figure 105: Arrhenius plot of **10META5-POL** showing the different relaxation times at different temperatures.*

DMTA was also performed on **10HEMA20-DAH2** and **40HEMA20-DAH2**. Comparable to **10AEMA20-DAM2**, **10HEMA20-DAH2** and **40HEMA20-DAH2** exhibit a glassy plateau storage modulus (*G'*) of approximately 2.0 GPa and rubbery plateau storage modulus (G'_{rubber}) of 1.0-1.5 MPa, extending up to 200 °C (*Figure 106, Figure 107*). As previously discussed in *2.3.3 Rheology,* a M_c of 3091 g.mol^{-1} and 1961 g.mol^{-1} can be calculated for **10HEMA20-DAH2** and **40HEMA20-DAH2**, respectively (*Equation 7*).

These values are lower than the reported *G'* = 3.0-5.5 GPa and G'_{rubber} = 1-3 MPa for step-growth PCL-based PMEs (M_n = 2 kg.mol^{-1}, T_g = −63 °C), which were cross-linked with the aromatic **DAH1**.[200] The T_g can be defined as the midpoint of the *G'* inflection

and was significantly higher for both networks than the one observed using DSC analysis.

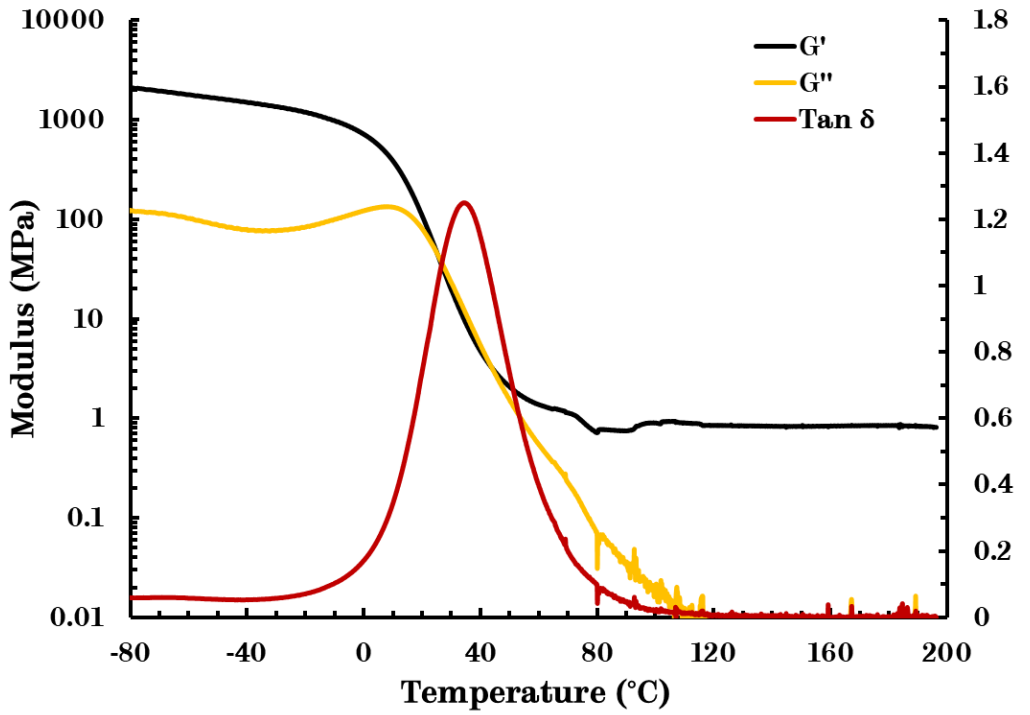

*Figure 106: Storage modulus, loss modulus and tan δ of **10HEMA20-DAH2** measured via DMTA (Heating rate 3 °C.min^{-1}).*

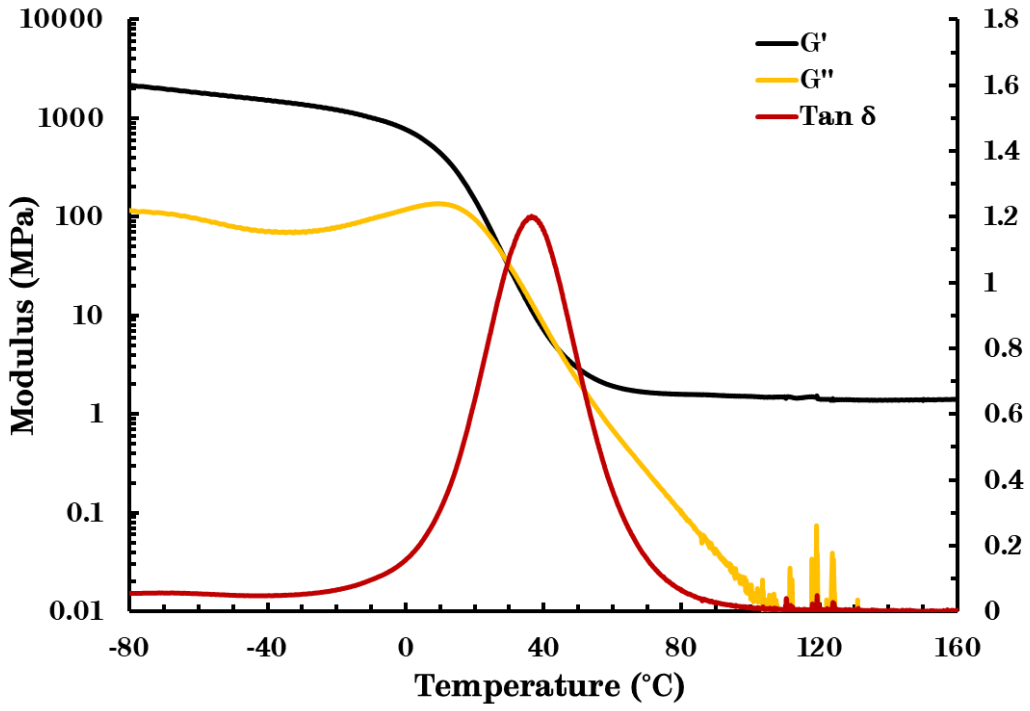

*Figure 107: Storage modulus, loss modulus and tan δ of **40HEMA20-DAH2** measured via DMTA (Heating rate 3 °C.min^{-1}).*

4.3.4 Mechanical properties

Tensile testing was performed to assess the mechanical properties of the transesterification networks. **10HEMA10-DAH2** was soft and highly elastic, with the final stress at break (σ_b) and elongation at break (ε_b) unable to be measured using the available experimental set-up, similar to the previously discussed **10AEMA5-DAM2** (*Figure 108*). This ε_b exceeding 1100% is comparable to the values reported of the homopolymer PEHMA.[170] Further, cross-referencing these results with the soluble fraction of **10HEMA10-DAH2** confirms the poor network formation as a consequence of the low average number of functional groups on the prepolymer chains. Furthermore, **10HEMA5-DAH2** was not tested due to the similar soluble fractions and lower average number of functional groups when compared to **10HEMA10-DAH2**. Thus, **10HEMA20-DAH2** is the only the network with a Young's modulus (E) and ε_b in the expected range.

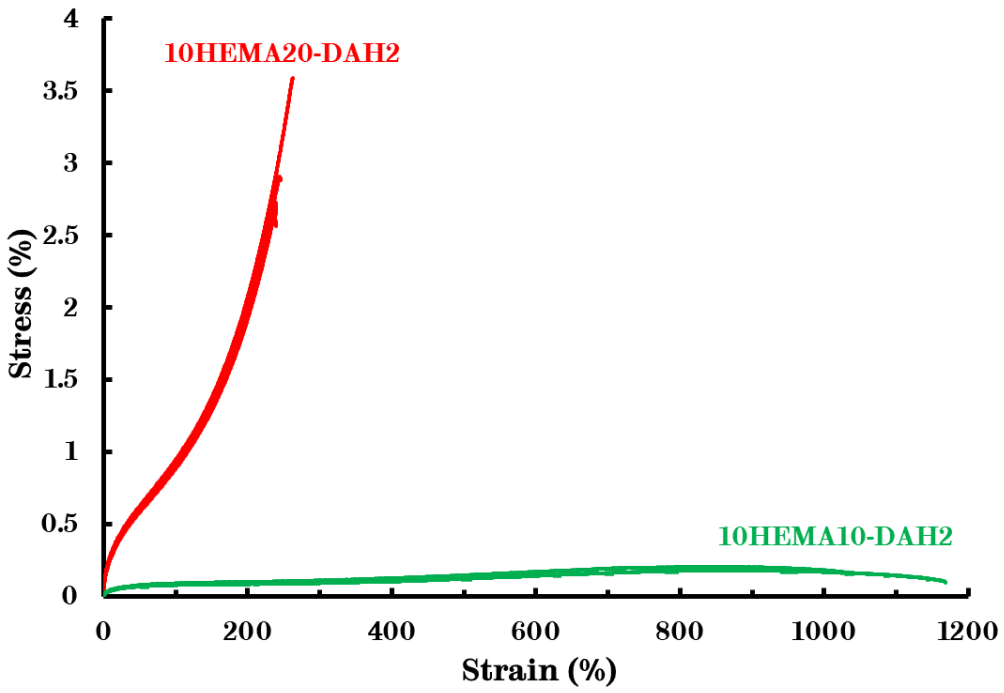

Figure 108: Stress-strain curves of the networks based on poly(EHMA-co-HEMA) with a targeted molecular weight M_n = 10 kg.mol^{-1} and different HEMA concentrations.

For the networks obtained from the higher molecular weight prepolymers, the same trend is visible as the Diels-Alder networks, namely the stiffness increases with the content of cross-linker units (*Figure 109*). Moreover, **40HEMA5-DAH2** lacks strain hardening, which is present in **40HEMA10-DAH2** and **40HEMA20-DAH2.** Further, it exhibits an elongation at break that is significantly higher than the expected range, which may be the result of incomplete curing since the network possesses a higher average number of functional groups than **10HEMA20-DAH2** (*vide supra*).

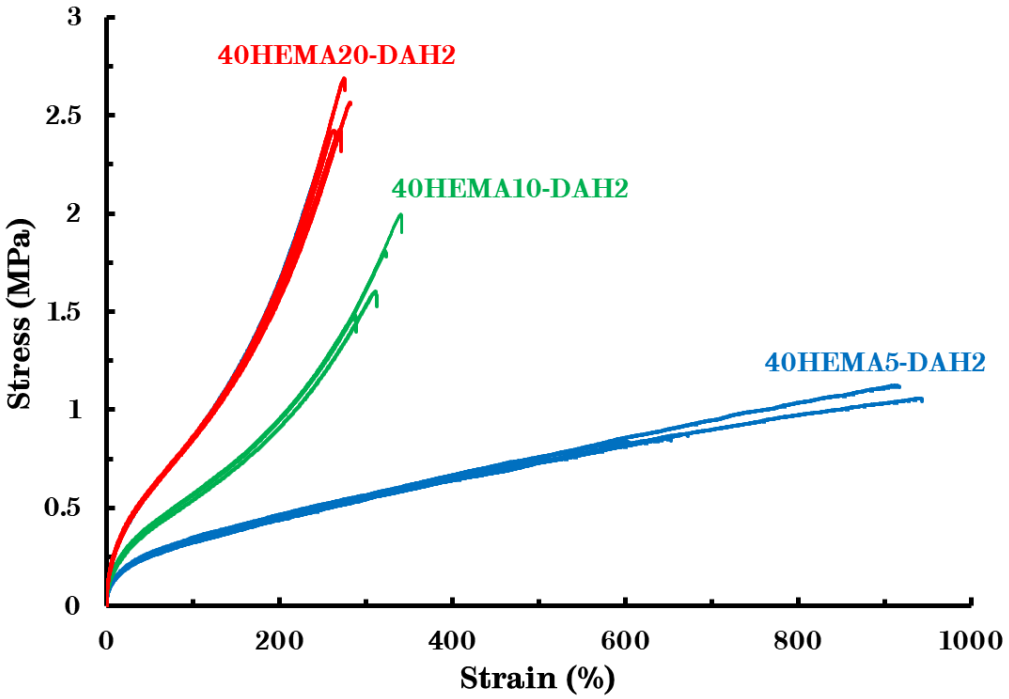

Figure 109: Stress-strain curves of the networks based on poly(EHMA-co-HEMA) with a targeted molecular weight M_n = 40 kg.mol^{-1} and different HEMA concentrations.

For the networks based on poly(EHMA-*co*-META), only **10META5-POL** and **10META10-POL** were investigated due to time constraints. **10META10-POL** exhibit a higher *E* and a significantly lower ε_b compared to **10HEMA10-DAH2** (*Figure 110*, *Table 37*). This can be explained by cross-referencing the tensile data with the functionality per chain (*vide supra*) (*Table 34, Table 35*). **10HEMA10-DAH2** and

10META10-POL possess on average 5.6 and 6.0 functional groups per chain, respectively. As previously discussed, an excess of 25% hydroxyl groups was selected during the synthesis of **10HEMA10-DAH2**. Thus, on average only 4.2 groups of the incorporated 5.6 groups reacted with the **DAH2** cross-linker. Furthermore, the functionality of **10META10-POL** remained 6.0 after forming the network. Consequently, the experimental average number of phthalic anhydride groups per chain that reacted with **POL** closely approximates the theoretical average number.

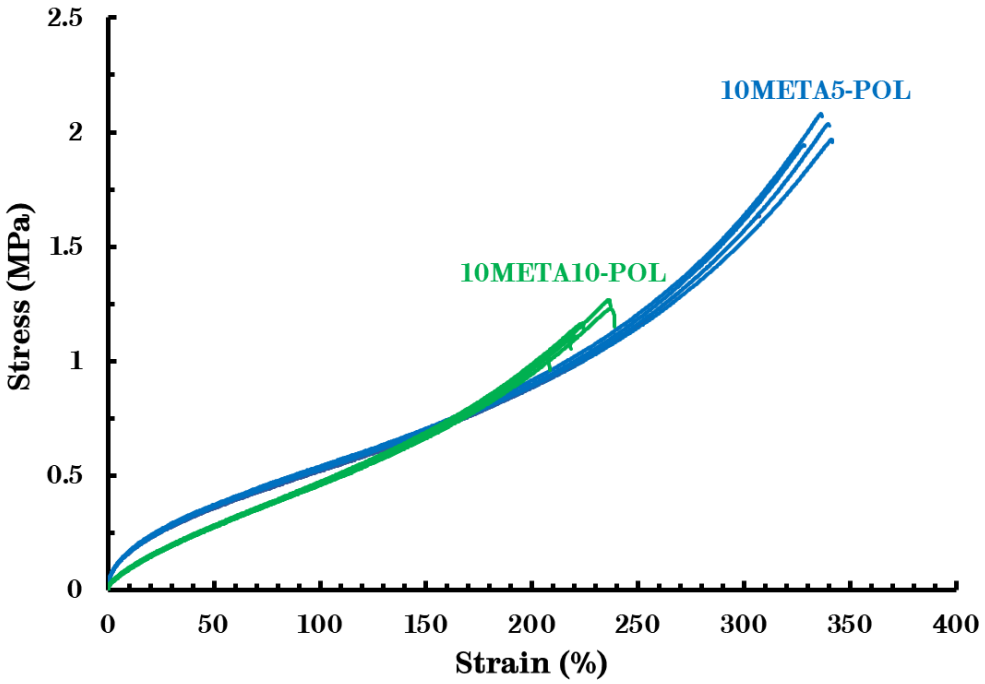

Figure 110: Stress-strain curves of the networks based on poly(EHMA-co-META) with a targeted molecular weight M_n = 10 kg.mol^{-1} and different META concentrations.

Moreover, the data of all transesterification networks show E in the range of 4-13 MPa, which is an improvement to the reported 5 ± 1 MPa for the homopolymer PEHMA (M_n = 53 kg.mol^{-1}) and 2.70 ± 0.06 MPa for the step-growth PMEs based on triol TMP, diol DEPD and phthalic dianhydride **DAH2**.[170, 199] However, the E range is exceeded by equivalent step-growth based PMEs with 1,6-hexanediol as the incorporated diol (E = 39 ± 6).[161]

Table 36: Tensile properties of the transesterification networks based on prepolymers with different HEMA concentrations.

Name	M_n (kg.mol^{-1})[a]	$F_{\%HEMA}$[b]	E (MPa)	σ_b (MPa)	ε_b (%)
10HEMA5-DAH2	**11.4**	**7.8**	**N/a**	**N/a**	**N/a**
10HEMA10-DAH2	**9.5**	**12.1**	**1.56 ± 0.62**	**N/a**	**N/a**
10HEMA20-DAH2	**8.4**	**21.7**	**12.78 ± 0.20**	**2.85 ± 0.16**	**243 ± 4**
40HEMA5-DAH2	**38.7**	**6.4**	**8.48 ± 0.06**	**0.94 ± 0.06**	**758 ± 71**
40HEMA10-DAH2	**38.1**	**12.8**	**11.23 ± 0.52**	**1.61 ± 0.10**	**311 ± 10**
40HEMA20-DAH2	**47.9**	**22.9**	**11.56 ± 0.17**	**2.44 ± 0.06**	**270 ± 5**

[a]Measured via SEC ($CHCl_3$, PMMA standards). [b]Calculated from ^{1}H NMR spectroscopy.

Table 37: Tensile properties of the transesterification networks based on prepolymers with different META concentrations.

Name	M_n (kg.mol^{-1})[a]	$F_{\%META}$[b]	E (MPa)	σ_b (MPa)	ε_b (%)
10META5-POL	**9.3**	**5.4**	**7.47 ± 0.17**	**1.93 ± 0.08**	**331 ± 6**
10META10-POL	**12.7**	**9.2**	**3.92 ± 0.28**	**1.02 ± 0.04**	**216 ± 5**

[a] Measured via SEC ($CHCl_3$, PMMA standards). [b]Calculated from ^{1}H NMR spectroscopy.

4.3.5 Ageing

Weathering experiments were conducted on **10HEMA20-DAH2** and **40HEMA20-DAH2** to investigate the longer-term stability of the material (*Figure 111, Figure 112*). Again, this experiment involved ageing the samples at 80 °C for 3 weeks and testing their tensile properties afterwards. This temperature ensured the samples would stay in the plateau region from DMTA (*vide supra*).

The E of **10HEMA20-DAH2** and **40HEMA20-DAH2** increased by 353% and 494%, respectively, and now exceeds all the values of the reported step-growth PMEs that were not aged (*vide supra*).[161, 199] Moreover, the samples displayed a higher stiffness (higher E, lower ε_b). Furthermore, this increase might be rationalised by a post-curing occurring in the material.

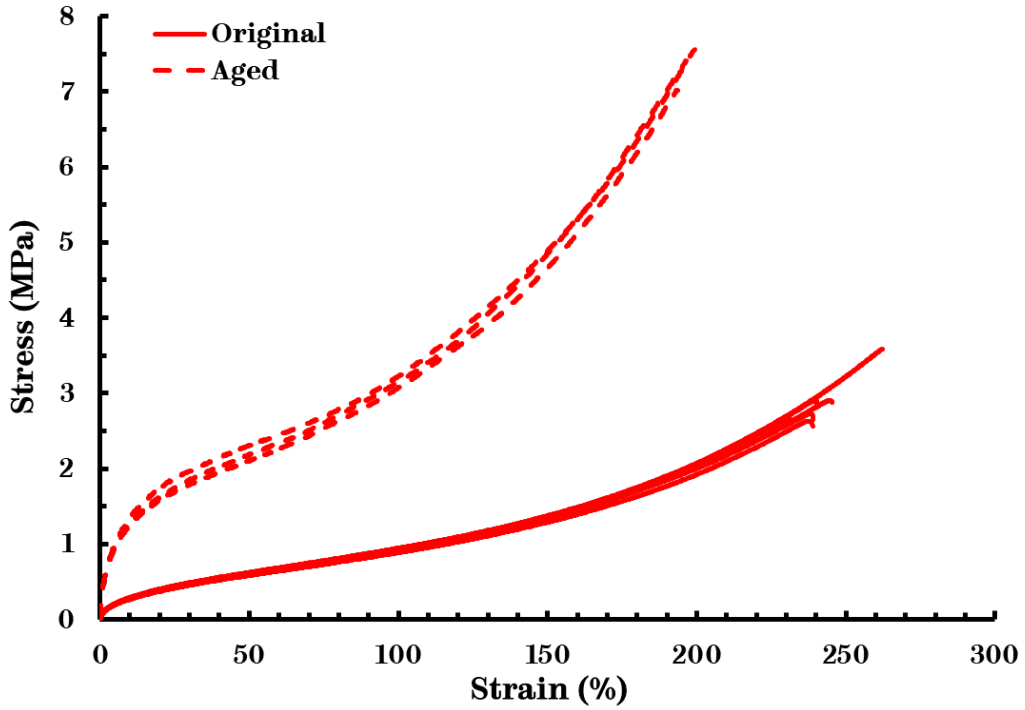

*Figure 111: Stress-strain curves of **10HEMA20-DAH2** before and after ageing at 80 °C for 3 weeks.*

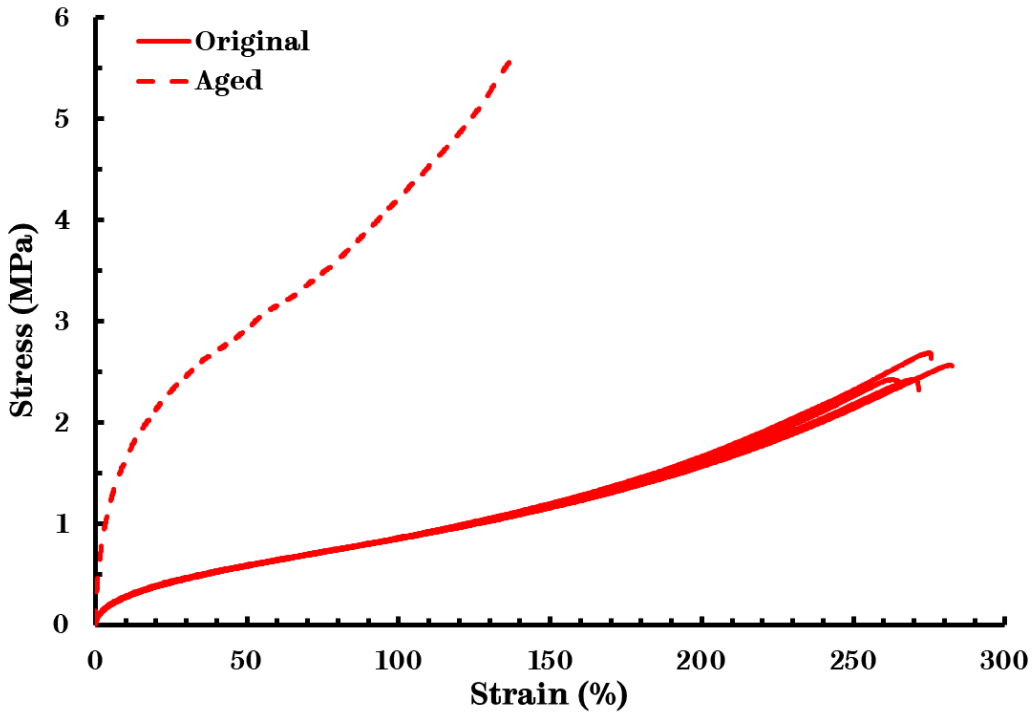

*Figure 112: Stress-strain curves of **40HEMA20-DAH2** before and after ageing at 80 °C for 3 weeks.*

Table 38: Results of the tensile testing of the networks based on poly(EHMA-co-HEMA) with 20% of HEMA before and after ageing at 80 °C for 3 weeks.

	Name	M_n (kg.mol^{-1})[a]	$F_{\%HEMA}$[b]	E (MPa)	σ_b (MPa)	ε_b (%)
Original	**10HEMA20-DAH2**	**8.4**	**21.7**	**12.78 ± 0.20**	**2.85 ± 0.16**	**243 ± 4**
Aged				**57.95 ± 2.69**	**7.33 ± 0.16**	**196 ± 2**
Original	**40HEMA20-DAH2**	**47.9**	**22.9**	**11.56 ± 0.17**	**2.44 ± 0.06**	**270 ± 5**
Aged				**68.61**	**5.65**	**139**

[a]Measured via SEC ($CHCl_3$, PMMA standards). [b]Calculated from ^1H NMR spectroscopy.

FTIR spectroscopy of both **10HEMA20-DAH2** and **40HEMA20-DAH2** was performed before and after ageing to investigate if any changes or degradation occurred (*Figure 113, Figure 114*). The IR spectra of both samples are nearly identical, indicating little degradation occurred during ageing.

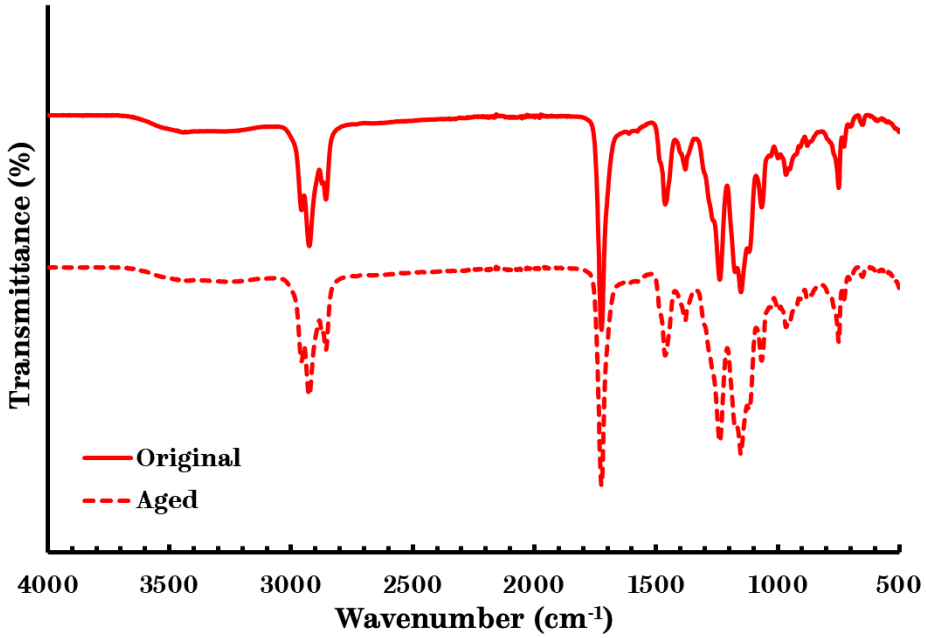

*Figure 113: IR spectrum of **10HEMA20-DAH2** before and after ageing at 80 °C for 3 weeks.*

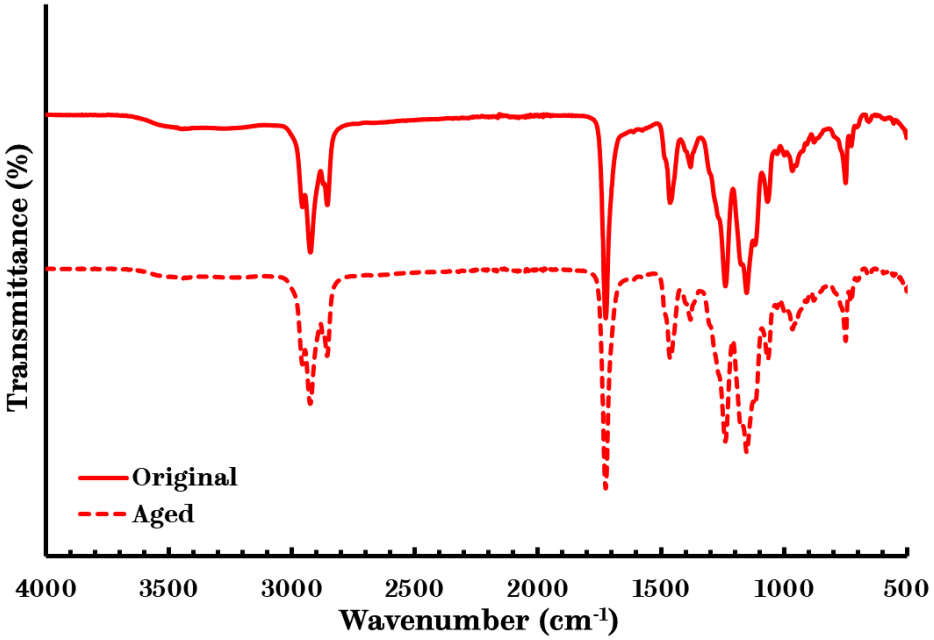

*Figure 114: IR spectrum of **40HEMA20-DAH2** before and after ageing at 80 °C for 3 weeks.*

4.3.6 Recyclability

In order to test the recyclability of the prepared networks, tensile testing was performed on different reprocessed cycles (recycles) and the results were compared to the pristine material (Original). Due to time constraints towards the end of the project, only one recycle (R1) was performed on **10HEMA20-DAH2** and **40HEMA20-DAH2** and two recycles (R2) on **40HEMA10-DAH2** (*Figure 115, Figure 116, Figure 117, respectively, and Table 39*).

Table 39: Reprocessing parameters of the transesterification networks based on poly(EHMA-co-HEMA) with different molecular weights and concentration of HEMA.

	Name	***M_n* (kg.mol^{-1})[a]**	***$F_{\%HEMA}$*[b]**	***P* (bar)**	***Temp* (°C)**	***Time* (min)**
Original	**10HEMA20-DAH2**	**8.4**	**21.7**	**40**	**170**	**20**
R1				**50**	**180**	**10**
Original	**40HEMA10-DAH2**	**38.1**	**12.8**	**50**	**190**	**5**
R1				**50**	**190**	**20**
R2				**40**	**195**	**35**
Original	**40HEMA20-DAM2**	**47.9**	**22.9**	**40**	**170**	**30**
R1				**50**	**190**	**40**

[a]Measured via SEC ($CHCl_3$, PMMA standards). [b]Calculated from ^1H NMR spectroscopy.

The reprocessing parameters of **40HEMA10-DAH2** and **40HEMA20-DAH2** were more stringent compared to the original processing parameters (*Table 30*). This may be the result of a post-cure combined with the slow exchange dynamics, previously discussed in *4.3.3. Rheology*.

After R1, the *E* of **10HEMA20-DAH2** and **40HEMA20-DAH2** increased by 549% and 786%, respectively. After R1 and R2, the *E* of **40HEMA10-DAH2** increased by 25% and 288%, respectively. Comparable to the previously discussed aged samples, these values now exceed all the values of the reported step-growth PMEs before recycling.[161, 199] Moreover, after R1 and R2, the σ_b of the reported step-growth PMEs based on triol TMP, diol DEPD and phthalic dianhydride **DAH2** is reduced by 14% and 17%, respectively.[199] This indicates the superior recyclability of **40HEMA10-DAH2**. A clear trend was observed again with samples showing an increased *E* and decreased ε_b similar to the aged samples. Moreover, this suggests that the materials have an increased stiffness rather than toughness. This may be the result of a post-cure during recycling.

FTIR spectroscopy of **40HEMA10-DAH2** was performed before and after recycling to investigate possible side reactions (*e.g.* hydrolysis) or degradation (*Figure 118*). The IR spectra before and after recycling are nearly identical, indicating no hydrolysis occurred during recycling. Thus, it appears that the PEHMA matrix was hydrophobic enough to minimise the risk of hydrolysis, which is preferable for most real-world applications where the material is exposed. Furthermore, hydrophilic backbones (*e.g.* networks based on a polyether matrix) must be avoided in applications where hydrolytic stability is required.[199]

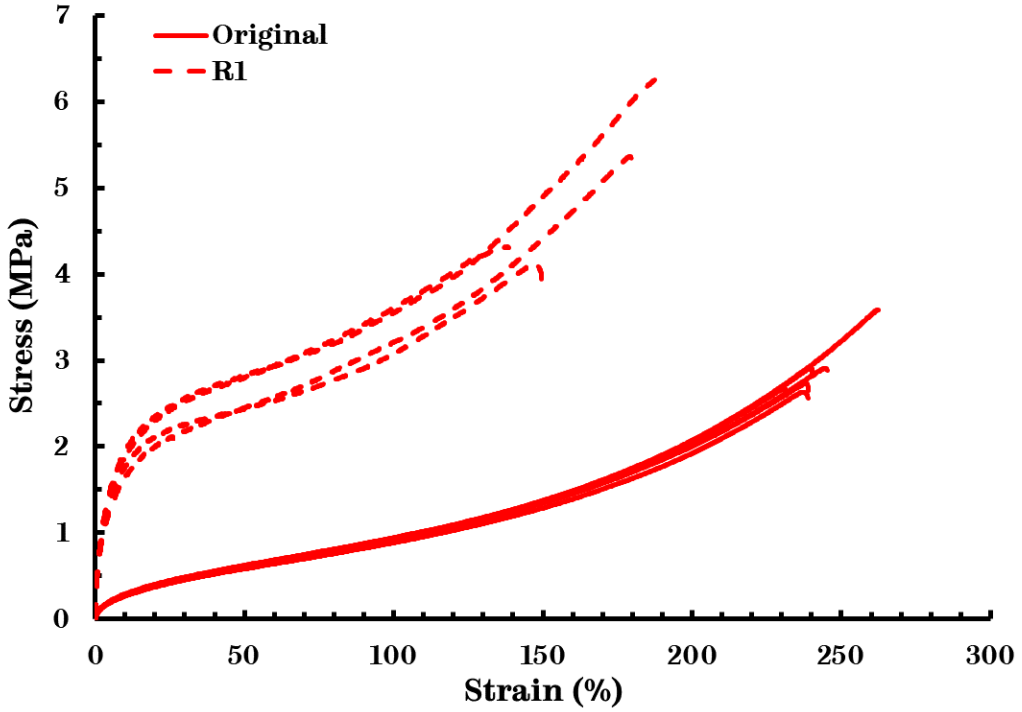

*Figure 115: Stress-strain curves of **10HEMA20-DAH2** before and after recycling.*

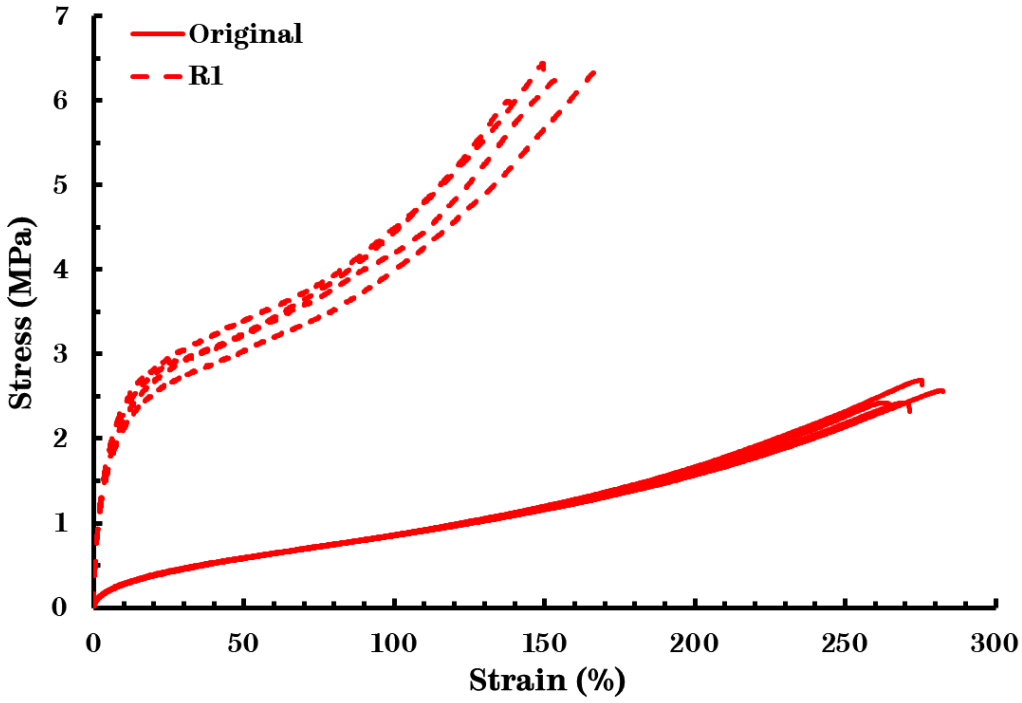

*Figure 116: Stress-strain curves of **40HEMA20-DAH2** before and after recycling.*

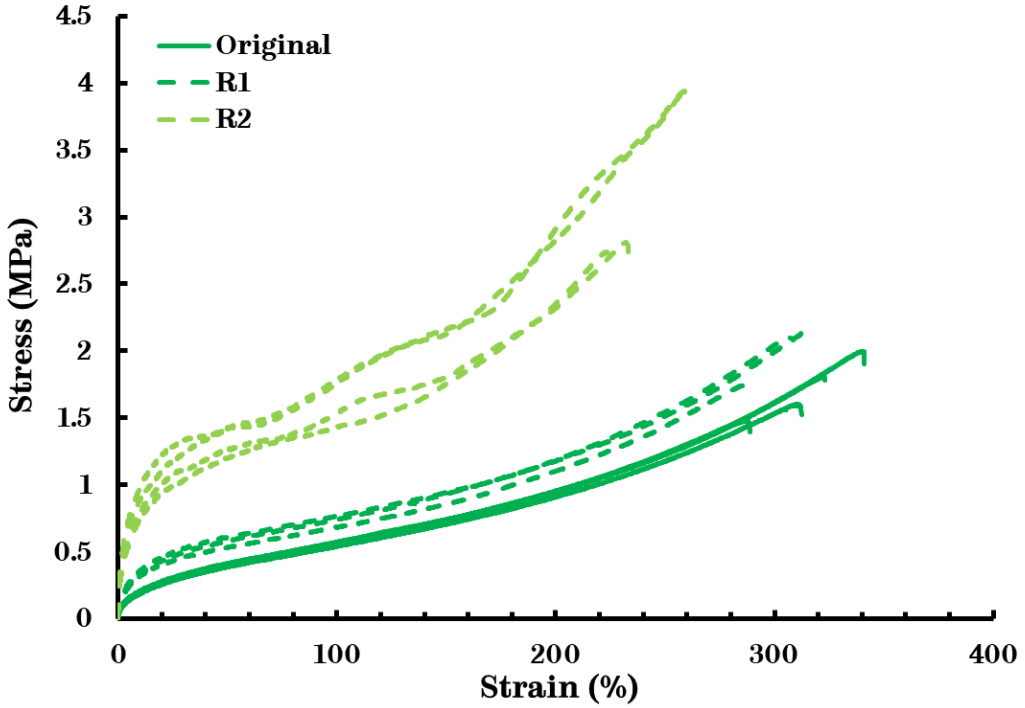

*Figure 117: Stress-strain curves of **40HEMA10-DAH2** before and after recycling.*

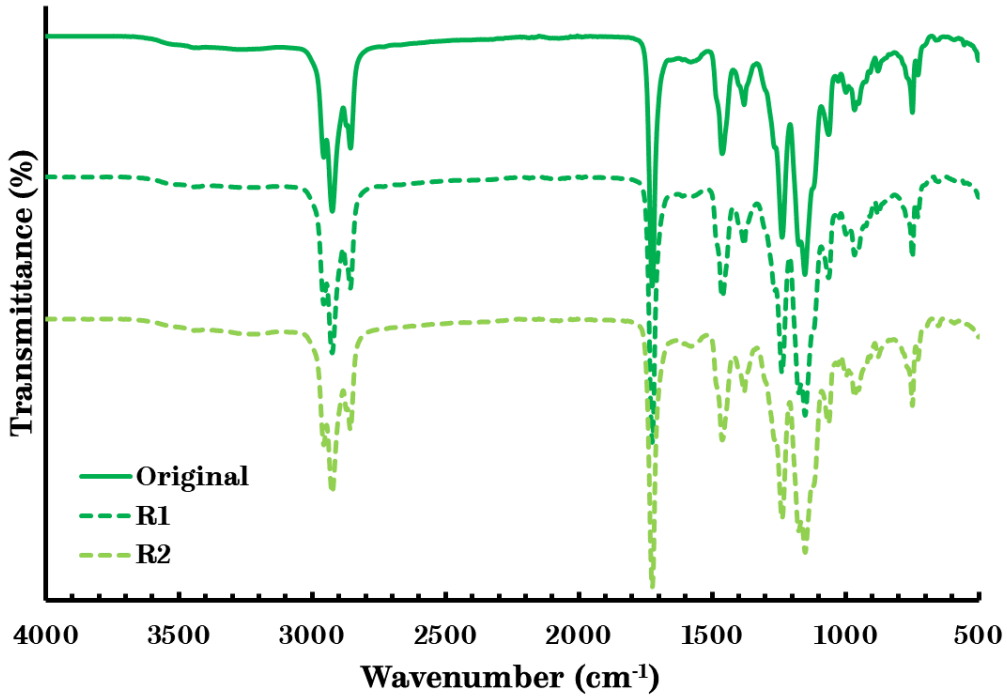

*Figure 118: IR spectrum of **40HEMA10-DAH2** before and after recycling.*

Table 40: Results of the tensile testing of the networks based on poly(EHMA-co-HEMA) with different targeted molecular weights and with different concentrations of HEMA before and after recycling.

	Name	M_n (kg.mol^{-1})[a]	$F_{\%HEMA}$[b]	E (MPa)	σ_b (MPa)	ε_b (%)
Original	**10HEMA20-DAH2**	**8.4**	**21.7**	**12.78 ± 0.20**	**2.85 ± 0.16**	**243 ± 4**
R1				**82.94 ± 2.11**	**4.96 ± 0.52**	**164 ± 12**
Original	**40HEMA10-DAH2**	**38.1**	**12.8**	**11.23 ± 0.52**	**1.61 ± 0.10**	**311 ± 10**
R1				**14.00 ± 0.81**	**1.96 ± 0.15**	**304 ± 9**
R2				**43.53 ± 3.02**	**3.29 ± 0.34**	**244 ± 9**
Original	**40HEMA20-DAH2**	**47.9**	**22.9**	**11.56 ± 0.17**	**2.44 ± 0.06**	**270 ± 5**
R1				**102.40 ± 1.25**	**6.21 ± 0.09**	**152 ± 6**

[a]Measured via SEC ($CHCl_3$, PMMA standards). [b]Calculated from ^{1}H NMR spectroscopy.

4.4 Conclusion

Functional copolymers were synthesised based on EHMA and varying concentrations of HEMA or META (5 – 20 mol.%). Actual compositions were close to feed compositions from standard free-radical polymerisation taken to high conversion. These copolymers were cross-linked with a flexible aliphatic cross-linker **DAH2** (0.65-0.8 eq. compared to the hydroxyl groups) to obtain homogeneous networks comprising PMEs. Different geometries were prepared by altering the processing parameters of the cured networks (temperature, time and pressure). These networks were characterised based on their different properties. They exhibit an improved thermal stability above 300 °C and lower T_g when compared to the prepolymers. They also possess low soluble fraction indicating good network formation, unless the average number of functional groups per chain was below the threshold value for this type of chemistry (4-5). Next, the solubility data suggested that the degree of swelling is only dependent on the number of cross-links per unit volume (cross-link density). Further, the dynamic behaviour of the material was confirmed *via* stress-relaxation experiments (E_a = 248-274 kJ.mol^{-1}). The tensile

properties were tested on the pristine samples (E = 4-13 MPa), after ageing at 80 °C for 3 weeks (E = 58-69 MPa) and after recycling (E = 44-102 MPa). Here, a substantial increase in E was observed (288-786%), which may be the result of a post-cure effect. Consequently, the tensile properties now exceed the values of the reported step-growth PMEs (E = 3–39 MPa) as a consequence of the post-cure effect and the PEHMA matrix.[161, 199]

Chapter 5 Comparison of Associative *vs.* Dissociative CANs

As defined in the aims of this work, a comprehensive comparison of novel recyclable acrylic polymers based on CANs was envisaged. Thus, after the synthesis and characterisation of the acrylic CANs based on dissociative Diels-Alder cycloaddition, associative transamination of vinylogous urethane bonds and hybrid transesterification of phthalate monoesters (PMEs), a direct comparison was conducted with one network of each dynamic chemistry. Furthermore, the networks based on the functional prepolymers with a targeted molecular weight of 40 kg.mol^{-1} and a targeted comonomer concentration of 10 mol.% were selected (*i.e.* **40FMA10-BMI2**, **40AEMA10-DAM2** and **40HEMA10-DAM2**). For the transesterification networks based on poly(EHMA-*co*-META) copolymers, the network **10META10-POL** was selected since **40META10-POL** could not be synthesised due to time constraints.

5.1 Thermal properties

Since all three types of networks are based on the same PEHMA matrix, the thermal stability of the networks was comparable with the $T_{deg5\%}$ ranging from 297 °C for **10META10-POL** up to 324 °C for **40HEMA10-DAH2** (*Figure 119*). Further, a general trend was observed where the thermal stability proportionally improved for all materials after cross-linking with the appropriate aliphatic cross-linker which may be the result of the identical C_{36} dimer core unit present in structure of the cross-linkers **BMI2**, **DAM2**, **DAH2** and **POL**.

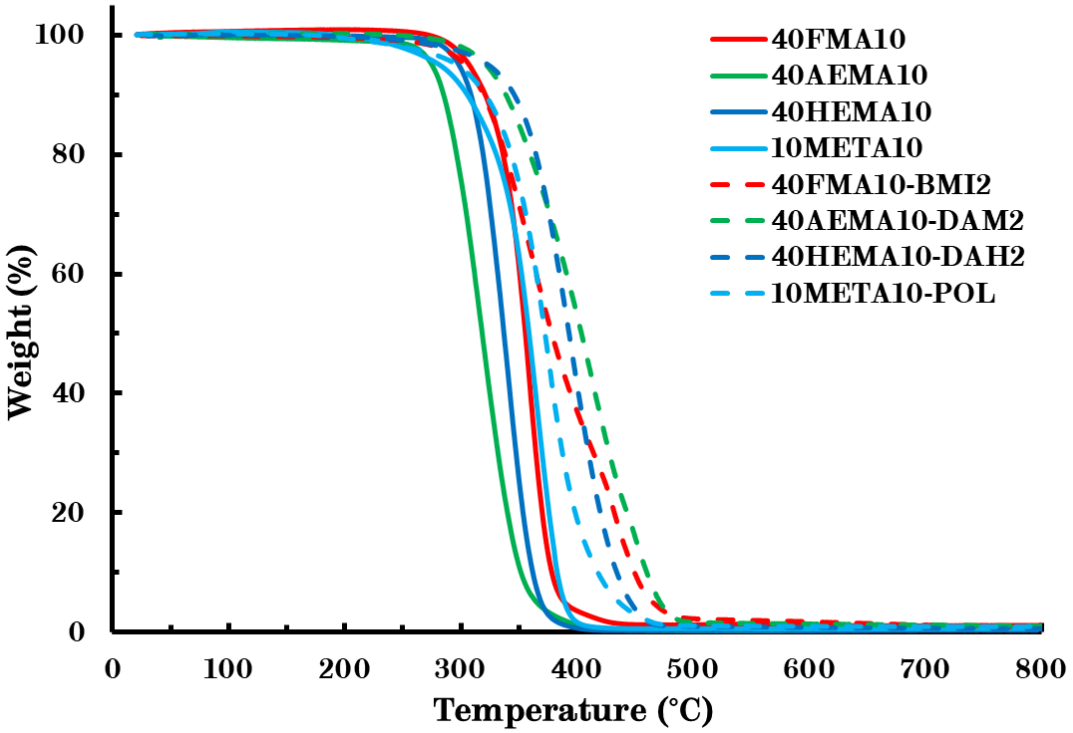

Figure 119: TGA thermograms of the prepolymers with targeted molecular weight M_n = 40 kg.mol^{-1} and targeted comonomer concentration of 10 mol.% and the resulting networks (N_2, heating rate 10 °C.min^{-1}).

Next, the glass-transition temperature (T_g) of the networks varied from -22 °C for **40FMA10-BMI2** to 3 °C for **40HEMA10-DAH2** (*Figure 120*). Generally, these T_g's are lower than the values obtained for the functional prepolymers as a result of the significantly lower T_g of the cross-linkers, which was -72 °C for **DAM2** up to -17 °C for **DAH2.** Thus, the lower values may be the result of an internal plasticisation effect of the flexible aliphatic cross-linker on the T_g, which was positively correlated with the concentration of the functional groups in the backbone and consequently with the amount of added cross-linker.

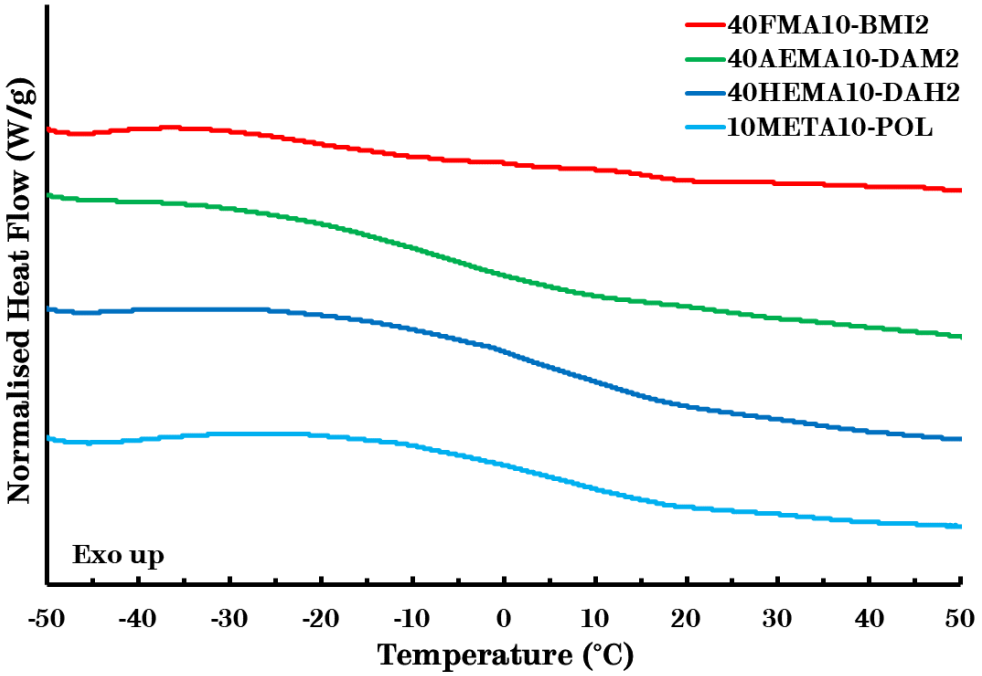

*Figure 120: DSC thermograms of the networks based on functional copolymers with a targeted molecular weight M_n = 40 kg.mol^{-1} and 10 mol.% of functional comonomer and **10META10-POL** (Second heating curve, heating rate 10 °C.min^{-1}).*

5.2 Solubility

Solubility experiments were conducted to investigated the extent of the network formation (*Figure 121, Table 41*). The extraction was performed in ethyl acetate (EtOAc) for **40FMA10-BMI2** and toluene for the other networks.

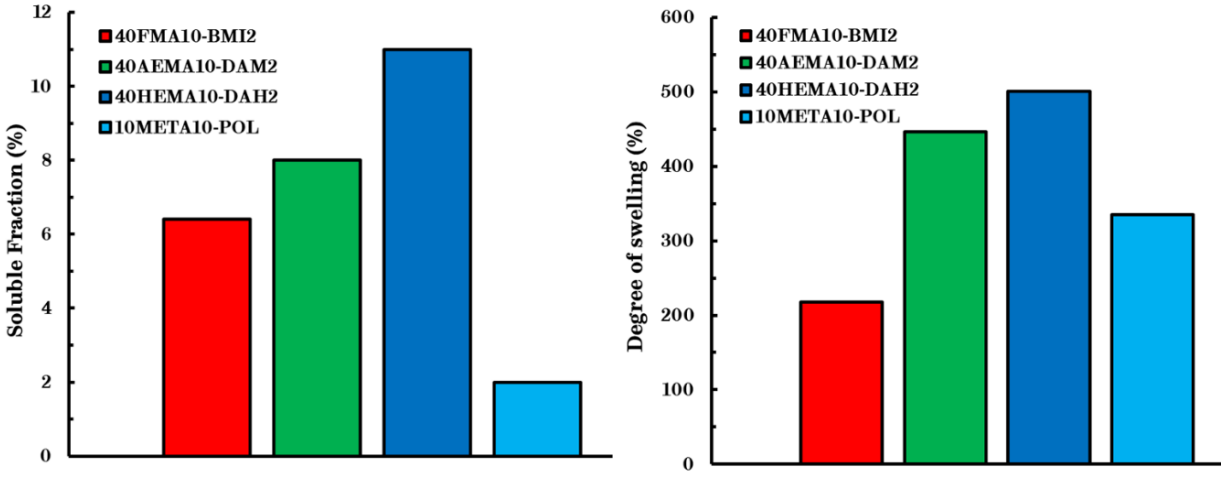

*Figure 121: Soluble fractions (left) and degree of swelling (right) of all the networks after extraction in EtOAc (**40FMA10-BMI2**) or toluene.*

10META10-POL possesses the lowest soluble fraction and consequently the highest network integrity. The soluble fractions of the other networks were similar in the range of 6-11% indicating that the soluble fractions are unaffected if the number of functional groups per chain are comparable (*Table 41*). Moreover, the degree of swelling ranged from 218-501% with **40FMA10-BMI2** and **40HEMA10-DAH2** displaying the lowest and highest value, respectively.

*Table 41: Results of the solubility experiments of the networks based on functional copolymers with a targeted molecular weight M_n = 40 kg.mol^{-1} and 10 mol.% of functional comonomer and **10META10-POL***

Name	***M*$_n$ (kg.mol^{-1})[a]**	***F*$_{\%com.}$[b]**	***Sol. Fr.* (%)[c]**	***Swell.* (%)[c]**	***Funct.*[a,b]**
40FMA10-BMI2	**38.2**	**9.9**	**6**	**218**	**19.4**
40AEMA10-DAM2	**43.8**	**10.3**	**8**	**446**	**22.5**
40HEMA10-DAH2	**38.1**	**12.8**	**11**	**501**	**25.5**
10META10-POL	**12.7**	**9.2**	**2**	**335**	**5.6**

[a]Measured via SEC (CHCl3, PMMA standards). [b]Calculated from ^{1}H NMR spectroscopy. [c]Measured via Soxhlet extraction.

5.3 Rheology and DMTA

The rheology of all three types of networks were compared *via* stress-relaxation experiments. These experiments were conducted at two different temperatures as a consequence of the different reversible exchange mechanisms (*Figure 122*). Furthermore, in order to assess the rheology of **40FMA10-BMI2**, 130 °C was selected due to the retro-Diels-Alder reaction (rDA) occurring between 120-150 °C. Thus, the network displayed significant relaxation without fully dissociating. **40FMA10-BMI2** possesses the shortest relaxation time (τ) of 109 s. This value is indicative of fast relaxation due to dissociation of the cross-links, which facilitates consequent reprocessing or recycling of the material. However, the service temperature is

limited up to moderate values below 120 °C to minimise the risk of creep as a consequence of premature dissociation of the DA cycloadducts.

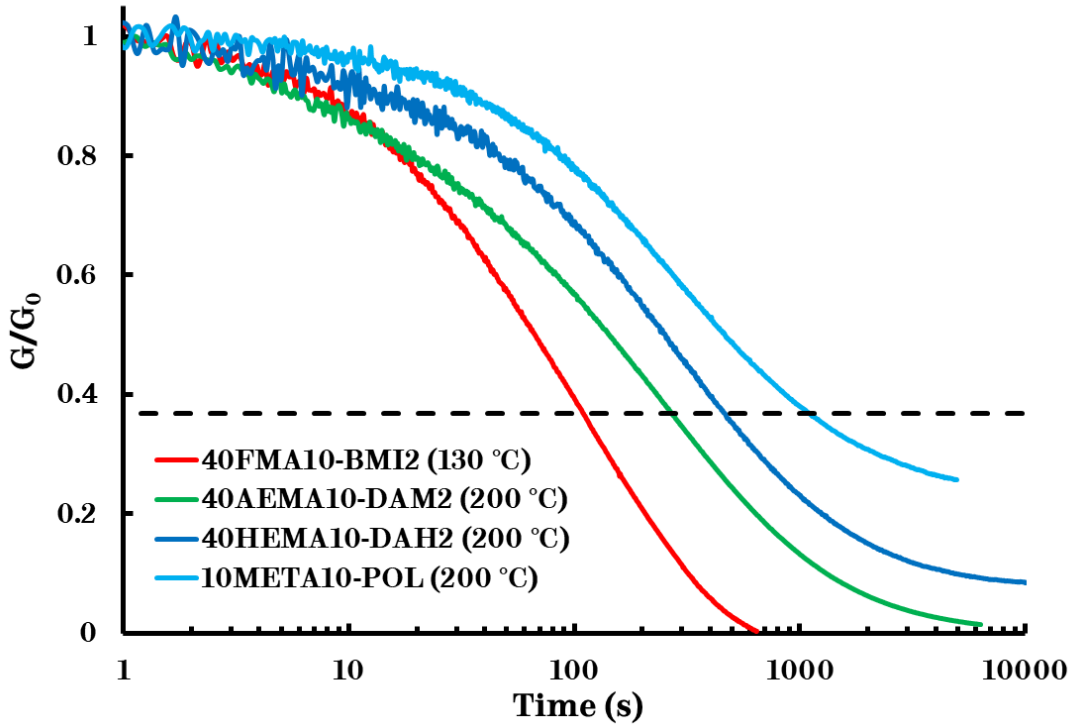

Figure 122: Stress-relaxation curves of the networks based on functional copolymers with M_n = 40 kg.mol^{-1} and $F_{\%com.}$ = 10 mol.% (1% strain).

The other networks required a significantly higher temperature of 200 °C in order to enable relaxation in a reasonable timeframe. The longest τ of 1100 s was observed for **10META10-POL** at 200 °C, which may be the result of sluggish exchange dynamics of the transesterification reaction. Furthermore, a build-up of stress can be found suggesting side reactions occurring, such as the formation of 1,2-diesters, tri-esters or tetra-esters. These moieties could render the network partially irreversible and impede the subsequent reprocessing and recycling process. Similar conclusion can be drawn for **40HEMA10-DAH2** due to the identical transesterification of PMEs. However, this network exhibited a τ of 464 s, which suggest faster exchange dynamics.

Finally, the τ of **40AEMA10-DAM2** was 270 s at 200 °C, which is a moderate value suggesting faster exchange dynamics of transamination, although a larger excess of amine was required. This renders the networks more reprocessable than **40HEMA10-DAH2** and **10META10-POL**.

Further, DMTA was only performed on the networks based on the functional prepolymers with a targeted molecular weight of 40 kg.mol^{-1} and a targeted comonomer concentration of 20 mol.%, namely **40FMA20-BMI2**, **40AEMA20-DAM2** and **40HEMA20-DAH2**, due to time constraints (*Figure 123*).

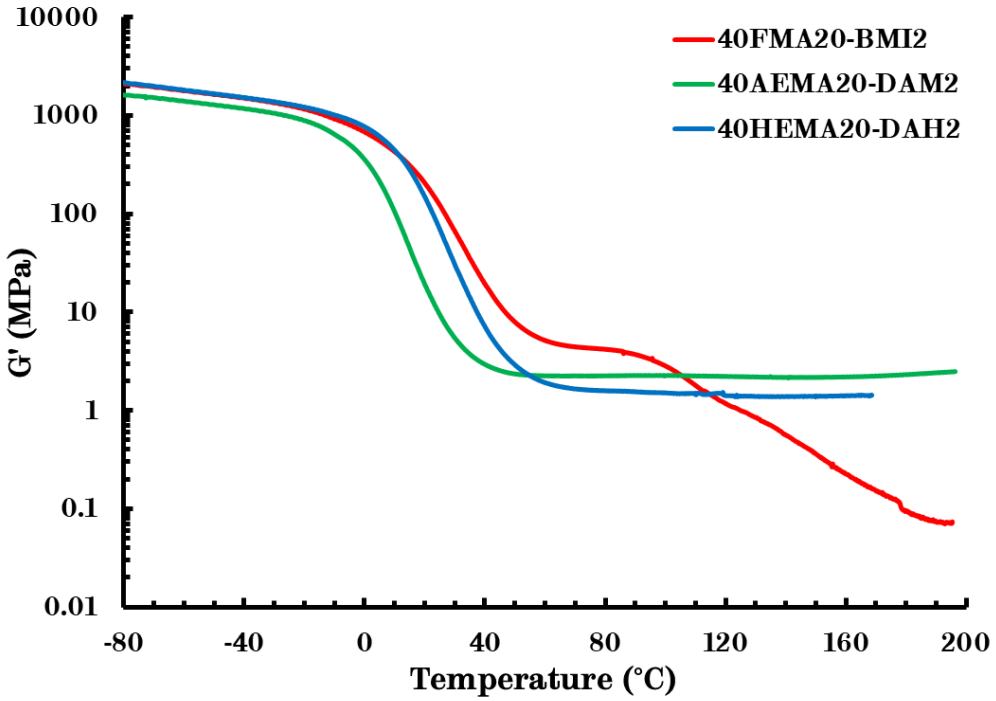

*Figure 123: Storage moduli of **40FMA20-BMI2**, **40AEMA20-DAM2** and **40HEMA20-DAH2** measured via DMTA (Heating rate 3 °C.min^{-1}).*

The data show that all networks possess a storage modulus G' of 1.6-2.1 GPa and rubbery plateau storage modulus (G'_{rubber}) of 1-4 MPa. This G'_{rubber} extends to 200 °C for **40AEMA20-DAM2** and to 170 °C for **40HEMA20-DAH2**, which prematurely broke during the experiment. The G'_{rubber} of **40FMA20-BMI2** only encompassed 60-90 °C as a consequence of the rDA reaction occurring above 100 °C. Further, the M_c

of all networks can be calculated using *Equation 7* (*2.3.3 Rheology*). At 80 °C, the calculated values were 0.7 kg.mol^{-1} for **40FMA20-BMI2**, 1.1 kg.mol^{-1} for **40AEMA20-DAM2** and 1.8 kg.mol^{-1} for **40HEMA20-DAH2**. Moreover, the average of all three networks was 1.2 kg.mol^{-1}. Considering the experimental error, this value indicates that the M_c remains constant if the cross-link density of all the networks remains constant.

5.4 Mechanical properties

The mechanical properties of all three types of networks were investigated *via* tensile testing (*Figure 124, Table 42*).

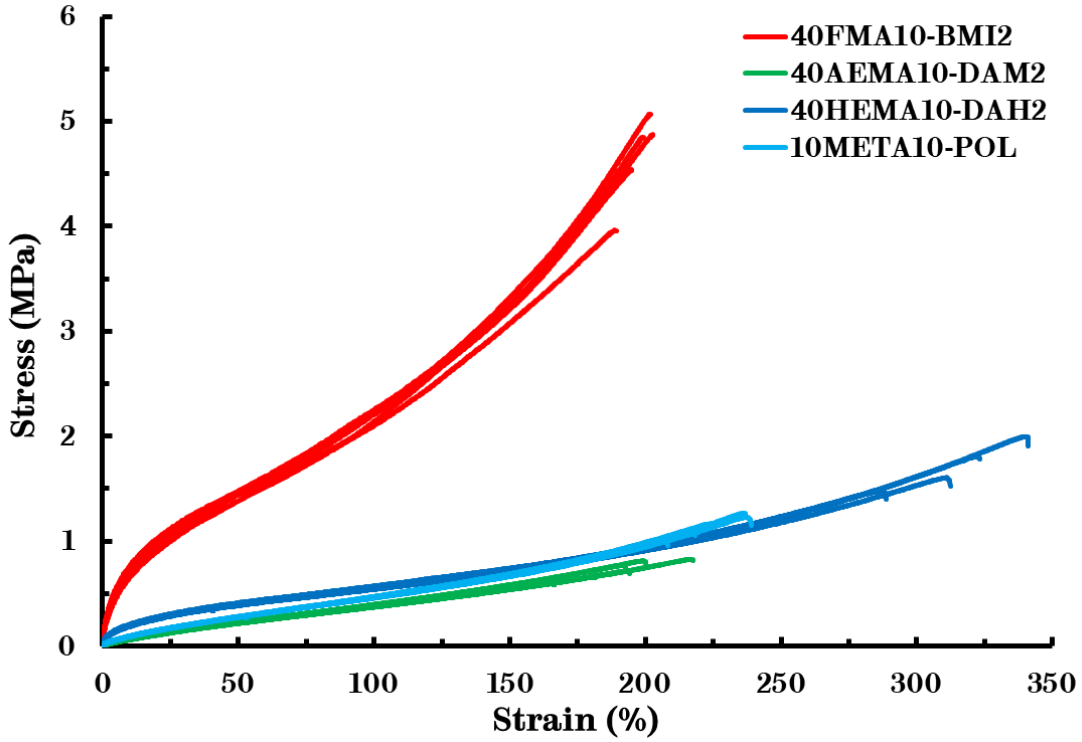

*Figure 124: Stress-strain curves of the networks based on functional copolymers with a targeted molecular weight M_n = 40 kg.mol^{-1} and 10 mol.% of functional comonomer and **10META10-POL***

40AEMA10-DAM2 exhibited the lowest Young's modulus (*E*) of 2 MPa, which is lower than the *E* of high molecular weight homopolymer PEHMA (M_n = 53 kg.mol^{-1})

(E = 5 MPa).[170] This could be rationalised by the large excess of **DAM2** (50 mol.%) present in the network. Further, the best mechanical properties were shown by **40FMA10-BMI2**, where the highest E of 30 MPa was observed, while having an identical elongation at break (ε_b) of 200% as **40AEMA10-DAM2**. An intermediate E of 11 MPa was found for **40HEMA10-DAH2**. Additionally, the ε_b was 311%, which suggest that the network is more ductile than the networks comprising the other chemistries. The lower E = 3.92 and ε_b = 216% of **10META10-POL** may be the result of the lower molecular weight of the functional prepolymers, rendering the material weaker and more brittle.

*Table 42: Results of the tensile testing of the networks based on functional copolymers with a targeted molecular weight M_n = 40 kg.mol^{-1} and 10 mol.% of functional comonomer and **10META10-POL***

Name	M_n (kg.mol^{-1})[a]	$F_{\%com.}$[b]	E (MPa)	σ_b (MPa)	ε_b (%)
40FMA10-BMI2	**38.2**	**9.9**	**27.99 ± 1.01**	**4.65 ± 0.20**	**198 ± 2**
40AEMA10-DAM2	**43.8**	**10.3**	**2.24 ± 0.10**	**0.75 ± 0.03**	**201 ± 6**
40HEMA10-DAH2	**38.1**	**12.8**	**11.23 ± 0.52**	**1.61 ± 0.10**	**311 ± 10**
10META10-POL	**12.7**	**9.2**	**3.92 ± 0.28**	**1.02 ± 0.04**	**216 ± 5**

[a]Measured via SEC ($CHCl_3$, PMMA standards). [b]Calculated from ^{1}H NMR spectroscopy.

5.5 Creep behaviour

Creep experiments were conducted to assess and compare the extent of permanent deformation of the different type of networks under a static load at elevated temperature for prolonged periods of time. The goal of the experiments was to simulate real-world applications, extending the characterisation beyond rheological analysis. Initially, small dog bones were used as the geometry to optimise the conditions of experiment, namely the static load, time and temperature. The static load was varied from 10 g to 100 g, the time ranged from 2 to 18 hours and the experimental temperature range was 25-100 °C. After these initial experiments, the

tested geometry was altered to bar samples with an increased cross-section, which facilitates the scale-up of the loads (*Figure 125*).

The best experimental results were observed at static loads between 10-50 g and an optimal temperature of 70 °C, which ensured creep in the material at long time scales without breaking the sample. It should be noted that all materials are above their T_g and within the scope of the plateau modulus observed *via* DMTA. After 18 hours, the load was removed and the elongation was measured. Next, the samples recovered without a load at 70 °C and the creep was measured after 2 hours, 4 hours and 24 hours. The obtained results support all the previous collected data in terms of the rheology and tensile properties.

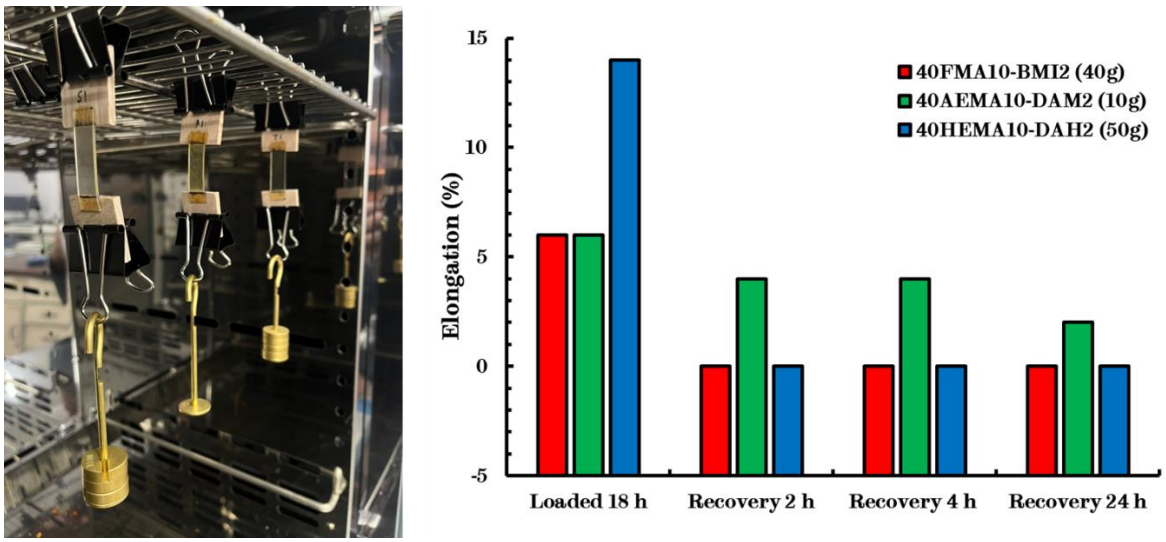

Figure 125: Experimental setup (left) and results (right) of the creep experiments at 70 °C.

First, **40AEMA10-DAM2**, which exhibits the lowest *E*, required the lowest load of 10 g and displayed a creep of 6%, which eventually recovered to 2% 24 hours after the load was removed. Next, **40HEMA10-DAH2**, which has a significantly higher *E* than **40AEMA10-DAM2**, required the highest load of 50 g, exhibiting an initial creep of 14%, which fully recovered within 2 hours. Finally, **40FMA10-BMI2**, which possesses the highest *E*, was tested with a load of 40 g and displayed a creep of 6%,

which fully recovered within 2 hours. Thus, the results are indicative of a creep resistance at 70 °C for the dissociative and hybrid network, which is absent for the transamination network.

5.6 Recyclability

In order to test the recyclability, the pristine materials were reprocessed twice into a plate geometry (*Table 43*). A trend was observed where the reprocessing times of the associative **40AEMA10-DAM2** and the hybrid **40HEMA10-DAH2** increased proportionally more during recycling than those for the dissociative **40FMA10-BMI2.** Here, the reprocessing time increased after R1 and stagnated afterwards. Furthermore, this suggests that the more difficult reprocessing of the transamination and transesterification networks may be the result of additional cross-links forming in the networks. Moreover, further experiments need to be conducted to investigate whether the formed cross-link bonds are dynamic or irreversible. After reprocessing, the tensile properties were measured for both recycles (R1, R2 respectively) (*Figure 126, Table 44*).

Table 43: Reprocessing parameters of the cross-linked networks based on functional copolymers with a targeted molecular weight M_n = 40 kg.mol^{-1} and 10 mol.% of functional comonomer.

	Name	M_n (kg.mol^{-1})[a]	$F_{\%com.}$[b]	*P* (bar)	*Temp.* (°C)	*Time* (min)
Original	**40FMA10-BMI2**	**38.2**	**9.9**	**30**	**140**	**5**
R1				**30**	**150**	**10**
R2				**30**	**150**	**12**
Original	**40AEMA10-DAM2**	**43.8**	**10.3**	**50**	**190**	**10**
R1				**40**	**180**	**20**
R2				**50**	**180**	**35**
Original	**40HEMA10-DAH2**	**38.1**	**12.8**	**50**	**190**	**5**
R1				**50**	**190**	**20**
R2				**40**	**195**	**35**

[a]*Measured via SEC ($CHCl_3$, PMMA standards).* [b]*Calculated from ^{1}H NMR spectroscopy.*

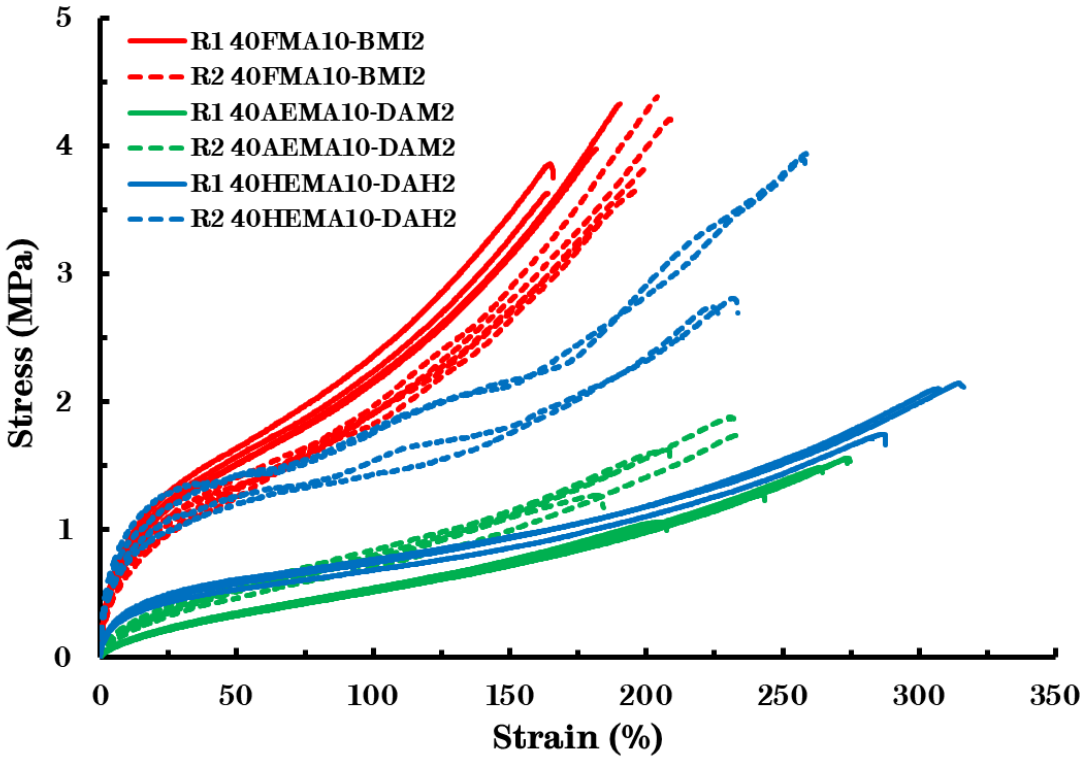

Figure 126: Stress-strain curves of the networks based on functional copolymers with a targeted molecular weight M_n = 40 kg.mol^{-1} and 10 mol.% of functional comonomer after recycling.

Cross-referencing the results with the previously discussed tensile properties on the pristine material (Original), both **40AEMA10-DAM2** and **40HEMA10-DAH2** display a large increase in E after R2 (268% and 288%, respectively), which is indicative of a post-cure occurring in the material. This post-cure may in part involve the formation of some permanent cross-links due to the high processing temperatures. However, **40FMA10-BMI2** exhibits an almost identical E = 28 MPa and ε_b = 200% as the original sample, which may be the result of the mild reprocessing conditions required as a consequence of the dissociative mechanism of the furan/maleimide system.

Table 44: Results of the tensile testing of the networks based on functional copolymers with a targeted molecular weight M_n = 40 kg.mol^{-1} and 10 mol.% of functional comonomer before after recycling.

	Name	M_n (kg.mol^{-1})[a]	$F_{\%com.}$[b]	E (MPa)	σ_b (MPa)	ε_b (%)
Original	**40FMA10-BMI2**	**38.2**	**9.9**	**27.99 ± 1.01**	**4.65 ± 0.20**	**198 ± 2**
R1				**31.69 ± 1.47**	**3.87 ± 0.13**	**175 ± 5**
R2				**28.02 ± 0.61**	**3.89 ± 0.18**	**199 ± 4**
Original	**40AEMA10-DAM2**	**43.8**	**10.3**	**2.24 ± 0.10**	**0.75 ± 0.03**	**201 ± 6**
R1				**4.15 ± 0.15**	**1.34 ± 0.10**	**253 ± 13**
R2				**8.24 ± 0.72**	**1.55 ± 0.12**	**210 ± 10**
Original	**40HEMA10-DAH2**	**38.1**	**12.8**	**11.23 ± 0.52**	**1.61 ± 0.10**	**311 ± 10**
R1				**14.00 ± 0.81**	**1.96 ± 0.15**	**304 ± 9**
R2				**43.53 ± 3.02**	**3.29 ± 0.34**	**244 ± 9**

[a]Measured via SEC ($CHCl_3$, PMMA standards). [b]Calculated from ^{1}H NMR spectroscopy.

5.7 Conclusion

After a direct comparative study on **40FMA10-BMI2**, **40AEMA10-DAM2**, **40HEMA10-DAH2** and **10META10-POL**, a conclusion can be drawn that each type of dynamic network displays advantages and disadvantages in terms of synthesis complexity, scalability, material processing, susceptibility to creep, thermal and mechanical properties (*Table 45*).

Table 45: Qualitative comparison of the advantages and disadvantages of all three incorporated dynamic chemistries in this work.

Dynamic chemistry	Synth.	Therm.	Rheol., Process.	DMTA	Sol.	Tensile, Creep
Cycloadd. of F-M						
Transam. of V-U						
Transest. of PME						

Firstly, the Diels-Alder cycloaddition networks show good processability and excellent recyclability as a consequence of their rheology, determined by the

dissociative mechanism. Moreover, solubility experiments indicate a good resistance against solvents. Further, the networks display good tensile properties and limited creep. The thermal stability and low T_g align with the expected value for the acrylic backbone. However, the rubbery plateau storage modulus (G'_{rubber}), measured *via* DMTA, is limited (60-90 °C). This narrows the service temperature window and limits the scope of possible applications.

Secondly, the transamination networks exhibit a moderate processability and a reduced recyclability due to the possible side reactions involving the free amine moieties, which are necessary in the associative mechanism. Solubility experiments show a moderate solvent resistance. Furthermore, the current excess (50 mol.%) of aliphatic cross-linker reduces the mechanical properties and renders the material susceptible to creep. The networks show good thermal stability and a low T_g, determined by the matrix and incorporated cross-linker. Moreover, this type of network can be employed at higher service temperatures as a result of the G'_{rubber} extending up to 200 °C. An optimised design of the system could mitigate these issues.

Finally, the transesterification networks display a moderate processability and poor reprocessability due to the slow exchange reactions in the current system, where high processing temperatures and longer processing times are required. Next, a good solvent resistance was observed *via* solubility experiments. Further, the tensile properties were promising and a low susceptibility toward creep was measured. Moreover, the thermal stability was high and the incorporated cross-linker lowered the T_g of the material. Nonetheless, the material exhibits an

excellent G'_{rubber}, which widens the service temperature window of this type of network. Again, the aforementioned issues could be resolved or minimised by an optimised design of the system.

Chapter 6 Conclusions

Initially, functional copolymers were synthesised based on 2-ethylhexyl methacrylate (EHMA) with different types of comonomers. The polymerisation technique that was employed was free radical polymerisation with a chain transfer agent (CTA) in bulk to ensure the synthesis was robust, economical and scalable. Two molecular weights were investigated, namely 10 and 40 kg.mol^{-1}, in order to assess the influence of chain entanglements in the backbone and the ratio between M_e and M_c. Next, these functional copolymers were cross-linked with a complementary cross-linker to the incorporated functional comonomers to form reversible cross-linking bonds, resulting in the synthesis of covalent adaptable networks (CANs). The three dynamic chemistries that were selected for the synthesis of these CANs were Diels-Alder cycloaddition (dissociative), transamination of vinylogous urethanes (associative) and the transesterification of phthalate monoesters (hybrid).

The first functional comonomer that was incorporated in the PEHMA matrix was furfuryl methacrylate (FMA) (5-20 mol.%). This poly(EHMA-*co*-FMA) copolymer was then cross-linked with an aliphatic bismaleimide **BMI2**, resulting in a dissociative Diels-Alder CAN. Different geometries were prepared *via* compression moulding. These networks were characterised based on their different properties. They display an improved thermal stability above 300 °C and a lowered T_g when compared to the prepolymers due to the plasticising cross-linker moiety. They also exhibit low soluble fractions (6-13%) indicating good network formation, unless the average number of functional groups per chain was below the threshold value for this type

of chemistry (< 3). Next, stress-relaxation experiments were conducted to confirm the dynamic behaviour of the material. At 130 °C, the material displays a fast relaxation. The tensile testing was performed on the pristine samples (E = 4-67 MPa), after ageing at 80 °C for 3 weeks (E = 31-141 MPa) and after recycling (E = 28-117 MPa). Here, an increased stiffness (higher E, lower ε_b) was observed, which may be the result of a post-cure effect.

The second functional comonomer that was incorporated in the PEHMA matrix was acetoacetoxyethyl methacrylate (AEMA) (5-20 mol.%). This poly(EHMA-*co*-AEMA) copolymer was then cross-linked with an aliphatic diamine **DAM2** (50 mol.%), resulting in an associative vinylogous urethane transamination CAN. The large excess of amines was required to process the material into different geometries using compression moulding within a reasonable timeframe. The material properties were investigated *via* different characterisation techniques. In terms of thermal stability, the material displays a stability up to a range of 320-340 °C. Furthermore, the cross-linker seems to have a plasticising effect on the T_g. The low soluble fraction (4-11%) that were obtained suggest a good network integrity, unless the average number of functional groups per chain was below the minimum threshold value for this type of chemistry. Moreover, an activation energy of 125 ± 4 kJ.mol^{-1} was calculated from stress-relaxation experiments confirming a similar dynamic behaviour as previously reported systems.[193, 196, 197] The Young's modulus (E) of the pristine samples that was calculated from the tensile experiments varied between 1.9-4.4 MPa. Increased values were obtained after ageing at 80 °C for 3 weeks (E = 6.8-9.1 MPa) and after recycling (E = 7.0-12.0 MPa). Here, the materials displayed an increased stiffness, which may be the result of a post-cure effect.

The third functional comonomer that was incorporated in the PEHMA matrix was 2-hydroxyethyl methacrylate (HEMA) (5-20 mol.%). This poly(EHMA-*co*-HEMA) copolymer was then cross-linked with an aliphatic phthalic dianhydride **DAH2** (0.65-0.80 eq. compared to -OH groups), resulting in an hybrid phthalate monoester transesterification CAN. A variety of geometries were processed *via* compression moulding. Characterisation was performed to investigate the different material properties. When compared to the functional prepolymers, all transesterification networks exhibit an improved thermal stability up to 335 °C and a reduced T_g due to the plasticising effect of the aliphatic cross-linker. The obtained soluble fraction were low (2-11%), which is indicative of a good network integrity, unless the average number of functional groups per chain was below the threshold value for this type of chemistry. Next, the reversible thermoresponsive behaviour of the material was confirmed using stress-relaxation experiments (E_a = 248-274 kJ.mol^{-1}). After testing the tensile properties, E = 4-13 MPa was obtained for the pristine material. Further, ageing (80 °C, 3 weeks) and recycling experiments significantly increased the E by 288% and 786%, respectively (E = 58-69 MPa and E = 44-102 MPa, respectively). Furthermore, this increase may be the result of additionally formed cross-links in the material (post-cure).

A comparative study was conducted on **40FMA10-BMI2**, **40AEMA10-DAM2**, **40HEMA10-DAH2** and **10META10-POL** to validate their advantages and disadvantages. Firstly, in terms of synthesis, they all exhibit a similar complexity. However, the scalability of **40FMA10-BMI2** and **10META10-POL** is limited by the commercial availability of the FMA and META comonomer. Next, all networks possess a similar thermal stability as a consequence of the same acrylic matrix and

a lowered T_g as a result of the plasticising cross-linkers that are incorporated. Further, the rheological properties and processability of the networks is mainly determined by their exchange mechanism. **40FMA10-BMI2** displays good processability and excellent recyclability due to the dissociative mechanism of the Diels-Alder cycloaddition. **40AEMA10-DAM2** and **40HEMA10-DAH2** show a moderate processability and poor recyclability. This could be rationalised by diffusion-controlled exchange dynamics and possible side reactions occurring at the high processing temperatures (*e.g.* oxidation of the free amine groups, formation of irreversible phthalic 1,2-diesters, triesters or tetra-esters). Furthermore, DMTA shows that the rubbery plateau storage modulus (G'_{rubber}) of both **40AEMA10-DAM2** and **40HEMA10-DAH2** extends up to 200 °C and vastly exceeds the G'_{rubber} range of **40FMA10-BMI2**, which is limited up to 90 °C. Thus, the service temperature window of **40AEMA10-DAM2** and **40HEMA10-DAH2** is significantly wider than **40FMA10-BMI2**. Moreover, solubility tests suggest a good solvent resistance for all three types of networks. Also, the DMTA and solubility data indicate that the G'_{rubber} and degree of swelling only depend on M_c. Thus, given $M_c < M_e$, these properties of the networks are dominated by the network topology.

Finally, the tensile properties of **40AEMA10-DAM2** are substantially lower and the measured creep is higher than the other networks, which may be the result of the large excess of incorporated amine. However, after two recycles, a large increase in Young's modulus (E) was measured in **40AEMA10-DAM2** and **40HEMA10-DAH2** (268% and 288%, respectively), which is indicative of a post-cure process occurring in these networks. Furthermore, the E of **40FMA10-BMI2** remained the same after two recycles, which suggests an excellent recyclability of this network.

In conclusion, CANs are a new paradigm in polymer science, where the understanding of the physical and mechanical properties on a macroscopic level is still limited but rapidly developing. Generally, there exists a compromise between their mechanical performance and recyclability. Furthermore, these smart novel polymers are a chemical platform that can be optimised for specific applications and could combine the best features from classical thermoplastic and thermosetting polymers.

Future work

In the future, it would be beneficial to conduct lap shear experiments and peel tests on different substrates (*e.g.* metal, plastic, wood) on the dynamic networks to investigated their adhesive properties. Furthermore, the self-healing and shape memory capabilities could be tested. Next, studies on the influence of the excess and structure of the cross-linking moiety on the kinetics of the dynamic exchange reactions would be useful. Further, the influence of incorporating a different polymer matrix on the mechanical properties of the resultant networks could be investigated. Here, the polarity of the matrix can be varied systematically, ranging from apolar to polar backbones. Finally, the influence of the morphology of the functional prepolymers on the properties of the networks can be studied in detail. For example, the structure of the prepolymer backbone can be expanded from linear copolymers to star copolymers, hyperbranched copolymers and dendrimers. Here, the functional groups can be introduced in the middle of one of the arms/branches or at the ends.

Chapter 7 Experimental Section

7.1 Materials

All (meth)acrylates were purified over a layer of basic aluminium oxide. All products were used without further purification unless specified otherwise.

Table 46: Used products and solvents

Name	CAS-No.	Supplier	Purity (%)
1,10-Decanediol	112-47-0	Fluorochem	N/A
1,3,5-Trioxane	110-88-3	Sigma-Aldrich	≥99
1,4-Dioxane (anhydrous)	123-91-1	Sigma Aldrich	≥99.8
1,5-Diamino-2-methylpentane	15520-10-2	Sigma-Aldrich	99
1-Butanol	71-36-3	Fisher Chemicals	≥99.8
1-Dodecanethiol	112-55-0	Sigma-Aldrich	≥98
2-(Methacryloyloxy)ethyl acetoacetate	21282-97-3	Sigma-Aldrich	95
2-Ethylhexyl methacrylate	688-84-6	Alfa Aesar	98
2-Hydroxyethyl methacrylate	868-77-9	Chemcruz	N/A
4-Methacryloxyethyl trimellitic anhydride	70293-55-9	Fluorochem	N/A
Aluminium oxide, basic	1344-28-1	VWR Chemicals	99
Azobisisobutyronitrile	78-67-1	Sigma-Aldrich	98
Benzyl Benzoate	120-51-4	Sigma-Aldrich	≥99
Chloroform	67-66-3	Merck Chemicals	≥99.8
Chloroform D	865-49-6	Sigma-Aldrich	99.8D
Ethanol	64-17-5	Fisher Chemicals	≥99.8
Ethyl acetate	141-78-6	Sigma-Aldrich	≥99.7
Furfuryl Methacrylate	3454-28-2	Sigma-Aldrich	97
Lauryl Methacrylate	142-90-5	Sigma-Aldrich	96
Methanol	67-56-1	Fisher Chemicals	≥99.8
m-Xylylenediamine	1477-55-0	Acros Organics	99
n-Butyl Acrylate	141-32-2	Merck Chemicals	≥99
n-Hexane	110-54-3	Merck Chemicals	≥97
Priamine™ 1075	N/A	CRODA	N/A
Pripol™ 2033	N/A	CRODA	N/A
Pyromellitic dianhydride	89-32-7	Alfa Aesar	97
SRM-1 (Hexyl ester bismaleimide)	N/A	Henkel	N/A
Tetrahydrofuran	109-99-9	Sigma Aldrich	≥99.9
Toluene	108-88-3	Fisher Chemicals	≥99.8
Trimellitic anhydride chloride	1204-28-0	Fluorochem	N/A

7.2 Instrumentation

7.2.1 Nuclear Magnetic Resonance

Proton (^{1}H) and Carbon (^{13}C) nuclear magnetic resonance (NMR) spectra were recorded using a Bruker Avance 400 spectrometer (400 MHz). Spectra were analysed on the TopSpin software of Bruker. Samples were prepared in $CDCl_3$ as the solvent. All chemical shifts were recorded in parts per million (ppm) relative to a reference peak of $CDCl_3$ solvent at δ = 7.26 ppm (^{1}H) and δ = 77. 2 ppm (^{13}C).

7.2.2 Size Exclusion Chromatography ($CHCl_3$)

Molecular weights and dispersities were determined *via* size-exclusion chromatography (SEC) using an Agilent 1260 Infinity GPC system equipped with a refractive index detector. Two Agilent PL-gel 5 μm Mixed-C columns and a guard column were connected in series and maintained at 35 °C. HPLC grade chloroform containing 0.25%-v/v NEt_3 was used as the eluent and the flow rate was set at 1.0 $mL.min^{-1}$. The refractive index detector was used for calculation of molecular weights and dispersities by calibration using a series of near-monodisperse poly(methyl methacrylate) standards. Analysis was performed on Agilent SEC software.

7.2.3 Differential Scanning Calorimetry

Differential scanning calorimetry (DSC) was performed on a Discovery DSC 25 TA instrument. All experiments were carried out under a nitrogen atmosphere and with a heating rate of 10 °$C.min^{-1}$. Pre-weighed samples of 5 ± 1 mg were loaded at 25 °C, cooled to -90 °C and heated to 200 °C. All T_g values were determined from the

midpoints in the second heating run using the TRIOS software of TA Instruments unless stated otherwise. Analysis was performed on TRIOS v5.1.1 software.

7.2.4 Thermogravimetric Analysis

A Perkin Elmer Pyris 1 instrument performed the thermogravimetric analysis (TGA). The measurements were performed in temperature range 25-800 °C under nitrogen atmosphere with a heating rate of 10 °C.min^{-1}. The thermograms were analysed using the Pyris 1 software.

7.2.5 Fourier Transform Infrared

Attenuated total reflectance Fourier transform infrared (ATR-FTIR) spectra was collected on a PerkinElmer Spectrum Two instrument with a UATR Two accessory. Analysis was performed on PerkinElmer Spectrum software.

7.2.6 Rheology

Rheological temperature sweeps were performed on an Anton Paar MCR502 with 8 mm disposable parallel plate geometry. Stress-relaxation experiments were run with a fixed amplitude (1%) in temperature range 110 – 200 °C. The samples were discs with a diameter and thickness of approximately 8 mm and 1 mm, respectively.

7.2.7 Dynamic Mechanical Analysis

Dynamic mechanical analysis (DMA) was performed on TA Instruments Q800 Dynamic Mechanical Analyser with an ACS-3 (Refrigerated Chiller System). Samples of approximately 40 × 5 × 1 mm were loaded at room temperature and clamped lightly. A sample length of 10 mm was used for all measurements. For each measurement, the sample was first cooled to -80 °C and held at this temperature for

a minimum of 5 minutes to fully equilibrate. The furnace was then opened and the sample clamped to a pressure of 4.5 p.s.i. using a small torque wrench. After clamping, the furnace was then immediately closed and temperature re-equilibration established at -80 °C. The method was then started. The thermal method used is: Motor Drive Off, Data Storage Off, equilibrate at -80 °C, isotherm 5 minutes, Motor Drive ON, Data Storage ON, ramp 3 °C.min^{-1} to 200 °C. The measurement parameters used were as follows: strain applied (0.05%), force track (110%), initial sample length (10 mm) with deformation frequency (1 Hz) fixed. Sample dimensions were calculated as follows: width was measured using digital callipers at three positions along the sample (End 1, Middle, End 2). The thickness was measured using digital callipers at three positions along the sample (End 1, Middle, End 2). Average values were calculated and used. The software used was TA Instruments Advantage Control Software and data analysis was performed on TA Instruments Universal Data Analysis Program.

7.2.8 Tensile Testing

Tensile tests were run on dogbone specimens approximately 1 mm thick, according to ISO 527-2 type 5B on a zwickiLine tensometer. The general procedure is as follows: dimensions of dog bone measured with digital calliper and noted on the system. The zero gap is set within Zwick software so the 170-gauge length is known. The sample is then securely clamped and the absolute cross head length is reset. The force is then zeroed. The test is run at a speed of 10 mm.min^{-1} until the sample fails. Results were analysed on TestXpert II software.

7.3 General synthesis of poly(EHMA-*co*-FMA)

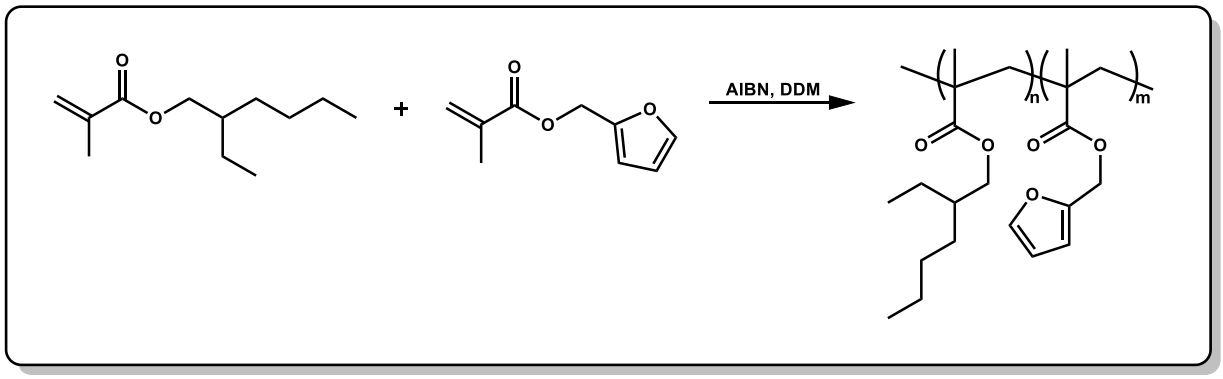

7.3.1 Synthesis of **10FMA3**

Azobisisobutyronitrile (AIBN) (54.8 mg, 0.334 mmol), 1-dodecanethiol (DDM) (1.350 g, 6.671 mmol), benzyl benzoate (289.0 mg, 1.362 mmol) as an internal NMR standard and furfuryl methacrylate (FMA) (2.332 g, 14.033 mmol) were dissolved in 2-ethylhexyl methacrylate (EHMA) (90.000 g, 453.835 mmol) in a two-neck round bottom flask. The flask was equipped with a septum and a mechanical stirrer. The reaction mixture was purged with N_2 for 30 minutes. The flask was placed in an oil bath at 80 °C and stirred for 3.5 hours. The conversion was monitored *via* ^{1}H NMR spectroscopy. After the reaction was completed, the polymer was dissolved in a minimal amount of ethyl acetate (*ca.* 125 mL). This solution was precipitated in a large excess of ice-cold ethanol (500 mL). The precipitated polymer was collected in a PTFE-lined Petri dish and dried in a vacuum oven at 80 °C. The precipitation was repeated until all residual monomer, observed by ^{1}H NMR spectroscopy, was removed.

Yield: 77.651 g (6.694 mmol, 84%)

SEC ($CHCl_3$): M_n = 11.6 kg.mol^{-1}, M_w = 20.3 kg.mol^{-1}, $Đ_M$ = 1.74

^{1}H-NMR (400 MHz, 298 K, $CDCl_3$): δ (ppm) = 0.81 – 0.95 (m, 6H, $CH_2 - CH_3$), 1.02 (s, 6H, $CH_3 - C$), 1.23 – 1.46 (m, 12H, CH_2), 1.54 (m, 1H, $CH - (CH_2)_3$), 3.83 (m, 2H, $O - CH_2$

– CH), 4.94 (s, 2H, O – CH_2 – C), 6.36 (d, 2H, C = CH – CH = CH), 7.40 (m, 1H, O – CH = CH)

ATR-FTIR: ν_{MAX} = 2958-2860*m* (C-H), 1725*s* (C=O), 1463*m* (C-H), 1381*m* (C-H), 1238*m* (C-O), 1176*m* (C-O), 1151*s* (C-O), 1061*w* (C-O), 966*w* (C=C) cm^{-1}.

7.3.2 Synthesis of **10FMA5**

Azobisisobutyronitrile (AIBN) (54.8 mg, 0.334 mmol), 1-dodecanethiol (DDM) (1.350 g, 6.671 mmol), benzyl benzoate (289.0 mg, 1.362 mmol) as an internal NMR standard and furfuryl methacrylate (FMA) (3.967 g, 23.872 mmol) were dissolved in 2-ethylhexyl methacrylate (EHMA) (90.000 g, 453.835 mmol) in a two-neck round bottom flask. The flask was equipped with a septum and a mechanical stirrer. The reaction mixture was purged with N_2 for 30 minutes. The flask was placed in an oil bath at 80 °C and stirred for 3.5 hours. The conversion was monitored *via* ^{1}H NMR spectroscopy. After the reaction was completed, the polymer was dissolved in a minimal amount of ethyl acetate (*ca.* 125 mL). This solution was precipitated in a large excess of ice-cold ethanol (500 mL). The precipitated polymer was collected in a PTFE-lined Petri dish and dried in a vacuum oven at 80 °C. The precipitation was repeated until all residual monomer, observed by ^{1}H NMR spectroscopy, was removed.

Yield: 77.993 g (7.958 mmol, 83%)

SEC ($CHCl_3$): M_n = 9.8 $kg.mol^{-1}$, M_w = 17.5 $kg.mol^{-1}$, $Đ_M$ = 1.79

^{1}H-NMR (400 MHz, 298 K, $CDCl_3$): δ (ppm) = 0.81 – 0.95 (m, 6H, CH_2 – CH_3), 1.02 (s, 6H, CH_3 – C), 1.23 – 1.46 (m, 12H, CH_2), 1.54 (m, 1H, CH – $(CH_2)_3$), 3.83 (m, 2H, O – CH_2 – CH), 4.94 (s, 2H, O – CH_2 – C), 6.36 (d, 2H, C = CH – CH = CH), 7.40 (m, 1H, O – CH = CH)

^{13}C-NMR (400 MHz, 298 K, $CDCl_3$, DEPT): δ (ppm) = 177.8 (C_q= O), 149.1 (C_q – O), 143.2 (*C*H – O), 110.4 (CH – *C*H – CH), 67.0 (*C*H – OCOR), 44.9 (C_q – *C*H_2 – C_q), 38.4 (*C*H_3 – C_q), 30.4 (CH_2 – *C*H2 –CH), 29.0 (CH_3 – *C*H_2 – CH), 23.9 (CH_2 – *C*H_2 – CH_2), 22.9 (CH_3 – *C*H_2 – CH_2), 14.1 (*C*H_3 – CH_2 – CH_2), 11.0 (*C*H_3 – CH_2 – CH)

ATR-FTIR: ν_{MAX} = 2958-2860*m* (C-H), 1725*s* (C=O), 1463*m* (C-H), 1381*m* (C-H), 1238*m* (C-O), 1176*m* (C-O), 1151*s* (C-O), 1061*w* (C-O), 966*w* (C=C) cm^{-1}.

7.3.3 Synthesis of **10FMA10**

Azobisisobutyronitrile (AIBN) (54.8 mg, 0.334 mmol), 1-dodecanethiol (DDM) (1.350 g, 6.671 mmol), benzyl benzoate (289.0 mg, 1.362 mmol) as an internal NMR standard and furfuryl methacrylate (FMA) (8.372 g, 50.376 mmol) were dissolved in 2-ethylhexyl methacrylate (EHMA) (90.000 g, 453.835 mmol) in a two-neck round bottom flask. The flask was equipped with a septum and a mechanical stirrer. The reaction mixture was purged with N_2 for 30 minutes. The flask was placed in an oil bath at 80 °C and stirred for 3.5 hours. The conversion was monitored *via* ^{1}H NMR spectroscopy. After the reaction was completed, the polymer was dissolved in a minimal amount of ethyl acetate (*ca.* 125 mL). This solution was precipitated in a large excess of ice-cold ethanol (500 mL). The precipitated polymer was collected in a PTFE-lined Petri dish and dried in a vacuum oven at 80 °C. The precipitation was repeated until all residual monomer, observed by ^{1}H NMR spectroscopy, was removed.

Yield: 65.614 g (6.190 mmol, 67%)

SEC ($CHCl_3$): M_n = 10.6 kg.mol^{-1}, M_w = 19.2 kg.mol^{-1}, $Đ_M$ = 1.81

^{1}H-NMR (400 MHz, 298 K, $CDCl_3$): δ (ppm) = 0.81 – 0.95 (m, 6H, CH_2 – C*H*$_3$), 1.02 (s, 6H, C*H*$_3$ – C), 1.23 – 1.46 (m, 12H, C*H*$_2$), 1.54 (m, 1H, C*H* – $(CH_2)_3$), 3.83 (m, 2H, O – C*H*$_2$

– CH), 4.94 (s, 2H, O – CH_2 – C), 6.36 (d, 2H, C = CH – CH = CH), 7.40 (m, 1H, O – CH = CH)

^{13}C-NMR (400 MHz, 298 K, $CDCl_3$, DEPT): δ (ppm) = 177.8 (C_q= O), 149.1 (C_q – O), 143.2 (*C*H – O), 110.4 (CH – *C*H – CH), 67.0 (*C*H – OCOR), 44.9 (C_q – *C*H_2 – C_q), 38.4 (*C*H_3 – C_q), 30.4 (CH_2 – *C*H2 –CH), 29.0 (CH_3 – *C*H_2 – CH), 23.9 (CH_2 – *C*H_2 – CH_2), 22.9 (CH_3 – *C*H_2 – CH_2), 14.1 (*C*H_3 – CH_2 – CH_2), 11.0 (*C*H_3 – CH_2 – CH)

ATR-FTIR: ν_{MAX} = 2958-2860*m* (C-H), 1725*s* (C=O), 1463*m* (C-H), 1381*m* (C-H), 1238*m* (C-O), 1176*m* (C-O), 1151*s* (C-O), 1061*w* (C-O), 966*w* (C=C) cm^{-1}.

7.3.4 Synthesis of **10FMA20**

Azobisisobutyronitrile (AIBN) (54.8 mg, 0.334 mmol), 1-dodecanethiol (DDM) (1.350 g, 6.671 mmol), benzyl benzoate (289.0 mg, 1.362 mmol) as an internal NMR standard and furfuryl methacrylate (FMA) (18.855 g, 113.460 mmol) were dissolved in 2-ethylhexyl methacrylate (EHMA) (90.000 g, 453.835 mmol) in a two-neck round bottom flask. The flask was equipped with a septum and a mechanical stirrer. The reaction mixture was purged with N_2 for 30 minutes. The flask was placed in an oil bath at 80 °C and stirred for 3.5 hours. The conversion was monitored *via* ^{1}H NMR spectroscopy. After the reaction was completed, the polymer was dissolved in a minimal amount of ethyl acetate (*ca.* 125 mL). This solution was precipitated in a large excess of ice-cold ethanol (500 mL). The precipitated polymer was collected in a PTFE-lined Petri dish and dried in a vacuum oven at 80 °C. The precipitation was repeated until all residual monomer, observed by ^{1}H NMR spectroscopy, was removed.

Yield: 94.160 g (7.414 mmol, 87%)

SEC ($CHCl_3$): M_n = 12.7 kg.mol^{-1}, M_w = 24.8 kg.mol^{-1}, $Đ_M$ = 1.96

^{1}H-NMR (400 MHz, 298 K, $CDCl_3$): δ (ppm) = 0.81 – 0.95 (m, 6H, $CH_2 – CH_3$), 1.02 (s, 6H, $CH_3 – C$), 1.23 – 1.46 (m, 12H, CH_2), 1.54 (m, 1H, $CH – (CH_2)_3$), 3.83 (m, 2H, $O – CH_2 – CH$), 4.94 (s, 2H, $O – CH_2 – C$), 6.36 (d, 2H, $C = CH – CH = CH$), 7.40 (m, 1H, $O – CH = CH$)

^{13}C-NMR (400 MHz, 298 K, $CDCl_3$, DEPT): δ (ppm) = 177.8 (C_q= O), 149.1 (C_q – O), 143.2 (CH – O), 110.4 ($CH – CH – CH$), 67.0 (CH – OCOR), 44.9 ($C_q – CH_2 – C_q$), 38.4 ($CH_3 – C_q$), 30.4 ($CH_2 – CH2 –CH$), 29.0 ($CH_3 – CH_2 – CH$), 23.9 ($CH_2 – CH_2 – CH_2$), 22.9 ($CH_3 – CH_2 – CH_2$), 14.1 ($CH_3 – CH_2 – CH_2$), 11.0 ($CH_3 – CH_2 – CH$)

ATR-FTIR: ν_{MAX} = 2958-2860*m* (C-H), 1725*s* (C=O), 1463*m* (C-H), 1381*m* (C-H), 1238*m* (C-O), 1176*m* (C-O), 1151*s* (C-O), 1061*w* (C-O), 966*w* (C=C) cm^{-1}.

7.3.5 Synthesis of **40FMA2**

Azobisisobutyronitrile (AIBN) (13.7 mg, 0.083 mmol), 1-dodecanethiol (DDM) (0.169 g, 0.834 mmol), benzyl benzoate (289.0 mg, 1.362 mmol) as an internal NMR standard and furfuryl methacrylate (FMA) (1.478 g, 8.895 mmol) were dissolved in 2-ethylhexyl methacrylate (EHMA) (90.000 g, 453.835 mmol) in a two-neck round bottom flask. The flask was equipped with a septum and a mechanical stirrer. The reaction mixture was purged with N_2 for 30 minutes. The flask was placed in an oil bath at 80 °C and stirred for 4.0 hours. The conversion was monitored *via* ^{1}H NMR spectroscopy. After the reaction was completed, the polymer was dissolved in a minimal amount of ethyl acetate (*ca.* 125 mL). This solution was precipitated in a large excess of ice-cold ethanol (500 mL). The precipitated polymer was collected in a PTFE-lined Petri dish and dried in a vacuum oven at 80 °C. The precipitation was repeated until all residual monomer, observed by ^{1}H NMR spectroscopy, was removed.

Yield: 52.142 g (0.887 mmol, 57%)

SEC ($CHCl_3$): M_n = 58.8 kg.mol^{-1}, M_w = 127.5 kg.mol^{-1}, $Đ_M$ = 2.17

^{1}H-NMR (400 MHz, 298 K, $CDCl_3$): δ (ppm) = 0.81 – 0.95 (m, 6H, $CH_2 – CH_3$), 1.02 (s, 6H, $CH_3 – C$), 1.23 – 1.46 (m, 12H, CH_2), 1.54 (m, 1H, $CH – (CH_2)_3$), 3.83 (m, 2H, $O – CH_2 – CH$), 4.94 (s, 2H, $O – CH_2 – C$), 6.36 (d, 2H, $C = CH – CH = CH$), 7.40 (m, 1H, $O – CH = CH$)

ATR-FTIR: ν_{MAX} = 2958-2860*m* (C-H), 1725*s* (C=O), 1463*m* (C-H), 1381*m* (C-H), 1238*m* (C-O), 1176*m* (C-O), 1151*s* (C-O), 1061*w* (C-O), 966*w* (C=C) cm^{-1}.

7.3.6 Synthesis of **40FMA5**

Azobisisobutyronitrile (AIBN) (13.7 mg, 0.083 mmol), 1-dodecanethiol (DDM) (0.169 g, 0.834 mmol), benzyl benzoate (289.0 mg, 1.362 mmol) as an internal NMR standard and furfuryl methacrylate (FMA) (3.967 g, 23.872 mmol) were dissolved in 2-ethylhexyl methacrylate (EHMA) (90.000 g, 453.835 mmol) in a two-neck round bottom flask. The flask was equipped with a septum and a mechanical stirrer. The reaction mixture was purged with N_2 for 30 minutes. The flask was placed in an oil bath at 80 °C and stirred for 3.5 hours. The conversion was monitored *via* ^{1}H NMR spectroscopy. After the reaction was completed, the polymer was dissolved in a minimal amount of ethyl acetate (*ca.* 125 mL). This solution was precipitated in a large excess of ice-cold ethanol (500 mL). The precipitated polymer was collected in a PTFE-lined Petri dish and dried in a vacuum oven at 80 °C. The precipitation was repeated until all residual monomer, observed by ^{1}H NMR spectroscopy, was removed.

Yield: 48.487 g (1.080 mmol, 52%)

SEC ($CHCl_3$): M_n = 44.9 kg.mol^{-1}, M_w = 95.4 kg.mol^{-1}, $Đ_M$ = 2.12

^{1}H-NMR (400 MHz, 298 K, $CDCl_3$): δ (ppm) = 0.81 – 0.95 (m, 6H, $CH_2 – CH_3$), 1.02 (s, 6H, $CH_3 – C$), 1.23 – 1.46 (m, 12H, CH_2), 1.54 (m, 1H, $CH – (CH_2)_3$), 3.83 (m, 2H, $O – CH_2 – CH$), 4.94 (s, 2H, $O – CH_2 – C$), 6.36 (d, 2H, $C = CH – CH = CH$), 7.40 (m, 1H, $O – CH = CH$)

^{13}C-NMR (400 MHz, 298 K, $CDCl_3$, DEPT): δ (ppm) = 177.8 (C_q= O), 149.1 (C_q – O), 143.2 (CH – O), 110.4 (CH – CH – CH), 67.0 (CH – OCOR), 44.9 ($C_q – CH_2 – C_q$), 38.4 ($CH_3 – C_q$), 30.4 ($CH_2 – CH2 –CH$), 29.0 ($CH_3 – CH_2 – CH$), 23.9 ($CH_2 – CH_2 – CH_2$), 22.9 ($CH_3 – CH_2 – CH_2$), 14.1 ($CH_3 – CH_2 – CH_2$), 11.0 ($CH_3 – CH_2 – CH$)

ATR-FTIR: ν_{MAX} = 2958-2860*m* (C-H), 1725*s* (C=O), 1463*m* (C-H), 1381*m* (C-H), 1238*m* (C-O), 1176*m* (C-O), 1151*s* (C-O), 1061*w* (C-O), 966*w* (C=C) cm^{-1}.

7.3.7 Synthesis of **40FMA10**

Azobisisobutyronitrile (AIBN) (27.4 mg, 0.167 mmol), 1-dodecanethiol (DDM) (0.338 g, 1.668 mmol), benzyl benzoate (289.0 mg, 1.362 mmol) as an internal NMR standard and furfuryl methacrylate (FMA) (8.372 g, 50.376 mmol) were dissolved in 2-ethylhexyl methacrylate (EHMA) (90.000 g, 453.835 mmol) in a two-neck round bottom flask. The flask was equipped with a septum and a mechanical stirrer. The reaction mixture was purged with N_2 for 30 minutes. The flask was placed in an oil bath at 80 °C and stirred for 3.5 hours. The conversion was monitored *via* ^{1}H NMR spectroscopy. After the reaction was completed, the polymer was dissolved in a minimal amount of ethyl acetate (*ca.* 125 mL). This solution was precipitated in a large excess of ice-cold ethanol (500 mL). The precipitated polymer was collected in a PTFE-lined Petri dish and dried in a vacuum oven at 80 °C. The precipitation was repeated until all residual monomer, observed by ^{1}H NMR spectroscopy, was removed.

Yield: 73.976 g (1.937 mmol, 75%)

SEC ($CHCl_3$): M_n = 38.2 kg.mol^{-1}, M_w = 77.7 kg.mol^{-1}, $Đ_M$ = 2.03

^{1}H-NMR (400 MHz, 298 K, $CDCl_3$): δ (ppm) = 0.81 – 0.95 (m, 6H, $CH_2 – CH_3$), 1.02 (s, 6H, $CH_3 – C$), 1.23 – 1.46 (m, 12H, CH_2), 1.54 (m, 1H, $CH – (CH_2)_3$), 3.83 (m, 2H, $O – CH_2 – CH$), 4.94 (s, 2H, $O – CH_2 – C$), 6.36 (d, 2H, $C = CH – CH = CH$), 7.40 (m, 1H, $O – CH = CH$)

^{13}C-NMR (400 MHz, 298 K, $CDCl_3$, DEPT): δ (ppm) = 177.8 (C_q= O), 149.1 (C_q – O), 143.2 (CH – O), 110.4 (CH – CH – CH), 67.0 (CH – OCOR), 44.9 ($C_q – CH_2 – C_q$), 38.4 ($CH_3 – C_q$), 30.4 ($CH_2 – CH2 –CH$), 29.0 ($CH_3 – CH_2 – CH$), 23.9 ($CH_2 – CH_2 – CH_2$), 22.9 ($CH_3 – CH_2 – CH_2$), 14.1 ($CH_3 – CH_2 – CH_2$), 11.0 ($CH_3 – CH_2 – CH$)

ATR-FTIR: ν_{MAX} = 2958-2860*m* (C-H), 1725*s* (C=O), 1463*m* (C-H), 1381*m* (C-H), 1238*m* (C-O), 1176*m* (C-O), 1151*s* (C-O), 1061*w* (C-O), 966*w* (C=C) cm^{-1}.

7.3.8 Synthesis of **40FMA20**

Azobisisobutyronitrile (AIBN) (19.4 mg, 0.118 mmol), 1-dodecanethiol (DDM) (0.239 g, 1.180 mmol), benzyl benzoate (289.0 mg, 1.362 mmol) as an internal NMR standard and furfuryl methacrylate (FMA) (18.855 g, 113.460 mmol) were dissolved in 2-ethylhexyl methacrylate (EHMA) (90.000 g, 453.835 mmol) in a two-neck round bottom flask. The flask was equipped with a septum and a mechanical stirrer. The reaction mixture was purged with N_2 for 30 minutes. The flask was placed in an oil bath at 80 °C and stirred for 3.5 hours. The conversion was monitored *via* ^{1}H NMR spectroscopy. After the reaction was completed, the polymer was dissolved in a minimal amount of ethyl acetate (*ca.* 125 mL). This solution was precipitated in a large excess of ice-cold ethanol (500 mL). The precipitated polymer was collected in a PTFE-lined Petri dish and dried in a vacuum oven at 80 °C. The precipitation was repeated until all residual monomer, observed by ^{1}H NMR spectroscopy, was removed.

Yield: 17.417 g (0.431 mmol, 16%)

SEC ($CHCl_3$): M_n = 40.4 kg.mol^{-1}, M_w = 115.1 kg.mol^{-1}, $Đ_M$ = 2.85

^{1}H-NMR (400 MHz, 298 K, $CDCl_3$): δ (ppm) = 0.81 – 0.95 (m, 6H, $CH_2 – CH_3$), 1.02 (s, 6H, $CH_3 – C$), 1.23 – 1.46 (m, 12H, CH_2), 1.54 (m, 1H, $CH – (CH_2)_3$), 3.83 (m, 2H, $O – CH_2 – CH$), 4.94 (s, 2H, $O – CH_2 – C$), 6.36 (d, 2H, $C = CH – CH = CH$), 7.40 (m, 1H, $O – CH = CH$)

^{13}C-NMR (400 MHz, 298 K, $CDCl_3$, DEPT): δ (ppm) = 177.8 (C_q= O), 149.1 (C_q – O), 143.2 (CH – O), 110.4 (CH – CH – CH), 67.0 (CH – OCOR), 44.9 ($C_q – CH_2 – C_q$), 38.4 ($CH_3 – C_q$), 30.4 ($CH_2 – CH2 –CH$), 29.0 ($CH_3 – CH_2 – CH$), 23.9 ($CH_2 – CH_2 – CH_2$), 22.9 ($CH_3 – CH_2 – CH_2$), 14.1 ($CH_3 – CH_2 – CH_2$), 11.0 ($CH_3 – CH_2 – CH$)

ATR-FTIR: ν_{MAX} = 2958-2860*m* (C-H), 1725*s* (C=O), 1463*m* (C-H), 1381*m* (C-H), 1238*m* (C-O), 1176*m* (C-O), 1151*s* (C-O), 1061*w* (C-O), 966*w* (C=C) cm^{-1}.

7.4 General synthesis of poly(EHMA-*co*-AEMA)

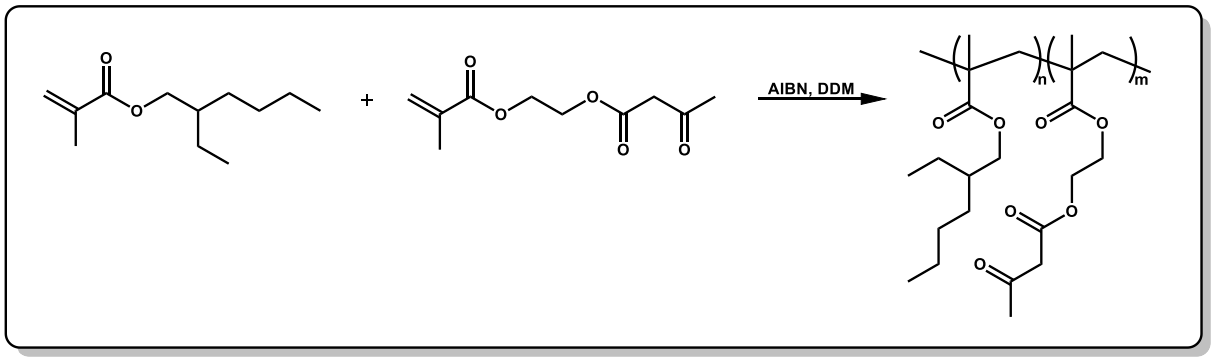

7.4.1 Synthesis of **10AEMA3**

Azobisisobutyronitrile (AIBN) (7.3 mg, 0.044 mmol), 1-dodecanethiol (DDM) (0.180 g, 0.890 mmol), 1,3,5-trioxane (54.5 mg, 0.605 mmol) as an internal NMR standard and acetoacetoxyethyl methacrylate (AEMA) (0.401 g, 1.870 mmol) were dissolved in 2-ethylhexyl methacrylate (EHMA) (12.000 g, 60.512 mmol) in a two-neck round bottom flask. The flask was equipped with a septum and a mechanical stirrer. The reaction mixture was purged with N_2 for 30 minutes. The flask was placed in an oil bath at 80 °C and stirred for 3.0 hours. The conversion was monitored *via* ^{1}H NMR spectroscopy. After the reaction was completed, the polymer was dissolved in a minimal amount of ethyl acetate (*ca.* 125 mL). This solution was precipitated in a large excess of ice-cold ethanol (500 mL). The precipitated polymer was collected in a PTFE-lined Petri dish and dried in a vacuum oven at 80 °C. The precipitation was repeated until all residual monomer, observed by ^{1}H NMR spectroscopy, was removed.

Yield: 9.772 g (0.949 mmol, 79%)

SEC ($CHCl_3$): M_n = 10.3 kg.mol^{-1}, M_w = 17.8 kg.mol^{-1}, $Đ_M$ = 1.73

^{1}H-NMR (400 MHz, 298 K, $CDCl_3$): δ (ppm) = 0.81 – 0.95 (m, 6H, $CH_2 - CH_3$), 1.02 (s, 6H, $CH_3 - C$), 1.23 – 1.46 (m, 12H, CH_2), 1.54 (m, 1H, $CH - (CH_2)_3$), 2.30 (s, 3H, $CH_3 - CO$),

3.60 (s, 2H, CO – CH_2 – CO), 3.83 (m, 2H, O – CH_2 – CH), 4.15 (m, 2H, O – CH_2 – CH_2), 4.32 (m, 2H, O – CH_2 – CH_2)

ATR-FTIR: ν_{MAX} = 2958-2860*m* (C-H), 1725*s* (C=O), 1463*m* (C-H), 1381*m* (C-H), 1238*m* (C-O), 1175*m* (C-O), 1150*s* (C-O), 1061*w* (C-O) cm^{-1}.

7.4.2 Synthesis of **10AEMA5**

Azobisisobutyronitrile (AIBN) (54.8 mg, 0.334 mmol), 1-dodecanethiol (DDM) (1.350 g, 6.671 mmol), 1,3,5-trioxane (122.6 mg, 1.362 mmol) as an internal NMR standard and acetoacetoxyethyl methacrylate (AEMA) (5.117 g, 23.886 mmol) were dissolved in 2-ethylhexyl methacrylate (EHMA) (90.000 g, 453.835 mmol) in a two-neck round bottom flask. The flask was equipped with a septum and a mechanical stirrer. The reaction mixture was purged with N_2 for 30 minutes. The flask was placed in an oil bath at 80 °C and stirred for 3.5 hours. The conversion was monitored *via* ^{1}H NMR spectroscopy. After the reaction was completed, the polymer was dissolved in a minimal amount of ethyl acetate (*ca.* 125 mL). This solution was precipitated in a large excess of ice-cold ethanol (500 mL). The precipitated polymer was collected in a PTFE-lined Petri dish and dried in a vacuum oven at 80 °C. The precipitation was repeated until all residual monomer, observed by ^{1}H NMR spectroscopy, was removed.

Yield: 90.171 g (8.588 mmol, 95%)

SEC ($CHCl_3$): M_n = 10.5 kg.mol^{-1}, M_w = 19.1 kg.mol^{-1}, $Đ_M$ = 1.82

^{1}H-NMR (400 MHz, 298 K, $CDCl_3$): δ (ppm) = 0.81 – 0.95 (m, 6H, CH_2 – CH_3), 1.02 (s, 6H, CH_3 – C), 1.23 – 1.46 (m, 12H, CH_2), 1.54 (m, 1H, CH – $(CH_2)_3$), 2.30 (s, 3H, CH_3 – CO), 3.60 (s, 2H, CO – CH_2 – CO), 3.83 (m, 2H, O – CH_2 – CH), 4.15 (m, 2H, O – CH_2 – CH_2), 4.32 (m, 2H, O – CH_2 – CH_2)

^{13}C-NMR (400 MHz, 298 K, $CDCl_3$, DEPT): δ (ppm) = 200.4 (C_q= O), 177.8 (C_q= O), 67.0 (*C*H – OCOR), 54.6 (CO – *C*H_2 – CO), 44.9 (C_q – *C*H_2 – C_q), 38.4 (*C*H_3 – C_q), 30.4 (CH_2 – *C*H2 –CH), 29.0 (CH_3 – *C*H_2 – CH), 23.9 (CH_2 – *C*H_2 – CH_2), 22.9 (CH_3 – *C*H_2 – CH_2), 14.1 (*C*H_3 – CH_2 – CH_2), 11.0 (*C*H_3 – CH_2 – CH)

ATR-FTIR: ν_{MAX} = 2958-2860*m* (C-H), 1725*s* (C=O), 1463*m* (C-H), 1381*m* (C-H), 1238*m* (C-O), 1175*m* (C-O), 1150*s* (C-O), 1061*w* (C-O) cm^{-1}.

7.4.3 Synthesis of **10AEMA10**

Azobisisobutyronitrile (AIBN) (54.8 mg, 0.334 mmol), 1-dodecanethiol (DDM) (1.350 g, 6.671 mmol), 1,3,5-trioxane (122.6 mg, 1.362 mmol) as an internal NMR standard and acetoacetoxyethyl methacrylate (AEMA) (10.791 g, 50.376 mmol) were dissolved in 2-ethylhexyl methacrylate (EHMA) (90.000 g, 453.835 mmol) in a two-neck round bottom flask. The flask was equipped with a septum and a mechanical stirrer. The reaction mixture was purged with N_2 for 30 minutes. The flask was placed in an oil bath at 80 °C and stirred for 3.5 hours. The conversion was monitored *via* ^{1}H NMR spectroscopy. After the reaction was completed, the polymer was dissolved in a minimal amount of ethyl acetate (*ca.* 125 mL). This solution was precipitated in a large excess of ice-cold ethanol (500 mL). The precipitated polymer was collected in a PTFE-lined Petri dish and dried in a vacuum oven at 80 °C. The precipitation was repeated until all residual monomer, observed by ^{1}H NMR spectroscopy, was removed.

Yield: 92.928 g (8.224 mmol, 92%)

SEC ($CHCl_3$): M_n = 11.3 $kg.mol^{-1}$, M_w = 20.2 $kg.mol^{-1}$, $Đ_M$ = 1.78

^{1}H-NMR (400 MHz, 298 K, $CDCl_3$): δ (ppm) = 0.81 – 0.95 (m, 6H, CH_2 – C*H*$_3$), 1.02 (s, 6H, C*H*$_3$ – C), 1.23 – 1.46 (m, 12H, C*H*$_2$), 1.54 (m, 1H, C*H* – $(CH_2)_3$), 2.30 (s, 3H, C*H*$_3$ – CO),

3.60 (s, 2H, CO – CH_2 – CO), 3.83 (m, 2H, O – CH_2 – CH), 4.15 (m, 2H, O – CH_2 – CH_2), 4.32 (m, 2H, O – CH_2 – CH_2)

^{13}C-NMR (400 MHz, 298 K, $CDCl_3$, DEPT): δ (ppm) = 200.4 (C_q= O), 177.8 (C_q= O), 67.0 (*C*H – OCOR), 54.6 (CO – *C*H_2 – CO), 44.9 (C_q – *C*H_2 – C_q), 38.4 (*C*H_3 – C_q), 30.4 (CH_2 – *C*H2 –CH), 29.0 (CH_3 – *C*H_2 – CH), 23.9 (CH_2 – *C*H_2 – CH_2), 22.9 (CH_3 – *C*H_2 – CH_2), 14.1 (*C*H_3 – CH_2 – CH_2), 11.0 (*C*H_3 – CH_2 – CH)

ATR-FTIR: ν_{MAX} = 2958-2860*m* (C-H), 1725*s* (C=O), 1463*m* (C-H), 1381*m* (C-H), 1238*m* (C-O), 1175*m* (C-O), 1150*s* (C-O), 1061*w* (C-O) cm^{-1}.

7.4.4 Synthesis of **10AEMA20**

Azobisisobutyronitrile (AIBN) (27.4 mg, 0.167 mmol), 1-dodecanethiol (DDM) (0.675 g, 3.336 mmol), 1,3,5-trioxane (61.3 mg, 0.681 mmol) as an internal NMR standard and acetoacetoxyethyl methacrylate (AEMA) (12.153 g, 56.729 mmol) were dissolved in 2-ethylhexyl methacrylate (EHMA) (45.000 g, 226.918 mmol) in a two-neck round bottom flask. The flask was equipped with a septum and a mechanical stirrer. The reaction mixture was purged with N_2 for 30 minutes. The flask was placed in an oil bath at 80 °C and stirred for 3.5 hours. The conversion was monitored *via* ^{1}H NMR spectroscopy. After the reaction was completed, the polymer was dissolved in a minimal amount of ethyl acetate (*ca.* 125 mL). This solution was precipitated in a large excess of ice-cold ethanol (500 mL). The precipitated polymer was collected in a PTFE-lined Petri dish and dried in a vacuum oven at 80 °C. The precipitation was repeated until all residual monomer, observed by ^{1}H NMR spectroscopy, was removed.

Yield: 47.151 g (4.668 mmol, 83%)

SEC ($CHCl_3$): M_n = 10.1 $kg.mol^{-1}$, M_w = 22.0 $kg.mol^{-1}$, $Đ_M$ = 2.19

^{1}H-NMR (400 MHz, 298 K, $CDCl_3$): δ (ppm) = 0.81 – 0.95 (m, 6H, CH_2 – CH_3), 1.02 (s, 6H, CH_3 – C), 1.23 – 1.46 (m, 12H, CH_2), 1.54 (m, 1H, CH – $(CH_2)_3$), 2.30 (s, 3H, CH_3 – CO), 3.60 (s, 2H, CO – CH_2 – CO), 3.83 (m, 2H, O – CH_2 – CH), 4.15 (m, 2H, O – CH_2 – CH_2), 4.32 (m, 2H, O – CH_2 – CH_2)

^{13}C-NMR (400 MHz, 298 K, $CDCl_3$, DEPT): δ (ppm) = 200.4 (C_q= O), 177.8 (C_q= O), 67.0 (*C*H – OCOR), 54.6 (CO – *C*H_2 – CO), 44.9 (C_q – *C*H_2 – C_q), 38.4 (*C*H_3 – C_q), 30.4 (CH_2 – *C*H2 –CH), 29.0 (CH_3 – *C*H_2 – CH), 23.9 (CH_2 – *C*H_2 – CH_2), 22.9 (CH_3 – *C*H_2 – CH_2), 14.1 (*C*H_3 – CH_2 – CH_2), 11.0 (*C*H_3 – CH_2 – CH)

ATR-FTIR: ν_{MAX} = 2958-2860*m* (C-H), 1725*s* (C=O), 1463*m* (C-H), 1381*m* (C-H), 1238*m* (C-O), 1175*m* (C-O), 1150*s* (C-O), 1061*w* (C-O) cm^{-1}.

7.4.5 Synthesis of **40AEMA2**

Azobisisobutyronitrile (AIBN) (13.7 mg, 0.083 mmol), 1-dodecanethiol (DDM) (0.169 g, 0.834 mmol), 1,3,5-trioxane (122.6 mg, 1.362 mmol) as an internal NMR standard and acetoacetoxyethyl methacrylate (AEMA) (1.993 g, 9.304 mmol) were dissolved in 2-ethylhexyl methacrylate (EHMA) (90.000 g, 453.835 mmol) in a two-neck round bottom flask. The flask was equipped with a septum and a mechanical stirrer. The reaction mixture was purged with N_2 for 30 minutes. The flask was placed in an oil bath at 80 °C and stirred for 4.0 hours. The conversion was monitored *via* ^{1}H NMR spectroscopy. After the reaction was completed, the polymer was dissolved in a minimal amount of ethyl acetate (*ca.* 125 mL). This solution was precipitated in a large excess of ice-cold ethanol (500 mL). The precipitated polymer was collected in a PTFE-lined Petri dish and dried in a vacuum oven at 80 °C. The precipitation was repeated until all residual monomer, observed by ^{1}H NMR spectroscopy, was removed.

Yield: 14.167 g (0.290 mmol, 15%)

SEC ($CHCl_3$): M_n = 48.8 kg.mol^{-1}, M_w = 101.9 kg.mol^{-1}, $Đ_M$ = 2.19

^{1}H-NMR (400 MHz, 298 K, $CDCl_3$): δ (ppm) = 0.81 – 0.95 (m, 6H, CH_2 – C*H*$_3$), 1.02 (s, 6H, C*H*$_3$ – C), 1.23 – 1.46 (m, 12H, C*H*$_2$), 1.54 (m, 1H, C*H* – $(CH_2)_3$), 2.30 (s, 3H, C*H*$_3$ – CO), 3.60 (s, 2H, CO – C*H*$_2$ – CO), 3.83 (m, 2H, O – C*H*$_2$ – CH), 4.15 (m, 2H, O – C*H*$_2$ – CH_2), 4.32 (m, 2H, O – CH_2 – C*H*$_2$)

ATR-FTIR: ν_{MAX} = 2958-2860*m* (C-H), 1725*s* (C=O), 1463*m* (C-H), 1381*m* (C-H), 1238*m* (C-O), 1175*m* (C-O), 1150*s* (C-O), 1061*w* (C-O) cm^{-1}.

7.4.6 Synthesis of **40AEMA5**

Azobisisobutyronitrile (AIBN) (18.3 mg, 0.111 mmol), 1-dodecanethiol (DDM) (0.225 g, 1.112 mmol), 1,3,5-trioxane (122.6 mg, 1.362 mmol) as an internal NMR standard and acetoacetoxyethyl methacrylate (AEMA) (5.117 g, 23.886 mmol) were dissolved in 2-ethylhexyl methacrylate (EHMA) (90.000 g, 453.835 mmol) in a two-neck round bottom flask. The flask was equipped with a septum and a mechanical stirrer. The reaction mixture was purged with N_2 for 30 minutes. The flask was placed in an oil bath at 80 °C and stirred for 4.0 hours. The conversion was monitored *via* ^{1}H NMR spectroscopy. After the reaction was completed, the polymer was dissolved in a minimal amount of ethyl acetate (*ca.* 125 mL). This solution was precipitated in a large excess of ice-cold ethanol (500 mL). The precipitated polymer was collected in a PTFE-lined Petri dish and dried in a vacuum oven at 80 °C. The precipitation was repeated until all residual monomer, observed by ^{1}H NMR spectroscopy, was removed.

Yield: 33.767 g (0.866 mmol, 36%)

SEC ($CHCl_3$): M_n = 39.0 kg.mol^{-1}, M_w = 84.2 kg.mol^{-1}, $Đ_M$ = 2.16

^{1}H-NMR (400 MHz, 298 K, $CDCl_3$): δ (ppm) = 0.81 – 0.95 (m, 6H, $CH_2 - CH_3$), 1.02 (s, 6H, $CH_3 - C$), 1.23 – 1.46 (m, 12H, CH_2), 1.54 (m, 1H, $CH - (CH_2)_3$), 2.30 (s, 3H, $CH_3 - CO$), 3.60 (s, 2H, $CO - CH_2 - CO$), 3.83 (m, 2H, $O - CH_2 - CH$), 4.15 (m, 2H, $O - CH_2 - CH_2$), 4.32 (m, 2H, $O - CH_2 - CH_2$)

^{13}C-NMR (400 MHz, 298 K, $CDCl_3$, DEPT): δ (ppm) = 200.4 (C_q= O), 177.8 (C_q= O), 67.0 ($CH - OCOR$), 54.6 ($CO - CH_2 - CO$), 44.9 ($C_q - CH_2 - C_q$), 38.4 ($CH_3 - C_q$), 30.4 ($CH_2 - CH2 - CH$), 29.0 ($CH_3 - CH_2 - CH$), 23.9 ($CH_2 - CH_2 - CH_2$), 22.9 ($CH_3 - CH_2 - CH_2$), 14.1 ($CH_3 - CH_2 - CH_2$), 11.0 ($CH_3 - CH_2 - CH$)

ATR-FTIR: ν_{MAX} = 2958-2860*m* (C-H), 1725*s* (C=O), 1463*m* (C-H), 1381*m* (C-H), 1238*m* (C-O), 1175*m* (C-O), 1150*s* (C-O), 1061*w* (C-O) cm^{-1}.

7.4.7 Synthesis of **40AEMA10**

Azobisisobutyronitrile (AIBN) (18.3 mg, 0.111 mmol), 1-dodecanethiol (DDM) (0.225 g, 1.112 mmol), 1,3,5-trioxane (122.6 mg, 1.362 mmol) as an internal NMR standard and acetoacetoxyethyl methacrylate (AEMA) (10.791 g, 50.376 mmol) were dissolved in 2-ethylhexyl methacrylate (EHMA) (90.000 g, 453.835 mmol) in a two-neck round bottom flask. The flask was equipped with a septum and a mechanical stirrer. The reaction mixture was purged with N_2 for 30 minutes. The flask was placed in an oil bath at 80 °C and stirred for 4.0 hours. The conversion was monitored *via* ^{1}H NMR spectroscopy. After the reaction was completed, the polymer was dissolved in a minimal amount of ethyl acetate (*ca.* 125 mL). This solution was precipitated in a large excess of ice-cold ethanol (500 mL). The precipitated polymer was collected in a PTFE-lined Petri dish and dried in a vacuum oven at 80 °C. The precipitation was repeated until all residual monomer, observed by ^{1}H NMR spectroscopy, was removed.

Yield: 35.680 g (0.815 mmol, 35%)

SEC ($CHCl_3$): M_n = 43.8 kg.mol^{-1}, M_w = 97.2 kg.mol^{-1}, $Đ_M$ = 2.22

^{1}H-NMR (400 MHz, 298 K, $CDCl_3$): δ (ppm) = 0.81 – 0.95 (m, 6H, $CH_2 - CH_3$), 1.02 (s, 6H, $CH_3 - C$), 1.23 – 1.46 (m, 12H, CH_2), 1.54 (m, 1H, $CH - (CH_2)_3$), 2.30 (s, 3H, $CH_3 - CO$), 3.60 (s, 2H, $CO - CH_2 - CO$), 3.83 (m, 2H, $O - CH_2 - CH$), 4.15 (m, 2H, $O - CH_2 - CH_2$), 4.32 (m, 2H, $O - CH_2 - CH_2$)

^{13}C-NMR (400 MHz, 298 K, $CDCl_3$, DEPT): δ (ppm) = 200.4 (C_q= O), 177.8 (C_q= O), 67.0 ($CH - OCOR$), 54.6 ($CO - CH_2 - CO$), 44.9 ($C_q - CH_2 - C_q$), 38.4 ($CH_3 - C_q$), 30.4 ($CH_2 - CH2 - CH$), 29.0 ($CH_3 - CH_2 - CH$), 23.9 ($CH_2 - CH_2 - CH_2$), 22.9 ($CH_3 - CH_2 - CH_2$), 14.1 ($CH_3 - CH_2 - CH_2$), 11.0 ($CH_3 - CH_2 - CH$)

ATR-FTIR: ν_{MAX} = 2958-2860*m* (C-H), 1725*s* (C=O), 1463*m* (C-H), 1381*m* (C-H), 1238*m* (C-O), 1175*m* (C-O), 1150*s* (C-O), 1061*w* (C-O) cm^{-1}.

7.4.8 Synthesis of **40AEMA20**

Azobisisobutyronitrile (AIBN) (18.6 mg, 0.113 mmol), 1-dodecanethiol (DDM) (0.113 g, 0.556 mmol), 1,3,5-trioxane (61.3 mg, 0.681 mmol) as an internal NMR standard and acetoacetoxyethyl methacrylate (AEMA) (12.153 g, 56.729 mmol) were dissolved in 2-ethylhexyl methacrylate (EHMA) (45.000 g, 226.918 mmol) in a two-neck round bottom flask. The flask was equipped with a septum and a mechanical stirrer. The reaction mixture was purged with N_2 for 30 minutes. The flask was placed in an oil bath at 70 °C and stirred for 5.0 hours. The conversion was monitored *via* ^{1}H NMR spectroscopy. After the reaction was completed, the polymer was dissolved in a minimal amount of ethyl acetate (*ca.* 125 mL). This solution was precipitated in a large excess of ice-cold ethanol (500 mL). The precipitated polymer was collected in a PTFE-lined Petri dish and dried in a vacuum oven at 80 °C. The precipitation was repeated until all residual monomer, observed by ^{1}H NMR spectroscopy, was removed.

Yield: 36.406 g (0.531 mmol, 64%)

SEC ($CHCl_3$): M_n = 68.5 kg.mol^{-1}, M_w = 200.0 kg.mol^{-1}, $Đ_M$ = 2.92

^{1}H-NMR (400 MHz, 298 K, $CDCl_3$): δ (ppm) = 0.81 – 0.95 (m, 6H, $CH_2 - CH_3$), 1.02 (s, 6H, $CH_3 - C$), 1.23 – 1.46 (m, 12H, CH_2), 1.54 (m, 1H, $CH - (CH_2)_3$), 2.30 (s, 3H, $CH_3 - CO$), 3.60 (s, 2H, $CO - CH_2 - CO$), 3.83 (m, 2H, $O - CH_2 - CH$), 4.15 (m, 2H, $O - CH_2 - CH_2$), 4.32 (m, 2H, $O - CH_2 - CH_2$)

^{13}C-NMR (400 MHz, 298 K, $CDCl_3$, DEPT): δ (ppm) = 200.4 (C_q= O), 177.8 (C_q= O), 67.0 ($CH - OCOR$), 54.6 ($CO - CH_2 - CO$), 44.9 ($C_q - CH_2 - C_q$), 38.4 ($CH_3 - C_q$), 30.4 ($CH_2 - CH2 - CH$), 29.0 ($CH_3 - CH_2 - CH$), 23.9 ($CH_2 - CH_2 - CH_2$), 22.9 ($CH_3 - CH_2 - CH_2$), 14.1 ($CH_3 - CH_2 - CH_2$), 11.0 ($CH_3 - CH_2 - CH$)

ATR-FTIR: ν_{MAX} = 2958-2860*m* (C-H), 1725*s* (C=O), 1463*m* (C-H), 1381*m* (C-H), 1238*m* (C-O), 1175*m* (C-O), 1150*s* (C-O), 1061*w* (C-O) cm^{-1}.

7.5 General synthesis of poly(EHMA-*co*-HEMA)

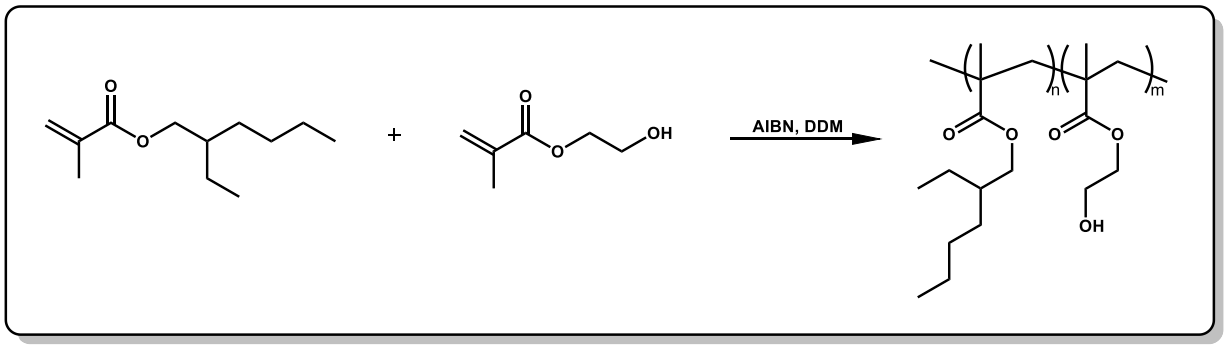

7.5.1 Synthesis of **10HEMA2**

Azobisisobutyronitrile (AIBN) (54.8 mg, 0.334 mmol), 1-dodecanethiol (DDM) (1.350 g, 6.671 mmol), 1,3,5-trioxane (122.6 mg, 1.362 mmol) as an internal NMR standard and 2-hydroxyethyl methacrylate (HEMA) (1.205 g, 9.258 mmol) were dissolved in 2-ethylhexyl methacrylate (EHMA) (90.000, 453.835 mmol) in a two-neck round bottom flask. The flask was equipped with a septum and a mechanical stirrer. The reaction mixture was purged with N_2 for 30 minutes. The flask was placed in an oil bath at 80 °C and stirred for 3.5 hours. The conversion was monitored *via* ^{1}H NMR spectroscopy. After the reaction was completed, the polymer was dissolved in a minimal amount of ethyl acetate (*ca.* 125 mL). This solution was precipitated in a large excess of ice-cold ethanol (500 mL). The precipitated polymer was collected in a PTFE-lined Petri dish and dried in a vacuum oven at 80 °C. The precipitation was repeated until all residual monomer, observed by ^{1}H NMR spectroscopy, was removed.

Yield: 82.267 g (8.395 mmol, 90%)

SEC ($CHCl_3$): M_n = 9.8 kg.mol^{-1}, M_w = 17.8 kg.mol^{-1}, $Đ_M$ = 1.81

^{1}H-NMR (400 MHz, 298 K, $CDCl_3$): δ (ppm) = 0.81 – 0.95 (m, 6H, CH_2 – CH_3), 1.02 (s, 6H, CH_3 – C), 1.23 – 1.46 (m, 12H, CH_2), 1.54 (m, 1H, CH – $(CH_2)_3$), 3.83 (m, 2H, O – CH_2 – CH), 4.15 (m, 2H, O – CH_2 – CH_2), 4.32 (m, 2H, O – CH_2 – CH_2)

^{13}C-NMR (400 MHz, 298 K, $CDCl_3$, DEPT): δ (ppm) = 177.8 (C_q= O), 67.0 (*C*H – OCOR), 60.7 (*C*H_2 – O), 44.9 (C_q – *C*H_2 – C_q), 38.4 (*C*H_3 – C_q), 30.4 (CH_2 – *C*H2 –CH), 29.0 (CH_3 – *C*H_2 – CH), 23.9 (CH_2 – *C*H_2 – CH_2), 22.9 (CH_3 – *C*H_2 – CH_2), 14.1 (*C*H_3 – CH_2 – CH_2), 11.0 (*C*H_3 – CH_2 – CH)

ATR-FTIR: ν_{MAX} = 3600-3400*w* (O-H), 2958-2861*m* (C-H), 1725*s* (C=O), 1463*m* (C-H), 1381*m* (C-H), 1239*m* (C-O), 1176*m* (C-O), 1151*s* (C-O), 1061*w* (C-O) cm^{-1}.

7.5.2 Synthesis of **10HEMA5**

Azobisisobutyronitrile (AIBN) (54.8 mg, 0.334 mmol), 1-dodecanethiol (DDM) (1.350 g, 6.671 mmol), 1,3,5-trioxane (122.6 mg, 1.362 mmol) as an internal NMR standard and 2-hydroxyethyl methacrylate (HEMA) (3.107 g, 23.872 mmol) were dissolved in 2-ethylhexyl methacrylate (EHMA) (90.000, 453.835 mmol) in a two-neck round bottom flask. The flask was equipped with a septum and a mechanical stirrer. The reaction mixture was purged with N_2 for 30 minutes. The flask was placed in an oil bath at 80 °C and stirred for 3.5 hours. The conversion was monitored *via* ^{1}H NMR spectroscopy. After the reaction was completed, the polymer was dissolved in a minimal amount of ethyl acetate (*ca.* 125 mL). This solution was precipitated in a large excess of ice-cold ethanol (500 mL). The precipitated polymer was collected in a PTFE-lined Petri dish and dried in a vacuum oven at 80 °C. The precipitation was repeated until all residual monomer, observed by ^{1}H NMR spectroscopy, was removed.

Yield: 81.282 g (7.130 mmol, 87%)

SEC ($CHCl_3$): M_n = 11.4 kg.mol^{-1}, M_w = 19.9 kg.mol^{-1}, $Đ_M$ = 1.75

^{1}H-NMR (400 MHz, 298 K, $CDCl_3$): δ (ppm) = 0.81 – 0.95 (m, 6H, CH_2 – CH_3), 1.02 (s, 6H, CH_3 – C), 1.23 – 1.46 (m, 12H, CH_2), 1.54 (m, 1H, CH – $(CH_2)_3$), 3.83 (m, 2H, O – CH_2 – CH), 4.15 (m, 2H, O – CH_2 – CH_2), 4.32 (m, 2H, O – CH_2 – CH_2)

^{13}C-NMR (400 MHz, 298 K, $CDCl_3$, DEPT): δ (ppm) = 177.8 (C_q= O), 67.0 (CH – OCOR), 60.7 (CH$_2$ – O), 44.9 (C_q – CH$_2$ – C_q), 38.4 (CH$_3$ – C_q), 30.4 (CH_2 – CH2 –CH), 29.0 (CH_3 – CH$_2$ – CH), 23.9 (CH_2 – CH$_2$ – CH_2), 22.9 (CH_3 – CH$_2$ – CH_2), 14.1 (CH$_3$ – CH_2 – CH_2), 11.0 (CH$_3$ – CH_2 – CH)

ATR-FTIR: ν_{MAX} = 3600-3400*w* (O-H), 2958-2861*m* (C-H), 1725*s* (C=O), 1463*m* (C-H), 1381*m* (C-H), 1239*m* (C-O), 1176*m* (C-O), 1151*s* (C-O), 1061*w* (C-O) cm^{-1}.

7.5.3 Synthesis of **10HEMA10**

Azobisisobutyronitrile (AIBN) (54.8 mg, 0.334 mmol), 1-dodecanethiol (DDM) (1.350 g, 6.671 mmol), 1,3,5-trioxane (122.6 mg, 1.362 mmol) as an internal NMR standard and 2-hydroxyethyl methacrylate (HEMA) (6.556 g, 50.376 mmol) were dissolved in 2-ethylhexyl methacrylate (EHMA) (90.000, 453.835 mmol) in a two-neck round bottom flask. The flask was equipped with a septum and a mechanical stirrer. The reaction mixture was purged with N_2 for 30 minutes. The flask was placed in an oil bath at 80 °C and stirred for 3.5 hours. The conversion was monitored *via* ^{1}H NMR spectroscopy. After the reaction was completed, the polymer was dissolved in a minimal amount of ethyl acetate (*ca.* 125 mL). This solution was precipitated in a large excess of ice-cold ethanol (500 mL). The precipitated polymer was collected in a PTFE-lined Petri dish and dried in a vacuum oven at 80 °C. The precipitation was repeated until all residual monomer, observed by ^{1}H NMR spectroscopy, was removed.

Yield: 87.866 g (9.249 mmol, 91%)

SEC ($CHCl_3$): M_n = 9.5 kg.mol^{-1}, M_w = 16.8 kg.mol^{-1}, $Đ_M$ = 1.76

^{1}H-NMR (400 MHz, 298 K, $CDCl_3$): δ (ppm) = 0.81 – 0.95 (m, 6H, CH_2 – CH_3), 1.02 (s, 6H, CH_3 – C), 1.23 – 1.46 (m, 12H, CH_2), 1.54 (m, 1H, CH – $(CH_2)_3$), 3.83 (m, 2H, O – CH_2 – CH), 4.15 (m, 2H, O – CH_2 – CH_2), 4.32 (m, 2H, O – CH_2 – CH_2)

^{13}C-NMR (400 MHz, 298 K, $CDCl_3$, DEPT): δ (ppm) = 177.8 (C_q= O), 67.0 (CH – OCOR), 60.7 (CH$_2$ – O), 44.9 (C_q – CH$_2$ – C_q), 38.4 (CH$_3$ – C_q), 30.4 (CH_2 – CH2 –CH), 29.0 (CH_3 – CH$_2$ – CH), 23.9 (CH_2 – CH$_2$ – CH_2), 22.9 (CH_3 – CH$_2$ – CH_2), 14.1 (CH$_3$ – CH_2 – CH_2), 11.0 (CH$_3$ – CH_2 – CH)

ATR-FTIR: ν_{MAX} = 3600-3400*w* (O-H), 2958-2861*m* (C-H), 1725*s* (C=O), 1463*m* (C-H), 1381*m* (C-H), 1239*m* (C-O), 1176*m* (C-O), 1151*s* (C-O), 1061*w* (C-O) cm^{-1}.

7.5.4 Synthesis of **10HEMA20**

Azobisisobutyronitrile (AIBN) (27.4 mg, 0.167 mmol), 1-dodecanethiol (DDM) (0.675 g, 3.336 mmol), 1,3,5-trioxane (61.3 mg, 0.681 mmol) as an internal NMR standard and 2-hydroxyethyl methacrylate (HEMA) (7.383 g, 56.730 mmol) were dissolved in 2-ethylhexyl methacrylate (EHMA) (45.000, 226.918 mmol) in a two-neck round bottom flask. The flask was equipped with a septum and a mechanical stirrer. The reaction mixture was purged with N_2 for 30 minutes. The flask was placed in an oil bath at 80 °C and stirred for 3.0 hours. The conversion was monitored *via* ^{1}H NMR spectroscopy. After the reaction was completed, the polymer was dissolved in a minimal amount of ethyl acetate (*ca.* 125 mL). This solution was precipitated in a large excess of ice-cold methanol (500 mL). The precipitated polymer was collected in a PTFE-lined Petri dish and dried in a vacuum oven at 80 °C. The precipitation was repeated until all residual monomer, observed by ^{1}H NMR spectroscopy, was removed.

Yield: 45.207 g (5.382 mmol, 86%)

SEC ($CHCl_3$): M_n = 8.4 kg.mol^{-1}, M_w = 16.5 kg.mol^{-1}, $Đ_M$ = 1.95

^{1}H-NMR (400 MHz, 298 K, $CDCl_3$): δ (ppm) = 0.81 – 0.95 (m, 6H, CH_2 – C*H*$_3$), 1.02 (s, 6H, C*H*$_3$ – C), 1.23 – 1.46 (m, 12H, C*H*$_2$), 1.54 (m, 1H, C*H* – $(CH_2)_3$), 3.83 (m, 2H, O – C*H*$_2$ – CH), 4.15 (m, 2H, O – C*H*$_2$ – CH_2), 4.32 (m, 2H, O – CH_2 – C*H*$_2$)

^{13}C-NMR (400 MHz, 298 K, $CDCl_3$, DEPT): δ (ppm) = 177.8 (C_q= O), 67.0 (*C*H – OCOR), 60.7 (*C*H_2 – O), 44.9 (C_q – *C*H_2 – C_q), 38.4 (*C*H_3 – C_q), 30.4 (CH_2 – *C*H2 –CH), 29.0 (CH_3 – *C*H_2 – CH), 23.9 (CH_2 – *C*H_2 – CH_2), 22.9 (CH_3 – *C*H_2 – CH_2), 14.1 (*C*H_3 – CH_2 – CH_2), 11.0 (*C*H_3 – CH_2 – CH)

ATR-FTIR: ν_{MAX} = 3600-3400*w* (O-H), 2958-2861*m* (C-H), 1725*s* (C=O), 1463*m* (C-H), 1381*m* (C-H), 1239*m* (C-O), 1176*m* (C-O), 1151*s* (C-O), 1061*w* (C-O) cm^{-1}.

7.5.5 Synthesis of **40HEMA2**

Azobisisobutyronitrile (AIBN) (13.7 mg, 0.083 mmol), 1-dodecanethiol (DDM) (0.169 g, 0.834 mmol), 1,3,5-trioxane (204.4 mg, 2.269 mmol) as an internal NMR standard and 2-hydroxyethyl methacrylate (HEMA) (1.205 g, 9.258 mmol) were dissolved in 2-ethylhexyl methacrylate (EHMA) (90.000, 453.835 mmol) in a two-neck round bottom flask. The flask was equipped with a septum and a mechanical stirrer. The reaction mixture was purged with N_2 for 30 minutes. The flask was placed in an oil bath at 80 °C and stirred for 4.0 hours. The conversion was monitored *via* ^{1}H NMR spectroscopy. After the reaction was completed, the polymer was dissolved in a minimal amount of ethyl acetate (*ca.* 125 mL). This solution was precipitated in a large excess of ice-cold ethanol (500 mL). The precipitated polymer was collected in a PTFE-lined Petri dish and dried in a vacuum oven at 80 °C. The precipitation was repeated until all residual monomer, observed by ^{1}H NMR spectroscopy, was removed.

Yield: 61.107 g (0.942 mmol, 67%)

SEC ($CHCl_3$): M_n = 64.9 kg.mol^{-1}, M_w = 122.6 kg.mol^{-1}, $Đ_M$ = 1.89

^{1}H-NMR (400 MHz, 298 K, $CDCl_3$): δ (ppm) = 0.81 – 0.95 (m, 6H, $CH_2 - CH_3$), 1.02 (s, 6H, $CH_3 - C$), 1.23 – 1.46 (m, 12H, CH_2), 1.54 (m, 1H, $CH - (CH_2)_3$), 3.83 (m, 2H, $O - CH_2 - CH$), 4.15 (m, 2H, $O - CH_2 - CH_2$), 4.32 (m, 2H, $O - CH_2 - CH_2$)

^{13}C-NMR (400 MHz, 298 K, $CDCl_3$, DEPT): δ (ppm) = 177.8 (C_q= O), 67.0 ($CH - OCOR$), 60.7 ($CH_2 - O$), 44.9 ($C_q - CH_2 - C_q$), 38.4 ($CH_3 - C_q$), 30.4 ($CH_2 - CH2 - CH$), 29.0 ($CH_3 - CH_2 - CH$), 23.9 ($CH_2 - CH_2 - CH_2$), 22.9 ($CH_3 - CH_2 - CH_2$), 14.1 ($CH_3 - CH_2 - CH_2$), 11.0 ($CH_3 - CH_2 - CH$)

ATR-FTIR: ν_{MAX} = 3600-3400*w* (O-H), 2958-2861*m* (C-H), 1725*s* (C=O), 1463*m* (C-H), 1381*m* (C-H), 1239*m* (C-O), 1176*m* (C-O), 1151*s* (C-O), 1061*w* (C-O) cm^{-1}.

7.5.6 Synthesis of **40HEMA5**

Azobisisobutyronitrile (AIBN) (13.7 mg, 0.083 mmol), 1-dodecanethiol (DDM) (0.169 g, 0.834 mmol), 1,3,5-trioxane (204.4 mg, 2.269 mmol) as an internal NMR standard and 2-hydroxyethyl methacrylate (HEMA) (3.107 g, 23.872 mmol) were dissolved in 2-ethylhexyl methacrylate (EHMA) (90.000, 453.835 mmol) in a two-neck round bottom flask. The flask was equipped with a septum and a mechanical stirrer. The reaction mixture was purged with N_2 for 30 minutes. The flask was placed in an oil bath at 80 °C and stirred for 4.0 hours. The conversion was monitored *via* ^{1}H NMR spectroscopy. After the reaction was completed, the polymer was dissolved in a minimal amount of ethyl acetate (*ca.* 125 mL). This solution was precipitated in a large excess of ice-cold ethanol (500 mL). The precipitated polymer was collected in a PTFE-lined Petri dish and dried in a vacuum oven at 80 °C. The precipitation was repeated until all residual monomer, observed by ^{1}H NMR spectroscopy, was removed.

Yield: 56.888 g (1.470 mmol, 61%)

SEC ($CHCl_3$): M_n = 38.7 kg.mol^{-1}, M_w = 84.4 kg.mol^{-1}, $Đ_M$ = 2.18

^{1}H-NMR (400 MHz, 298 K, $CDCl_3$): δ (ppm) = 0.81 – 0.95 (m, 6H, $CH_2 - CH_3$), 1.02 (s, 6H, $CH_3 - C$), 1.23 – 1.46 (m, 12H, CH_2), 1.54 (m, 1H, $CH - (CH_2)_3$), 3.83 (m, 2H, $O - CH_2 - CH$), 4.15 (m, 2H, $O - CH_2 - CH_2$), 4.32 (m, 2H, $O - CH_2 - CH_2$)

^{13}C-NMR (400 MHz, 298 K, $CDCl_3$, DEPT): δ (ppm) = 177.8 (C_q= O), 67.0 ($CH - OCOR$), 60.7 ($CH_2 - O$), 44.9 ($C_q - CH_2 - C_q$), 38.4 ($CH_3 - C_q$), 30.4 ($CH_2 - CH2 - CH$), 29.0 ($CH_3 - CH_2 - CH$), 23.9 ($CH_2 - CH_2 - CH_2$), 22.9 ($CH_3 - CH_2 - CH_2$), 14.1 ($CH_3 - CH_2 - CH_2$), 11.0 ($CH_3 - CH_2 - CH$)

ATR-FTIR: ν_{MAX} = 3600-3400*w* (O-H), 2958-2861*m* (C-H), 1725*s* (C=O), 1463*m* (C-H), 1381*m* (C-H), 1239*m* (C-O), 1176*m* (C-O), 1151*s* (C-O), 1061*w* (C-O) cm^{-1}.

7.5.7 Synthesis of **40HEMA10**

Azobisisobutyronitrile (AIBN) (27.4 mg, 0.167 mmol), 1-dodecanethiol (DDM) (0.338 g, 1.668 mmol), 1,3,5-trioxane (102.2 mg, 1.135 mmol) as an internal NMR standard and 2-hydroxyethyl methacrylate (HEMA) (6.497 g, 49.922 mmol) were dissolved in 2-ethylhexyl methacrylate (EHMA) (90.000, 453.835 mmol) in a two-neck round bottom flask. The flask was equipped with a septum and a mechanical stirrer. The reaction mixture was purged with N_2 for 30 minutes. The flask was placed in an oil bath at 80 °C and stirred for 3.5 hours. The conversion was monitored *via* ^{1}H NMR spectroscopy. After the reaction was completed, the polymer was dissolved in a minimal amount of ethyl acetate (*ca.* 125 mL). This solution was precipitated in a large excess of ice-cold ethanol (500 mL). The precipitated polymer was collected in a PTFE-lined Petri dish and dried in a vacuum oven at 80 °C. The precipitation was repeated until all residual monomer, observed by ^{1}H NMR spectroscopy, was removed.

Yield: 74.785 g (1.963 mmol, 76%)

SEC ($CHCl_3$): M_n = 38.1 kg.mol^{-1}, M_w = 69.7 kg.mol^{-1}, $Đ_M$ = 1.83

^{1}H-NMR (400 MHz, 298 K, $CDCl_3$): δ (ppm) = 0.81 – 0.95 (m, 6H, $CH_2 - CH_3$), 1.02 (s, 6H, $CH_3 - C$), 1.23 – 1.46 (m, 12H, CH_2), 1.54 (m, 1H, $CH - (CH_2)_3$), 3.83 (m, 2H, $O - CH_2 - CH$), 4.15 (m, 2H, $O - CH_2 - CH_2$), 4.32 (m, 2H, $O - CH_2 - CH_2$)

^{13}C-NMR (400 MHz, 298 K, $CDCl_3$, DEPT): δ (ppm) = 177.8 (C_q= O), 67.0 ($CH - OCOR$), 60.7 ($CH_2 - O$), 44.9 ($C_q - CH_2 - C_q$), 38.4 ($CH_3 - C_q$), 30.4 ($CH_2 - CH2 - CH$), 29.0 ($CH_3 - CH_2 - CH$), 23.9 ($CH_2 - CH_2 - CH_2$), 22.9 ($CH_3 - CH_2 - CH_2$), 14.1 ($CH_3 - CH_2 - CH_2$), 11.0 ($CH_3 - CH_2 - CH$)

ATR-FTIR: ν_{MAX} = 3600-3400*w* (O-H), 2958-2861*m* (C-H), 1725*s* (C=O), 1463*m* (C-H), 1381*m* (C-H), 1239*m* (C-O), 1176*m* (C-O), 1151*s* (C-O), 1061*w* (C-O) cm^{-1}.

7.5.8 Synthesis of **40HEMA20**

Azobisisobutyronitrile (AIBN) (233.3 mg, 1.421 mmol), 1-dodecanethiol (DDM) (0.144 g, 0.710 mmol), 1,3,5-trioxane (122.6 mg, 1.362 mmol) as an internal NMR standard and 2-hydroxyethyl methacrylate (HEMA) (14.766 g, 113.460 mmol) were dissolved in 2-ethylhexyl methacrylate (EHMA) (90.000, 453.835 mmol) in a two-neck round bottom flask. The flask was equipped with a septum and a mechanical stirrer. The reaction mixture was purged with N_2 for 30 minutes. The flask was placed in an oil bath at 70 °C and stirred for 1.0 hours. The conversion was monitored *via* ^{1}H NMR spectroscopy. After the reaction was completed, the polymer was dissolved in a minimal amount of ethyl acetate (*ca.* 125 mL). This solution was precipitated in a large excess of ice-cold methanol (500 mL). The precipitated polymer was collected in a PTFE-lined Petri dish and dried in a vacuum oven at 80 °C. The precipitation was repeated until all residual monomer, observed by ^{1}H NMR spectroscopy, was removed.

Yield: 75.641 g (1.579 mmol, 72%)

SEC ($CHCl_3$): M_n = 47.9 kg.mol^{-1}, M_w = 116.7 kg.mol^{-1}, $Đ_M$ = 2.44

^{1}H-NMR (400 MHz, 298 K, $CDCl_3$): δ (ppm) = 0.81 – 0.95 (m, 6H, $CH_2 - CH_3$), 1.02 (s, 6H, $CH_3 - C$), 1.23 – 1.46 (m, 12H, CH_2), 1.54 (m, 1H, $CH - (CH_2)_3$), 3.83 (m, 2H, $O - CH_2 - CH$), 4.15 (m, 2H, $O - CH_2 - CH_2$), 4.32 (m, 2H, $O - CH_2 - CH_2$)

^{13}C-NMR (400 MHz, 298 K, $CDCl_3$, DEPT): δ (ppm) = 177.8 (C_q= O), 67.0 ($CH - OCOR$), 60.7 ($CH_2 - O$), 44.9 ($C_q - CH_2 - C_q$), 38.4 ($CH_3 - C_q$), 30.4 ($CH_2 - CH2 - CH$), 29.0 ($CH_3 - CH_2 - CH$), 23.9 ($CH_2 - CH_2 - CH_2$), 22.9 ($CH_3 - CH_2 - CH_2$), 14.1 ($CH_3 - CH_2 - CH_2$), 11.0 ($CH_3 - CH_2 - CH$)

ATR-FTIR: ν_{MAX} = 3600-3400*w* (O-H), 2958-2861*m* (C-H), 1725*s* (C=O), 1463*m* (C-H), 1381*m* (C-H), 1239*m* (C-O), 1176*m* (C-O), 1151*s* (C-O), 1061*w* (C-O) cm^{-1}.

7.6 General synthesis of poly(EHMA-*co*-META)

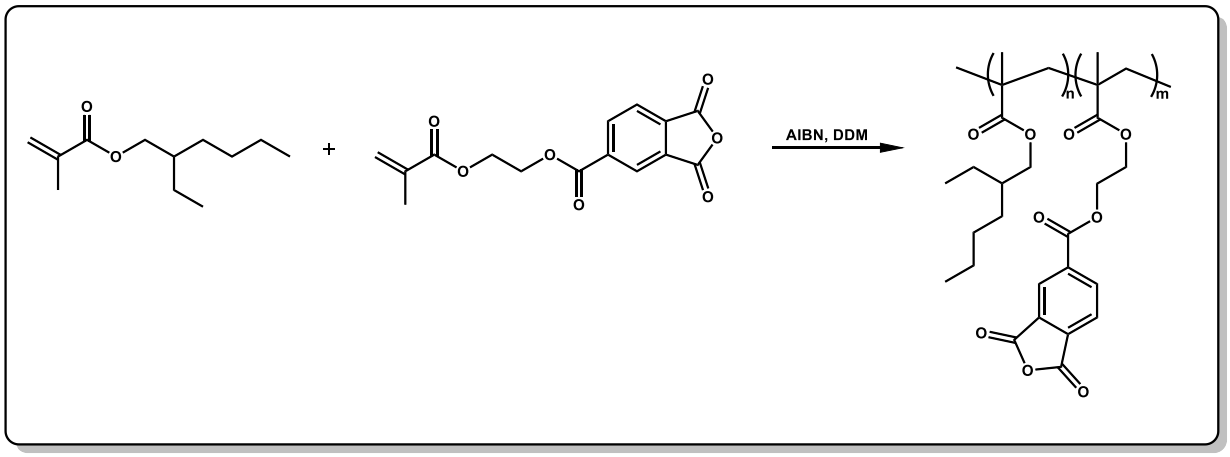

7.6.1 Synthesis of **10META5**

Azobisisobutyronitrile (AIBN) (11.7 mg, 0.071 mmol), 1-dodecanethiol (DDM) (143.8 mg, 0.710 mmol), 1,3,5-trioxane (61.3 mg, 0.681 mmol) as an internal NMR standard and 4-methacryloxyethyl trimellitic anhydride (META) (3.632 g, 11.936 mmol) were dissolved in 2-ethylhexyl methacrylate (EHMA) (45.000 g, 226.918 mmol) and 1,4-dioxane (20 mL, 233.799 mmol) in a two-neck round bottom flask. The flask was equipped with a septum and a mechanical stirrer. The reaction mixture was purged with N_2 for 30 minutes. The flask was placed in an oil bath at 70 °C and stirred for 6.0 hours. The conversion was monitored *via* ^{1}H NMR spectroscopy. After the reaction was completed, the polymer was dissolved in a minimal amount of THF (*ca.* 50 mL). This solution was precipitated in a large excess of ice-cold ethanol (300 mL). The precipitated polymer was collected in a PTFE-lined Petri dish and dried in a vacuum oven at 80 °C. The precipitation was repeated until all residual monomer, observed by ^{1}H NMR spectroscopy, was removed.

Yield: 42.358 g (4.555 mmol, 87%)

SEC ($CHCl_3$): M_n = 9.3 kg.mol^{-1}, M_w = 16.3 kg.mol^{-1}, $Đ_M$ = 1.76

^{1}H-NMR (400 MHz, 298 K, $CDCl_3$): δ (ppm) = 0.81 – 0.95 (m, 6H, CH_2 – CH_3), 1.02 (s, 6H, CH_3 – C), 1.23 – 1.46 (m, 12H, CH_2), 1.54 (m, 1H, CH – $(CH_2)_3$), 3.83 (m, 2H, O – CH_2 – CH), 4.15 (m, 2H, O – CH_2 – CH_2), 4.32 (m, 2H, O – CH_2 – CH_2), 8.23 – 8.73 (m, 3H, ArH)

^{13}C-NMR (400 MHz, 298 K, $CDCl_3$, DEPT): δ (ppm) = 177.8 (C_q= O), 164.7 (C_q= O), 125.2 (*C*H, Ar.), 67.0 (*C*H – OCOR), 60.7 (*C*H_2 – O), 44.9 (C_q – *C*H_2 – C_q), 38.4 (*C*H_3 – C_q), 30.4 (CH_2 – *C*H2 –CH), 29.0 (CH_3 – *C*H_2 – CH), 23.9 (CH_2 – *C*H_2 – CH_2), 22.9 (CH_3 – *C*H_2 – CH_2), 14.1 (*C*H_3 – CH_2 – CH_2), 11.0 (*C*H_3 – CH_2 – CH)

ATR-FTIR: ν_{MAX} = 2958-2861*m* (C-H), 1841*w* (C=O), 1725*s* (C=O), 1463*m* (C-H), 1381*m* (C-H), 1239*m* (C-O), 1176*m* (C-O), 1151*s* (C-O), 1061*w* (C-O), 799*w* (C=C), 707*w* (C-H) cm^{-1}.

7.6.2 Synthesis of **10META10**

Azobisisobutyronitrile (AIBN) (19.4 mg, 0.118 mmol), 1-dodecanethiol (DDM) (12.0 mg, 0.590 mmol), 1,3,5-trioxane (20.4 mg, 0.227 mmol) as an internal NMR standard and 4-methacryloxyethyl trimellitic anhydride (META) (2.555 g, 8.396 mmol) were dissolved in 2-ethylhexyl methacrylate (EHMA) (15.000 g, 75.640 mmol) and 1,4-dioxane (12 mL, 140.279 mmol) in a two-neck round bottom flask. The flask was equipped with a septum and a mechanical stirrer. The reaction mixture was purged with N_2 for 30 minutes. The flask was placed in an oil bath at 70 °C and stirred for 4.5 hours. The conversion was monitored *via* ^{1}H NMR spectroscopy. After the reaction was completed, the polymer was dissolved in a minimal amount of THF (*ca.* 50 mL). This solution was precipitated in a large excess of ice-cold ethanol (300 mL). The precipitated polymer was collected in a PTFE-lined Petri dish and dried in a vacuum oven at 80 °C. The precipitation was repeated until all residual monomer, observed by ^{1}H NMR spectroscopy, was removed.

Yield: 14.342 g (1.129 mmol, 82%)

SEC ($CHCl_3$): M_n = 12.7 kg.mol^{-1}, M_w = 19.4 kg.mol^{-1}, $Đ_M$ = 1.53

^{1}H-NMR (400 MHz, 298 K, $CDCl_3$): δ (ppm) = 0.81 – 0.95 (m, 6H, CH_2 – CH_3), 1.02 (s, 6H, CH_3 – C), 1.23 – 1.46 (m, 12H, CH_2), 1.54 (m, 1H, CH – $(CH_2)_3$), 3.83 (m, 2H, O – CH_2 – CH), 4.15 (m, 2H, O – CH_2 – CH_2), 4.32 (m, 2H, O – CH_2 – CH_2), 8.23 – 8.73 (m, 3H, ArH)

^{13}C-NMR (400 MHz, 298 K, $CDCl_3$, DEPT): δ (ppm) = 177.8 (C_q= O), 164.7 (C_q= O), 125.2 (*C*H, Ar.), 67.0 (*C*H – OCOR), 60.7 (*C*H_2 – O), 44.9 (C_q – *C*H_2 – C_q), 38.4 (*C*H_3 – C_q), 30.4 (CH_2 – *C*H2 –CH), 29.0 (CH_3 – *C*H_2 – CH), 23.9 (CH_2 – *C*H_2 – CH_2), 22.9 (CH_3 – *C*H_2 – CH_2), 14.1 (*C*H_3 – CH_2 – CH_2), 11.0 (*C*H_3 – CH_2 – CH)

ATR-FTIR: ν_{MAX} = 2958-2861*m* (C-H), 1841*w* (C=O), 1725*s* (C=O), 1463*m* (C-H), 1381*m* (C-H), 1239*m* (C-O), 1176*m* (C-O), 1151*s* (C-O), 1061*w* (C-O), 799*w* (C=C), 707*w* (C-H) cm^{-1}.

7.6.3 Synthesis of **40META5**

Azobisisobutyronitrile (AIBN) (19.4 mg, 0.118 mmol), 1-dodecanethiol (DDM) (12.0 mg, 0.590 mmol), 1,3,5-trioxane (20.4 mg, 0.227 mmol) as an internal NMR standard and 4-methacryloxyethyl trimellitic anhydride (META) (1.211 g, 3.979 mmol) were dissolved in 2-ethylhexyl methacrylate (EHMA) (15.000 g, 75.640 mmol) and 1,4-dioxane (7 mL, 81.830 mmol) in a two-neck round bottom flask. The flask was equipped with a septum and a mechanical stirrer. The reaction mixture was purged with N_2 for 30 minutes. The flask was placed in an oil bath at 70 °C and stirred for 3.0 hours. The conversion was monitored *via* ^{1}H NMR spectroscopy. After the reaction was completed, the polymer was dissolved in a minimal amount of THF (*ca.* 50 mL). This solution was precipitated in a large excess of ice-cold ethanol (300 mL). The precipitated polymer was collected in a PTFE-lined Petri dish and dried in a vacuum oven at 80 °C. The precipitation was repeated until all residual monomer, observed by ^{1}H NMR spectroscopy, was removed.

Yield: 12.953 g (0.320 mmol, 80%)

SEC ($CHCl_3$): M_n = 40.5 kg.mol^{-1}, M_w = 99.3 kg.mol^{-1}, $Đ_M$ = 2.46

^{1}H-NMR (400 MHz, 298 K, $CDCl_3$): δ (ppm) = 0.81 – 0.95 (m, 6H, CH_2 – C*H*$_3$), 1.02 (s, 6H, C*H*$_3$ – C), 1.23 – 1.46 (m, 12H, C*H*$_2$), 1.54 (m, 1H, C*H* – $(CH_2)_3$), 3.83 (m, 2H, O – C*H*$_2$ – CH), 4.15 (m, 2H, O – C*H*$_2$ – CH_2), 4.32 (m, 2H, O – CH_2 – C*H*$_2$), 8.23 – 8.73 (m, 3H, Ar*H*)

^{13}C-NMR (400 MHz, 298 K, $CDCl_3$, DEPT): δ (ppm) = 177.8 (C_q= O), 164.7 (C_q= O), 125.2 (*C*H, Ar.), 67.0 (*C*H – OCOR), 60.7 (*C*H_2 – O), 44.9 (C_q – *C*H_2 – C_q), 38.4 (*C*H_3 – C_q), 30.4 (CH_2 – *C*H2 –CH), 29.0 (CH_3 – *C*H_2 – CH), 23.9 (CH_2 – *C*H_2 – CH_2), 22.9 (CH_3 – *C*H_2 – CH_2), 14.1 (*C*H_3 – CH_2 – CH_2), 11.0 (*C*H_3 – CH_2 – CH)

ATR-FTIR: ν_{MAX} = 2958-2861*m* (C-H), 1841*w* (C=O), 1725*s* (C=O), 1463*m* (C-H), 1381*m* (C-H), 1239*m* (C-O), 1176*m* (C-O), 1151*s* (C-O), 1061*w* (C-O), 799*w* (C=C), 707*w* (C-H) cm^{-1}.

7.7 Cross-linking of poly(EHMA-*co*-FMA) with bismaleimides

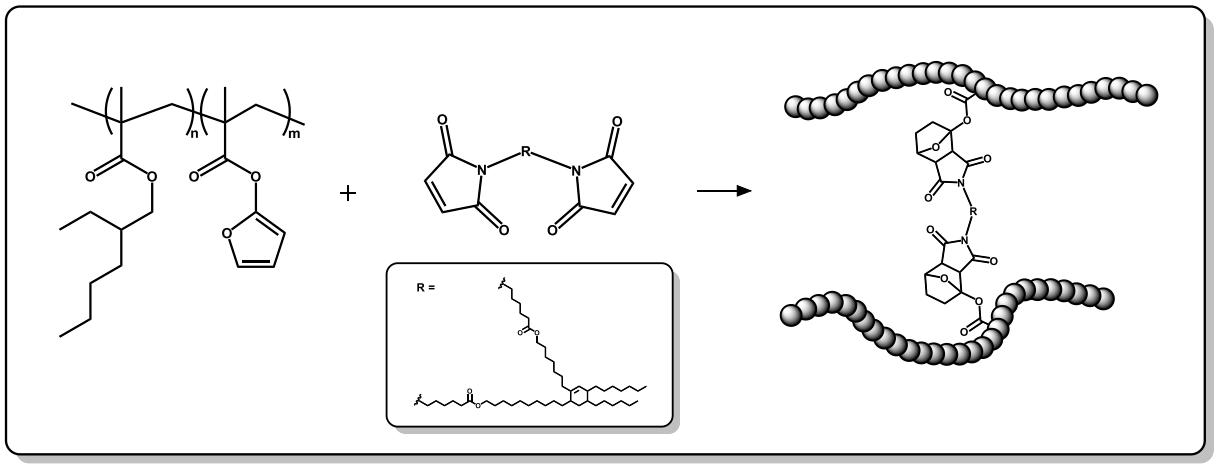

Poly(EHMA-*co*-FMA) was dissolved in a minimal amount of THF (35 mL) and **BMI2** was dissolved in 8 mL of THF and added to the copolymer solution (*Table 47*). The mixture was vigorously shaken for 30 seconds and poured onto a PTFE-lined Petri dish. The solvent was evaporated at ambient temperature for 1 hour and the residual solvent was evaporated overnight in a vacuum oven at 80 °C.

ATR-FTIR: ν_{MAX} = 2957-2859*m* (C-H), 1726*s* (C=O), 1463*m* (C-H), 1380*m* (C-H), 1239*m* (C-N), 1175*m* (C-O), 1150*s* (C-O), 1062*w* (C-O), 967*w* (C=C) cm^{-1}.

Table 47: Amount of BMI2 used in the cross-linking of poly(EHMA-co-FMA)

	Poly(EHMA-*co*-FMA)		**BMI2**	
	g	**mmol**	**g**	**mmol**
10FMA5-BMI2	**10**	**1.020**	**1.198**	**1.300**
10FMA10-BMI2	**10**	**0.943**	**2.384**	**2.587**
10FMA20-BMI2	**10**	**0.787**	**4.706**	**5.108**
40FMA5-BMI2	**10**	**0.223**	**1.259**	**1.366**
40FMA10-BMI2	**10**	**0.262**	**2.338**	**2.538**
40FMA20-BMI2	**10**	**0.248**	**5.325**	**5.779**

7.8 Cross-linking of poly(EHMA-*co*-AEMA) with diamines

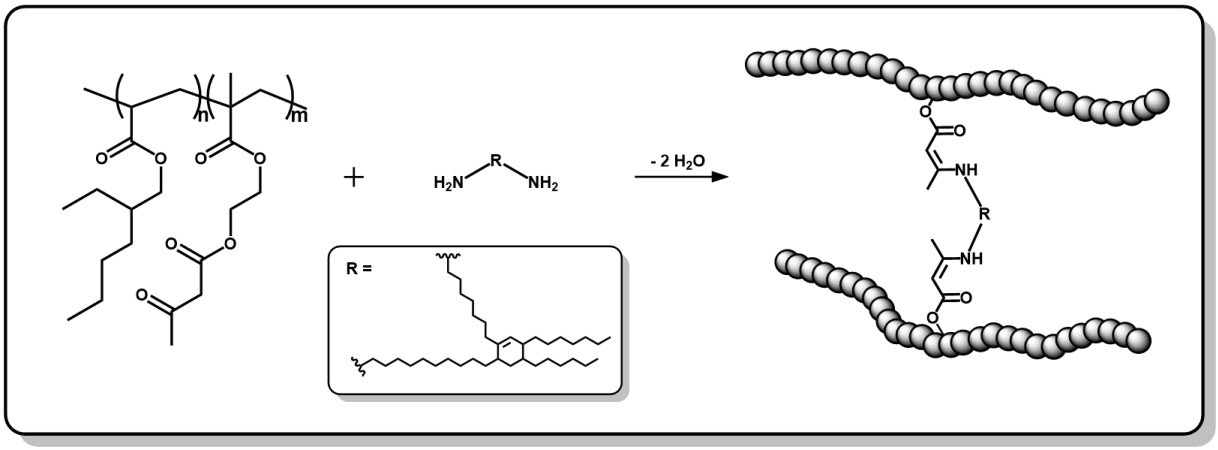

Poly(EHMA-*co*-AEMA) was dissolved in a minimal amount of ethyl acetate (35 mL), **DAM2** was dissolved in 8 mL of ethyl acetate and added to the copolymer solution (*Table 48*). The mixture was vigorously shaken for 30 seconds and poured onto a PTFE-lined Petri dish. The solvent was evaporated at ambient temperature for 1 hour and the residual solvent was evaporated overnight in a vacuum oven at 80 °C.

ATR-FTIR: ν_{MAX} = 3400-3300*w* (*br.*, free N-H), 2957-2859*m* (C-H), 1726*s* (C=O), 1656*s* (NR_2-H), 1608*s* (C=C), 1463*m* (C-N), 1380*m* (C-N), 1239*m* (C-O), 1150*s* (C-O) cm^{-1}.

Table 48: Amount of DAM2 used in the cross-linking of poly(EHMA-co-AEMA)

	Poly(EHMA-*co*-AEMA)		**DAM2**	
	g	**mmol**	**g**	**mmol**
10AEMA5-DAM2	**10**	**0.952**	**0.705**	**1.288**
10AEMA10-DAM2	**10**	**0.885**	**1.869**	**3.414**
10AEMA20-DAM2	**10**	**0.99**	**3.6**	**6.575**
40AEMA5-DAM2	**10**	**0.256**	**0.753**	**1.375**
40AEMA10-DAM2	**10**	**0.228**	**2.112**	**3.858**
40AEMA20-DAM2	**10**	**0.146**	**4.133**	**7.549**

7.9 Synthesis of **DAH2**

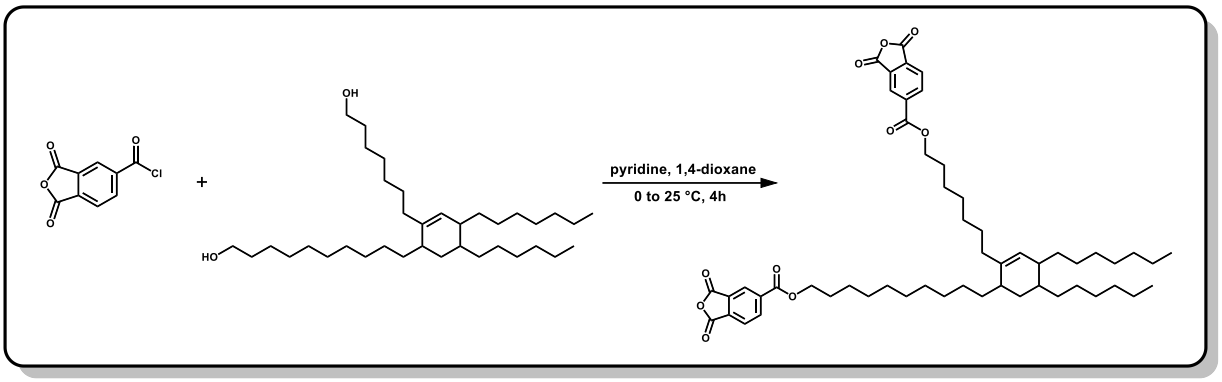

In a two-neck 500 mL round bottom flask, trimellitic anhydride chloride (15.041 g, 71.4 mmol) was dissolved in 200 mL of dry 1,4-dioxane. The mixture was cooled to 0 °C and placed under nitrogen. Pripol™ 2033 (20.000 g, 35.7 mmol) was dissolved in 100 mL of dry 1,4-dioxane together with 5.75 mL of dry pyridine (5.650 g, 71.4 mmol). This alcohol solution was dropwise added to the cooled acid chloride. The mixture was stirred at 0 °C for 2 hours, slowly heated to room temperature and stirred for an additional 2 hours. The mixture was filtrated to remove the formed pyridine salts and concentrated in a vacuum oven at 80 °C to obtain **DAH2**, which was used without further purification.

Yield: 28.272 g yellow viscous oil (31.1 mmol, 87%).

MW: 908.24 g.mol^{-1}

^{1}H NMR (400 MHz, 298 K, $CDCl_3$): δ (ppm) = 0.74 – 0.97 (m, 6H, $CH_2 - CH_3$), 0.98 – 1.37 (m, 60H, -CH_2-), 1.54 (m, 4H, -C*H*-), 4.41 (t, 4H, O – CH_2), 8.11 (m, 2H, Ar*H*), 8.57 (m, 2H, Ar*H*), 8.64 (m, 2H Ar*H*).

ATR-FTIR: ν_{MAX} = 2920-2852*m* (C-H), 1841*m* (C=O), 1726*s* (C=O), 1463*m* (C-H), 1377*m* (C-H), 1072*w* (C-O), 793*w* (C=C), 722*w* (C-H) cm^{-1}.

7.10 Cross-linking of poly(EHMA-*co*-HEMA) with phthalic dianhydrides

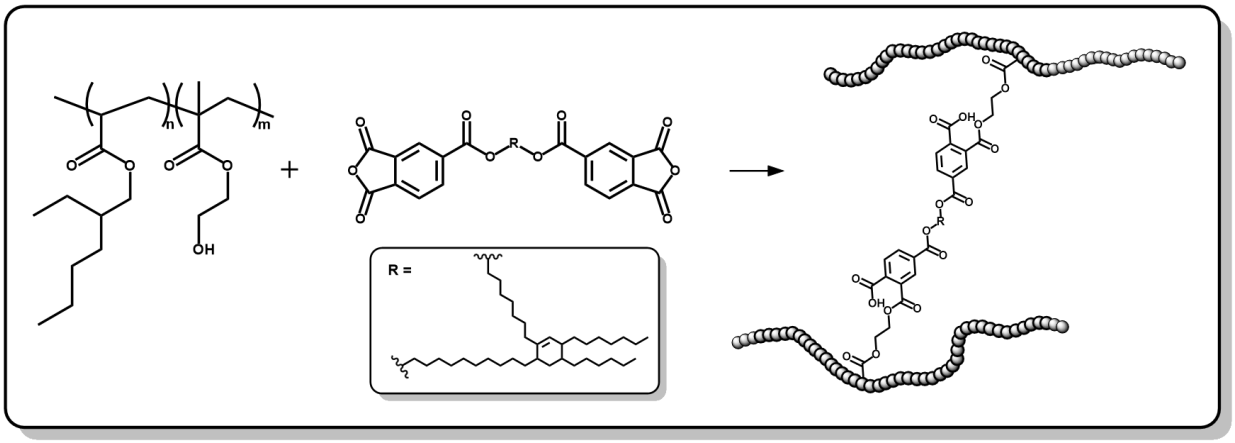

Poly(EHMA-*co*-HEMA) was dissolved in a minimal amount of THF (35 mL) and **DAH2** was dissolved in 8 mL of THF and added to the copolymer solution (*Table 49*). The mixture was vigorously shaken for 30 seconds and poured onto a PTFE-lined Petri dish. The solvent was evaporated at ambient temperature for 1 hour and the residual solvent was evaporated overnight in a vacuum oven at 80 °C.

ATR-FTIR: ν_{MAX} = 3550-3200*w* (*br.*, free O-H), 2957-2859*m* (C-H), 1841*w* (C=O), 1726*s* (C=O), 1463*m* (C-H), 1380*m* (C-H), 1239*m* (C-O), 1150*s* (C-O), 1062*w* (C-O), 799*w* (C=C), 707*w* (C-H) cm^{-1}.

Table 49: Amount of DAH2 used in the cross-linking of poly(EHMA-co-HEMA)

	Poly(EHMA-*co*-HEMA)		**DAH2**	
	g	**mmol**	**g**	**mmol**
10HEMA5-DAH2	**10**	**0.877**	**1.512**	**1.665**
10HEMA10-DAH2	**10**	**1.053**	**2.307**	**2.540**
10HEMA20-DAH2	**10**	**1.190**	**3.946**	**4.345**
40HEMA5-DAH2	**10**	**0.258**	**1.261**	**1.389**
40HEMA10-DAH2	**10**	**0.262**	**2.422**	**2.667**
40HEMA20-DAH2	**10**	**0.209**	**4.124**	**4.540**

7.11 Cross-linking of poly(EHMA-*co*-META) with diols

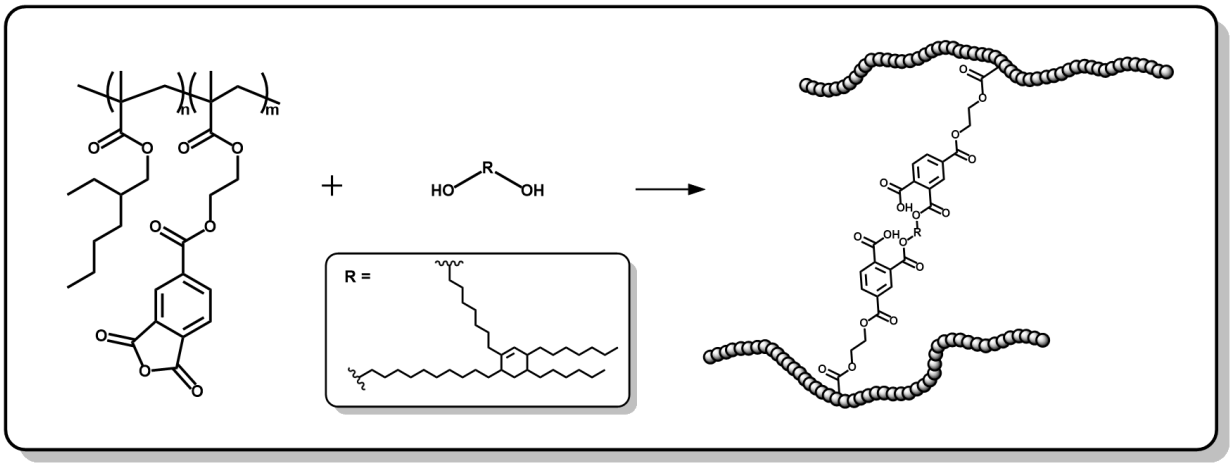

Poly(EHMA-*co*-META) was dissolved in a minimal amount of THF (35 mL) and **POL** was dissolved in 8 mL of THF and added to the copolymer solution (*Table 50*). The mixture was vigorously shaken for 30 seconds and poured onto a PTFE-lined Petri dish. The solvent was evaporated at ambient temperature for 1 hour and the residual solvent was evaporated overnight in a vacuum oven at 80 °C.

ATR-FTIR: ν_{MAX} = 3550-3200*w* (*br.*, free O-H), 2957-2859*m* (C-H), 1841*w* (C=O), 1726*s* (C=O), 1463*m* (C-H), 1380*m* (C-H), 1239*m* (C-O), 1150*s* (C-O), 1062*w* (C-O), 799*w* (C=C), 707*w* (C-H) cm^{-1}.

Table 50: Amount of POL used in the cross-linking of poly(EHMA-co-META)

	Poly(EHMA-*co*-META)		**POL**	
	g	**mmol**	**g**	**mmol**
10META5-POL	**5**	**0.538**	**0.408**	**0.729**
10META10-POL	**5**	**0.394**	**0.676**	**1.207**
40META5-POL	**5**	**0.123**	**0.408**	**0.729**

7.12 Solubility experiments

This Soxhlet extraction method involves weighing samples (m_0) and exposing them to a refluxing solvent in an extractor chamber for a prolonged period of time (usually 24 hours). During this time, the solvent with possible solutes drains after reaching a certain level starting a new cycle where fresh solvent is introduced into the extractor chamber. After extraction, the wet samples are weighed (m_{sw}) and a degree of swelling can be calculated using *Equation 9*. Next, the samples are dried in a vacuum oven at 80 °C and weighed again (m_{dry}). The soluble fraction can then be calculated using *Equation 8*.

$$Soluble\ fraction = \frac{m_0 - m_{dry}}{m_0}\ x\ 100\% \qquad (8)$$

$$Degree\ of\ swelling = \frac{m_{sw} - m_0}{m_0}\ x\ 100\% \qquad (9)$$

Furthermore, the gel fraction can be calculated by subtracting the soluble fraction from 100%. The lower the soluble fraction, the lower the number of solutes extracted from the network, the higher the extent of the network formation and integrity.

7.13 Functionality

The number of functional groups per chain (functionality) can be calculated be using *Equation 10*.

$$Functionality = \left(\frac{M_{\mathrm{n}}}{M_{unit}}\right) x\ F_{\%com.} \qquad (10)$$

With M_{n} as the number average molecular weight of the copolymer determined by SEC, M_{unit} as the average molecular weight of a repeating unit of the polymer (calculated using the molar feed ratios of the comonomers) and $F_{\%\mathrm{com.}}$ as the molar concentration of the incorporated functional comonomer in the product copolymer, which was determined by ^{1}H NMR spectroscopy.

References

1. W. Abdallah, J. S. Buckley, A. Carnegie, J. Edwards, B. Herold, E. Fordham, A. Graue, T. Habashy, N. Seleznev and C. Signer, *Technology*, 1986, **38**, 268.
2. W.-S. Kim, I.-H. Yun, J.-J. Lee and H.-T. Jung, *International Journal of Adhesion and Adhesives*, 2010, **30**, 408-417.
3. H. W. Engels, H. G. Pirkl, R. Albers, R. W. Albach, J. Krause, A. Hoffmann, H. Casselmann and J. Dormish, *Angewandte Chemie International Edition*, 2013, **52**, 9422-9441.
4. N. Saba, M. Jawaid, O. Y. Alothman, M. Paridah and A. Hassan, *Journal of Reinforced Plastics and Composites*, 2016, **35**, 447-470.
5. Y. Li and C. Wong, *Materials Science and Engineering: R: Reports*, 2006, **51**, 1-35.
6. L. A. Modesti, A. S. de Vargas and E. L. Schneider, *International Journal of Adhesion and Adhesives*, 2020, **101**, 102645.
7. A. Pizzi and K. L. Mittal, *Handbook of Adhesive Technology*, CRC Press, Boca Raton (Florida, USA), 2017, p. 415-441, 9781498736473.
8. Technavio, Global Structural Adhesives Market Projected to Grow to 7,862 Kilotons by 2021, https://www.businesswire.com/news/home/20170613006056/en/Global-Structural-Adhesives-Market-Projected-Grow-7862, accessed July 18th, 2019.
9. D. A. Dillard, *Advances in Structural Adhesive Bonding*, CRC Press, Boca Raton (Florida, USA), 2010, 9781439802175.

10. M. A. Droesbeke, R. Aksakal, A. Simula, J. M. Asua and F. E. Du Prez, *Progress in Polymer Science*, 2021, **117**, 101396.

11. M. Donkerwolcke, F. Burny and D. Muster, *Biomaterials*, 1998, **19**, 1461-1466.

12. H. S. Tan and W. R. Pfister, *Pharmaceutical Science & Technology Today*, 1999, **2**, 60-69.

13. A. Tutunchi, R. Kamali and A. Kianvash, *The Journal of Adhesion*, 2015, **91**, 663-676.

14. J. Del Real, Y. Ballesteros, R. Chamochin, J. Abenojar and L. Molisani, *The Journal of Adhesion*, 2011, **87**, 366-381.

15. M. D. Banea, *Reviews of Adhesion and Adhesives*, 2019, **7**, 33-50.

16. A. Santamaria, M. E. Muñoz, M. Fernandez and M. Landa, *Journal of Applied Polymer Science*, 2013, **129**, 1643-1652.

17. S. Salimi, T. S. Babra, G. S. Dines, S. W. Baskerville, W. Hayes and B. W. Greenland, *European Polymer Journal*, 2019, **121**, 109264-109271.

18. D. S. Morehouse Jr and R. J. Tetreault, *Expansible thermoplastic polymer particles containing volatile fluid foaming agent and method of foaming the same*, US3615972A, USA, 1971.

19. M. D. Banea, L. F. da Silva, R. D. Campilho and C. Sato, *The Journal of Adhesion*, 2014, **90**, 16-40.

20. H. Onusseit, *Resources, Conservation and Recycling*, 2006, **46**, 168-181.

21. L. O. Oyedele, M. Regan, J. von Meding, A. Ahmed, O. J. Ebohon and A. Elnokaly, *World Journal of Science, Technology and Sustainable Development*, 2013, **10**, 131-142.

22. S. O. Ajayi, L. O. Oyedele, O. O. Akinade, M. Bilal, H. A. Owolabi, H. A. Alaka and K. O. Kadiri, *Journal of Building Engineering*, 2016, **5**, 185-193.

23. R. Geyer, J. R. Jambeck and K. L. Law, *Science Advances*, 2017, **3**, 1700782-1700786.

24. M. Geissdoerfer, P. Savaget, N. M. P. Bocken and E. J. Hultink, *Journal of Cleaner Production*, 2017, **143**, 757-768.

25. L. K. Ncube, A. U. Ude, E. N. Ogunmuyiwa, R. Zulkifli and I. N. Beas, *Recycling*, 2021, **6**, 12.

26. A. L. Volynskii and N. F. Bakeev, *Solvent crazing of polymers*, Elsevier, Amsterdam (The Netherlands), 2012, vol. 13, 0444818480.

27. E. MacArthur, D. Waughray and M. Stuchtey, *The New Plastics Economy, Rethinking the Future of Plastics*, World Economic Forum, London (UK), 2016.

28. H. Dodiuk and S. H. Goodman, *Handbook of Thermoset Plastics*, William Andrew (Elsevier), Oxford (UK), 2013, 1455731099.

29. J. D. Smith, K. F. Schoch Jr and W.-F. A. Su, *Electrical insulation using liquid crystal thermoset epoxy resins*, US5904984A, USA, 1999.

30. F. Delrector, W. W. Blount and D. R. Leonard, *J. Coat. Technol.*, 1989, **61**, 31-37.

31. G. De Santis, *Polyurethane sealant-primer system*, US3779794A, USA, 1973.

32. S. T. Lin, S. Conjeevaram and D. J. Henderson, *Moldable bone-implant material*, US4645503A, USA, 1987.

33. C. Soutis, *Progress in Aerospace Sciences*, 2005, **41**, 143-151.

34. S. Ma and D. C. Webster, *Progress in Polymer Science*, 2018, **76**, 65-110.

35. W. H. Carothers, *Transactions of the Faraday Society*, 1936, **32**, 39-49.

36. W. H. Stockmayer, *The Journal of Chemical Physics*, 1943, **11**, 45-55.

37. P. J. Flory, *Journal of the American Chemical Society*, 1941, **63**, 3083-3090.

38. P. J. Flory, *Principles of Polymer Chemistry*, Cornell University Press, Ithaca (New York, USA), 1953, 0801401348.

39. A. N. Wilkinson and A. J. Ryan, *Polymer Processing and Structure Development*, Kluwer Academic Publishers, Dordrecht (The Netherlands), 1998, 0751403636.

40. G. Burnett and G. Duncan, *Macromolecular Chemistry and Physics*, 1962, **51**, 171-176.

41. G. Bristow, *Transactions of the Faraday Society*, 1958, **54**, 1064-1068.

42. K. Matyjaszewski and T. P. Davis, *Handbook of Radical Polymerization*, John Wiley & Sons, Hoboken (New Jersey, USA), 2002, 9780471392743.

43. P. Nesvadba, *Radical Polymerization in Industry*, John Wiley & Sons, Chichester (UK), 2012, 9781119953678.

44. N. Platzer, *Industrial & Engineering Chemistry*, 1970, **62**, 6-20.

45. M. P. McDaniel, *A Review of the Phillips Chromium Catalyst for Ethylene Polymerization*, John Wiley & Sons, Chichester (UK), 2018, 9781119242130

46. G. Odian, *Principles of Polymerization*, John Wiley & Sons, Hoboken (New Jersey, USA), 2004, 0471274003.

47. J. M. G. Cowie and V. Arrighi, *Polymers: Chemistry and Physics of Modern Materials*, CRC press, Boca Raton (Florida, USA), 2007, 1420009877.

48. A. Rudin and P. Choi, *The Elements of Polymer Science and Engineering*, Academic Press (Elsevier), Oxford (UK), 2012, 9780123821782.

49. J. P. Heuts, T. P. Davis and G. T. Russell, *Macromolecules*, 1999, **32**, 6019-6030.

50. Y. Kaneko, K. Sakai, A. Kikuchi, R. Yoshida, Y. Sakurai and T. Okano, *Macromolecules*, 1995, **28**, 7717-7723.

51. M. Kato, M. Kamigaito, M. Sawamoto and T. Higashimura, *Macromolecules*, 1995, **28**, 1721-1723.

52. K. Matyjaszewski, S. Gaynor and J.-S. Wang, *Macromolecules*, 1995, **28**, 2093-2095.

53. M. D. Saban, M. K. Georges, R. P. Veregin, G. K. Hamer and P. M. Kazmaier, *Macromolecules*, 1995, **28**, 7032-7034.

54. J. Chiefari, Y. Chong, F. Ercole, J. Krstina, J. Jeffery, T. P. Le, R. T. Mayadunne, G. F. Meijs, C. L. Moad and G. Moad, *Macromolecules*, 1998, **31**, 5559-5562.

55. C. J. Kloxin, T. F. Scott, B. J. Adzima and C. N. Bowman, *Macromolecules*, 2010, **43**, 2643-2653.

56. G. M. Scheutz, J. J. Lessard, M. B. Sims and B. S. Sumerlin, *Journal of the American Chemical Society*, 2019, **141**, 16181-16196.

57. W. Denissen, J. M. Winne and F. E. Du Prez, *Chem. Sci.*, 2016, **7**, 30-38.

58. H. Yang, K. Yu, X. Mu, X. Shi, Y. Wei, Y. Guo and H. J. Qi, *Soft Matter*, 2015, **11**, 6305-6317.

59. O. Diels and K. Alder, *Berichte der Deutschen Chemischen Gesellschaft*, 1929, **62**, 554-562.

60. G. Brieger and J. N. Bennett, *Chemical Reviews*, 1980, **80**, 63-97.

61. R. R. Schmidt, *Accounts of Chemical Research*, 1986, **19**, 250-259.

62. J. Clayden, N. Greeves and S. Warren, *Organic Chemistry*, Oxford University Press, Oxford (UK), 2012, 9780199270293.

63. A. Cohen and F. L. Warren, *Journal of the Chemical Society*, 1937, 1315-1320.

64. E. G. Mackay and M. S. Sherburn, *Synthesis*, 2015, **47**, 1-21.

65. Z.-K. Liu, J. Ågren and M. Hillert, *Fluid Phase Equilibria*, 1996, **121**, 167-177.

66. H. Durmaz, B. Colakoglu, U. Tunca and G. Hizal, *Journal of Polymer Science Part A: Polymer Chemistry*, 2006, **44**, 1667-1675.

67. B. Gacal, H. Durmaz, M. Tasdelen, G. Hizal, U. Tunca, Y. Yagci and A. Demirel, *Macromolecules*, 2006, **39**, 5330-5336.

68. T. D. Kim, J. Luo, J. W. Ka, S. Hau, Y. Tian, Z. Shi, N. M. Tucker, S. H. Jang, J. W. Kang and A. Y. Jen, *Advanced Materials*, 2006, **18**, 3038-3042.

69. Y. Chung, B. F. Duerr, T. A. McKelvey, P. Nanjappan and A. W. Czarnik, *The Journal of Organic Chemistry*, 1989, **54**, 1018-1032.

70. J. R. Jones, C. L. Liotta, D. M. Collard and D. A. Schiraldi, *Macromolecules*, 1999, **32**, 5786-5792.

71. X. Lei and J. A. Porco, *Organic Letters*, 2004, **6**, 795-798.

72. J. P. Kennedy and K. F. Castner, *Journal of Polymer Science: Polymer Chemistry Edition*, 1979, **17**, 2055-2070.

73. X. Chen and E. Ruckenstein, *Journal of Polymer Science Part A: Polymer Chemistry*, 2000, **38**, 1662-1672.

74. X. Chen and E. Ruckenstein, *Journal of Polymer Science Part A: Polymer Chemistry*, 2000, **38**, 4373-4384.

75. J. S. Park, H. S. Kim and H. T. Hahn, *Composites Science and Technology*, 2009, **69**, 1082-1087.

76. A. J. Inglis, L. Nebhani, O. Altintas, F. G. Schmidt and C. Barner-Kowollik, *Macromolecules*, 2010, **43**, 5515-5520.

77. A. Gandini and M. N. Belgacem, *Progress in Polymer Science*, 1997, **22**, 1203-1379.

78. J. M. Craven, *Cross-linked thermally reversible polymers produced from condensation polymers with pendant furan groups cross-linked with maleimides*, US3435003A, USA, 1969.

79. M. P. Stevens and A. D. Jenkins, *Journal of Polymer Science: Polymer Chemistry Edition*, 1979, **17**, 3675-3685.

80. Y. Chujo, K. Sada and T. Saegusa, *Macromolecules*, 1990, **23**, 2636-2641.

81. S. A. Canary and M. P. Stevens, *Journal of Polymer Science Part A: Polymer Chemistry*, 1992, **30**, 1755-1760.

82. C. Goussé, A. Gandini and P. Hodge, *Macromolecules*, 1998, **31**, 314-321.

83. E. Goiti, M. B. Huglin and J. M. Rego, *Polymer*, 2001, **42**, 10187-10193.

84. A. Gandini, *Progress in Polymer Science*, 2013, **38**, 1-29.

85. R. C. Boutelle and B. H. Northrop, *The Journal of Organic Chemistry*, 2011, **76**, 7994-8002.

86. Y. L. Liu and C. Y. Hsieh, *Journal of Polymer Science Part A: Polymer Chemistry*, 2006, **44**, 905-913.

87. M. Watanabe and N. Yoshie, *Polymer*, 2006, **47**, 4946-4952.

88. R. Gheneim, C. Perez-Berumen and A. Gandini, *Macromolecules*, 2002, **35**, 7246-7253.

89. A. A. Kavitha and N. K. Singha, *Macromolecular Chemistry and Physics*, 2007, **208**, 2569-2577.

90. C. Toncelli, D. C. De Reus, F. Picchioni and A. A. Broekhuis, *Macromolecular Chemistry and Physics*, 2012, **213**, 157-165.

91. N. B. Pramanik, G. B. Nando and N. K. Singha, *Polymer*, 2015, **69**, 349-356.

92. S. Das, S. Samitsu, Y. Nakamura, Y. Yamauchi, D. Payra, K. Kato and M. Naito, *Polymer Chemistry*, 2018, **9**, 5559-5565.

93. A. Gandini, *Green Chemistry*, 2011, **13**, 1061-1083.

94. L. Ye, S.-F. Zhang, Y.-C. Lin, J.-K. Min, L. Ma and T. Tang, *Chinese Journal of Polymer Science*, 2018, **36**, 1011-1018.

95. T. F. Scott, A. D. Schneider, W. D. Cook and C. N. Bowman, *Science*, 2005, **308**, 1615-1617.

96. R. Nicolay, J. Kamada, A. Van Wassen and K. Matyjaszewski, *Macromolecules*, 2010, **43**, 4355-4361.

97. Y. Amamoto, J. Kamada, H. Otsuka, A. Takahara and K. Matyjaszewski, *Angewandte Chemie*, 2011, **123**, 1698-1701.

98. Y. Amamoto, H. Otsuka, A. Takahara and K. Matyjaszewski, *Advanced Materials*, 2012, **24**, 3975-3980.

99. D. Montarnal, M. Capelot, F. Tournilhac and L. Leibler, *Science*, 2011, **334**, 965-968.

100. G. Urbain, Y. Bottinga and P. Richet, *Geochimica et Cosmochimica Acta*, 1982, **46**, 1061-1072.

101. J. I. Steinfeld, J. S. Francisco and W. L. Hase, *Chemical Kinetics and Dynamics*, Prentice Hall Inc., Upper Saddle River (New Jersey, USA), 1999, vol. 3, 0137371233.

102. T. Masuko and J. H. Magill, *Nihon Reoroji Gakkaishi*, 1988, **16**, 22-26.

103. M. L. Williams, R. F. Landel and J. D. Ferry, *Journal of the American Chemical Society*, 1955, **77**, 3701-3707.

104. C. A. Angell, *Science*, 1995, **267**, 1924-1935.

105. P. Richet, Y. Bottinga, L. Denielou, J. Petitet and C. Tequi, *Geochimica et Cosmochimica Acta*, 1982, **46**, 2639-2658.

106. D. J. Plazek and V. M. O'Rourke, *Journal of Polymer Science Part A-2: Polymer Physics*, 1971, **9**, 209-243.

107. D. J. Plazek, C. A. Bero and I.-C. Chay, *Journal of non-crystalline solids*, 1994, **172**, 181-190.

108. J. C. Dyre, *Reviews of Modern Physics*, 2006, **78**, 953-972.

109. Z. P. Zhang, M. Z. Rong and M. Q. Zhang, *Progress in Polymer Science*, 2018, **80**, 39-93.

110. T. Witten Jr and L. M. Sander, *Physical Review Letters*, 1981, **47**, 1400-1403.

111. C. J. Kloxin and C. N. Bowman, *Chemical Society Reviews*, 2013, **42**, 7161-7173.

112. M. Röttger, T. Domenech, R. van der Weegen, A. Breuillac, R. Nicolaÿ and L. Leibler, *Science*, 2017, **356**, 62-65.

113. X. Niu, F. Wang, X. Li, R. Zhang, Q. Wu and P. Sun, *Industrial & Engineering Chemistry Research*, 2019, **58**, 5698-5706.

114. F. Cuminet, D. Berne, S. Lemouzy, É. Dantras, C. Joly-Duhamel, S. Caillol, É. Leclerc and V. Ladmiral, *Polymer Chemistry*, 2022, **13**, 2651-2658.

115. L. Imbernon and S. Norvez, *European Polymer Journal*, 2016, **82**, 347-376.

116. A. Demongeot, R. Groote, H. Goossens, T. Hoeks, F. Tournilhac and L. Leibler, *Macromolecules*, 2017, **50**, 6117-6127.

117. M. M. Obadia, B. P. Mudraboyina, A. Serghei, D. Montarnal and E. Drockenmuller, *Journal of the American Chemical Society*, 2015, **137**, 6078-6083.

118. B. P. Mudraboyina, M. M. Obadia, I. Allaoua, R. Sood, A. Serghei and E. Drockenmuller, *Chemistry of Materials*, 2014, **26**, 1720-1726.

119. B. Hendriks, J. Waelkens, J. M. Winne and F. E. Du Prez, *ACS Macro Letters*, 2017, **6**, 930-934.

120. R. H. Grubbs and S. Chang, *Tetrahedron*, 1998, **54**, 4413-4450.

121. R. R. Schrock, *Journal of Molecular Catalysis A: Chemical*, 2004, **213**, 21-30.

122. Y.-X. Lu, F. Tournilhac, L. Leibler and Z. Guan, *Journal of the American Chemical Society*, 2012, **134**, 8424-8427.

123. G. C. Vougioukalakis and R. H. Grubbs, *Chemical Reviews*, 2009, **110**, 1746-1787.

124. W. Denissen, G. Rivero, R. Nicolaÿ, L. Leibler, J. M. Winne and F. E. Du Prez, *Adv. Funct. Mater.*, 2015, **25**, 2451-2457.

125. S. E. Eldred, D. A. Stone, S. H. Gellman and S. S. Stahl, *Journal of the American Chemical Society*, 2003, **125**, 3422-3423.

126. J. M. Hoerter, K. M. Otte, S. H. Gellman, Q. Cui and S. S. Stahl, *Journal of the American Chemical Society*, 2008, **130**, 647-654.

127. H. Ying, Y. Zhang and J. Cheng, *Nature Communications*, 2014, **5**, 3218-3226.

128. B. Jousseaume, C. Laporte, T. Toupance and J.-M. Bernard, *Tetrahedron Letters*, 2002, **43**, 6305-6307.

129. E. Delebecq, J.-P. Pascault, B. Boutevin and F. Ganachaud, *Chemical Reviews*, 2012, **113**, 80-118.

130. R. C. Fuson, *Chemical Reviews*, 1935, **16**, 1-27.

131. A. Blatt, *The Journal of Organic Chemistry*, 1936, **1**, 154-158.

132. S. Krishnamurthy, *Journal of Chemical Education*, 1982, **59**, 543.

133. W. Denissen, *Vitrimers based on vinylogous acyl exchange reactions*, PhD thesis, Ghent University, 2017.

134. O. Exner and J. Lakomý, *Collection of Czechoslovak Chemical Communications*, 1970, **35**, 1371-1386.

135. W. Denissen, M. Droesbeke, R. Nicolay, L. Leibler, J. M. Winne and F. E. Du Prez, *Nature Communications*, 2017, **8**, 1-7.

136. M. Guerre, C. Taplan, R. Nicolaÿ, J. M. Winne and F. E. Du Prez, *Journal of the American Chemical Society*, 2018, **140**, 13272-13284.

137. H. A. Stefani, I. M. Costa and D. de O Silva, *Synthesis*, 2000, **2000**, 1526-1528.

138. S. Tariq, L. Irusta, M. Fernández and M. Paulis, *Progress in Organic Coatings*, 2023, **174**, 107292-107301.

139. S. Tariq, L. Irusta, M. Fernández and M. Paulis, *Progress in Organic Coatings*, 2022, **165**, 106732-106739.

140. P. J. Geurink, L. van Dalen, L. G. van der Ven and R. R. Lamping, *Progress in Organic Coatings*, 1996, **27**, 73-78.

141. W. Denissen, I. De Baere, W. Van Paepegem, L. Leibler, J. Winne and F. E. Du Prez, *Macromolecules*, 2018, **51**, 2054-2064.

142. N. J. Van Zee and R. Nicolaÿ, *Progress in Polymer Science*, 2020, **104**, 101233-101271.

143. B. Krishnakumar, R. P. Sanka, W. H. Binder, V. Parthasarthy, S. Rana and N. Karak, *Chemical Engineering Journal*, 2020, **385**, 123820-123832.

144. J. Zheng, Z. M. Png, S. H. Ng, G. X. Tham, E. Ye, S. S. Goh, X. J. Loh and Z. Li, *Materials Today*, 2021, **51**, 586-625.

145. K. Yu, P. Taynton, W. Zhang, M. L. Dunn and H. J. Qi, *RSC Advances*, 2014, **4**, 10108-10117.

146. J. P. Brutman, P. A. Delgado and M. A. Hillmyer, *ACS Macro Letters*, 2014, **3**, 607-610.

147. T. Liu, B. Zhao and J. Zhang, *Polymer*, 2020, **194**, 122392-122408.

148. X. Yang, L. Guo, X. Xu, S. Shang and H. Liu, *Materials & Design*, 2020, **186**, 108248-108258.

149. P. Muller, *Pure and Applied Chemistry*, 1994, **66**, 1077-1184.

150. M. I. Page, *Chemical Society Reviews*, 1973, **2**, 295-323.

151. D. J. Cox and A. J. Fairbanks, *Tetrahedron: Asymmetry*, 2009, **20**, 773-780.

152. L. N. Ferguson, *Journal of Chemical Education*, 1970, **47**, 46-53.

153. D. Williams, E. Bienvenüe-Goetz and J. Dubois, *Journal of the Chemical Society B: Physical Organic*, 1969, 517-522.

154. Ö. K. Kovács, G. Schneider, L. Lang and J. Apjok, *Tetrahedron*, 1967, **23**, 4181-4196.

155. H. W. Heine, A. D. Miller, W. H. Barton and R. W. Greiner, *Journal of the American Chemical Society*, 1953, **75**, 4778-4779.

156. B. Capon, *Quarterly Reviews, Chemical Society*, 1964, **18**, 45-111.

157. M. Gibson, J. M. Goodman, L. J. Farrugia and R. C. Hartley, *Tetrahedron Letters*, 2003, **44**, 2841-2844.

158. J. Gierer and I. Pettersson, *Canadian Journal of Chemistry*, 1977, **55**, 593-599.

159. G. A. Morrison and J. B. Wilkinson, *Journal of the Chemical Society, Perkin Transactions 1*, 1990, 345-351.

160. F. Cuminet, S. Caillol, É. Dantras, E. Leclerc and V. Ladmiral, *Macromolecules*, 2021, **54**, 3927-3961.

161. M. Delahaye, F. Tanini, J. O. Holloway, J. M. Winne and F. E. Du Prez, *Polymer Chemistry*, 2020, **11**, 5207-5215.

162. N. Ballard and J. M. Asua, *Progress in Polymer Science*, 2018, **79**, 40-60.

163. N. M. Ahmad, F. Heatley and P. A. Lovell, *Macromolecules*, 1998, **31**, 2822-2827.

164. N. M. Ahmad, B. Charleux, C. Farcet, C. J. Ferguson, S. G. Gaynor, B. S. Hawkett, F. Heatley, B. Klumperman, D. Konkolewicz and P. A. Lovell, *Macromolecular Rapid Communications*, 2009, **30**, 2002-2021.

165. N. Ballard, J. C. de la Cal and J. M. Asua, *Macromolecules*, 2015, **48**, 987-993.

166. M. Destarac, *Polymer Chemistry*, 2018, **9**, 4947-4967.

167. K. Liang, R. A. Hutchinson, J. Barth, S. Samrock and M. Buback, *Macromolecules*, 2011, **44**, 5843-5845.

168. K. Liang and R. A. Hutchinson, *Macromolecular Rapid Communications*, 2011, **32**, 1090-1095.

169. H. H. Pham, J. Farinha and M. A. Winnik, *Macromolecules*, 2000, **33**, 5850-5862.

170. C. L. Elkins, T. Park, M. G. McKee and T. E. Long, *Journal of Polymer Science Part A: Polymer Chemistry*, 2005, **43**, 4618-4631.

171. S. Jung, J. T. Liu, S. H. Hong, D. Arunbabu, S. M. Noh and J. K. Oh, *Polymer*, 2017, **109**, 58-65.

172. S. Jung, S. Y. Kim, J. C. Kim, S. M. Noh and J. K. Oh, *RSC Advances*, 2017, **7**, 26496-26506.

173. S. Jung and J. K. Oh, *Materials Today Communications*, 2017, **13**, 241-247.

174. L. J. Fetters, D. J. Lohse, S. T. Milner and W. W. Graessley, *Macromolecules*, 1999, **32**, 6847-6851.

175. S. Wu, *Journal of Polymer Science Part B: Polymer Physics*, 1989, **27**, 723-741.

176. J. J. Rogalski, L. Botto, C. W. Bastiaansen and T. Peijs, *Journal of Applied Polymer Science*, 2020, **137**, 48963.

177. F. Jahanzad, M. Kazemi, S. Sajjadi and F. A. Taromi, *Polymer*, 1993, **34**, 3542-3544.

178. M. Thiessen and V. Abetz, *Polymers*, 2021, **13**, 1189.

179. C. Goussé and A. Gandini, *Polymer International*, 1999, **48**, 723-731.

180. I. Brown and T. Sandreczki, *Macromolecules*, 1990, **23**, 94-100.

181. M.-F. Grenier-Loustalot and L. Da Cunha, *European Polymer Journal*, 1998, **34**, 95-102.

182. J. L. Hopewell, D. J. Hill and P. J. Pomery, *Polymer*, 1998, **39**, 5601-5607.

183. G. Scheltjens, M. Diaz, J. Brancart, G. Van Assche and B. Van Mele, *Reactive and Functional Polymers*, 2013, **73**, 413-420.

184. F. Orozco, Z. Niyazov, T. Garnier, N. Migliore, A. T. Zdvizhkov, P. Raffa, I. Moreno-Villoslada, F. Picchioni and R. K. Bose, *Molecules*, 2021, **26**, 2230-2237.

185. B. D. Mather, K. Viswanathan, K. M. Miller and T. E. Long, *Progress in Polymer Science*, 2006, **31**, 487-531.

186. Z. Czech, K. Agnieszka, P. Ragańska and A. Antosik, *Journal of Thermal Analysis and Calorimetry*, 2015, **119**, 1157-1161.

187. A. Cuvellier, R. Verhelle, J. Brancart, B. Vanderborght, G. Van Assche and H. Rahier, *Polymer Chemistry*, 2019, **10**, 473-485.

188. A. A. Kavitha and N. K. Singha, *ACS Applied Materials & Interfaces*, 2009, **1**, 1427-1436.

189. P. J. Flory and J. Rehner Jr, *The Journal of Chemical Physics*, 1943, **11**, 512-520.

190. M. Doi and S. F. Edwards, *The Theory of Polymer Dynamics*, Oxford University Press, Oxford (UK), 1988, vol. 73, 0198520336.

191. J. D. Ferry, *Viscoelastic Properties of Polymers*, John Wiley & Sons, Chichester (UK), 1980, 0471048941.

192. A. A. Kavitha and N. K. Singha, *Macromolecules*, 2010, **43**, 3193-3205.

193. J. J. Lessard, L. F. Garcia, C. P. Easterling, M. B. Sims, K. C. Bentz, S. Arencibia, D. A. Savin and B. S. Sumerlin, *Macromolecules*, 2019, **52**, 2105-2111.

194. P. R. Christensen, A. M. Scheuermann, K. E. Loeffler and B. A. Helms, *Nature Chemistry*, 2019, **11**, 442-448.

195. Y. Zhu, F. Gao, J. Zhong, L. Shen and Y. Lin, *European Polymer Journal*, 2020, **135**, 109865-109870.

196. J. Tellers, R. Pinalli, M. Soliman, J. Vachon and E. Dalcanale, *Polymer Chemistry*, 2019, **10**, 5534-5542.

197. J. J. Lessard, G. M. Scheutz, R. W. Hughes and B. S. Sumerlin, *ACS Applied Polymer Materials*, 2020, **2**, 3044-3048.

198. S. Weerathaworn and V. Abetz, *Macromolecular Chemistry and Physics*, 2023, **224**, 2200248.

199. M. Delahaye, J. M. Winne and F. E. Du Prez, *Journal of the American Chemical Society*, 2019, **141**, 15277-15287.

200. H. Zhang, S. Majumdar, R. A. van Benthem, R. P. Sijbesma and J. P. Heuts, *ACS Macro Letters*, 2020, **9**, 272-277.